AN EVALUATION OF THE EFFECT OF BLAST-GENERATED FRAGMENT SIZE DISTRIBUTION ON THE UNIT COSTS OF A MINING OPERATION, USING MODELING AND SIMULATION TECHNIQUES

by

Solomon Augustine Tucker

A dissertation submitted to the faculty of
The University of Utah
in partial fulfillment of the requirements for the degree of

Doctor of Philosophy

Department of Mining Engineering

The University of Utah

May 2015

The University of Utah Graduate School

STATEMENT OF DISSERTATION APPROVAL

The dissertation of **Solomon Augustine Tucker**

has been approved by the following supervisory committee members:

Michael K. McCarter	, Chair	**12/19/2014** Date Approved
Michael G. Nelson	, Member	**12/19/2014** Date Approved
Thomas A. Hethmon	, Member	**12/19/2014** Date Approved
Hyung Min Park	, Member	**12/19/2014** Date Approved
Raj K. Rajamani	, Member	**12/19/2014** Date Approved

and by **Michael G. Nelson** , Chair of

the Department of **Mining Engineering**

and by David B. Kieda, Dean of The Graduate School.

ABSTRACT

This research was undertaken to investigate the impacts of finer rock fragmentation (arising from higher energy blasting) on the unit costs of a hard-rock surface mine. The investigation was carried out at a copper operation in southern Utah, which exploits its deposits by conventional methods, including drilling, blasting, loading, and truck haulage. The run of mine is processed in a three-stage crushing circuit and a two-stage grinding circuit, which feed a flotation plant that produces a copper concentrate.

The research was carried out using modeling and simulation techniques. Fifty-five blast designs in total were developed for ore and waste units, with energy inputs ranging from 100 kcal/st to 400 kcal/st. For each design, fragmentation was predicted using the Kuz-Ram method. Crushing of the predicted ore fragment size distributions was simulated using MODSIM™.

Data from pit face imaging and timed motion studies were collected and analyzed for the influence of fragmentation on shovel and truck productivity. Analyses indicated that fragment size distribution alone does not significantly impact this productivity.

From simulation of the crushing circuit, it was found that the impact of differences in the blast-generated fragment distribution on the crusher energy is limited to the primary crusher, where a vast range of feed size distributions are introduced. No such relationships were evident at the secondary and tertiary crushers. Energy savings from

increasing blasting intensity proved negligible and would not justify the costs of higher energy blasting.

There was no evidence from this work that any beneficial influences of blast-generated fragment size distribution reach the grinding mill.

Costs were estimated for drilling, blasting, and crushing, which were the principal unit operations inferred to be affected in some meaningful way by the varying intensities of blast energy input.

The research shows that, principally as a result of jaw crusher gape restrictions and the significant unit costs of secondary reduction for both ore and waste, the net of all breakage (primary blast, secondary reduction, and crushing) does reduce to a transient minimum before they begin to ramp up again, thus fitting a classical mine-to-mill curve.

To Yie and Papa

TABLE OF CONTENTS

ACKNOWLEDGEMENTS

Many people contributed in many different ways to make my research possible. I owe these people my sincere thanks.

Firstly, my heartfelt thanks to W.U.S. Copper (a pseudonym) for kindly and generously granting me access to their mine and their incredible personnel. My experience with them has built me up in many invaluable ways, and I wish them the success that they work so hard for and that they so greatly deserve. While I would love to name and thank specific persons working at or in relation to this operation, the company's desire for anonymity prevents my saying thanks to these persons by name. However, I say to them a big thank you for all the help, time, and other resources they so graciously gave me.

My heartfelt thanks to the Fulbright Program for sponsoring my studies, and to the Institute for International Education (IIE) for stoutly and vigilantly shepherding me through. I am forever grateful for your support.

I am indebted to my committee, whose dedicated and thoughtful review of my evolving concepts, thoughts, and drafts made this dissertation possible. Each member gave more support than duty required. As a result, I come out a confident professional in issues of mine-to-mill optimization. Thank you, Dr. Kim McCarter, Dr. Mike Nelson, Dr. Raj Rajamani, Prof. Tom Hethmon, and Dr. Hyung Min Park.

I am grateful to Pam Hofmann, Samantha Davis, and Darrel Cameron for their kindness of heart and their stalwart support throughout the course of my studies. Special thanks to Rob Byrnes for patiently giving me guidance in my geotechnical test work.

My incredible colleagues and fellow travelers, Mahesh Kumar Shriwas, Siavash Nadimi, Ankit Jha, Anirban Bhattacharyya, Hossein Changani, Kirk Erickson, and Rao Latchireddi, I am grateful to have known you, and to have shared the bond and trials of learning. I thank you, Jessica Wempen, for being such sound counsel and encouragement. Many times, I have wished you were not so uncannily spot-on with your shot-in-the-dark predictions!

My family bore the most sacrifice to make my studies possible. The rest of my life is committed to making up for my absence in your lives over this period. Thank you, Annette, Kwame, Hinga, Nyapo, and Ama!

My thanks to Chris Adjei, Hannah David, Joseph Morrison, Marie Rogers, Amelia Liberty, Martha Munezhi, Henok Eyob, Michelle Twali, Betty Jonah, John and Amie Tucker, and the Newlove family for giving me socio-psycho-emotional support and succor through this period. I hope I have been a good enough friend and brother, and I dearly look forward to keeping the bond through the rest of our lives.

CHAPTER 1

INTRODUCTION

1.1 Problem Statement

The view is held widely in the mining industry that more intense fragmentation created by blasting yields increasingly better economic benefits to some key aspects of the mine-to-mill value chain (MacKenzie 1966, 1967; Edgar and Pfleider 1972; Workman and Eloranta 2003; Singh and Narendrula 2005; Eloranta et al. 2007; Brandt et al. 2011). Those aspects that are said to benefit from blasting improvement include the load and haul segments (with associated improvement in productivity), crushing, grinding, and general processing throughput potential. However, a closer examination suggests that, while the anticipated benefits may be realized in some specific situations, there may actually not be as much economic merit to increasing blast fragmentation (reducing the particle size distribution) on these elements as the widely held notion suggests. Process performance improvements, such as increased mining productivity, plant throughput and decreased comminution energy consumption, which are conventionally attributed to blast-induced particle size reduction, may actually be due to additional or entirely different causes, such as better-blended ore grades and changing material hardness (Dance et al. 2007). Similarly, the productivity of loading machines may be affected not by particle size distribution alone, but by several other factors,

including the looseness, angle of repose, moisture content of the muck pile (Singh and Narendrula 2005), the degree of interlock between fragments, and operator efficiency.

Additionally, it is common experience that a wide range of fragmentation size profiles result within the same rock domain (as observed in this research), even when based on a constant level of blast energy infusion. Indeed, such an observation that blasting provides inconsistent particle size distributions and muck pile characteristics further confuses evidence or undermines the prospect that any observed downstream benefits actually would arise directly from blasting alone. The ambiguity therefore triggers the question: how consistent can the effects of blasting be expected to be along the mine-to-mill pathway? The anticipated benefits are sometimes not even necessarily evident, possibly being far too negligible to be considered significant. In effect, the process of physically and objectively tracing the cause-and-effect relationships between the blast results, load and haul productivity, grinding effort (Eloranta 2014), and the overall economics of the operation is often far too fraught with obscurities to provide conclusive results.

Thus, it remains a challenge to provide definitive answers to the question: how does blasting and blast-generated particle size distribution affect the economics of a hard-rock operation?

1.2 Hypothesis

The hypothesis for this research has been formulated to investigate the validity of the above-described notion which is prevalently held about the mine-to-mill concept, that is:

Increased intensity of blasting leads to reduced particle size distributions which eventually lead to a diminishing and minimization of net mine-to-mill costs.

The alternative proposition to this hypothesis is that the increased energies and reduced particle size distributions do not lead to a reduction and minimization of the net mine-to-mill costs.

1.3 Objectives of the research

In pursuit of evidence for the above hypothesis, the following objectives were outlined for this research:

1. Carry out preliminary rock (ore and waste) characterization
    - From these, generate modeling and simulation parameters (for blasting, crushing, and grinding);
2. Produce a range of blast designs with energy inputs ranging from low to high;
3. For each blast design, predict the resulting particle size distribution (PSD) using the Kuz-Ram model;
4. For each design, estimate the unit costs of all the mining unit operations;
5. Simulate the comminution process for all feed PSDs
    - Crushing;
    - Grinding;
6. Evaluate the effect of feed size (PSD) changes on:
    - Mining : drilling, blasting, loading, hauling;
    - Energy consumption, throughput/feed rate;
    - Costs

7. Compare the savings/losses from the mine to the mill, based on the changes in energy input into the blast.

1.4 Description of the host operation

This research was carried out at the operations of W.U.S. Copper, a private-equity-funded company located in the western United States, whose real name has been disguised in this dissertation for reasons of privacy. Typically, copper, silver, and gold mineralization in the deposits of W.U.S. Copper is associated with low-iron skarn alterations within clastic sedimentary rocks and in limestone lying immediately above a monzonite intrusive stock.

The company extracts ore by open pit methods, and employs drilling and blasting techniques to dislodge and fragment ore and waste. Drilling and blasting services are provided by a contractor, based on terms that are reviewed periodically. The mine uses conventional load and haul processes to move ore to the crusher and waste to the adjacent dumps.

A three-stage crushing circuit (one jaw and two cone crushers) produces feed for a two-stage grinding plant. At each stage of grinding, there are two ball mills operating in parallel with each other. Each ball mill operates in standard closed circuit configuration. The cyclone product from the first-stage of grinding is screened at 140 Tyler mesh (105 microns), and the screen undersize is caught in a sump that feeds the second-stage ball mill. The screen oversize forms part of the grinding circuit's final product. The P_{80} size of the final grinding product (screen undersize plus Stage 2 cyclone overflow), combined from the parallel circuits, is 140 Tyler mesh (105 microns). Figure 1.1 is a schematic of

the whole comminution circuit. The liberated copper content in the grinding product is recovered in a flotation circuit to form the final product which is a concentrate. The grade of the concentrate is 22% Cu.

1.5 Scope of the research

This research focused on the stages from drilling to grinding, and did not consider any of the processes downstream of the comminution circuit, including flotation.

The reader may notice that, even though grinding studies are outlined in Section 1.3 as a part of the objectives of this research, the topic of grinding has not been included in the list of chapters. This exclusion was made as a consequence of findings during the research that the crushing product streams remain invariant irrespective of the size profiles generated in the blasting product (crusher head feed). This finding implied that, irrespective of the range of blast energies considered, only a single particle size distribution of feed would be available for a grinding study, and this lack of variety would render pointless the plan to simulate grinding performance for a variety of blast energy-related feed particle size profiles.

However, it must be noted that a significant amount of the research time, especially at the early stages, was devoted to studying the grinding characteristics of the ore, in anticipation of using that understanding to assess the effect of blasting. The decision was therefore made to include the grinding report (with the related literature reviews, modeling theory, and a full account of the grinding test procedures) in Appendix A for interested readers. The remark is made in Section 4.2 that the outcomes of the grinding study presented in Appendix A remain valid considerations for a grinding optimization

effort at the mine, for as long as the ores being treated in the ball mills remain the same as those that were being treated at the time of the grinding sample collection. Should those ores change, which they will as mining progresses downwards in the pits, fresh samples of crusher product will need to be taken, and the full range of fresh grinding tests performed on the new material.

1.6 Units of measure

The primary units of measure in this dissertation are the S.I. units. However, the blasting industry in the United States is solidly based on customary English units, with designs and measurements being prevalently carried out and expressed using the latter. In order to minimize the chances for loss of communication in this operating context, the design procedures have all adhered to the customary practice, and metric equivalents of measure have been provided throughout. Appendix B provides a selection of conversions of the units used in this research.

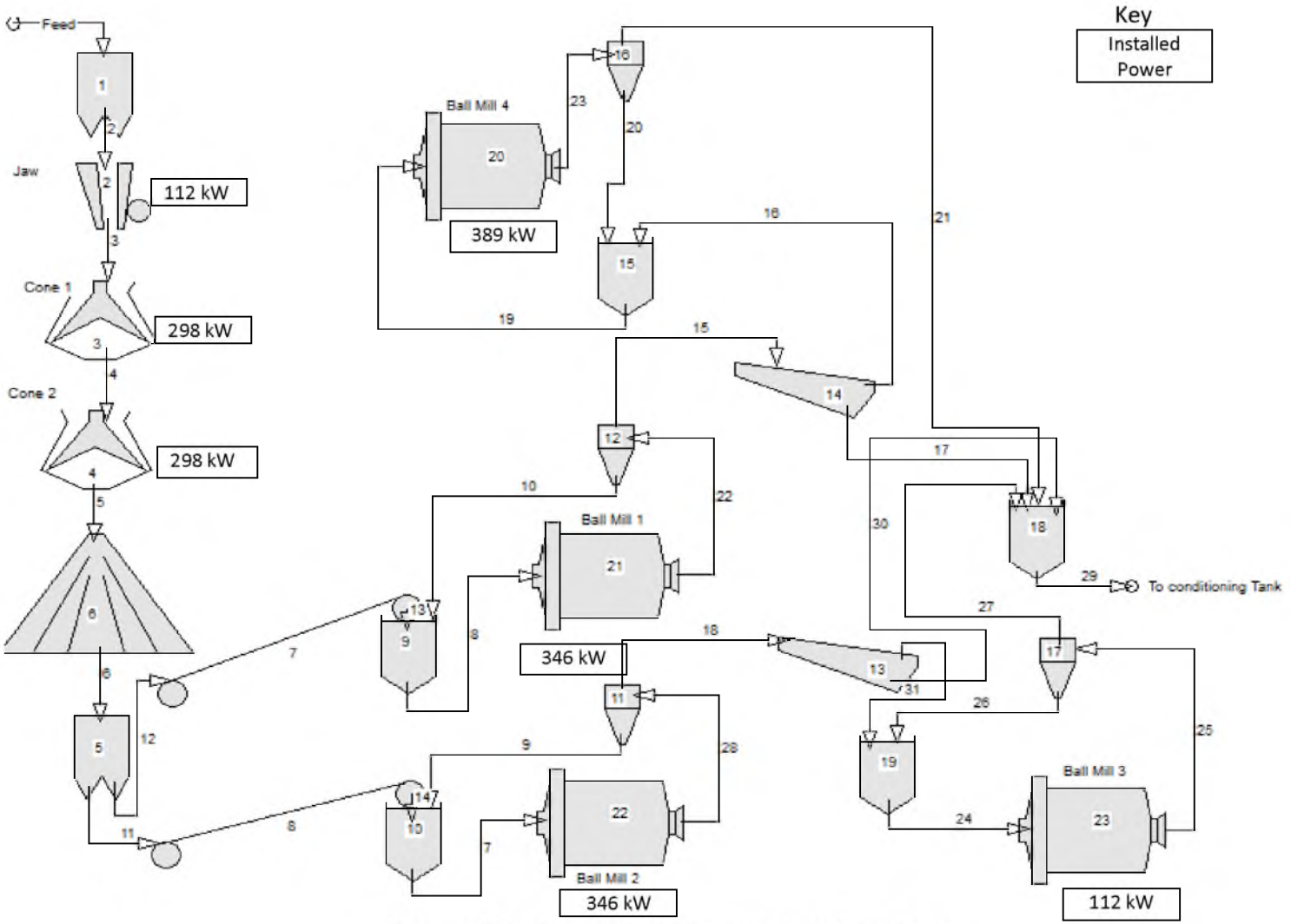

Source: Based on W.U.S. Copper plant flow sheet

FIGURE 1.1 A schematic layout of the comminution circuit at W.U.S. Copper

CHAPTER 2

UNDERSTANDING MINE-TO-MILL PROCESS OPTIMIZATION

2.1 Overview of mine-to-mill process optimization

Between 1990 and 2010, the mining industry saw a surge of interest in the field now commonly called mine-to-mill process optimization, mine-to-mill (Julius Kruttschnitt Mineral Research Center, or JKMRC, 2012), mine-to-mill integration, and process improvement and optimization (PIO) (Dance et al. 2007; Mwansa et al. 2010). The basic concept in this field is that the unit processes in the mining and mineral processing phases of mineral extraction are all related and interdependent, and that they should therefore be treated with an integrated approach, rather than as unrelated processes. Accordingly, it is argued that all benefits and costs accruing at each stage should be reckoned and optimized together against (or in), as it were, a unified overall cost center.

In the traditional system, which is still practiced in many operations around the world, the optimizations of the mine and mill are done separately, with the following typical characteristics being evident (JKMRC 2012):

- mine and mill are under different management structures and cost centers;
- each process has production targets and cost budgets that are optimized without due consideration for the implications of this said optimization either upstream or downstream;

- in the case of costs, the optimization objective for each cost center is to achieve a minimum, and the production volume objective is a maximum. Thus, effectively, the effort is a bid for quantity rather than quality.

Commenting on the traditional approach, Workman and Eloranta (2003) say, "in the past, the primary focus was the ability of the excavation equipment to productively dig the blasted rock and the amount of oversize chunks produced".

In an analysis of the syndromes of the traditional approach to mining optimization, the Julius Kruttschnitt Mineral Research Centre (JKMRC 2012) notes that there is often inadequate communication between different processes to understand the interactions and changes. Furthermore, there is usually no incentive to improve the overall efficiency or value added. These commentators describe this approach as mainly cost oriented rather than value oriented, as the key performance indices (KPIs) do not encourage the maximization of the overall economic value across the operation. However, according to JKMRC (2012) "the focus …. (should be) to maximize the overall value of the operation rather than just to minimize the unit costs".

2.2 Evolution of mine-to-mill

Although the surge of industry interest in mine-to-mill was seen mostly around the turn of the millennium, focus on the impact of the degree of rock fragmentation on the economics of an operation was brought to the fore much earlier, principally through the writings and conference presentations of MacKenzie (1966, 1967). MacKenzie produced what are now considered the classical curves representing the relationships between the

degree of fragmentation and the individual as well as cumulative costs of the various unit processes, from drilling to crushing (Figure 2.1).

This set of curves demonstrates the cost dependence of the various mining unit operations on the degree of fragmentation. The costs of these unit operations, namely, drilling, blasting, loading, hauling, and primary crushing, will increase (or decrease) as shown, with the degree of fragmentation. Summing the curves together, the overall cost versus degree-of-fragmentation curve shown last in the set of curves is obtained. This curve has the form of a saddle, indicating that there is a certain set of values of the degree of fragmentation for which the overall cost is a minimum. According to MacKenzie's presentations, the base of the saddle is quite broad, suggesting that the overall costs change little over a wide range of fragmentation. MacKenzie (1966, 1967) and later Hustrulid (1999) explain the logic and mechanism behind MacKenzie's curves in detail.

Probably due to the central thought in MacKenzie's presentations, the mining industry has prevalently viewed the concept of mine-to-mill integration as leaning almost entirely on rock fragmentation, especially by blasting. However, this view is misleading. Dance et al. (2007) clarify that it is really about (producing) "a more suitable, higher value or higher quality concentrator feed". They stress that what "higher quality feed" means will vary from operation to operation. "In some cases, it is finer fragmentation, in others it is feed that is well blended for grade and lacking in contaminants; it can even indicate that certain ore types are, in fact, not profitable and should be considered mineralized waste" (Dance et al. 2007). They add that "process improvement and optimization (or mine-to-mill) reflects the fact that optimizing concentrator feed goes beyond run-of-mine (ROM) fragmentation and considers all aspects of improving mill

performance from throughput, recovery and final concentrate grade to lower operating costs".

Mine-to-mill philosophy follows a more-or-less 5-stage methodology in its implementation that is highly similar to the workflow of the widely known six-sigma process improvement methodology. This protocol typically involves benchmarking, rock characterization, measurements, modeling/simulation and, if necessary, material tracking.

2.3 "Optimum blasting" not based on cost alone

MacKenzie (1966, 1967) defined optimum blasting as that blasting practice that gives the degree of fragmentation necessary to obtain the lowest unit cost of the combined operations of drilling, blasting, loading, hauling, and crushing. Quoting a popular saying in mine management at the time of his writing, MacKenzie says: "the place for primary crushing is in the mine, not in the crushing plant". He adds, "It has been known for many years that the key to an efficient, low cost hard rock operation is in the mine" (MacKenzie, 1966). He then goes ahead to state as the objective (of his study) the identification of the minimum cost method for the chain of activities under review.

In fact, MacKenzie's focus on mine-to-mill was principally one of cost optimization. He sought to optimize the mine-to-crusher pathway by aggregating the process (unit operation) options which together achieved an overall cost minimum. However, as was later demonstrated by Kanchibotla (2001), this may well lead to a kind of false efficiency, as it overlooks the influence of revenue changes related to various degrees of fragmentation.

According to Kanchibotla (2001), revenue is a principal component of the optimization effort. Whilst recognizing that costs for some subprocesses actually need to be *increased* (rather than decreased) in order to reduce the overall costs of the chain, he notes that the profitability of an operation can be improved either by increasing the revenues or by decreasing the costs, or both. Inherently, he argues, various scenarios exist which shift the optimal choice across a whole spectrum of possible combinations of blasting and processing cost. Some of these scenarios are commodity-specific.

As an example, Kanchibotla reports studies he carried out that demonstrate that purely minimizing total operating costs does not necessarily result in optimum solution unless the impact on unit fixed costs and revenues are also considered. Indeed, the optimum, which may be defined as the maximization of profit, may as well occur on either side of the total cost minimum as on it. This reality of uncertain merits and outcomes for a fragmentation objective thus necessitates a systematic study to determine the conceptually more correct notion of value chain optimization. Figures 2.2 and 2.3 demonstrate Kanchibotla's value chain curves.

Thus, according to Kanchibotla (referring to the contents of Figure 2.3), "optimum" is where the results deliver the maximum net returns on the investment while maintaining the safety and environmental standards.

2.4 How blasting influences fragmentation and filters into mine-to-mill

Various authors have reviewed the nature of rock fragmentation produced by blasting, and opined on the mechanisms by which that fragmentation affects the mine-to-mill pathway (Nielsen and Kristiansen 1996; Hustrulid 1999; Valery and Jankovic 2002;

Ouchterlony 2003; Workman and Eloranta 2003; Valery et al. 2004; Eloranta et al. 2007; JKMRC 2012). All views embrace the notion by Workman and Eloranta (2003) that there are two important aspects of blasting effect on fragmentation, namely, the seen and the unseen. The seen part is the size distribution of blasted fragments, and the unseen effect is in the form of fractures or cracks within the blasted fragments.

It appears to be a consensus among these commentators that improvements in yield from blasting typically consist of some combination of the following features:

- A larger throughput in crushers and mills;
- A lower total energy expenditure in the process;
- Smaller volumes of worthless or cost-prone fractions like fines and oversize;
- A higher ore concentrate grade;
- A higher processing recovery arising from improved liberation (Ouchterlony 2003);
- An improved or, at least, a maintained fragmentation with a lower consumption of explosives.

2.5 The focus of this research

This research focuses principally on the seen aspect of blast fragmentation, namely the particle size distribution. It neither attempts to assess microfractures nor to evaluate the processing impacts of those microfractures on the liberation characteristics of the ore.

Liberation requirements that determine the target grind size were previously investigated by the host mine. Based on verbal advice received, and on current practices at the mine, the assumption was made here that maximum liberation of all of the copper

ore for economic metallurgical recovery is achieved at a grind of 80% passing size of 105 microns (150 Tyler Mesh or 140 US Mesh). This comminution target is the final grind size at the mill of the host mine. Indeed, this size is the sum of all of the breakage goals, contributed to at each stage of "comminution" from the mine to the mill.

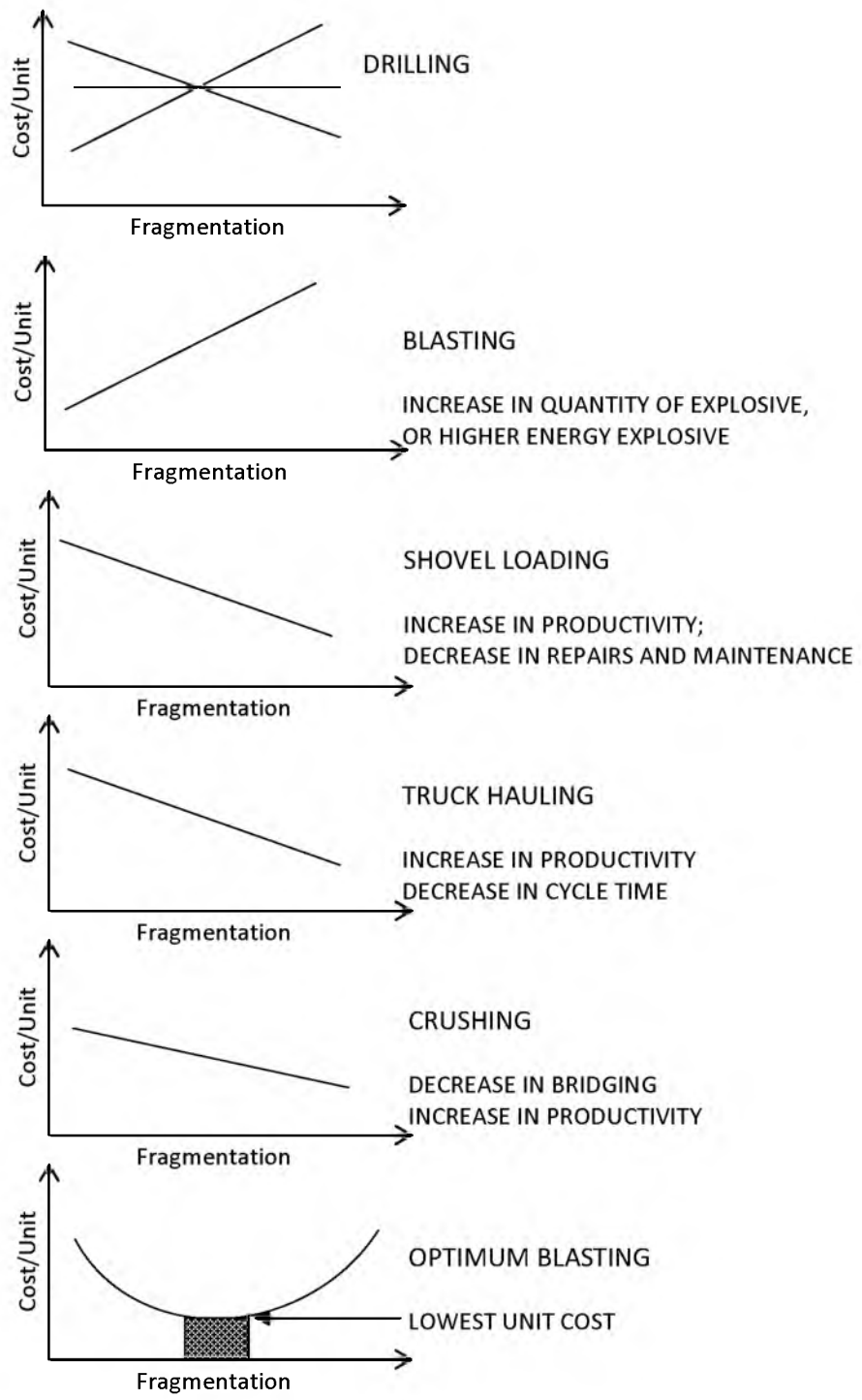

After Mackenzie 1966, 1967

FIGURE 2.1 The effect of the degree of fragmentation on the individual unit operations and on the overall cost

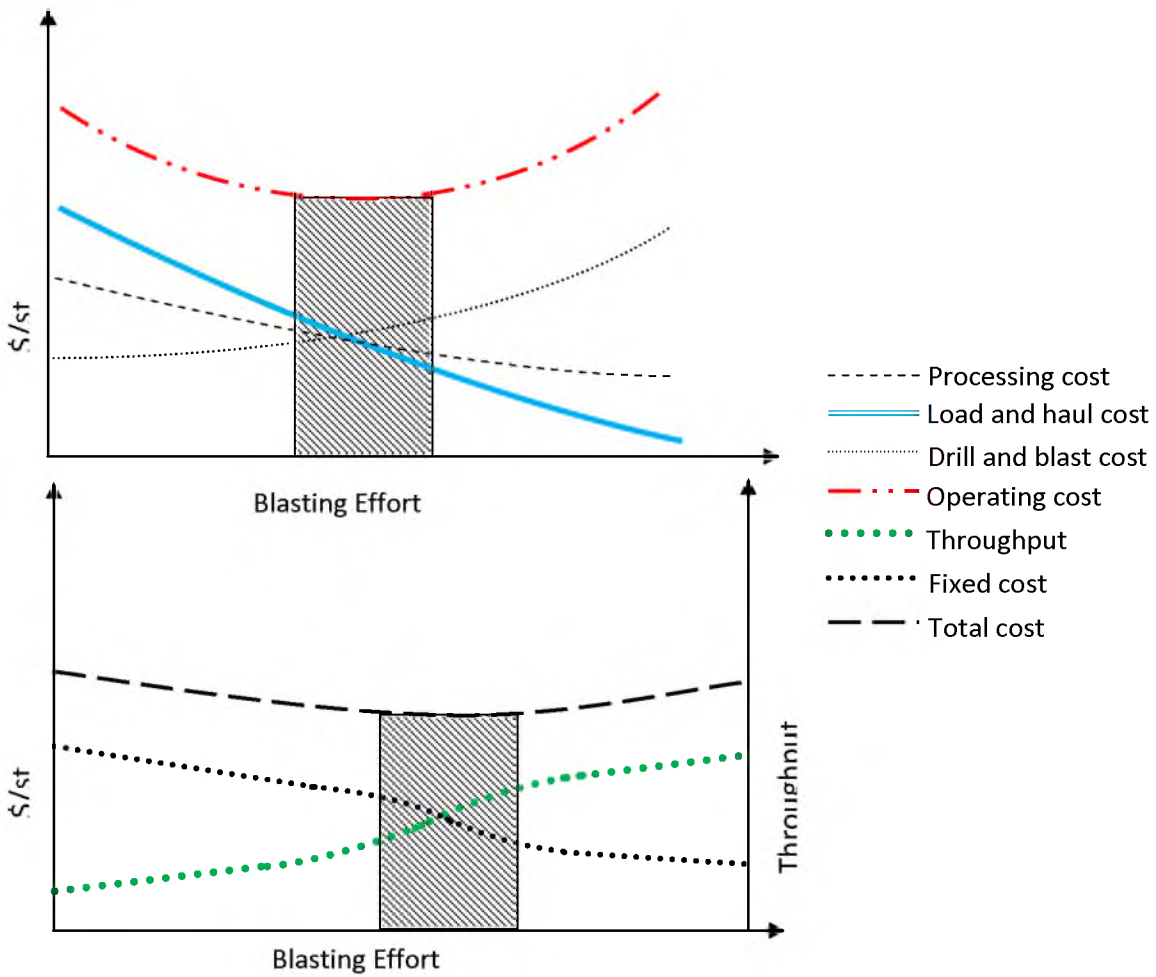

Adapted from Kanchibotla et al. (2001)

FIGURE 2.2 An adaptation of MacKenzie's fragmentation curves to account for impact on throughput

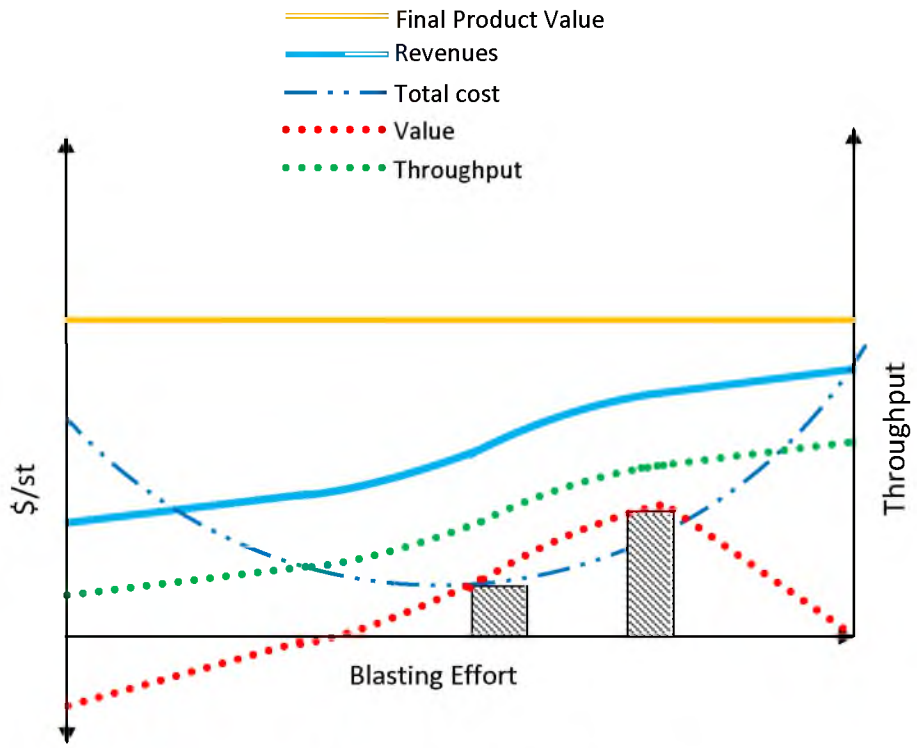

Adapted from JKMRC (2012)

FIGURE 2.3 An adaptation of MacKenzie's curves to reflect the contribution of revenue and overall value to the determination of optimum blast performance

CHAPTER 3

PRINCIPLES FOR THE DESIGN, MEASUREMENT, MODELING, AND SIMULATION OF BLAST FRAGMENTATION

3.1 Introduction

In this chapter, the objectives and fundamentals of surface blast design are reviewed briefly, and some key methods of bench blast design are discussed. A justification is provided for the selection of the design method that is used in this research. Methods for the description and measurement of blasting results are reviewed, and the basis is laid out for the techniques used in this work to model and predict or simulate the blasting product particle size distributions.

3.2 Blast design objectives, fundamentals, and methods

3.2.1 The objectives and fundamentals of blast design

All blast design efforts for open pit mining seek, partly, to find suitable values for the following geometrical elements: the blast hole diameter (D), the burden (B), the spacing (S), the sub-drill (J) and the stemming (T). Together, these elements define the region of rock space that will be directly impacted by the infusion of chemical energy in the process of blasting. The combination of these dimensions with the choice and characteristics of the explosive, as well as the manner and sequence of initiation of the

explosive throughout all or part of the blast, constitute the totality of the blast design.

In a bench blast, the burden (B) is defined as the distance between the individual rows of holes (see Figure 3.1). The burden is also usually reckoned as the distance between the front row of holes and the free face. The spacing (S) is the distance between holes in a given row. Typically, the holes are drilled to a finite depth below the desired final grade. This extra depth of drilling is called the sub-drill (J). Generally, a fraction of the length of the drill hole is left uncharged with explosive, and is usually filled with crushed rock or drill chippings, or just simply left unfilled. This fraction is the stemming (T). The drilled length of the blast hole (L) is equal to the bench height (H) plus the sub-drill (J). The total length of the explosive column (L_e) equals the hole length (L) less the stemming (T).

3.2.2 The methods of blast design

According to Hustrulid (1999), most geometrical designs for a surface mine blast operate, not arbitrarily, but on the basis of some kind of a rational relationship between two or more of the geometric elements listed above, that seeks to optimize energy distribution. He lists the five most fundamental of these relationships as follows:

1 Spacing – Burden

$$S = K_S B$$

Where:

K_S is a constant relating spacing, S, to the burden. B. For a square pattern, K_S = 1; it grades into a rectangular pattern for values between 1 to 1.5. For staggered patterns, the best energy distribution is achieved with $K_S = 1.15$.

2 Burden – Diameter

$$B = K_B D$$

Where:

K_B is a constant relating burden to the hole diameter, and incorporates explosive energy factors and rock density.

3 Subdrill - Burden

$$J = K_J B$$

Where:

K_J is a constant relating sub-drill to the burden. Values range from 0.23 to 0.32. A typical value is 0.3.

4 Stemming - Burden

$$T = K_T B$$

Where:

K_T is a constant relating stemming to the burden. Typically, $K_T \geq 0.7$

5 Bench height – Burden

$$H = K_H B$$

Where:

K_H is a constant relating bench height to the burden. Typically, $K_H > 1$, but is more commonly between 1.5 and 2.

Hustrulid (1999) combines relationships 2 and 5, and devises the following:

$$H \geq K_B D$$

John Floyd (n.d.) validates this relationship by recommending the following:

$$D(in) \leq \frac{1}{3} * H\ (ft)$$

There are many blast design methods in use in the mining industry today, the most common of which include: Konya's method, Ash's method, Powder Factor method, Blast Dynamics method, and Blast Dynamics Energy method. All of these methods have emerged or evolved from empirical observations and/or rules of thumb, focused on deducing the values for the above-listed ratios which yield the most efficient energy coverage in the mass of rock to be blasted. Details of the various methods are documented in various places (Ash 1963; Konya 1968; Hustrulid 1999; Floyd n.d.). In this dissertation, the method used to design blasts is the Blast Dynamics Energy method.

3.2.3 The Blast Dynamics Energy method

This method has been promoted in industry by John Floyd of Blast Dynamics. Like the other methods, it applies suitable values for all of the ratios outlined above that, in the experience of the proponent, enhances explosive energy distribution. The uniqueness of this method is based first on a decision to apply a certain level of energy to the rock. This desired energy infusion is specified in terms of an energy factor (EF), expressed in kcal/st. A list of recommended energy factors, viewed by Floyd as suitable in the described situations, is presented in Table 3.1. Once the energy level is selected, a back-calculation is done (see Equation 3.1) to determine the various dimensions of the design factors that would yield the specified energy input.

The advantage of using the Blast Dynamics Energy method is that it gives an excellent index for comparing energy inputs. For example, an EF of 100 kcal/st is clearly smaller than one of 400 kcal/st. This scale then provides an objective means for a systematic investigation like the one in this dissertation, to progressively change blast energy input and assess the key outcomes and impacts.

Although it is somewhat similar to the Powder Factor method in terms of the ability to rank levels of explosive energy input into blasts, it differs in the sense that it considers the actual explosive energy input rather than (as in the Powder Factor method) just the weight of the explosive used. Thus, various explosives of different formulations can be compared on a consistent and rational energy-based scale.

The design process by this method is as follows (McCarter 2014; Floyd n.d.):

i. Calculate stem length, T, by the formula:

$$T = \begin{cases} De(22/12) \text{ (for explosive density} < 0.9 \text{ g/ cm}^3) \\ De(24/12) \text{ (for explosive density} > 0.9 \text{ g/cm}^3) \end{cases}$$

ii. Calculate: Subdrill, J = D_e*(7/12)

iii. Calculate: Loading density = 0.3405*(Explosive Density)*D_e^2

iv. Calculate: Charge weight = (H + subdrill - stem length)*(loading density)

v. Calculate: Charge energy = 0.454*(charge weight)*(AWS)

vi. Calculate: Burden (B in feet) by the formula:

$$B = \left[1739 * \left[\frac{\text{Charge Energy}}{\text{Desired Energy Factor} * \text{Rock Density} * \text{Bench Height}}\right]\right]^{0.5} \quad (3.1)$$

Where:

Charge Energy is in kcal/blast hole

Desired Energy Factor is in kcal/st

Rock Density is in lb/ft^3

Bench Height, H, is in ft

Hole Diameter, D_e, is in inches

Explosive Density is in g/cm^3

AWS is in cal/g

vii. Calculate Spacing (S) (ft) = 1.15*B

3.3 Description and modeling of blast fragmentation

For many years, an unambiguous representation of blast-related fragmentation outcomes was difficult to produce. This difficulty was closely related to the problem of measuring or evaluating fragmentation outcomes. Aspects of measurement and evaluation are treated in Section 3.4. It is noteworthy that MacKenzie (1966, 1967) in his

accounts of the results of his study of fragmentation never stated the difficulty he encountered in evaluating the outcomes. His solution was to represent fragmentation by indirect means. He represented the "degree of fragmentation" by shovel loading speed (exclusive of operating delays).

This method to describe fragmentation is classified as indirect, in that it does not really produce an objective quantitative representation of the fragmentation, but instead makes reference to performance values, such as shovel loading speed, that depend on the degree of fragmentation. In addition to this loading rate which MacKenzie favored, other workers (Hustrulid 1999) have indicated other methods such as the quantity of secondary breakage required, secondary breakage costs, bridging delays at the crusher, crusher energy consumption, the type, strength, and size of the feed material, the size of the crushed product, and crusher throughput.

The effectiveness of these various means to represent the degree of fragmentation is, at best, left to personal proof. All of those measures are subject to a wide range of extraneous influences. While MacKenzie's shovel productivity may be valid in some situations, it is fraught with a lot of issues such as will be demonstrated in this work (see Sections 8.5 and 8.6).

3.3.1 An objective description of the degree of fragmentation

The most common and objective representation of the degree of fragmentation today is the PSD. It is a mathematical description of the fraction of discrete or cumulative mass(es), P, passing a screen with a given size, x.

In its simplest form, the PSD is expressed as the equivalent of a frequency table, listing the various fractions of mass appearing in each of a set of discrete size ranges. A suitable graphical representation would be patterned after the frequency distribution model, P(a), such that all size fractions are displayed as size interval-bound frequencies.

In its cumulative form (the cumulative distribution function or CDF), it itemizes the probability, P(x), of fractions of the masses in question appearing below (or passing) a specified mesh size, x. The function, P(x) then varies from 0 to 1 or from 0 to 100%. Figure 3.2 is an example of a graphical output from this kind of a function.

In relation to Figure 3.2, the following features are relevant to this discussion:

X_{50} is a measure of mean fragmentation, which equates to the mesh size through which half of the muckpile (P = 0.5 or 50%) passes.

X_N is some other percentage-related fragmentation size, where N = 20, 30, 75, 80, 90, etc.

P_O is the percentage of fragments larger than a typical size, x_O. This percentage is related to the handling of big blocks (or oversize) by trucks or the size of blocks that the primary crusher cannot swallow.

P_F is the percentage of fine material smaller than a typical size, x_F. In certain contexts, this percentage may be related to sizes below which a penalty for the product's generation is accounted.

The above method of representation of fragmentation or particle size distribution is very prevalently used in mineral processing.

3.3.2 The modeling of particle size distribution

The CDF discussed in Section 3.3.1 is typically discretized, as it is obtained over a number of fractions, retained or passing specified sizes, from sieving with a finite number of screens. A common related practice is to represent the CDF by a continuous function, P(x). A number of standard continuous functions of this nature are used to model particle size distributions, the most common of which are the Rosin-Rammler function (Rosin and Rammler 1933) and the Gaudin-Schuhmann function (Schuhmann et al. 1940). Both distribution functions will be discussed here.

3.3.2.1 The Rosin-Rammler Distribution function

This function is given as follows:

$$Y = 1 - \exp\left[-\left(\frac{x}{x_c}\right)^n\right] \tag{3.2}$$

Where:

Y is the cumulative fraction finer than x

x is the particle size

x_c is the size modulus or characteristic size, or absolute size constant (theoretical maximum particle size)

n is the distribution or dispersion modulus (the spread of the distribution)

The expression can be transformed to

$$\log\left[\ln\left(\frac{1}{1-Y}\right)\right] = n \cdot \log x - n \cdot \log x_c \tag{3.3}$$

This model generally fits coarse particle distributions, which is both a strength and a weakness. The model is known to not adequately predict in the fines range. The relationship is relatively linear over the entire range of particle sizes. Other variations of this expression are used in mining and mineral processing, as will be seen in Section 3.6.1.2.

3.3.2.2 The Gaudin-Schuhmann Distribution function

This distribution function is more commonly used in mineral processing, and generally fits fine particle distributions, such as a ball mill product. It tends to best fit below the 75 to 80% passing size, and has been used in this dissertation in the description of particle size distributions of test ball mill feed and product streams. The relationship is:

$$Y = \left(\frac{x}{k}\right)^m \tag{3.4a}$$

Re-expressed,

$$\log Y = m \cdot \log x - m \cdot \log k \tag{3.4b}$$

Where:

Y is the cumulative fraction finer than x

x is the particle size

k is the size modulus (theoretical maximum particle size)

m is the distribution modulus (spread of the distribution)

3.4 The measurement and estimation of blast fragmentation

The pertinent question is how should the particle size of a muck pile be measured or estimated? Either direct or indirect methods can be used. Direct methods include sieving the whole muck pile, counting boulders, and measuring boulders. Sieving the muck pile is a particularly tedious option that may be impractical or nonviable, and is certainly time-consuming and very costly. Boulder evaluation (counting and measuring) does provide some information, but is restricted to assessing the coarse extremes of the distribution.

On the other hand, the indirect methods, which may be somewhat less accurate, are usually the most practical methods. Two categories of viable indirect methods are (1) the photographic (or photogrammetric) methods, and (2) the measurement of parameters that can be quantitatively related to the degree of fragmentation.

Both of these methods have been used in this dissertation. Photographic methods have been used to estimate the particle size distribution on the mining face, and time-and-motion studies have been used, with very limited success, to attempt to establish a relationship between the particle size distribution and the rate at which loading of rock is done. The inability, encountered in this work (Sections 8.4 and 8.5) to establish a statistically significant relationship between loading rate and PSD underscores the unreliability and ineffectiveness of this kind of indirect method.

3.4.1 Photographic granulometry methods

The theoretical basis and operating details of photographic methods of size distribution analysis are well documented in literature (Kemeny et al. 1993; Bedair 1996;

Maerz 1998; Maerz et al. 1998; Kemeny et al. 2001; Maerz et al. 2001; Palangio et al. 2005; Eloranta et al. 2007; Bobo, n.d.), and will not be given any extensive treatment here. Photographic methods involve less of measurement and more of estimation. However, it is important to note that, imperfect as photographic methods are, they are the speediest, most practical, and most cost-friendly evaluation methods that provide quantitative descriptions of the blast product distribution. In the fast-paced contemporary production environments, these methods can return fairly dependable results in close to real-time, and provide a means for rapid evaluation and pro-active or corrective decision making.

Typically, the results of photographic granulometry estimates of particle size distribution are provided in the form of the particle size distributions, as shown in Figure 3.2. A key issue in these techniques is that evaluation of fines can be quite tenuous below a certain size. Only estimates can be made of fines below certain sizes, these size limits being influenced by the capabilities of the specific piece of software in use. Estimates of the particle distribution profile below this cutoff may be done using curve characteristic options, including Rosin-Rammler (Split Desktop and WipFrag software), Gaudin-Schuhmann (in Split Desktop software), or the Swebrec function (WipFrag software).

Importantly, photographic methods also provide a means for validation of predictive and simulation models. Without such a practical tool for comparison, and given the impracticality of direct sizing techniques, the predictive models would probably have no means to be validated or checked for effectiveness.

3.5 The prediction of blast fragmentation

Blasting literature documents various methods that have developed over the years that attempt to predict the size distribution resulting from a blast design (Hall and Brunton 2001; Ouchterlony 2005). According to Cunningham (2005), the majority of these methods generally fall into two categories, empirical and mechanistic modeling techniques.

Empirical models are predominantly based on the assumption that increased energy levels result in reduced fragmentation across the whole range of sizes. A broader assessment of the characteristics of these models is provided in a review by Ouchterlony (2005), which is summarized in Section 3.5.1.

Mechanistic models track the physics of detonation and the process of energy transfer in a well-defined medium (rock) for specific blast layouts. The models are also able to derive the whole range of blasting results. By its very nature, the mechanistic approach is intrinsically able to map out and demonstrate or "play out" the individual mechanisms in the detonation and breakage process. The approach takes into consideration the physics of both the explosion process and the response characteristics of the blasted medium. Extensive work has been carried out by Dale Preece (2001, 2003, 2008), employing finite element and discrete element methods.

Mechanistic models typically entail a visual element to their depiction of the fragmentation outcome, and are therefore very compelling to potential end-users. However, Cunningham (2005) insists that they are not necessarily any more accurate than the more prevalently used empirical models. He outlines the major shortcoming of the mechanistic models as that they are limited in scale, require long run times, and involve

great difficulty in collecting adequate data about the detonation, the rock, and the end results.

3.5.1 Ouchterlony's review

At about the same time as Cunningham's analysis above, Ouchterlony (2003) carried out an extensive review of fragmentation prediction models. Quoting Rustan (1981), Ouchterlony concluded that, almost invariably, the existing models, which are predominantly empirical in nature, predict the average fragment size (x_{50}) and how that average size depends on the different factors which govern blasting. Some of the models, in addition, venture to describe the fragment size distribution, P(x). Importantly, Ouchterlony observed that rarely do these models attempt to predict the shape of the fragments or their internal microfracture status. This latter fact is a shortcoming, as it leaves a gap in the full evaluation of blast outcomes.

Ouchterlony reports that Rustan (1981) had produced a summary in which he (Rustan) noted that the Kuznetsov formula (which eventually became one element of the Kuz-Ram model) tended to have the best basis of all the methods, with a reported accuracy of ±15%.

Ouchterlony observed that the general build up of the x_{50} equation in all instances contained the three factors in the following structure:

$$x_{50} = \text{constant}*(\text{rock factor})*(\text{geometry factor})*(\text{explosives factor}) \qquad (3.5)$$

The prediction models listed and discussed by Ouchterlony (2003) are as follows:

- SveDeFo's fragmentation equations, based on work by Langefors and Kihlstrom (1963), Holmberg (1974), and Larsson (1974)
- The Kou-Rustan fragmentation equation (Saroblast) - (Kou and Rustan 1993)
- The Kuz-Ram model (Cunningham 1983, 1987, 2005)
- The Chung and Katsabanis model (CK model) – (Chung and Katsabanis 2000)
- The model of Bergmann, Riggle, and Wu (BRW model) – (Bergmann et al. 1973)
- The models of the Julius Kruttschnitt Mineral Research Center (JKMRC or JK models) (Hall and Brunton, 2001)
    - The Crush(ed) Zone model (CZM)
    - The Two-Component model (TCM)
- The Swebrec Function (Ouchterlony 2003)
- The Natural Breakage Characteristic (NBC) model (Moser 2003).

For practical reasons, and given the extent of industry affirmation of the Kuz-Ram model (albeit with some significantly acknowledged shortcomings), only the Kuz-Ram model has been discussed and used in this research work.

3.6 The Kuz-Ram model

The Kuz-Ram model is probably the best known and most widely used empirical approach to estimating fragmentation from blasting (Cunningham, 2005). It was introduced by Cunningham (1987), and has undergone a number of modifications and seen several applications since its first introduction.

There are three key equations constituting the Kuz-Ram model, namely the adapted Kuznetsov equation, the adapted Rosin-Rammler function, and the uniformity equation.

The Kuznetsov equation predicts the mean particle size resulting from a given blasting situation as a function of the in situ rock condition and the explosive energy infused into the blast. The Rosin-Rammler function describes the particle size distribution over the entire range of fragmentation to be achieved. The uniformity equation predicts the spread of the distribution around the Rosin-Rammler profile, and is an indicator of the precision or statistical spread of particle sizes around the expected distribution profile.

3.6.1 The Kuznetsov equation

Hustrulid (1999) has provided an account of the relationship developed by Kuznetsov (1973) between the mean fragment size and the blast energy applied per unit volume of rock (powder factor), expressed as a function of rock type. The development below is sourced from Hustrulid (1999). According to Kuznetsov,

$$\bar{X} = A\left(\frac{V_o}{Q_T}\right)^{0.8} Q_T^{1/6} \tag{3.6}$$

Where:

$\bar{X}$ is the mean fragment size, cm

A is the rock factor. Rock factor is 7 for medium rocks; 10 for hard, highly fissured rocks; 13 for hard, weakly fissured rocks

V_o is the rock volume (cubic meters) broken per blast hole.

V_o = Burden * Spacing * Bench Height

Q_T is the mass (kg) of TNT containing the energy equivalent of the explosive charge in each blast hole

Expressing the TNT strength in Equation 3.6 in terms of ANFO strength (where the relative weight strength of TNT compared to ANFO is 115, ANFO relative strength being 100), then:

$$\bar{X} = A\left(\frac{V_o}{Q_e}\right)^{0.8} Q_e^{1/6} \left(\frac{S_{ANFO}}{115}\right)^{-19/30} \tag{3.7}$$

Where:

Q_e is the mass of explosive being used (kg)

S_{ANFO} is the weight strength of the explosive relative to ANFO

But:

$$\frac{V_o}{Q_e} = \frac{1}{K} \tag{3.8}$$

Where:

K is the powder factor (or specific charge, in kg/m^3)

Hence, Equation 3.7 becomes:

$$\bar{X} = A(K)^{-0.8} Q_e^{1/6} \left(\frac{115}{S_{ANFO}}\right)^{19/30} \tag{3.9}$$

The mean fragment size can, therefore, now be calculated from a given powder factor.

This form (Equation 3.9), as well as that in Equation 3.7, is the preferred form employed by Cunningham in the Kuz-Ram model.

Various applications have been found for this equation, including the calculation of the quantity of a given explosive required to achieve a certain mean fragmentation from a blast.

3.6.1.1 The rock factor, A

Cunningham (1983) reckoned initially that values of rock factor, A, range from 8 to 12, with 8 being the lower limit even for very weak rocks and 12 the upper limit even for hard rocks. Cunningham has since taken several steps to improve estimates of the factor, A. A significant milestone along this path was the adoption and modification of Lilly's Blastability Index (Lilly 1986; Widzyk-Capehart and Lilly 2001).

Lilly (1986) defined the Blastability Index (BI) as:

$$BI = \frac{1}{2}[RMD + JPS + JPO + SGI + H] \tag{3.10}$$

Where:

RMD is the rock mass description

JPS is the joint plane spacing

JPO is the joint plane orientation

SGI is the specific gravity influence

H is rock hardness

Values that Lilly provided for the terms in this relationship are given in Table 3.2.

Cunningham (1987) initially proposed an adaptation for Lilly's scheme as follows:

$$A = 0.06 \times (RMD + JF + RDI + HF) \tag{3.11}$$

Where:

JF, the Joint Factor, replaces the Joint Plane Spacing (JPS) and Joint Plane Orientation (JPO) in Lilly's formulation.

As will be shown in Equation 3.17, this replacement would be subsequently modified further in Cunningham's revision of the algorithm.

3.6.2 Adoption of the Rosin-Rammler equation

Cunningham observed that the Rosin Rammler formula (see Equation 3.2) provides a reasonable description of the fragment size distribution in blasted rock, the preferred formulation being:

$$R = e^{-\left(\frac{x}{x_c}\right)^n} \tag{3.12}$$

or

$$W_r = 100e^{-\left(\frac{x}{x_c}\right)^n} \tag{3.13}$$

Where:

R is the proportion of material retained on a given mesh, x

W_r is the percentage of the weight retained on that mesh

x is a given screen size

x_c is the characteristic size, a scale factor dictating the size through which 63.2% of the particles pass

Cunningham (1983) and Hustrulid (1999) show that x_c can be obtained from a rearrangement of Equation 3.12, such that:

$$x_c = \frac{x}{\left[\ln\frac{1}{R}\right]^{\frac{1}{n}}} \tag{3.14}$$

Given that the Kuznetsov formula gives the 50%-passing screen size $\overline{X}$, then substituting $\overline{X}$ for x and R = 0.5 in Equation 2.12, then:

$$x_c = \frac{\overline{X}}{[0.693]^{1/n}} \tag{3.15}$$

The requirement for completeness of the prediction model, then, is to determine "n", the uniformity constant.

3.6.3 The Uniformity equation

From field results, Cunningham (1987) found that, for a square drilling pattern,

$$n = \left(2.2 - 14\frac{B}{D}\right)\left[\frac{1+\frac{S}{B}}{2}\right]^{0.5}\left(1 - \frac{W}{B}\right)\left(\frac{L}{H}\right) \tag{3.16}$$

Where:

B is the burden (m)

S is the spacing (m)

D is the hole diameter (mm)

W is the standard deviation of drilling accuracy (m)

L is the total charge length (m)

H is the bench height (m)

For a staggered pattern, 'n' increases by 10%.

In general, it is desirable to have uniform fragmentation, so high values of 'n' may be preferred. Cunningham (1987) has observed the following pattern:

- The normal range of 'n' for blasting fragmentation in reasonably competent ground is from 0.75 to 1.5, with the average being around 1.0. More competent rocks have higher values.
- Values of 'n' below 0.75 represent a situation of "dust and boulders" which, if it occurs on a wide scale in practice, indicates that the rock conditions are not conducive to control of fragmentation through changes in blasting. Cunningham observed that "dust and boulders" typically happens when stripping overburden in weathered ground.
- For values below 1, variations in the uniformity index, 'n', are more critical to oversize and fines. For n = 1.5 and higher, muck pile texture does not change much, and errors in judgment are less punitive.
- The rock at a given site will tend to break into a particular shape. These shapes may be loosely termed "cubes", "plates", or "shards". The shape factor has an important influence on the results of sieving tests, as the mesh used is generally

square, and will retain the majority of fragments having any dimension greater than the mesh size.

3.7 Important limitations to the original Kuz-Ram model

As the mining industry embraced the original Kuz-Ram model, a number of shortcomings became apparent, as shown below. Some of these shortcomings still exist today.

i. The model failed to consider the effect of timing on fragmentation (Ouchterlony 2005; Kanchibotla et al. 1999)
ii. It did not expressly consider the effect of gas pressure and brisance
iii. It did not account for microfractures resulting in the broken rock
iv. It did not model fines sufficiently effectively (Ouchterlony 2005)
v. It did not account for boosters and primers

In the light of some the above limitations, Cunningham (2005) proposed a set of changes to the original Kuz-Ram model. The changes aimed at improving estimation of mean fragmentation $\bar{X}$, and uniformity, 'n', both of which he reckoned were partly outcomes of the initiation methods. He ascribes the possibility of these changes to advancements related to the introduction of electronic delay detonators.

3.7.1 Important changes to the algorithm

One significant change in the mean fragmentation algorithm lies in the inclusion of a correction factor, C(A). Need for this correction typically arises when it is apparent that the rock factor, A, is either greater or smaller than the original algorithm dictates.

Cunningham (2005) recommends that, rather than tweak the input, thus possibly losing some valid input, a correction factor is applied to the rock factor, to adjust to what is reckoned to be the reasonable value.

There is also a minor change in the sub-algorithm to quantify the Joint Plane Angle (JPA) influence. This change is as shown in Table 3.3.

The revised algorithm, which has been used in this dissertation, is:

$$A = 0.06(RMD + RDI + HF)\cdot C(A) \tag{3.17}$$

C(A) has values well within the range 0.5 to 2.

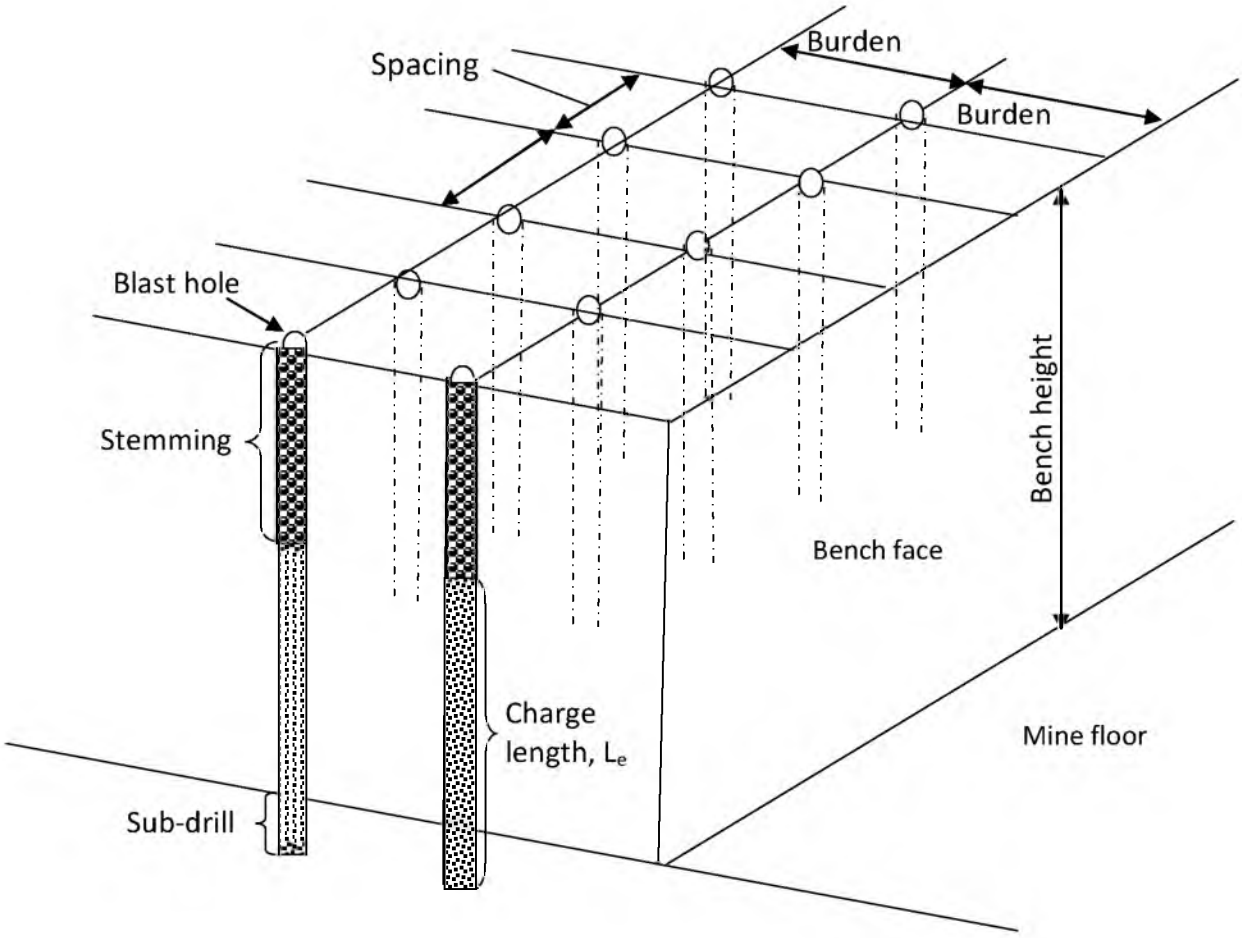

Adapted from Latham et al. (2006)

FIGURE 3.1 A schematic of key design features in a bench blast

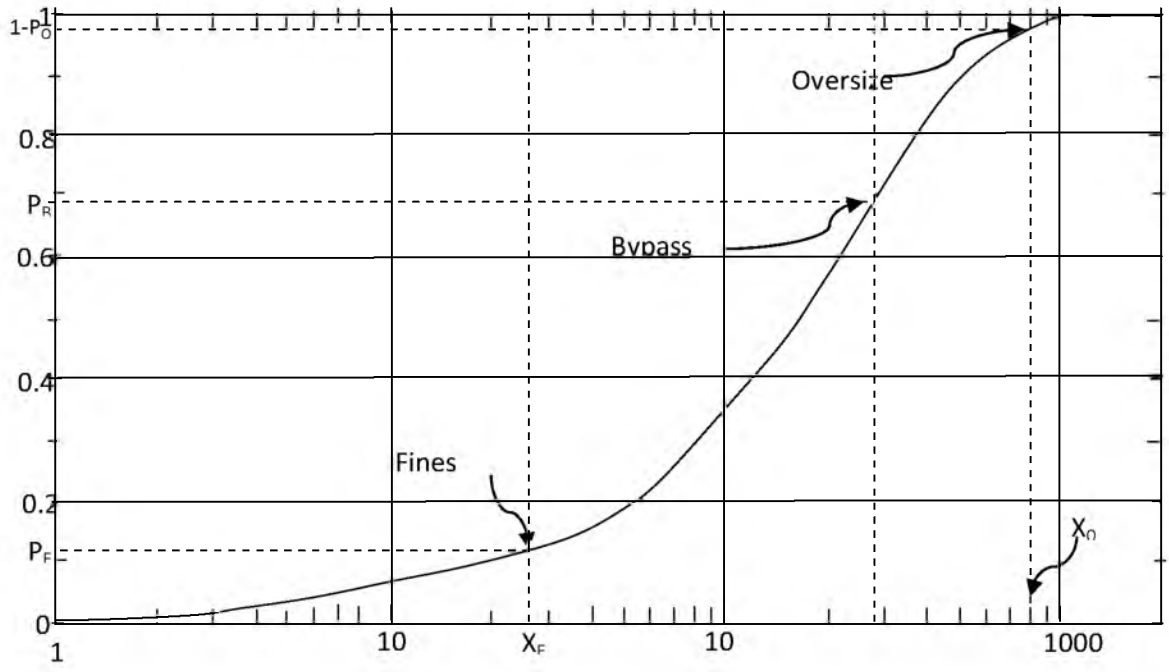

Adapted from Ouchterlony (2003)

FIGURE 3.2 An example of a fragmentation curve

TABLE 3.1 A list of energy factors recommended for various blasting situations

Operating Situation	Recommended Energy Factor (kcal/st)
Very weak rock	100
Well jointed, harder rock	140
Average rock	180
Hard rock	220
Blocky, very hard rock	250
Mine-to-mill blasting	350
Very high energy blasts	500
Upper limit	1200

Source: J. Floyd, 2012: *Efficient Blasting Techniques*

TABLE 3.2: Ratings for Lilly's rock factor parameters

Parameter	Description	Rating
Rock Mass Description (RMD)	Powdery/Friable	10
	Blocky	20
	Totally Massive	50
Joint Plane Spacing (JPS)	Close (< 0.1m)	10
	Intermediate (0.1 to 1m)	20
	Wide (> 1m)	50
Joint Plane Orientation (JPO)	Horizontal	10
	Dip out of face	20
	Strike normal to face	30
	Dip into face	40
Specific Gravity Influence (SGI)	SGI = 25* SG – 50 (where SG is in t/m^3)	
Hardness (H)	Mohr's Hardness	1 to 10

Adapted from Lilly, 1986

TABLE 3.3: Modifications to assigned values for joint plane angle (JPA)

Direction of rock fabric	Value 1987	Value 2005
Dip out of face	20	40
Strike out of face	30	30
Dip into face	40	20

CHAPTER 4

PRINCIPLES, TRENDS, AND METHODS FOR COMMINUTION MODELING AND THE SIMULATION OF CRUSHING SYSTEMS

4.1 Overview

In this chapter, the principles and theories behind the range of process simulation models used in this research are reviewed. Because comminution processes are typically supported and accompanied by classification phenomena and processes, the applicable models for these accompanying phenomena and processes have been included in this discussion.

4.2 The discussion and reporting of grinding simulation

The original plan for reporting on the outcomes of this research included providing a detailed discussion of the theory of grinding simulation. The plan also included providing a complete account of the grinding work that was carried out as part of this research in anticipation of the need to appraise (by simulation) the grinding performance of various streams of hypothetical mill feed that may arise from crushing simulated fragment size distributions for the range of blast designs considered.

In the pursuit of the original research plans, the key findings and conclusions that are presented in Chapters 7, 8, and 9 demonstrated that the initially anticipated analysis of

grinding are not justified as a central component of this dissertation. However, in view of the amount of effort devoted to this process, the grinding simulation literature review, the details of the modeling parameter development, and the grinding simulation work itself are included as Appendix A. The outcomes presented in this appendix remain valid considerations for a grinding optimization effort at the mine, for as long as the ores being treated in the ball mills remain the same as those that were being treated at the time of the grinding sample collection. Should those ores change, which they will as mining progresses downwards in the pits, fresh samples of crusher product will need to be taken, and the full range of grinding tests performed on the material.

In light of the situation described above, the discussions and reviews in this chapter have been provided with very broad attention to comminution in general, and a very specific focus on crushing. Minimal space is given to grinding considerations in the main text.

4.3 The simulation of mineral processing circuits

According to Thomas et al. (2014), "Simulation is the imitation of the operation of a real-world process or system over time. The act of simulating something first requires that a model be developed; this model represents the key characteristics or behaviors/functions of the selected physical or abstract system or process".

In mineral processing technology, Lynch and Morrison (1999) maintain that, modeling and simulation are concerned with the design and optimization of circuits. According to them, realistic simulation relies heavily on the availability of accurate and

physically meaningful mathematical models, of which there are three types: theoretical, empirical, and phenomenological.

Detailed discussions about the characteristics and formulation of these models are well dispersed in literature (Mular 1989; Sastry and Lofftus 1989; Sastry 1990; Wills 2006) and will, therefore, not be given further treatment here.

4.3.1 The Bond model

Bond's (1952) model is one of three popular empirical energy-size relationships for the modeling and scale up and simulation of comminution systems. The others are by Rittinger (1867) and Kick (1883). According to Bond, the energy required for comminution is proportional to the new crack tip length produced. Reconciling Rittinger's and Kick's laws, a practical form of Bond's law contains three parameters: a feed size parameter, a product size parameter, and a work index, all of which are used to compute the specific energy requirement for a commercial size reduction process. It is given as:

$$\bar{E} = 10W_i\left(\frac{1}{\sqrt{P_{80}}} - \frac{1}{\sqrt{F_{80}}}\right) \tag{4.1}$$

Where:

$\bar{E}$ is the Specific Energy, $(\frac{kWh}{t})$

W_i is the Bond's Work Index

P_{80} is the 80% product passing size

F_{80} is the 80% feed passing size

A major problem with Bond's formulation is that it is inherently a gross over-simplification of especially the grinding system (Herbst and Fuerstenau 1968) and is typically in error by large margins, increasing design risk by up to ±20 % (Blasket 1970; Herbst et al. 1977; Smith 1979).

The shortcomings in the performance of the Bond model, especially in wet comminution systems, seem to arise from its failure to explicitly account for some important circuit subprocesses in the grinding process (Siddique 1977). Instead, it lumps them all into a single empirical correlation (Herbst and Fuerstenau 1968; Herbst et al. 1983). These important subprocesses include the breakage kinetics, particle transport through the mill, and size classification.

Perhaps the most significant detailed phenomenological models for grinding are derived from population balance considerations (Siddique 1977). These models explicitly account for the grinding circuit subprocesses, namely, size reduction kinetics, size classification, and material transport in the mill. By including these critical elements, the population balance models become significantly more effective than the simpler energy—size reduction equations.

4.3.2 Justification for the use of modeling and simulation in this research

It is notoriously challenging to include or provide adequately for research work within the normal mining and processing activity of an operation. Even where an operation approves such a project, the demands and pressures of production usually and quickly cause many aspects of such research work to be de-prioritized, and focus tends to

be drawn to them only if the production is facing significant enough technical challenges whose solution may lie in the research outcomes.

Modeling and simulation are essentially nonobtrusive methods and provide a convenient answer not only for operating mines, but also especially for academic research. In academic research, the objectives and focus may have little overlap with those of a particular mine. By using these techniques, it is usually feasible and convenient to study the processes without necessarily incurring the penalty of the physical outcome of the processes themselves (Tucker 2001). Thus, modeling and simulation methods have been used in this work, to investigate all stages from blasting to grinding.

4.4 The modeling and simulation of crushing systems

A variety of models are available in literature for the simulation and modeling of crusher performance (King 2012; Wills 2006). Not all of these models take into consideration the particle size distribution of the feed. To be applicable to this study, only models which are susceptible to effective simulation of input and output particle size distributions are considered. In addition, the particle size distribution of the product from such models would normally be strongly related (directly or indirectly) to the particle size distribution of the feed. Lastly, the product characteristics arising from such a model must also bear evidence of the influences of the comminution system and the prevailing breakage and classification phenomena.

4.4.1 The jaw crusher model

The jaw crusher model used in this research is the Empirical Model for Jaw and Gyratory Crushers (EMJC)). This model is a simple normalized logarithmic distribution predictor, (Csoke et al. 1996) that is based on the idea that material in the feed smaller than the gap passes straight through the crusher and the larger material is crushed to a predefined size distribution that is modeled by the relation:

$$B(r) = (r/r_{max})^m \tag{4.2}$$

Where:

B is the size distribution function for product arising from feed with size characteristic "r", which is defined below

$r = d_p/GAP$

d_p is the size of the feed particle being broken

$r_{max} = d_{p(max)}/GAP$

$d_{p(max)}$ is the maximum size of the feed particle in the feed stream

GAP is the Open Side Setting (OSS) of the crusher

m is the exponent

In addition to these inputs into the EJMC model, the impact work index of the material in this crusher is an important input.

4.4.2 The cone crusher model

The cone crusher model selected for use in this research is the Classification-Breakage Cycle Model (or CBCM) (after Whiten 1973). This model provides perhaps

the most effective and useful description of the crushing action of a crusher. Also considered the standard model for crushers (Whiten et al. 1973), the CBCM is developed from population balance considerations, and is amenable to use for jaw, gyratory, and cone crushers. In this work, the CBCM has been used to simulate the performance of only the cone crushers.

The model formulation is based on the fact that the operation of a crusher is periodic, with each period consisting of a nipping action and an opening action. In the opening stage of the cycle, some fresh feed is taken in, while material already inside and further up moves downward into the crusher. In the process, some material falls through and out. This set (or cycle) of events can then be described quantitatively in terms of a discrete size distribution for both feed and product.

Consider a feed stream with various size classes, i, where i = 1 to n, with class 1 containing the largest particles.

Let:

p_i be the fraction of the product in size class i

p_i^F the fraction of feed in size class i

M the mass of material held in the crusher

b_{ij} the fraction of particles breaking in size class j that end up in size class i

m_i the fraction of material in the crusher in size class i

$c_i = c(d_i)$, the fraction of material in size class i that is retained for breakage during the next nip of the crusher

W is the mass of total feed that is accepted during a single opening of the crusher, which is also the mass of product discharged from the crusher.

In this scheme, the size distribution in a product is completely determined from the size distribution in the feed and a knowledge of the classification and breakage functions, c_i and b_{ij}, respectively. The size distribution in the product can be calculated from the following relationship:

$$p_i = \frac{(1-c_i)Mm_i}{W} = \frac{1-c_i}{1-c_i b_{ii}}\left(p_i^F + \sum_{j=1}^{i-1} c_j \frac{Mm_j}{W} b_{ij}\right) \quad (4.3)$$

An account of the development of this relationship is provided by King (2012).

For a specific crusher, this model reduces to the specification of the appropriate classification and breakage functions. These two features are directly related to the characteristics of the crusher, rather than to the characteristics of the material.

4.4.2.1 The crusher classification function

For the range $d_1 < d_{pi} < d_2$, a useful form of the crusher classification function, c_i, in Equation 4.3 is typically of the form:

$$c_i = 1 - \left[\frac{d_{pi}-d_2}{d_1-d_2}\right]^n \quad (4.4)$$

For $dpi \leq d_1$, $c_i = 0$

For, $d_{pi} \geq d_2$. $c_i = 1$

Where:

d_1 is the smallest size particle that can be retained in the crushing zone during the opening phase of the cycle

d_2 is the largest particle size that can fall through the crushing zone during the opening phase of the cycle

The parameters, d_1 and d_2, are characteristic of the crusher, and are determined primarily by the setting of the crusher. King (2012) reports that data from crushing machines indicate that both of these parameters are proportional to the closed side setting (CSS) of the crusher. For both the standard and short-head Symons cone crushers, the relationship is as follows:

$$d_1 = \alpha_1 \, CSS \tag{4.5}$$

$$d_2 = \alpha_2 \, CSS + d^* \tag{4.6}$$

In general, α_1 varies from about 0.5 to 0.95, and α_2 varies from about 1.7 to 3.5. The power, n, is usually approximately 2, but can be as low as 1 and as high as 3. The value of d^* is normally set to 0.

4.4.2.2 The crusher breakage function

According to King (2012), the breakage function that describes crushed product behavior is of the form:

$$B(x;y) = K\left(\frac{x}{y}\right)^{n_1} + (1-K)\left(\frac{x}{y}\right)^{n_2} \tag{4.7}$$

The values of b_{ij} are obtained from the cumulative breakage function by the relationship:

$$b_{ij} = B(D_i\text{-}1;\ d_{pj}) - B(D_i;\ d_{pj}) \tag{4.8}$$

Where:

b_{ij} is the fraction of material that enters size interval i from size interval j.

The values of b_{jj} are determined from the relationship:

$$b_{jj} = 1\text{-}B(D_j;\ d_{pj}) \tag{4.9}$$

Where:

b_{jj} is the fraction of material that remains in size interval j after breakage.

4.4.3 Estimation of crusher classification and breakage functions

The parameters in the classification and breakage functions are specific to crusher type and size. According to King (2012), not many studies have been done to establish their values under a range of actual operating conditions using predictive equations. The recommended practical means to estimate these quantities is from measured particle size distributions in the products from operating crushers. However, once established for a particular material in a particular crusher, they remain independent of the CSS. Hence, crusher performance can be simulated as the CSS is varied. This method to estimate selection and breakage functions has been used in this research.

4.4.4 Estimating the crusher work index

Utley (2002) and Luz and Milhomem (2013) maintain that the classical Bond equation is useful for the estimation of comminution power estimation, including crushing power. However, this procedure has come under criticism from authors such as Magdalinovic (1989, 1990) and Magdalinovic et al. (2011), who proposed a modification (see Jankovic et al., 2004; Luz and Milhomem 2013):

$$\bar{E} = 10 * \frac{A}{\sqrt{P_{80}}} * W_i * \left(\frac{1}{\sqrt{P_{80}}} - \frac{1}{\sqrt{F_{80}}}\right) \tag{4.10}$$

Where:

A is a material- and crusher-dependent parameter.

In the absence of a first-principles approach to the determination of the crusher work index or Magdalinovic's parameter, A, a representative value for the work index can be estimated by more practical ways. Of note is the usefulness of a back-calculation method involving the use of the Operating Work Index (Rajamani 2012; Rowland and McIvor 2009). Based in principle on Bond's original theory (Section 4.3.1), this approach does not involve using conventional testing equipment, but instead relies on actual specific energies expended at the comminution plant (in this case, the crusher) during normal operation. It also relies on measures from actual (or estimated) feed and product 80%-passing particle sizes (P_{80} and F_{80}). The adapted Bond relationship applied at each crusher in the circuit is as follows (Rajamani 2012; Rowland and McIvor 2009):

$$\bar{\bar{E}} = \frac{P_C}{F_f} = 10W_B\left(\frac{1}{\sqrt{P_{80}}} - \frac{1}{\sqrt{F_{80}}}\right) \tag{4.11}$$

Where:

$\bar{\bar{E}}$ is the specific energy, $(\frac{kWh}{t})$

P_C is crusher power, (kW)

F_f is fresh feed rate into crusher (tonnes per hour)

W_B is the Bond's crusher work index (kWh/ton)

P_{80} is the 80% product passing size, (microns)

F_{80} is the 80% feed passing size, (microns)

All terms in this relationship, with the exception of the work index, can be obtained from actual operational data. Hence, the operating work index can be estimated.

It is noteworthy that the value W_B, which is also Bond's crusher work index in Equation 4.11, may be considered equivalent to Magdalinovic's aggregate term $\frac{A}{\sqrt{P_{80}}} * W_i$, so that:

$$\frac{A}{\sqrt{P_{80}}} * W_i = W_B \tag{4.12}$$

Importantly, this relationship makes the value of W_B both crusher- and material-dependent, rather than just material-dependent. Indeed, this phenomenon is observed in parameter development in Section 6.2.3.

CHAPTER 5

FRAGMENTATION MODELING PARAMETERS, BLAST DESIGNS, AND FRAGMENTATION PREDICTION

5.1 Overview

In this chapter, three aspects of this research work are treated. Firstly, the rock characterization procedure used to generate parameters for blast fragmentation modeling and simulation is presented. This stage of work was almost entirely geotechnical in content. The outcome was a set of Kuz-Ram factors for the entire suite of rocks treated in the research.

The second stage involved the development of blast designs. All blast designs resulting from that phase of work are presented.

The third stage involved prediction of the blast fragment size distributions.

5.2 Determination of rock factor, A

Cunningham's formula for rock factor is given in equation 3.17 as:

$$A = 0.06 \cdot (RMD + RDI + HF) \cdot C(A) \qquad (5.1)$$

Where:

RMD is the Rock Mass Description

RDI is the Rock Density Influence

HF is the Hardness Factor

C(A) is the Correction Factor

In this scheme, the value of RMD is 10 for powdery/friable rock and 50 for massive rock; and RMD is equal to JF, for vertically jointed rock. These values are fixed and there is no gradation between them.

The RMD is an in situ rock parameter, and the RDI and HF are laboratory-assessed.

The in situ rock characteristics (RDI) were evaluated with the input of the mine geologists at W.U.S. Copper. To aid an unbiased and objective characterization of the in situ rock condition, a questionnaire was developed, based on Cunningham's algorithm. By carefully posing questions related to the rock condition and obtaining answers from the geologists, it was possible to use this questionnaire to evaluate the rock mass description (RMD). Table 5.1 shows a typical form, populated with answers (from both in situ and laboratory-derived data), related to the skarn ore in Bom pit. The forms for the rest of the rock types are presented in Appendix C.

5.2.1 Sample collection and preparation

Specimens of rock of various sizes were obtained from selected piles of blasted ore and waste at the mine site of W.U.S. Copper. This selection was guided by W.U.S. Copper personnel, based on the specimens' apparent representativeness of the visually assessed physical characteristics of the rock category of interest. Specimens were

obtained from both Bom and Sembehun pits, in dimensions ranging in diameter from a few centimeters (for point load tests) to about a quarter of a meter for coring and use in uniaxial compressive strength and related tests.

All tests were carried out in the geotechnical laboratories of the Department of Mining Engineering at the University of Utah.

Preparation of the rock specimens intended for compressive strength testing involved the casting of the blocks of rock in concrete, to facilitate good positioning and a firm grip during coring. Four separate blocks of rock (2 ore, 2 waste) were cast in concrete. After curing, these blocks were cored into cylindrical specimens of two main diameters, using the radial drill. Cored specimens were cut to sizes suitable for UCS testing, as specified in ASTM D7012. A total of 17 cores of size NX (nominal 54.7 mm, or 2.16 in.) and six of 31.4 mm nominal size were obtained. Appendix D shows, in addition to other data, details of the dimensions of the specimen cores used in this work. The target Length/Diameter (L/D) ratio was 2:1. However, where it was not possible to achieve that ratio, the specimen was cut to the nearest ratio possible. Appendix E shows selected photos of some of the cores produced.

The cut ends of the cylindrical rock cores were ground to achieve smooth and parallel ends to each specimen. The cores of softer rock (particularly from Bom pit) were not subjected to grinding, as it was perceived that this would massively degrade the specimens.

Those specimens whose ends were not ground were observed to have markedly irregular ends. To ensure that they had the end-parallelism necessary for the strength tests, the ends of these specimens were lined with a quick-set, epoxy-based filler, and

molded between cylinders of stainless steel. Strips of cellophane sheet were used to promote the separation of the samples from the cylinders. Although end-parallelism was still not fully achieved, the samples were significantly better than before.

5.2.2 Testing

5.2.2.1 Density tests

All samples were weighed using a Sartorius™ scale model 3713. Their lengths and diameters were determined using digital calipers. The values from these measurements were recorded and used to calculate the density of the rocks. The densities so obtained became key inputs into the derivation of the Kuz-Ram factor.

For good comparison of the density values of the rocks, density data were obtained from the Ore Control Section at W.U.S. Copper (Appendix F). Overall, the densities reported by the mine compared well with those calculated. Where differences were apparent, judgment was used to decide which values to use in the determination of the Kuz-Ram rock factor.

5.2.2.2 Ultrasonic velocity testing

Ultrasonic velocity testing was carried out on the cylindrical samples. In this procedure, the p- and s-wave velocities of the specimens were obtained by standard ASTM procedures (ASTM D 2845 – 00). Primarily, the purpose of this was to obtain values of the dynamic Young's modulus of these rocks. According to Cunningham, (2005) uniaxial compressive strength values for soft rocks are meaningless as an input to the derivation of rock factor, and should be replaced by the dynamic Young's Modulus in

the algorithm (obtained from ultrasonic velocity testing). The data obtained from this process are presented along with the core dimension data in Appendix D.

5.2.2.3 Uniaxial Compressive Strength (UCS) testing

UCS tests were performed by standard ASTM methods (ASTM 7012). Two types of testing machine were used, namely, the Rock Mechanics Testing Machine, (RMTS machine) and a testing machine specifically constructed for low-strength samples (a low-strength sample testing machine, or LSTM). The softer samples, predominantly obtained from Bom Pit, were tested using the LSTM. The harder, larger samples, predominantly waste rock from Sembehun Pit, which had been cored with NX bits, were tested using the RMTS machine.

The results obtained from the uniaxial compressive strength tests are summarized in Appendix G.

5.2.2.4 Point Load Index (PLI) tests

Point load index testing was done on the smaller-sized, irregular-shaped specimens obtained from the mine site. Procedures were based on the ASTM methods (ASTM D5731). The results obtained are presented in Appendix H. The results were used to corroborate UCS values. Where cores were unavailable, the point load test values were used to estimate the UCS values (example, Sembehun low-grade ore).

5.2.3 Computation of rock factor, A

From the results of the various tests outlined above, and using the forms in Table 5.1 and Appendix C, the rock factor was estimated for the major rocks that are blasted at the mine. The summary of these factors, along with values of various relevant rock parameters used in this research, are shown in Table 5.2.

In addition to Cunningham's procedure, Lilly (1986) proposed an alternative method to determine the Kuz-Ram rock factor. According to Lilly's experience in Australia, the rock factor can be obtained from the blastability index by the equation:

$$A = 0.12*(BI) \tag{5.2}$$

Using this scheme, a parallel estimate of the rock factor, A, was obtained (see Table 5.2). These results show remarkable similarity. However, only the results from Cunningham's model were used in blast prediction in this work.

5.3 Blast design

Eleven blast designs were developed using the Blast Dynamics Energy Factor method (see Section 3.2.3) (Floyd, n.d.). The base case energy design, which is one of the 11 designs, was that arising from the contract blasting pattern agreed between W.U.S. Copper and the blasting contractor. These contract patterns are approximately replicated in Table 5.3. The differences among the energy factors as shown in the table are accounted for by the differences in design formula used by this researcher and the mine.

The researcher retains the use of the Energy Factor method because of its perceived superiority to the Powder Factor method favored by the mine.

The following are the characteristics of the blast design exercise and its scope:

i. The energy levels chosen for this set of designs range from 100 kcal/st to 400 kcal/st. For each of the six rock categories that are mined by W.U.S. Copper, a blast design has been developed at each of 10 energy levels, based on Equation 3.1.

ii. The explosive of choice in each design is bulk ANFO. While ANFO is effective and relatively inexpensive explosive, the peculiar specification of the explosive does not really matter to the investigation concept. The energy factor is the true driver of the investigation. However, the energy factor does not address the issue of differences in certain other strength characteristics such as the brisance and gas-production capacity. The effect of these other characteristics on blasting outcomes is beyond the scope of this investigation.

iii. Precise timing has been assumed for NONEL initiation.

5.3.1 Details of blast design

Tables 5.4 to 5.8 are summaries of the patterns resulting from the energy factor-driven blast designs for each of the lithologies under consideration.

5.4 Prediction of blast fragmentation

Using the Kuz-Ram model, predictions of particle size distributions were done. The results of the ore shot size prediction are provided in Table 5.9. Figures 5.1, 5.2, and 5.3

are graphs showing the ore particle size distributions from that prediction. Table 5.10 is the result of the predictions of waste shot particle size distributions. Figures 5.4 and 5.5 are plots of these particle size distributions.

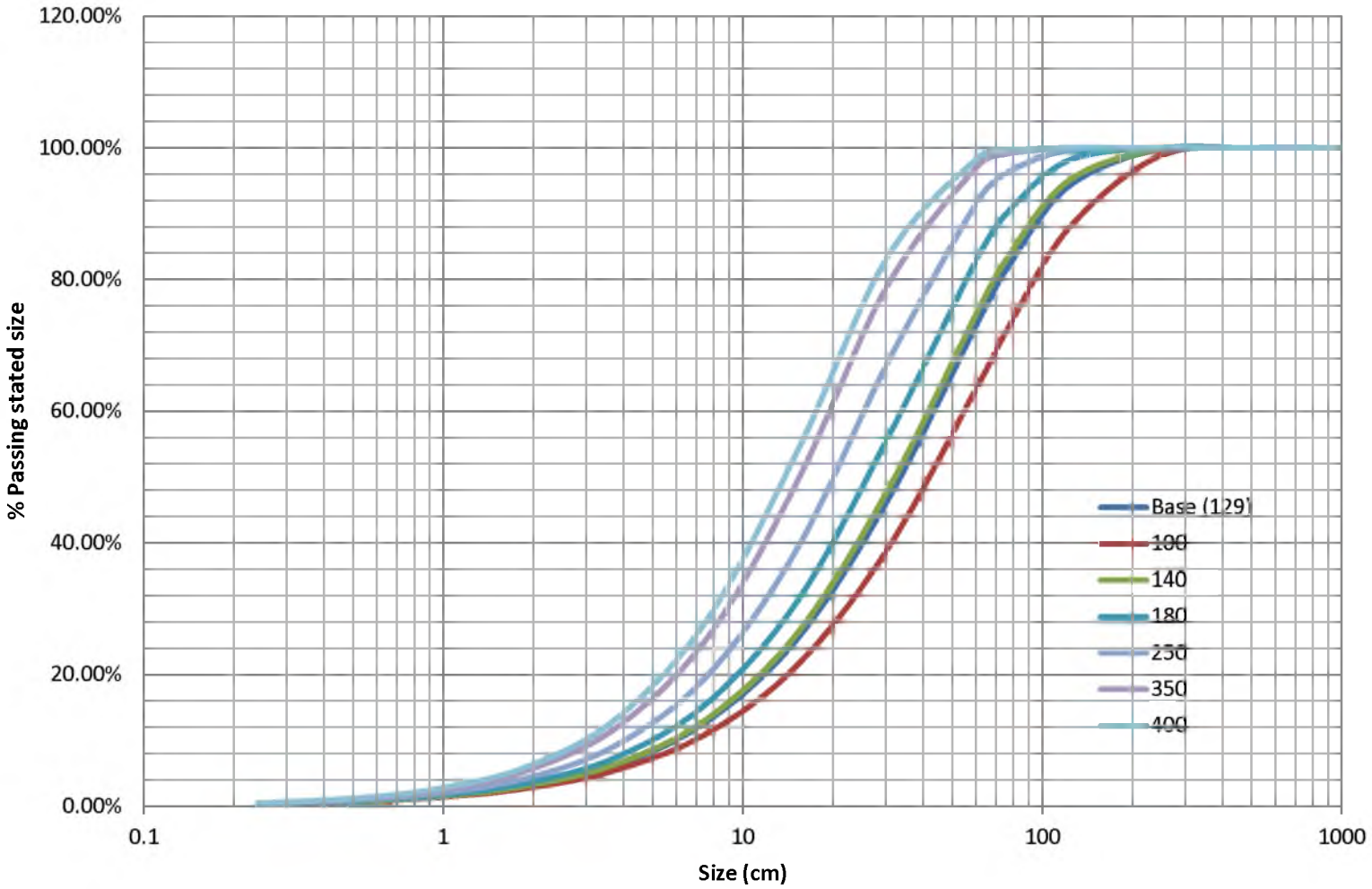

FIGURE 5.1 Plot of fragment size distribution prediction for Bom ore. Fragment size distributions are shown at different blast energies

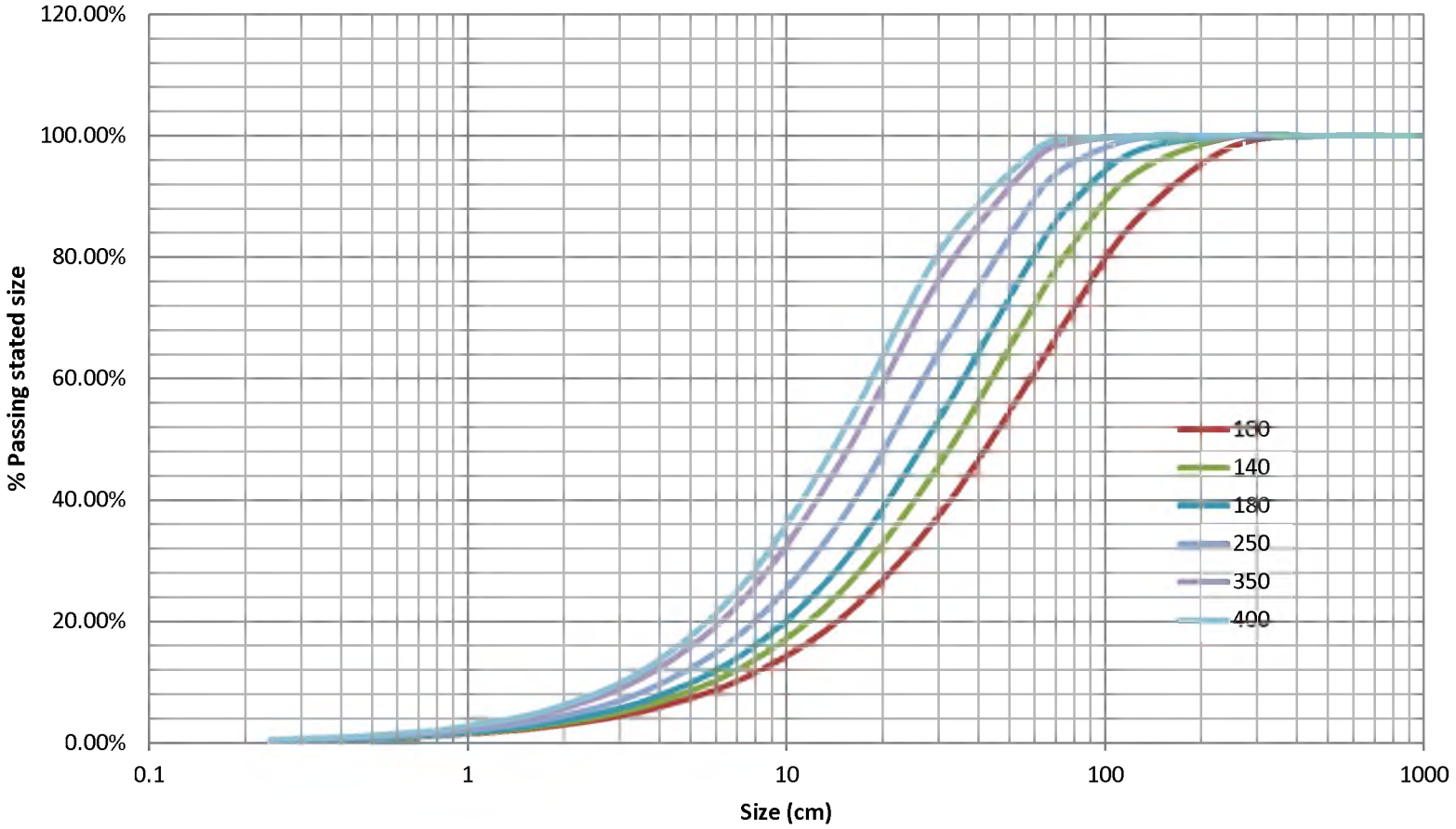

FIGURE 5.2 Plot of fragment size distribution prediction for Sembehun high-grade ore. Fragment size distributions are shown at different blast energies

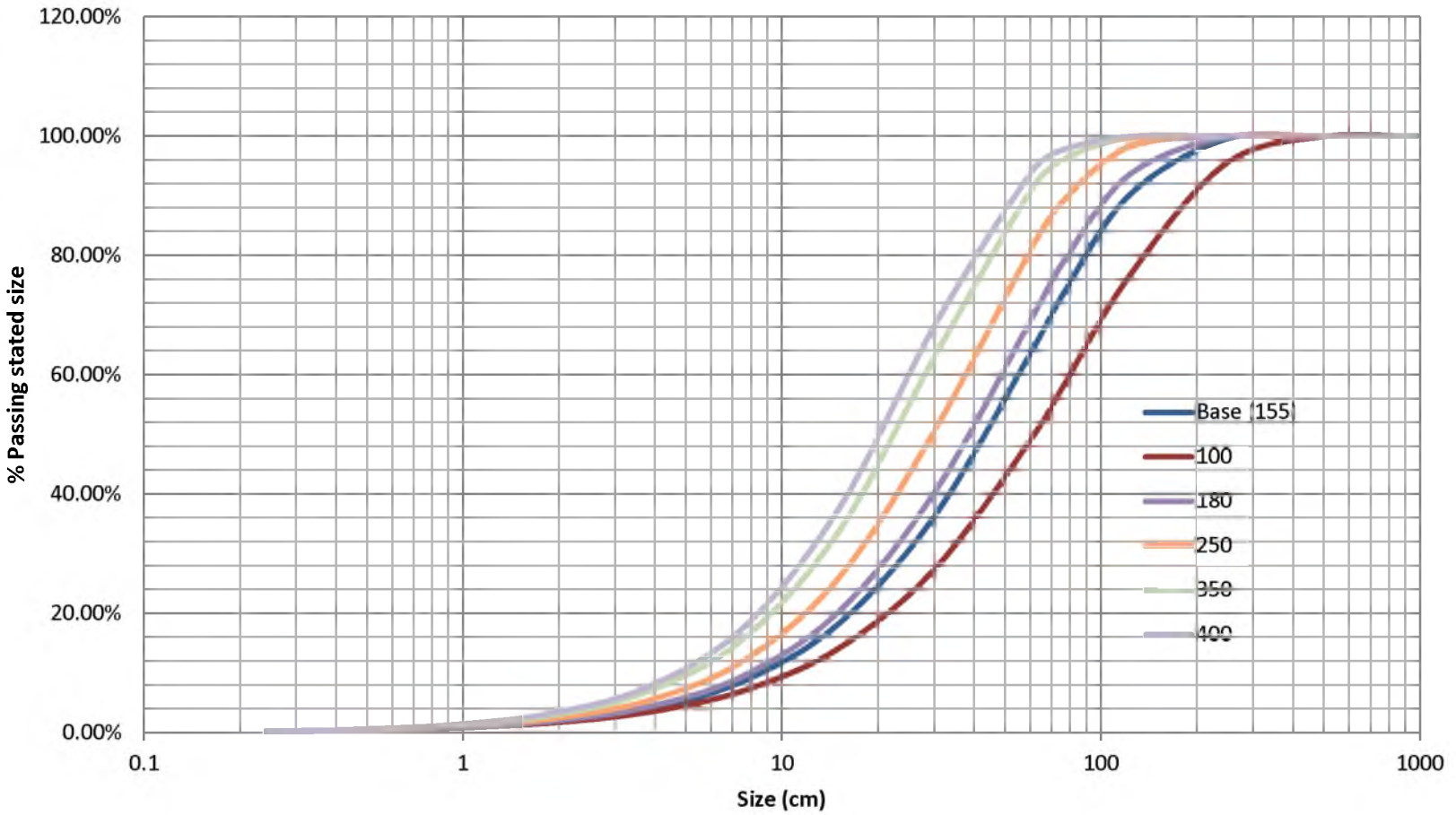

FIGURE 5.3 Plot of fragment size distribution prediction for Sembehun low-grade ore. Fragment size distributions are shown at different blast energies

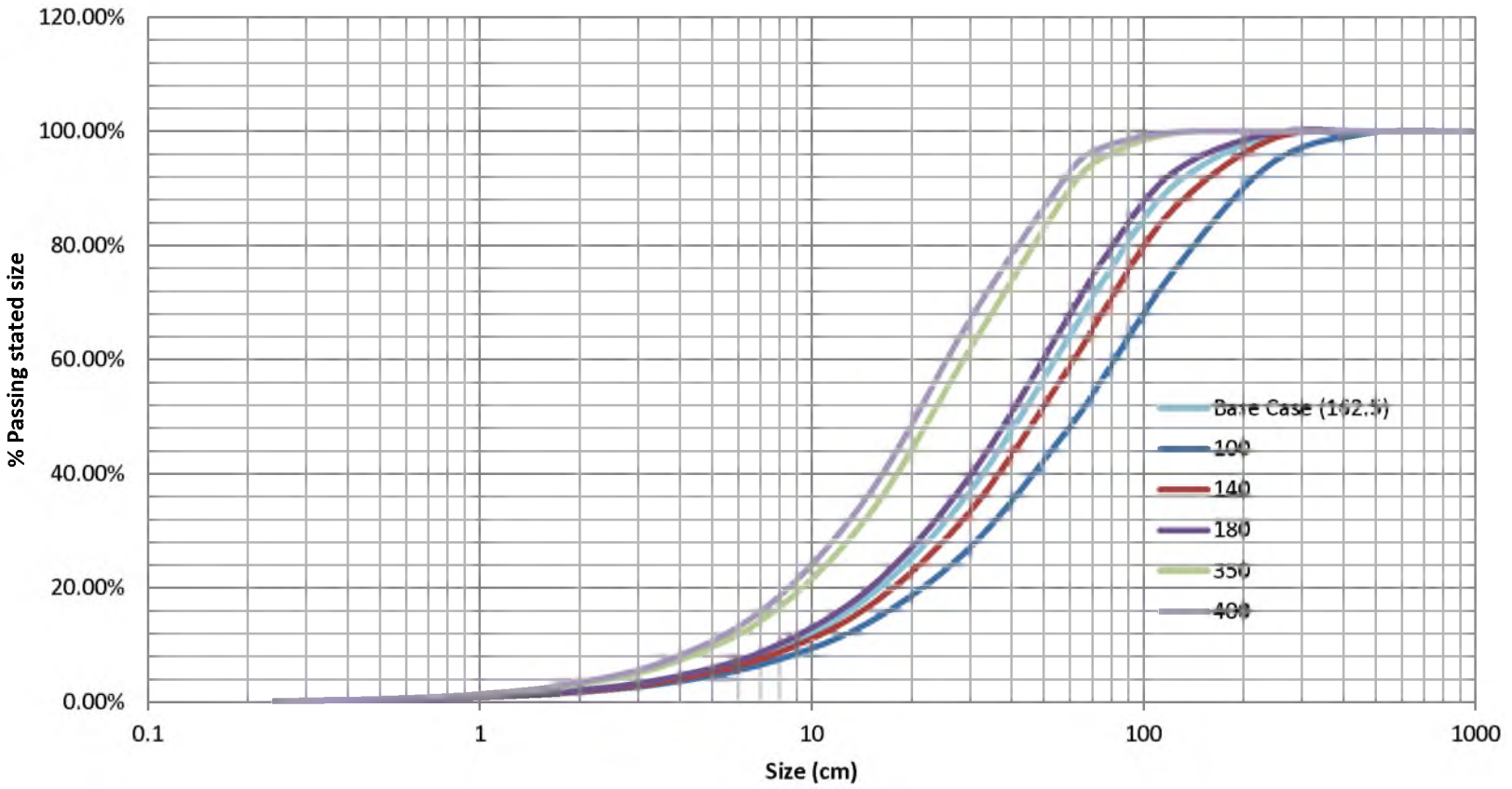

FIGURE 5.4 Plot of fragment size distribution prediction for waste rock (limestone). Fragment size distributions are shown at different blast energies

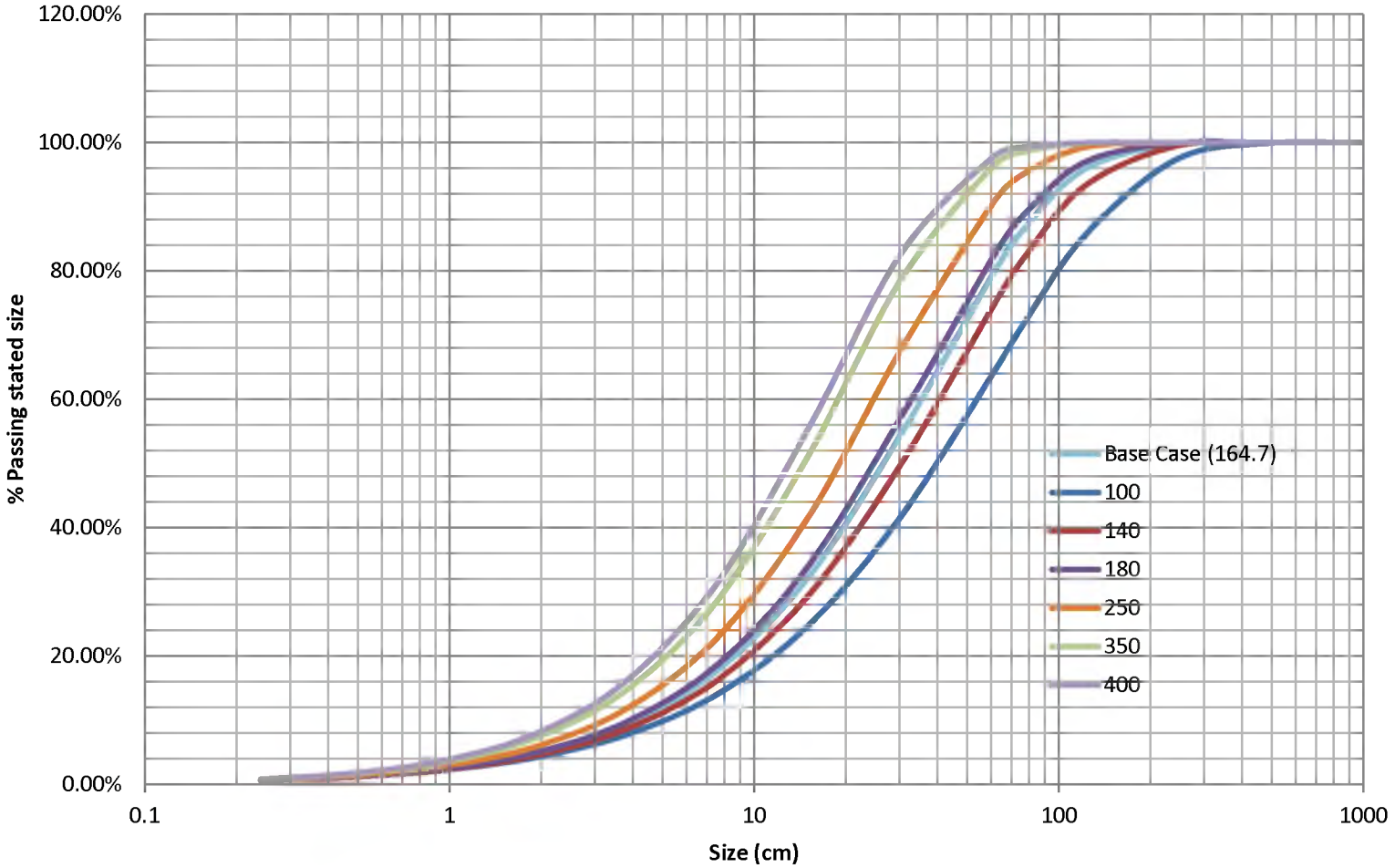

FIGURE 5.5 Plot of fragment size distribution prediction for granodiorite. Fragment size distributions are shown at different blast energies

TABLE 5.1 A sample of the form used to compute the Kuz-Ram rock factor, A.

Estimation of the Kuz-Ram Rock Factor, A

A = 0.06 * (RMD + RDI + HF) * C(A)		
A = Kuz-Ram Factor	***RDI = Rock Density Influence Factor***	
RMD = Rock Mass Description		***HF = Hardness Factor C(A) = Correction Factor***

Rock Type: Bom Ore (Soft)

Section 1: RMD				
RMD = 10 for powdery/friable rock; RMD = 50 for massiver Rock; RMD = JF, for vertically jointed				
Section 1a: Rock Mass Description (RMD)				
Please choose **yes (Y)** *to* ***only one*** *of the following three questions:*				
i. Is this rock friable (powdery)?(y/n)	n			
ii. Is this rock massive, with no jointing, or with joint spacing > blast hole spacing ? (y/n)	n			
iii. Is the rock vertically jointed? (y/n)	y			
Section 1b: Joint Factor, JF - ***(Only valid if you answered "Y" to Question iii in Section 1a, above)***				
Note: **JF = (JCF * JPS) + JPA**			JF = Joint Factor	
JCF = Joint Condition Factor		*JPA = Vertical Joint Plane Angle Factor*		
JPS = Joint Plane Spacing Factor				
JCF ***Range of values: 1 to 2***				
Describe th joint condition in the box below. Please, choose only one of three options, namely:				
"Tight", "Relaxed" or "Gouge-filled": if "Tight", input "1"; if "Relaxed", input "1.5";				
If joint is "gouge-filled", input "2"				
What is the condition of the joint? (1, 1.5 or 2)	1.5			
JPS ***Range: 10 to 50***				
Relevant factors: Reduced Pattern (P) and Joint Spacing (S)				
P = Reduced Pattern = $(B*S)^{0.5}$				
What is the average spacing of joints, in meters?	0.25		P =	4.56
What is the blast Burden (in meters)?	4.27		95% P	4.33
What is the blast Spacing (in meters)?	4.88		JPS	20.00
JPA ***Note that only one answer can be "Yes", although all can be "No"***				
Do the joints dip out of the face at >30°? (Y or N)	y			
Do the joints dip into the face at >30°? (Y or N)	n		JPA	40
Do the joints Strike out of the face? (Y or N)	n		**RMD**	**65**
Section 2: RDI (Rock Density Influence)				
Rock Density (kg//m^3)	3268			
Rock Density Influence Factor (RDI) =	**31.7**			
Section 3: Hardness Factor (HF)				
Young's Modulus, Y (Gpa)	44.56			
UCS (MPa)	28.76			
Hence, Hardness Factor, HF =	**14.85**			
Kuz-Ram Factor				
Uncorrected Kuz-Ram Factor	6.69			
Correction	1			
Kuz-Ram Factor (Estimate)	**6.69**			

TABLE 5.2 Summary of the estimated rock characteristics

Rock	SG (t/m3)	K-Factor 1	K-Factor2 (Lilly)	Blastability Index	P-wave vel (km/s)
Bom ore (Skarn)	3.27	6.69	6.94	57.85	4.43
Sembehun high-grade (soft) (Skarn)	2.97	6.51	5.43	54.33	5.36
Sembehun low-grade (hard) (Skarn)	2.72	8.49	8.04	67.04	5.36
Waste (Limestone)	2.59	8.33	7.94	66.19	5.92
Monzonite	2.66	8.72	8.07	67.24	5.92
Granodiorite	2.56	8.19	6.09	50.79	5.92

TABLE 5.3 The contract blast pattern and its approximate representation in this research work. (Note: 1 ft = 0.3048 m)

Rock	Contract Pattern			Research Approximation			
	Burden (ft)	Spacing (ft)	Powder factor (lb/yd^3)	Burden (ft)	Spacing (ft)	Powder factor (lb/yd^3)	Energy factor (kcal/st)
Bom	14	16	0.6	14.0	16.1	0.9	129.0
Sembehun high-grade	14	16	0.6	14.0	16.1	0.9	142.0
Sembehun low-grade	14	16	0.6	14.0	16.1	0.9	155.0
Waste	14	16	1.2	14.0	16.1	0.9	162.5
Monzonite	12	14	1.35	12.2	14.0	1.2	210.2
Granodiorite	14	16	1.2	14.0	16.1	0.9	164.5

TABLE 5.4 Blast pattern for Bom ore (Note: 1 ft = 0.3048 m)

Explosive energy (kcal/st)	129	100	140	160	180	220	250	280	300	350	400
Bench height, L (ft)	20	20	20	20	20	20	20	20	20	20	20
Burden (ft)	14.01	15.92	13.45	12.58	11.86	10.73	10.07	9.51	9.19	8.51	7.96
Spacing (ft)	16.12	18.30	15.47	14.47	13.64	12.34	11.58	10.94	10.57	9.78	9.15
Subdrill (ft)	3.94	3.94	3.94	3.94	3.94	3.94	3.94	3.94	3.94	3.94	3.94
Stemming (ft)	12.38	12.38	12.38	12.38	12.38	12.38	12.38	12.38	12.38	12.38	12.38
Total hole length (ft)	23.94	23.94	23.94	23.94	23.94	23.94	23.94	23.94	23.94	23.94	23.94
L/B (Stiffness ratio)	1.43	1.26	1.49	1.59	1.69	1.86	1.99	2.10	2.18	2.35	2.51
Powder factor (lb/st)	0.32	0.25	0.35	0.40	0.45	0.54	0.62	0.69	0.74	0.87	0.99
Powder factor (lb/yd^3)	0.88	0.68	0.95	1.09	1.23	1.50	1.70	1.91	2.04	2.39	2.73

TABLE 5.5 Blast pattern for Sembehun high-grade ore (Note: 1 ft = 0.3048 m)

Explosive energy (kcal/st)	142	100	140	160	180	220	250	280	300	350	400
Bench height (L) (ft)	20	20	20	20	20	20	20	20	20	20	20
Burden (ft)	14.02	16.71	14.12	13.21	12.45	11.26	10.57	9.98	9.65	8.93	8.35
Spacing (ft)	16.12	19.21	16.24	15.19	14.32	12.95	12.15	11.48	11.09	10.27	9.61
Subdrill (ft)	3.94	3.94	3.94	3.94	3.94	3.94	3.94	3.94	3.94	3.94	3.94
Stemming (ft)	12.38	12.38	12.38	12.38	12.38	12.38	12.38	12.38	12.38	12.38	12.38
Total hole length (ft)	23.94	23.94	23.94	23.94	23.94	23.94	23.94	23.94	23.94	23.94	23.94
L/B (Stiffness ratio)	1.43	1.20	1.42	1.51	1.61	1.78	1.89	2.00	2.07	2.24	2.39
Powder factor (lb/st)	0.35	0.25	0.35	0.40	0.45	0.54	0.62	0.69	0.74	0.87	0.99
Powder factor (lb/yd^3)	0.88	0.62	0.87	0.99	1.11	1.36	1.55	1.73	1.86	2.17	2.47

TABLE 5.6 Blast pattern for Sembehun low-grade ore (Note: 1 ft = 0.3048 m)

Explosive Energy (kcal/st)	155	100	140	160	180	220	250	280	300	350	400
Bench Height, L (ft)	20	20	20	20	20	20	20	20	20	20	20
Burden (ft)	14.00	17.44	14.74	13.78	13.00	11.75	11.03	10.42	10.07	9.32	8.72
Spacing (ft)	16.10	20.05	16.95	15.85	14.94	13.52	12.68	11.98	11.58	10.72	10.03
Subdrill (ft)	3.94	3.94	3.94	3.94	3.94	3.94	3.94	3.94	3.94	3.94	3.94
Stemming (ft)	12.38	12.38	12.38	12.38	12.38	12.38	12.38	12.38	12.38	12.38	12.38
Total Hole length (ft)	23.94	23.94	23.94	23.94	23.94	23.94	23.94	23.94	23.94	23.94	23.94
L/B (Stiffness ratio)	1.43	1.15	1.36	1.45	1.54	1.70	1.81	1.92	1.99	2.15	2.29
Powder Factor (lb/st)	0.38	0.25	0.35	0.40	0.45	0.54	0.62	0.69	0.74	0.87	0.99
Powder Factor (lb/yd^3)	0.88	0.57	0.80	0.91	1.02	1.25	1.42	1.59	1.70	1.99	2.27

TABLE 5.7 Blast pattern for limestone (Note: 1 ft = 0.3048 m)

Explosive energy (kcal/st)	162.5	100	140	160	180	220	250	280	300	350	400
Bench height, L (ft)	20	20	20	20	20	20	20	20	20	20	20
Burden (ft)	14.01	17.86	15.09	14.12	13.31	12.04	11.30	10.67	10.31	9.55	8.93
Spacing (ft)	16.11	20.54	17.36	16.24	15.31	13.85	12.99	12.27	11.86	10.98	10.27
Subdrill (ft)	3.94	3.94	3.94	3.94	3.94	3.94	3.94	3.94	3.94	3.94	3.94
Stemming (ft)	12.38	12.38	12.38	12.38	12.38	12.38	12.38	12.38	12.38	12.38	12.38
Total hole length (ft)	23.94	23.94	23.94	23.94	23.94	23.94	23.94	23.94	23.94	23.94	23.94
L/B (Stiffness ratio)	1.43	1.12	1.32	1.42	1.50	1.66	1.77	1.87	1.94	2.09	2.24
Powder factor (lb/st)	0.40	0.25	0.35	0.40	0.45	0.54	0.62	0.69	0.74	0.87	0.99
Powder factor (lb/yd^3)	0.88	0.54	0.76	0.87	0.97	1.19	1.35	1.52	1.62	1.89	2.17

TABLE 5.8 Blast pattern for granodiorite (Note: 1 ft = 0.3048 m)

Explosive energy (kcal/st)	164.7	100	140	160	180	220	250	280	300	350	400
Bench height, L (ft)	20	20	20	20	20	20	20	20	20	20	20
Burden (ft)	14.00	17.97	15.19	14.21	13.40	12.12	11.37	10.74	10.38	9.61	8.99
Spacing (ft)	16.10	20.67	17.47	16.34	15.40	13.93	13.07	12.35	11.93	11.05	10.33
Subdrill (ft)	3.94	3.94	3.94	3.94	3.94	3.94	3.94	3.94	3.94	3.94	3.94
Stemming (ft)	12.38	12.38	12.38	12.38	12.38	12.38	12.38	12.38	12.38	12.38	12.38
Total hole length (ft)	23.94	23.94	23.94	23.94	23.94	23.94	23.94	23.94	23.94	23.94	23.94
L/B (Stiffness ratio)	1.43	1.11	1.32	1.41	1.49	1.65	1.76	1.86	1.93	2.08	2.23
Powder factor (lb/st)	0.41	0.25	0.35	0.40	0.45	0.54	0.62	0.69	0.74	0.87	0.99
Powder factor (lb/yd^3)	0.88	0.53	0.75	0.86	0.96	1.18	1.34	1.50	1.60	1.87	2.14

TABLE 5.9 Particle size distributions predicted for a range of blasting energy factors within the various ore types

E. Factor (kcal/st)		129	142	155	100			140			160			180			220		
	Material	Bum	SHG	SLG	Bum	SHG	SLG	Bum	SHG	SLG	Bum	SHG	SLG	Bum	SHG	SLG	Bum	SHG	SLG
Inches	cm																		
384.00	975.36	100.00%	100.00%	100.00%	100.00%	100.00%	100.00%	100.00%	100.00%	100.00%	100.00%	100.00%	100.00%	100.00%	100.00%	100.00%	100.00%	100.00%	100.00%
192.00	487.68	100.00%	100.00%	100.00%	99.99%	99.96%	99.83%	100.00%	100.00%	100.00%	100.00%	100.00%	100.00%	100.00%	100.00%	100.00%	100.00%	100.00%	100.00%
96.00	243.84	99.75%	99.72%	99.42%	98.64%	97.96%	95.19%	99.83%	99.69%	98.94%	99.94%	99.88%	99.53%	99.98%	99.96%	99.80%	100.00%	99.99%	99.97%
48.00	121.92	94.09%	93.82%	89.97%	87.67%	85.51%	76.32%	94.97%	93.56%	87.21%	96.85%	95.78%	90.77%	98.05%	97.26%	93.41%	99.27%	98.87%	96.73%
30.00	76.20	81.66%	81.37%	73.59%	72.33%	69.92%	58.07%	83.24%	80.93%	69.89%	87.08%	84.95%	74.73%	90.10%	88.18%	78.90%	94.26%	92.80%	85.49%
24.00	60.96	73.57%	73.35%	64.19%	63.91%	61.66%	49.53%	75.31%	72.87%	60.53%	79.72%	77.33%	65.35%	83.41%	81.12%	69.69%	89.01%	87.02%	77.04%
12.00	30.48	46.53%	46.64%	36.78%	39.13%	37.86%	27.71%	48.02%	46.24%	34.32%	52.12%	50.15%	37.59%	55.96%	53.83%	40.78%	62.87%	60.53%	46.88%
6.00	15.24	25.52%	25.80%	18.51%	21.47%	21.04%	14.28%	26.38%	25.57%	17.31%	28.82%	27.85%	18.91%	31.23%	30.11%	20.54%	35.89%	34.51%	23.81%
3.00	7.62	12.94%	13.22%	8.73%	11.11%	11.06%	7.05%	13.35%	13.11%	8.24%	14.52%	14.20%	8.90%	15.71%	15.30%	9.60%	18.09%	17.53%	11.04%
1.50	3.81	6.31%	6.51%	4.00%	5.57%	5.65%	3.41%	6.48%	6.47%	3.81%	6.99%	6.93%	4.06%	7.50%	7.41%	4.33%	8.56%	8.40%	4.90%
0.75	1.90	3.01%	3.14%	1.80%	2.75%	2.84%	1.63%	3.08%	3.12%	1.74%	3.28%	3.30%	1.82%	3.49%	3.50%	1.92%	3.93%	3.90%	2.13%
0.38	0.95	1.43%	1.50%	0.81%	1.35%	1.42%	0.78%	1.45%	1.50%	0.79%	1.53%	1.56%	0.81%	1.61%	1.64%	0.85%	1.78%	1.80%	0.92%
0.18	0.48	0.68%	0.73%	0.37%	0.67%	0.71%	0.37%	0.69%	0.72%	0.36%	0.72%	0.74%	0.37%	0.75%	0.77%	0.38%	0.81%	0.83%	0.40%
0.09	0.24	0.32%	0.35%	0.16%	0.32%	0.36%	0.18%	0.32%	0.34%	0.16%	0.33%	0.35%	0.16%	0.34%	0.36%	0.17%	0.37%	0.38%	0.17%

% O/S	18.34%	18.63%	26.41%	27.67%	30.08%	41.93%	16.76%	19.07%	30.11%	12.92%	15.05%	25.27%	9.90%	11.82%	21.10%	5.74%	7.20%	14.51%
O/S in Crusher feed	21.1%			33.2%			22.0%			17.7%			14.3%			9.1%		
U/S in Crusher Feed	78.9%			66.8%			78.0%			82.3%			85.7%			90.9%		

Note: SHG refers to Sembehun high-grade ore; SLG refers to Sembehun low-grade ore.

TABLE 5.9 (Continued)

E. Factor (kcal/st)		250			280			300			350			400		
	Material -	Bum	SHG	SLG	Bum	SHG	SLG	Bum	SHG	SLG	Bum	SHG	SLG	Bum	SHG	SLG
Inches	cm															
384	975.36	100.00%	100.00%	100.00%	100.00%	100.00%	100.00%	100.00%	100.00%	100.00%	100.00%	100.00%	100.00%	100.00%	100.00%	100.00%
192.00	487.68	100.00%	100.00%	100.00%	100.00%	100.00%	100.00%	100.00%	100.00%	100.00%	100.00%	100.00%	100.00%	100.00%	100.00%	100.00%
96.00	243.84	100.00%	100.00%	99.99%	100.00%	100.00%	100.00%	100.00%	100.00%	100.00%	100.00%	100.00%	100.00%	100.00%	100.00%	100.00%
48.00	121.92	99.66%	99.43%	98.11%	99.84%	99.72%	98.93%	99.91%	99.82%	99.27%	99.98%	99.95%	99.73%	99.99%	99.98%	99.90%
30.00	76.20	96.23%	95.08%	89.16%	97.54%	96.66%	91.97%	98.16%	97.43%	93.45%	99.12%	98.68%	96.12%	99.59%	99.33%	97.74%
24.00	60.96	91.99%	90.27%	81.49%	94.20%	92.74%	85.17%	95.33%	94.04%	87.24%	97.32%	96.40%	91.33%	98.48%	97.84%	94.18%
12.00	30.48	67.43%	65.00%	51.17%	71.49%	69.02%	55.20%	73.93%	71.46%	57.75%	79.23%	76.83%	63.62%	83.53%	81.25%	68.80%
6.00	15.24	39.25%	37.69%	26.25%	42.48%	40.75%	28.67%	44.55%	42.73%	30.26%	49.48%	47.44%	34.17%	54.03%	51.83%	37.95%
3.00	7.62	19.87%	19.19%	12.14%	21.63%	20.85%	13.25%	22.79%	21.94%	14.00%	25.66%	24.65%	15.88%	28.46%	27.29%	17.75%
1.50	3.81	9.37%	9.16%	5.35%	10.18%	9.92%	5.81%	10.73%	10.43%	6.12%	12.09%	11.71%	6.90%	13.44%	12.98%	7.69%
0.75	1.90	4.27%	4.22%	2.30%	4.61%	4.55%	2.48%	4.84%	4.76%	2.60%	5.42%	5.31%	2.90%	6.01%	5.87%	3.22%
0.38	0.95	1.92%	1.92%	0.98%	2.06%	2.06%	1.05%	2.15%	2.15%	1.09%	2.39%	2.37%	1.21%	2.64%	2.60%	1.33%
0.18	0.48	0.87%	0.88%	0.42%	0.92%	0.94%	0.45%	0.96%	0.97%	0.47%	1.06%	1.06%	0.51%	1.16%	1.16%	0.55%
0.09	0.24	0.39%	0.40%	0.18%	0.41%	0.42%	0.19%	0.42%	0.43%	0.20%	0.46%	0.47%	0.21%	0.50%	0.51%	0.23%

% O/S	3.77%	4.92%	10.84%	2.46%	3.34%	8.03%	1.84%	2.57%	6.55%	0.88%	1.32%	3.88%	0.41%	0.67%	2.26%
O/S in Crusher feed	6.5%			4.6%			3.7%			2.0%			1.1%		
U/S in Crusher Feed	93.5%			95.4%			96.3%			98.0%			98.9%		

Note: SHG refers to Sembehun high-grade ore; SLG refers to Sembehun low-grade ore.

TABLE 5.10 Particle size distributions predicted for a range of blasting energy factors within limestone (LS) and granodiorite (GD)

E. Factor (kcal/st)		162.5	164.7	100		140		160		180		220	
	Material ------	LS	GD	LS	GD	LS	GD	LS	GD	LS	GD	LS	GD
Inches	cm												
384	975.36	100.00%	100.00%	100.00%	100.00%	100.00%	100.00%	100.00%	100.00%	100.00%	100.00%	100.00%	100.00%
192.00	487.68	100.00%	100.00%	99.76%	99.90%	99.99%	100.00%	100.00%	100.00%	100.00%	100.00%	100.00%	100.00%
96.00	243.84	99.45%	99.83%	94.52%	97.40%	98.69%	99.51%	99.39%	99.80%	99.73%	99.92%	99.95%	99.99%
48.00	121.92	90.31%	95.89%	75.22%	85.55%	86.23%	93.29%	89.92%	95.48%	92.69%	96.98%	96.25%	98.66%
30.00	76.20	74.22%	86.33%	57.21%	71.57%	68.85%	81.83%	73.66%	85.56%	77.84%	88.56%	84.51%	92.88%
24.00	60.96	64.91%	79.61%	48.85%	64.13%	59.61%	74.61%	64.35%	78.74%	68.64%	82.23%	75.97%	87.67%
12.00	30.48	37.49%	54.73%	27.54%	41.92%	33.92%	50.11%	37.10%	53.88%	40.20%	57.41%	46.15%	63.75%
6.00	15.24	19.01%	32.63%	14.34%	25.02%	17.26%	29.73%	18.81%	32.08%	20.39%	34.40%	23.57%	38.86%
3.00	7.62	9.02%	17.87%	7.17%	14.15%	8.30%	16.39%	8.94%	17.58%	9.61%	18.80%	11.01%	21.23%
1.50	3.81	4.15%	9.34%	3.51%	7.77%	3.88%	8.68%	4.12%	9.21%	4.38%	9.77%	4.94%	10.92%
0.75	1.90	1.88%	4.76%	1.70%	4.19%	1.79%	4.49%	1.87%	4.71%	1.96%	4.94%	2.17%	5.44%
0.38	0.95	0.85%	2.40%	0.82%	2.24%	0.82%	2.30%	0.84%	2.38%	0.87%	2.47%	0.95%	2.68%
0.18	0.48	0.39%	1.22%	0.40%	1.21%	0.38%	1.19%	0.39%	1.21%	0.39%	1.24%	0.42%	1.32%
0.09	0.24	0.17%	0.61%	0.19%	0.64%	0.17%	0.60%	0.17%	0.61%	0.17%	0.62%	0.18%	0.64%

Determination of Oversise in waste blasts

% U/S		97.16%	98.85%	89.69%	94.44%	95.58%	97.96%	97.02%	98.72%	97.97%	99.18%	99.02%	99.66%
% O/S		2.84%	1.15%	10.31%	5.56%	4.42%	2.04%	2.98%	1.28%	2.03%	0.82%	0.98%	0.34%

TABLE 5.10 (Continued)

E. Factor (kcal/st)		250		280		300		350		400	
	Material -----	LS	GD	LS	GD	LS	GD	LS	GD	LS	GD
Inches	cm										
384	975.36	100.00%	100.00%	100.00%	100.00%	100.00%	100.00%	100.00%	100.00%	100.00%	100.00%
192.00	487.68	100.00%	100.00%	100.00%	100.00%	100.00%	100.00%	100.00%	100.00%	100.00%	100.00%
96.00	243.84	99.99%	100.00%	100.00%	100.00%	100.00%	100.00%	100.00%	100.00%	100.00%	100.00%
48.00	121.92	97.78%	99.29%	98.70%	99.62%	99.10%	99.75%	99.65%	99.92%	99.87%	99.97%
30.00	76.20	88.28%	95.03%	91.20%	96.55%	92.76%	97.30%	95.60%	98.55%	97.38%	99.22%
24.00	60.96	80.46%	90.66%	84.19%	92.94%	86.32%	94.15%	90.54%	96.37%	93.54%	97.75%
12.00	30.48	50.35%	67.93%	54.31%	71.66%	56.82%	73.91%	62.61%	78.82%	67.75%	82.84%
6.00	15.24	25.94%	42.05%	28.30%	45.10%	29.85%	47.05%	33.66%	51.65%	37.34%	55.89%
3.00	7.62	12.09%	23.03%	13.17%	24.81%	13.90%	25.98%	15.73%	28.84%	17.56%	31.61%
1.50	3.81	5.37%	11.80%	5.82%	12.68%	6.12%	13.27%	6.89%	14.73%	7.67%	16.18%
0.75	1.90	2.33%	5.83%	2.51%	6.23%	2.62%	6.50%	2.92%	7.17%	3.23%	7.84%
0.38	0.95	1.01%	2.84%	1.07%	3.01%	1.12%	3.13%	1.23%	3.42%	1.35%	3.72%
0.18	0.48	0.44%	1.39%	0.46%	1.46%	0.48%	1.51%	0.52%	1.64%	0.57%	1.77%
0.09	0.24	0.19%	0.67%	0.20%	0.70%	0.20%	0.72%	0.22%	0.77%	0.23%	0.82%

Determination of Oversise in waste blasts

%U/S		99.43%	99.82%	99.67%	99.90%	99.77%	99.94%	99.91%	99.98%	99.97%	99.99%
%O/S		0.57%	0.18%	0.33%	0.10%	0.23%	0.06%	0.09%	0.02%	0.03%	0.01%

CHAPTER 6

ESTIMATION OF CRUSHER SIMULATION PARAMETERS

6.1 Overview

In this chapter, the procedures that were used to generate the crushing simulation parameters are described. Due to the limitations discussed in Sections 4.4.3 and 4.4.4, no direct testing could have been done to generate those parameters. Therefore, indirect methods of estimation were used.

6.2 Estimation of crushing simulation parameters

The crusher parameters which required estimation for use in this simulation work are listed in Table 6.1, each parameter in relation to the crusher to which it is relevant.

The parameter that is common to all the crushers is the crusher work index. In addition, the cone crushers (Cones 1 and 2) require the classification and breakage functions to be estimated. As discussed in Section 4.3.2.1 (and in King 2012), previous work has provided viable ranges for these latter parameters, and these ranges were explored in this work.

In order to be considered valid, the estimated parameters had to meet the following criteria:

i. The use of the set of estimated parameters must lead to the prediction of a particle size distribution of simulated final product that is comparable to the particle size distribution actually measured at the crusher product stockpile.

ii. For baseline operating feed size distributions, the simulated energy consumption at the crusher must be roughly identical to that observed under baseline operating conditions.

Obtaining a fair representation of blast product size distribution on-site for validation purposes was a challenge. Kuz-Ram predictions are averages, and values estimated by photo-granulometry are often very localized and tend to depart significantly from shot averages. Consequently, a very rough approximation was made on the basis of degree of oversize produced by the blasts. The prediction of ore oversize in this work is a mean of about 21%, and a maximum of 26%. Observed oversize ranged from about 7% to about 20% in ore. The researcher's judgment is that, given the natural inhomogeneities in rocks, and the lack of resources to do detailed verification and validation of photo-granulometry with sieving of a whole muckpile, this is an acceptable difference. The simple and broad assumption is made, therefore, that the crusher feed particle size distribution produced by the contract blasting practice is roughly equivalent to that which is predicted by the revised Kuz-Ram model in this research.

6.2.1 Preliminaries for parameter estimation

The following preliminaries were carried out, leading to the parameter estimation process itself.

i. In MODSIM simulation package, the crushing circuit was built (see Figure 6.1), with features including a jaw crusher, two cone crushers, screens, and feed and product stockpiles.

ii. Characteristics of the circuit were specified, including crusher gap dimensions, open and closed side settings, screen perforation sizes, dimensions of all screen surface areas, screen inclinations, and circuit paths between crushers, screens, and crushers. Details of the circuit characteristics are provided in Appendix I (crushing circuit parameters).

iii. The feed characteristics were specified. These characteristics included the ore type (Bom ore, Sembehun low-grade ore, and Sembehun high-grade ore), density, and particle size distribution. The base case particle size distribution specified was a modified form of that predicted by the Kuz-Ram model for the blast pattern established by the contractor. The modification was done to account for the contribution of secondary breakage of all oversize (>30 inches) ore. The particle size distribution of the secondary-broken ore was assumed to be identical to the size distribution of the blast-generate sub-30-in material. This method of size reconstitution was used for all the crusher feeds produced by the various energy factor blasts (Tables 6.2a, b, c).

iv. Key process features were specified. These features included the head feed rates and the feed blending proportions. Blending was in the ratio:

Bom/Sembehun high-grade/Sembehun low-grade (1:1:1)

v. A preliminary and arbitrary crusher work index value of 30 kWh/t was assumed.

6.2.2 Crusher and screen settings and characteristics

An important aspect of the specifications that were made in the simulation of the crushing system was the set of physical characteristics and settings of the crushers and screens in the system. To be representative of the operating situation at the mine, the data (dimensions and settings) of the equipment at the mine were obtained and used as input, as required, at the model parameter specification stage of the simulation.

The data specified in this research have been presented in Tables 6.3a (settings and features of the jaw crusher), 6.3b (settings and features of the cone crushers), 6.3c (settings and features for Screen 1), and 6.3d (settings and features for Screen 2).

6.2.3 The crusher breakage and classification functions

i. These two functions were estimated for only the cone crushers.

ii. Initially, the crusher breakage and classification functions were specified in MODSIM to match average values of the recommended ranges of setting for both the breakage and classification functions. These ranges are mentioned in Section 4.4.2.1.

iii. A simulation was then run, and the simulated product particle size distributions overlain on a plot of the actual mill feed (or crusher run) particle size distribution. Details of the sampling and size analysis procedure for mill feed are given in Appendix A. After each run, the departure from the reference plot formed the basis of adjustment of parameters. All the parameters were gradually adjusted in suitable directions, until an approximate overlap was achieved (see Figure 6.2). The settings at which this approximate overlap occurred were chosen as the

circuit's parameter settings for the rest of the simulation. These settings are presented in Table 6.4.

6.2.4 The crusher work index

i. The crusher work index was estimated using the operating work index method described in Section 4.4.4, using the equation:

$$\overline{E} = \frac{P_c}{F_f} = 10W_B\left(\frac{1}{\sqrt{P_{80}}} - \frac{1}{\sqrt{F_{80}}}\right)$$

All terms are as described in Equation 4.11.

ii. For the reconstituted base case feed (simulated) and crushing product (also simulated), the 80% passing sizes F_{80} and P_{80} were determined. The 80% passing feed and product sizes for each of the three crushers were determined.

iii. Values of crusher power draw at the time of the crusher product sampling were obtained from the mine power team.

iv. Setting $\left(\frac{1}{\sqrt{P_{80}}} - \frac{1}{\sqrt{F_{80}}}\right) = k$, and using average crusher power draw (P_c) and feed tonnes of fresh feed rate (F_f), the operating work index $W_{i(o)}$ was computed as shown in the table.

v. Assuming motor efficiencies of 80% at each crusher motor, an estimate of true work index, W_i, was made by de-rating the operating work index ($W_{i(o)}$). However, the operating work index was the value eventually used in all subsequent simulations, as no provision lies within MODSIM to account for

motor efficiency in the estimation of power draw. A weighted average operating work index of 20.86 kWh/t is calculated (prorated by mass flow through the plant), and a "true" work index estimate of 16.69 kwh/t is made. This value is consistent with various published values of typical copper ores or in related rocks such as dolomite in skarn deposits (from 1.8 to 40 kWh/t – and averaging 12 to 20 kWh/t) (Bergstrom 1985; Nematollahi 1994; Tavares and Carvalho 2007). All values of input parameters leading to this estimate, as well as the estimate of the crusher work index, are shown in Table 6.5.

vi. The variation of crusher work index in the different crushers for the blended ore is in line with Magdalinovic's observation (Section 4.4.4) which indicates that the work index is material and crusher specific.

6.2.5 Verification of crushing simulation parameters

In Table 6.5, note that the power draw for each crusher is the same as that provided by the power supply staff at W.U.S. Copper. This equality of predicted and actual values of power draw meets one of the criteria for parameter verification, as specified in i and ii of Section 6.2. The other validation is provided by the approximate overlap of actual and simulated product particle size distributions, as shown in Figure 6.2

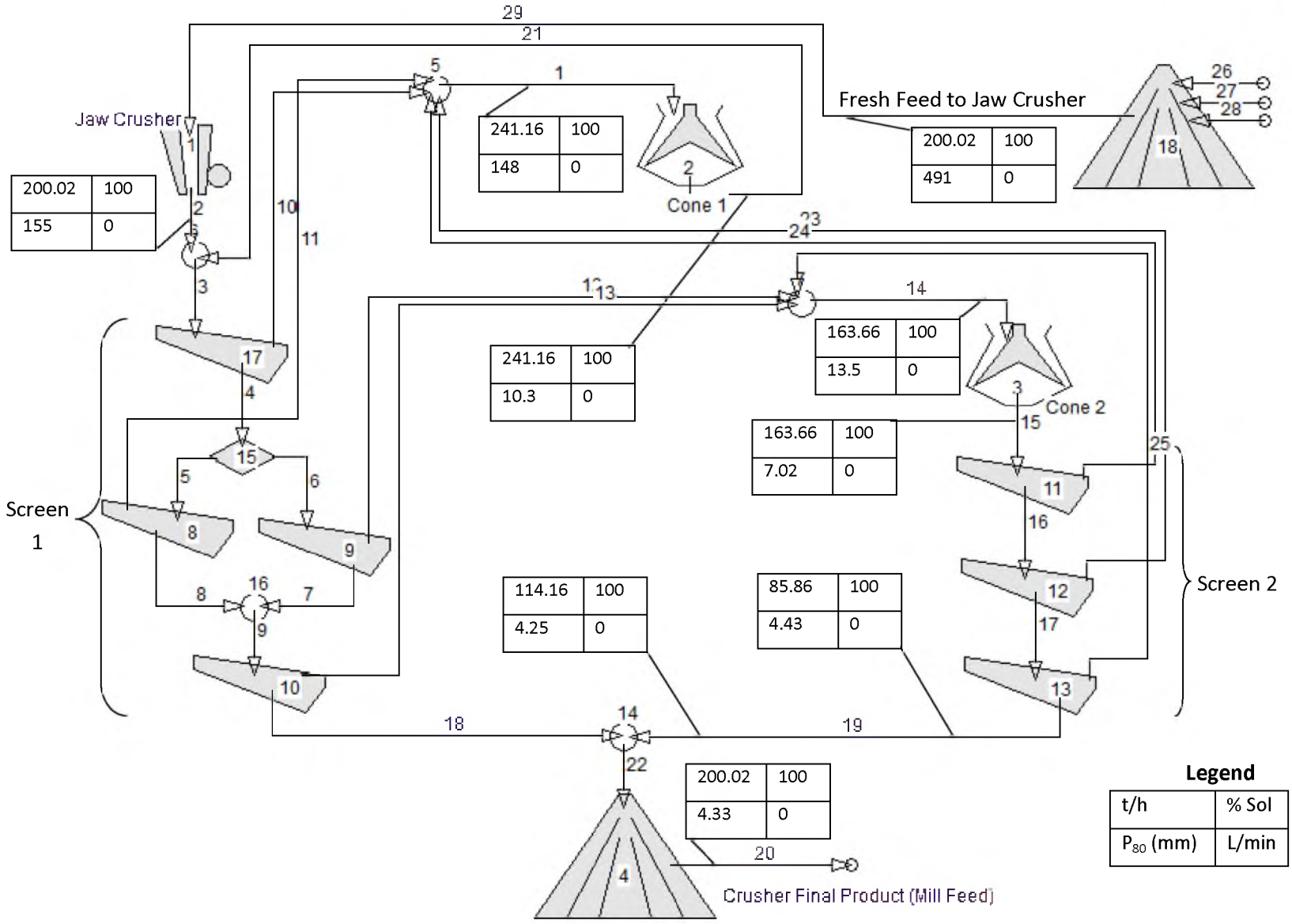

FIGURE. 6.1 Flowsheet of the crushing circuit, showing mass flow. This mass flow is based on jaw crusher feed size estimates from the blend of fragmentation profiles from contract blasts

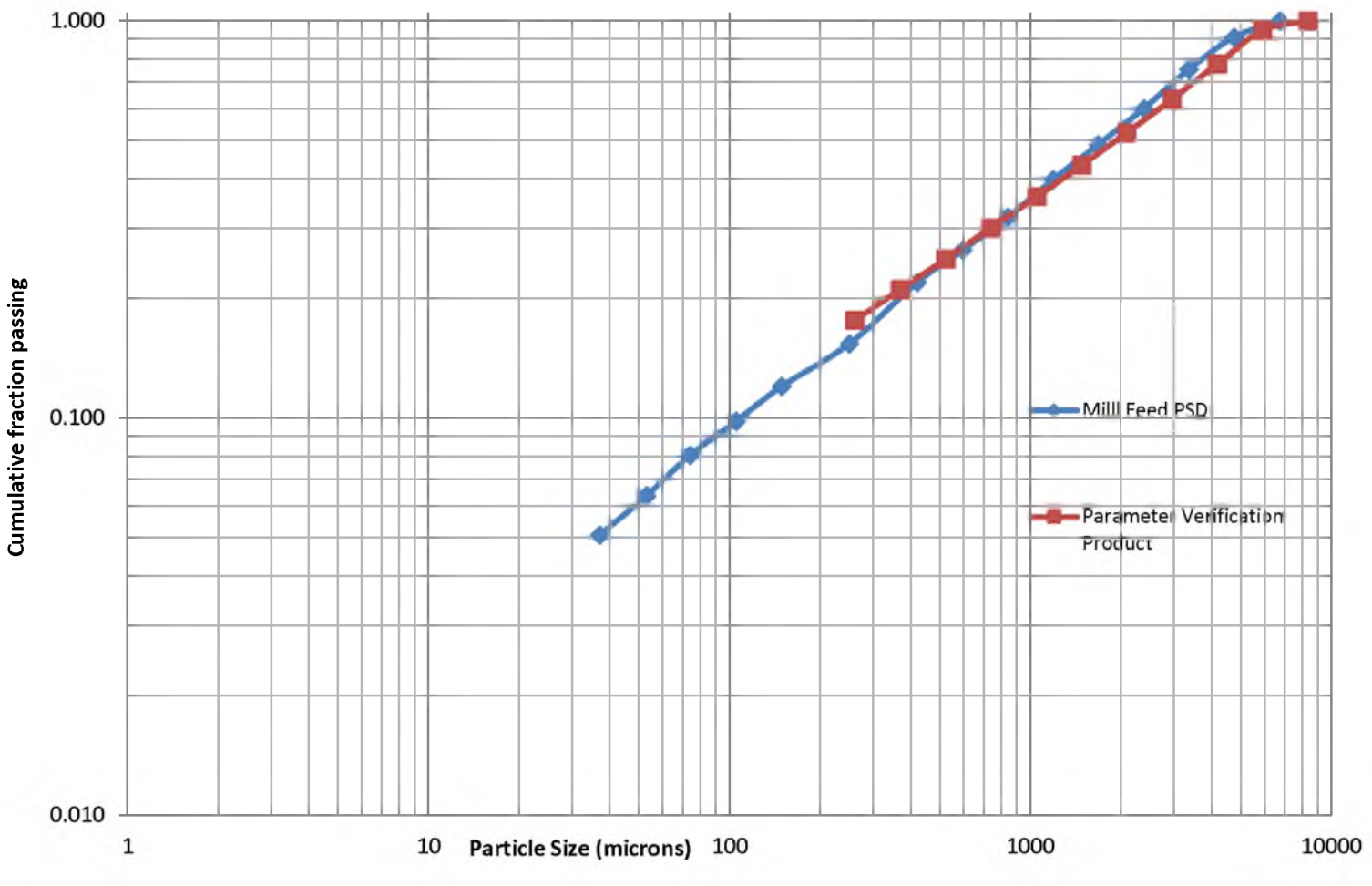

FIGURE. 6.2 Parameter verification plot of simulated and actual product particle size distributions. The test crush simulation product is overlaid on the measured crusher product (mill feed) particle size profile.

TABLE 6.1 The set of parameters whose estimation was required for the simulations

Crusher	Model	Parameter to estimate
Jaw	The Empirical Model for Jaw and Gyratory Crushers (EJMC)	The crusher work index (kWh/t)
Cone 1	The Standard Cone Crusher Model (CRSH)	Classification proportionality constants, α_1 and α_2
		The cumulative breakage function, B_{ij}
		The crusher work index
Cone 2	The Short-Head Cone Crusher Model (SHHD)	Classification proportionality constants, α_1 and α_2
		The cumulative breakage function, B_{ij}
		The crusher work index (kWh/t)

TABLE 6.2a Crusher feed, reconstituted for oversize (100 to 160 kcal/st)

			129	142	155	100			140			160		
mm	Inches	cm	Bum	SHG	SLG	Bum	SHG	SLG	Bum	SHG	SLG	Bum	SHG	SLG
762	30 00	76 20	100 00%	100 00%	100 00%	100 00%	100 00%	100 00%	100 00%	100 00%	100 00%	100 00%	100 00%	100 00%
610	24 00	60 96	90 09%	90 14%	87 23%	88 36%	88 19%	85 29%	90 47%	90 04%	86 61%	91 55%	91 03%	87 44%
305	12 00	30 48	56 98%	57 32%	49 98%	54 09%	54 15%	47 73%	57 70%	57 14%	49 10%	59 85%	59 03%	50 30%
152	6 00	15 24	31 25%	31 71%	25 16%	29 69%	30 09%	24 59%	31 69%	31 60%	24 77%	33 09%	32 79%	25 31%
76	3 00	7 62	15 85%	16 24%	11 87%	15 35%	15 82%	12 14%	16 04%	16 20%	11 78%	16 68%	16 71%	11 92%
38	1 50	3 81	7 73%	8 00%	5 43%	7 70%	8 08%	5 87%	7 79%	7 99%	5 45%	8 02%	8 16%	5 44%
19	0 75	1 90	3 69%	3 86%	2 45%	3 80%	4 06%	2 81%	3 70%	3 86%	2 48%	3 76%	3 89%	2 44%
10	0 38	0 95	1 75%	1 85%	1 10%	1 86%	2 03%	1 34%	1 75%	1 85%	1 13%	1 75%	1 84%	1 09%
5	0 18	0 48	0 84%	0 89%	0 50%	0 92%	1 02%	0 64%	0 83%	0 89%	0 52%	0 82%	0 88%	0 49%
2	0 09	0 24	0 39%	0 42%	0 22%	0 45%	0 51%	0 31%	0 39%	0 43%	0 23%	0 38%	0 41%	0 22%

Note: SHG refers to Sembehun high-grade ore; SLG refers to Sembehun low-grade ore

TABLE 6.2b Crusher feed, reconstituted for oversize (180 to 280 kcal/st)

		180			220			250			280		
Inches	cm	Bum	SHG	SLG	Bum	SHG	SLG	Bum	SHG	SLG	Bum	SHG	SLG
30.00	76.20	100.00%	100.00%	100.00%	100.00%	100.00%	100.00%	100.00%	100.00%	100.00%	100.00%	100.00%	100.00%
24.00	60.96	92.58%	92.00%	88.32%	94.43%	93.78%	90.11%	95.60%	94.94%	91.40%	96.57%	95.94%	92.61%
12.00	30.48	62.11%	61.04%	51.68%	66.70%	65.23%	54.83%	70.07%	68.36%	57.39%	73.29%	71.40%	60.02%
6.00	15.24	34.66%	34.15%	26.03%	38.08%	37.19%	27.85%	40.79%	39.64%	29.45%	43.55%	42.16%	31.18%
3.00	7.62	17.43%	17.35%	12.17%	19.19%	18.89%	12.91%	20.64%	20.19%	13.61%	22.17%	21.57%	14.41%
1.50	3.81	8.33%	8.40%	5.49%	9.09%	9.05%	5.74%	9.74%	9.63%	6.00%	10.44%	10.26%	6.31%
0.75	1.90	3.87%	3.96%	2.43%	4.17%	4.21%	2.49%	4.43%	4.44%	2.58%	4.73%	4.70%	2.69%
0.38	0.95	1.78%	1.85%	1.07%	1.89%	1.94%	1.08%	1.99%	2.02%	1.10%	2.11%	2.13%	1.14%
0.18	0.48	0.83%	0.87%	0.48%	0.86%	0.90%	0.47%	0.90%	0.93%	0.48%	0.95%	0.97%	0.49%
0.09	0.24	0.38%	0.41%	0.21%	0.39%	0.41%	0.20%	0.40%	0.42%	0.20%	0.42%	0.43%	0.21%

Note: SHG refers to Sembehun high-grade ore; SLG refers to Sembehun low-grade ore

TABLE 6.2c Crusher feed, reconstituted for oversize (300 to 400 kcal/st)

		300			350			400		
Inches	cm	Bum	SHG	SLG	Bum	SHG	SLG	Bum	SHG	SLG
30.00	76.20	100.00%	100.00%	100.00%	100.00%	100.00%	100.00%	100.00%	100.00%	100.00%
24.00	60.96	97.12%	96.52%	93.36%	98.18%	97.68%	95.02%	98.89%	98.50%	96.36%
12.00	30.48	75.32%	73.34%	61.80%	79.94%	77.85%	66.19%	83.87%	81.80%	70.39%
6.00	15.24	45.39%	43.85%	32.39%	49.92%	48.08%	35.55%	54.26%	52.18%	38.82%
3.00	7.62	23.22%	22.52%	14.98%	25.89%	24.98%	16.52%	28.58%	27.47%	18.17%
1.50	3.81	10.93%	10.70%	6.54%	12.19%	11.86%	7.18%	13.50%	13.07%	7.87%
0.75	1.90	4.93%	4.89%	2.78%	5.47%	5.38%	3.02%	6.04%	5.91%	3.29%
0.38	0.95	2.19%	2.20%	1.17%	2.41%	2.41%	1.26%	2.65%	2.62%	1.36%
0.18	0.48	0.98%	1.00%	0.50%	1.07%	1.08%	0.53%	1.16%	1.17%	0.57%
0.09	0.24	0.43%	0.44%	0.21%	0.47%	0.48%	0.22%	0.50%	0.51%	0.23%

Note: SHG refers to Sembehun high-grade ore; SLG refers to Sembehun low-grade ore

TABLE 6.3a Jaw Crusher Settings and features

Parameter	Value
Gap (m)	0.1778
r_{max}	1.251
Exponent, *m*	0.843
Gape (mm)	1117.6 mm x 787.4 mm (44 in. x 31 in.)
Installed power (kW)	112

Source: Processing staff at W.U.S. Copper

TABLE 6.3b Settings and features of cone crushers

Setting	Cone 1	Cone 2
Open-Side Set (OSS) (meters)	127 mm (5 in.)	44.45 mm (1.75 in.)
Closed-Side Set (CSS) (meters)	12.7 mm (0.5 in.)	6.35 mm (0.25 in.)
Installed power (kW)	298	298

Source: Processing staff at W.U.S. Copper

TABLE 6.3c Settings and features for Screen 1

Feature/Setting	Value
Number of decks of screen	3
Deck 1	
No. of screen panels in parallel	5
Size of screen panels in parallel	31.75 mm
Modsim screen model used	SCRN
Crusher receiving screen oversize	Cone 1
Deck 2	
No. of screen panels in parallel	5
Mesh size of screen panels in parallel	4 screens: 9.525 mm; 1 screen: 28.575 mm
Modsim screen model used	SCRN
Crusher receiving screen oversize	Cone 1 (from 4 screens); Cone 2 (from one screen)
Deck 3	
No. of screen panels in parallel	5
Size of screen panels in parallel	6.35 mm
Modsim Screen model used	SCRN
Crusher receiving screen oversize	Cone 2

Source: Processing staff at W.U.S. Copper

TABLE 6.3d Settings and features for Screen 2

Feature/Setting	Value
Number of decks of screen	3
Deck 1	
No. of screen panels in parallel	5
Size of screen panels in parallel	15.88 mm
Modsim screen model used	SCRN
Crusher receiving screen oversize	Cone 1
Deck 2	
No. of screen panels in parallel	5
Mesh size of screen panels in parallel	12.70 mm
Modsim screen model used	SCRN
Crusher receiving screen oversize	Cone 1
Deck 3	
No. of screen panels in parallel	5
Size of screen panels in parallel	6.35 mm
Modsim Screen model used	SCRN
Crusher receiving screen oversize	Cone 2

Source: Processing staff at W.U.S. Copper

TABLE 6.4 The values inferred for the crushing simulation parameters

Crusher	Parameter(s)	Value
Cone 1	Classification proportionality constants, α_1 and α_2	0.5; 1.85
	The cumulative breakage function, B_{ij}	0.6
Cone 2	Classification proportionality constants, α_1 and α_2	0.5; 1.85
	The cumulative breakage function, B_{ij}	0.6

TABLE 6.5 The values of work index inferred for the crushing circuit

Crusher	F_{80} (µm)	P_{80} (µm)	k	10k	Feed, tph	Op Kilowatts	kWh/t	Op. Work Index ($W_{i(o)}$)	W_i
Jaw	490,640	155,130	0.00111	0.01111	200.02	81	0.4050	36.44	29.15
Cone 1	148,090	10,300	0.00725	0.07255	241.2	101	0.4187	5.77	4.62
Cone 2	13,500	7,020	0.00333	0.03329	163.7	131	0.8002	24.04	19.23
							Weighted average W_i =	**20.86**	**16.69**

CHAPTER 7

SIMULATION OF THE CRUSHING OPERATION

7.1 Overview

Simulations were carried out to assess the influence of the blast-generated feed particle size distributions on crushing outcomes. This simulation was done using MODSIM. All simulations were performed on streams of material hypothetically mined from three sources: Bom, Sembehun high-grade and Sembehun low-grade ore domains. These ores were blended in the ratio 1:1:1. All materials in each blend were hypothetically shot with the same specific energy. Each processed stream in this work was uniquely identified by the energy factor with which that material was shot. Hence, Bom ore that was shot with 100 kcal/st was blended with Sembehun high-grade ore and Sembehun low-grade ore, each of which was shot with 100 kcal/st. This blend produced Stream 100 kcal/st.

7.2 Simulation setup

The modeled/simulated crushing circuit configuration was the same as that used for the parameter estimation exercise described in all of Section 6.2. The circuit included one jaw crusher, two cone crushers (Cones 1 and 2), and 2 banks of screens, as shown in Figures 1.1 and 6.1. The settings within the crusher circuit (including screens) are

outlined in Tables 6.3a 6.3b, 6.3c, and 6.3d, with further details provided in Appendix I. The model parameters are outlined in Tables 6.4 and 6.5.

The main variable in each cycle of simulation was the particle size distribution of the feed, dictated and identified by the blasting energy used to generate the particle size distributions.

An important aspect of the crushing circuit is the feed particle size limit imposed by the dimensions of the jaw crusher's throat. The maximum crushable particle size is 0.76 meters (30 inches). Any size larger than this must be set aside and secondary-broken, using a rock breaker. Usually, this re-break is done either at the crusher or at the mining pit, and at an extra cost beyond the basic rates for blast fragmentation. The extra cost is borne by the contractor, after an allowed maximum of 5% oversize.

This limitation to the features of the crushing circuit were taken into account in the evaluation. To do this, the following assumptions were made:

i. The recovery of blasted ore to the crusher stockpile is 100%
ii. All oversize must be crushed to ensure all materials are fed into the crusher
iii. The distribution of particle sizes of daughter fragments produced from the broken oversize is unknown, but may be assumed to follow the distribution of the original on-spec feed size distribution (of size less than 30 inches). Thus, the mass fractions of the feed in the sub-30 inch discrete size brackets were determined, and used as the basis to prorate the feed oversize daughter fragment redistribution. Accordingly, a new cumulative particle size distribution was inferred, accounting for all initial undersize and all redistributed oversize.

iv. The percentage oversize in the original feed distribution is shown at the bottom of Table 5.9a and 5.9b, and the new adjusted "true" feed particle size distribution to the crusher is shown in Table 6.2a and 6.2b.

v. The cost of secondary breakage was reckoned, not against crushing costs, but against blasting costs.

7.2.1 Results

Crushing simulation was carried out for all 11 oversize-reconstituted feed streams, produced after "blasting" at the various energy factors and doing secondary breakage of the oversize. Figure 7.1 is a plot of the size distributions of a number of the simulated products from the range of feed distribution crushes. Importantly, it shows that there is no difference in the particle size distribution produced, irrespective of the head feed particle size distribution.

At a first glance, this result appears to be counter-intuitive. However, it does make sense considering that each of the products only emerges if their particle sizes are finer than the perforations of the same set of screens. Any larger size is recycled until it is broken into a size smaller than the screen size.

7.2.2 Performance evaluation criteria

Beyond the particle size distribution, which has been shown above to be invariant with the feed, the following criteria were used to evaluate the impact of blast energy factor on crushing performance:

i. By-pass (fall-through) material and its potential impact on crusher throughput.

ii. The effect on crushing specific energy and crushing energy costs

It was not possible by the methods used in this work to assess the relative wear rates of crusher linings, based on feed particle size distribution.

Tables 7.1a to 7.1h provide a summary of various results, including: crusher throughput, percentage of fall-through material, power draw, specific energy, and costs.

7.2.2.1 By-pass (fall-through) material and throughput potential

As blasting energy intensity increases, the amount of fall-through material also increases. Fall-through material is material which passes through the crusher without being broken. The percentage of this kind of material in feed rises up to 55% at 400 kcal/st. Figure 7.2 is a plot of the percentage of fall-through material in blended crusher feed. Theoretically, the benefit of this scale of fall-through is to aid potential throughput capacity by allowing for scalping of the original feed and letting only larger sizes reach the primary crusher. The scalped undersize should then bypass the primary crusher and proceed to the secondary or tertiary crusher. Such an arrangement is particularly important in situations where maximum throughput capacity is desired.

However, throughput capacity is not a challenge at W.U.S. Copper, as the crusher generally operates up to a maximum of 12 hours a day and there is enough time slack to crush further if such additional crushing is required. Adding a scalping facility to the circuit would be making an unnecessary investment.

The other potential implication is for energy savings, as the amount of potential bypass material should ideally not use up energy at the primary crusher.

This potential, too, does not seem to serve W.U.S. Copper well. The theory of the crusher model is that material draws power only when the material is actually crushed. No power is drawn from the passage of fall-through material. Thus, power saving appears to have already been accounted for in the differences in energy draw at the crusher. These differences are discussed further, in Section 7.2.2.2.

7.2.2.2 The effect on specific energy and energy unit costs

Figure 7.3 is a graph of specific energy values at the various stages of crushing. The graph is based on the specific energy consumption data in Table 7.1d.

Specific energy at the crushing circuit appears to be affected only at the primary crusher. The secondary and tertiary crushers show no significant differences in the specific energies for the range of blast feed streams.

Even though there is some relative variation in specific energy at the primary crusher, these variations do not bear significant economic advantage. The insignificance of the economic advantage is owed to the fact that the differences in unit costs of crushing energy ($/st) are negligible (see Table 7.1g). Between 100 kcal/st and 400 kcal/st, the difference in unit cost of crushing energy is 1 cent. The monthly value of this difference is approximately $510 (Table 7.1.h)

7.2.3 Conclusions about the impact on crushing

The economic or cost impact of blast intensity changes on this crushing circuit is not significant. Expressed in terms of unit costs (of crushing specific energy), the cost advantage for increasing blast energy factor is minimal. This situation is demonstrated in

Figure 7.4. However, the true importance of this marginal difference needs to be explored further in terms of other costs that flow from the blast energy variations. These impacts are evaluated collectively in Chapter 9.

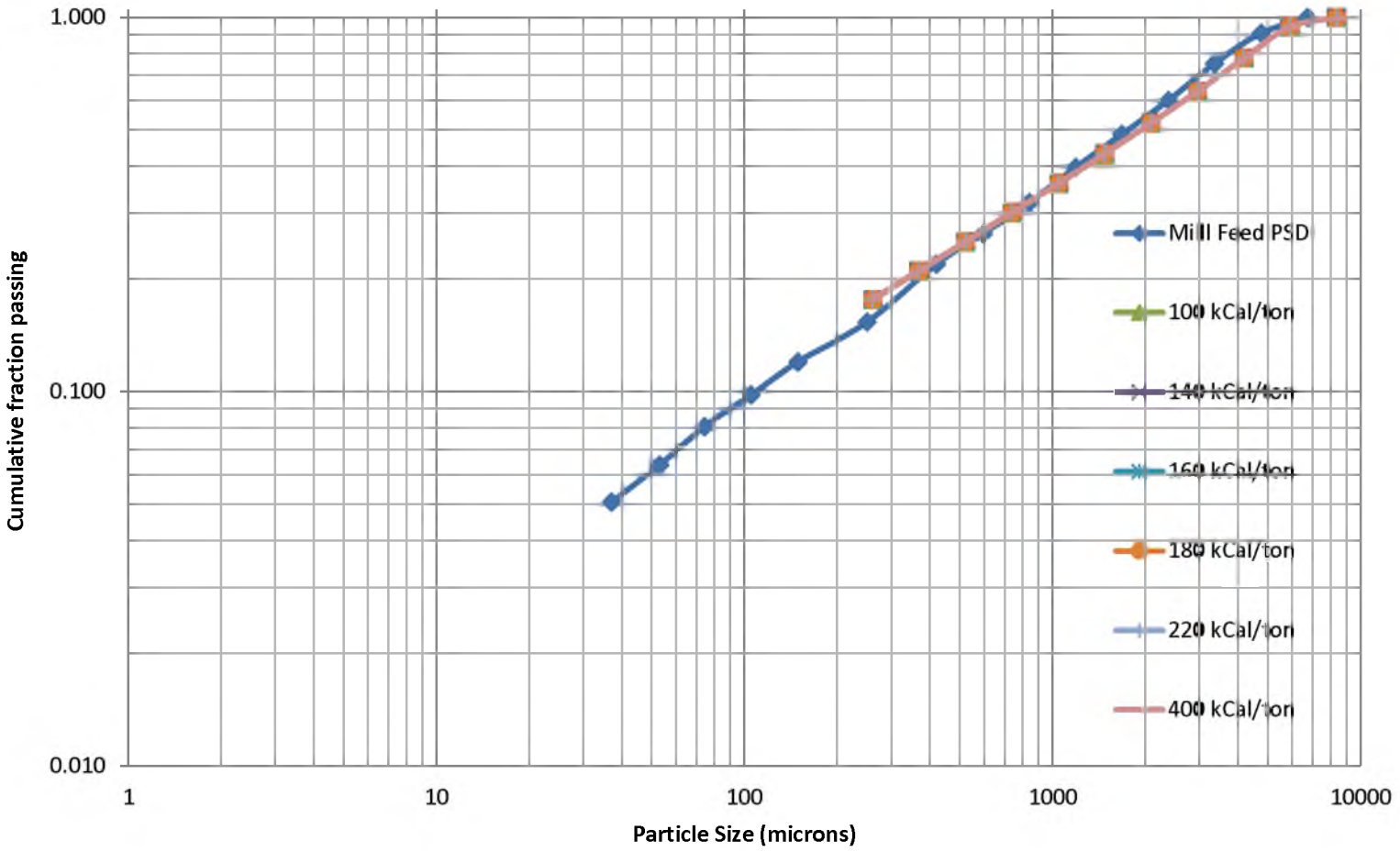

FIGURE 7.1 A plot of crushing product particle size distributions from ores blasted at 100, 140, 160, 180, 220, and 400 kcal/st. These results are superimposed on a plot of the actual mill feed (crusher product) particle size distribution.

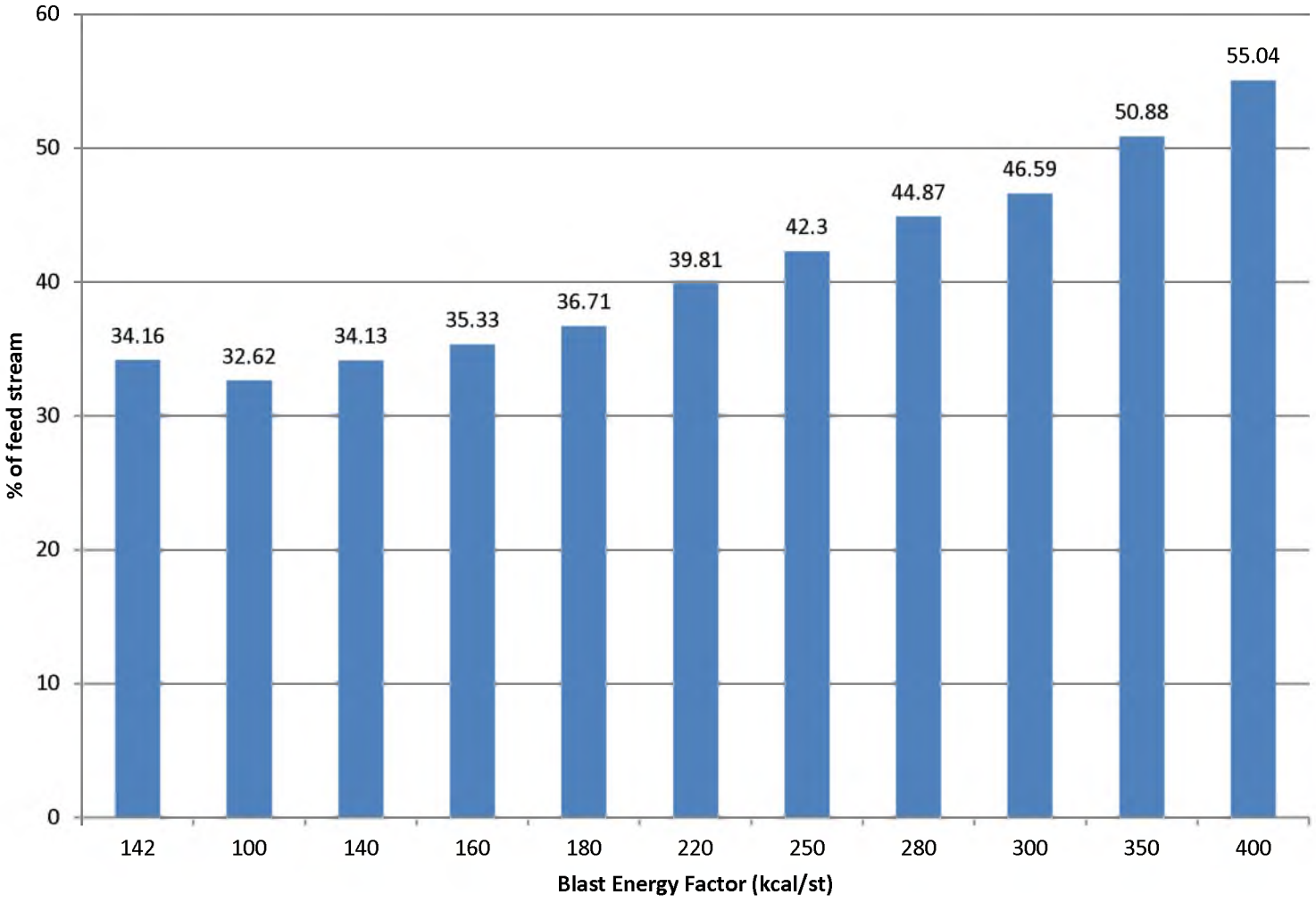

FIGURE 7.2 Percentage of fall-through material in feed vs. blast energy factors

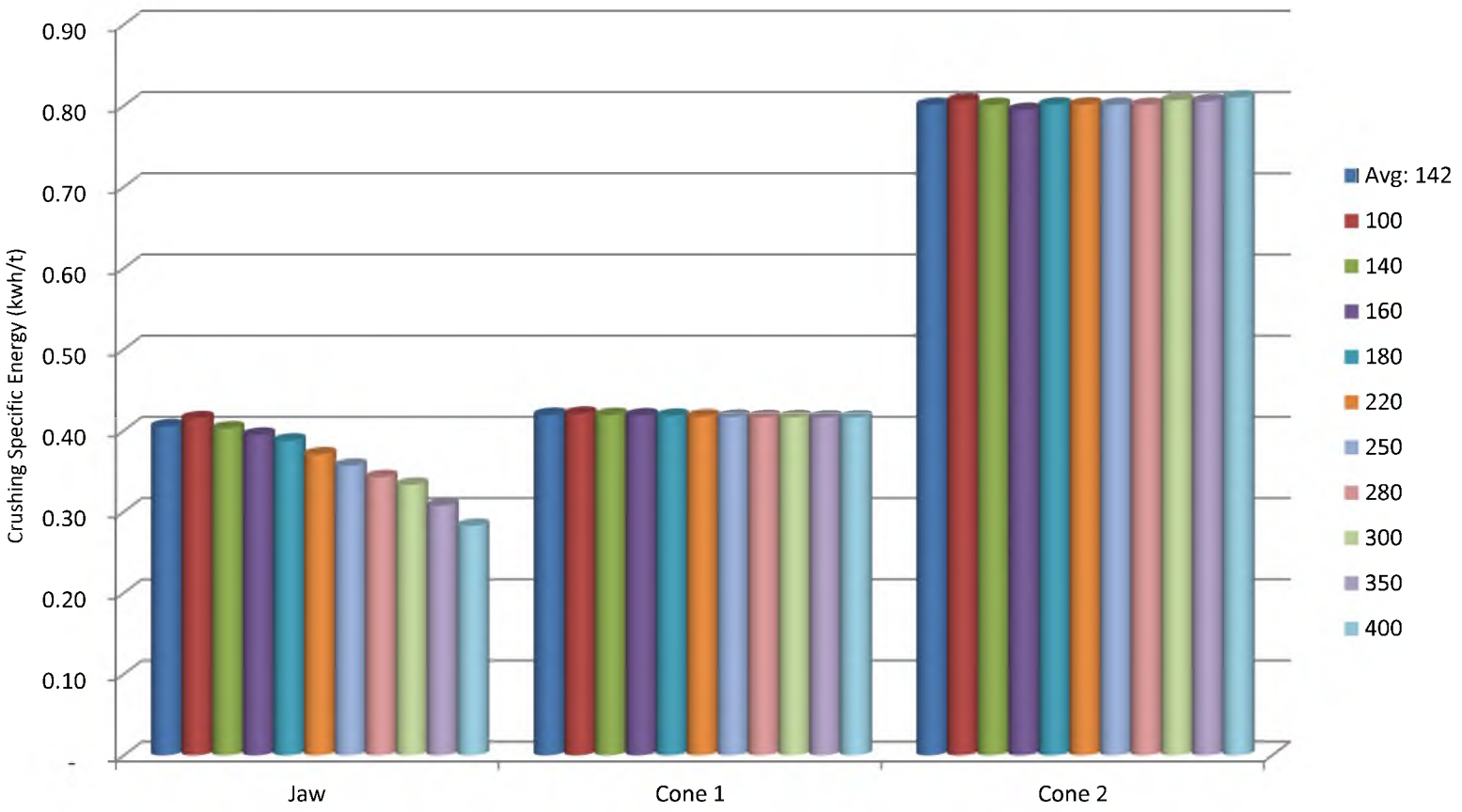

FIGURE 7.3 Variation of crushing specific energy with blasting energy factor

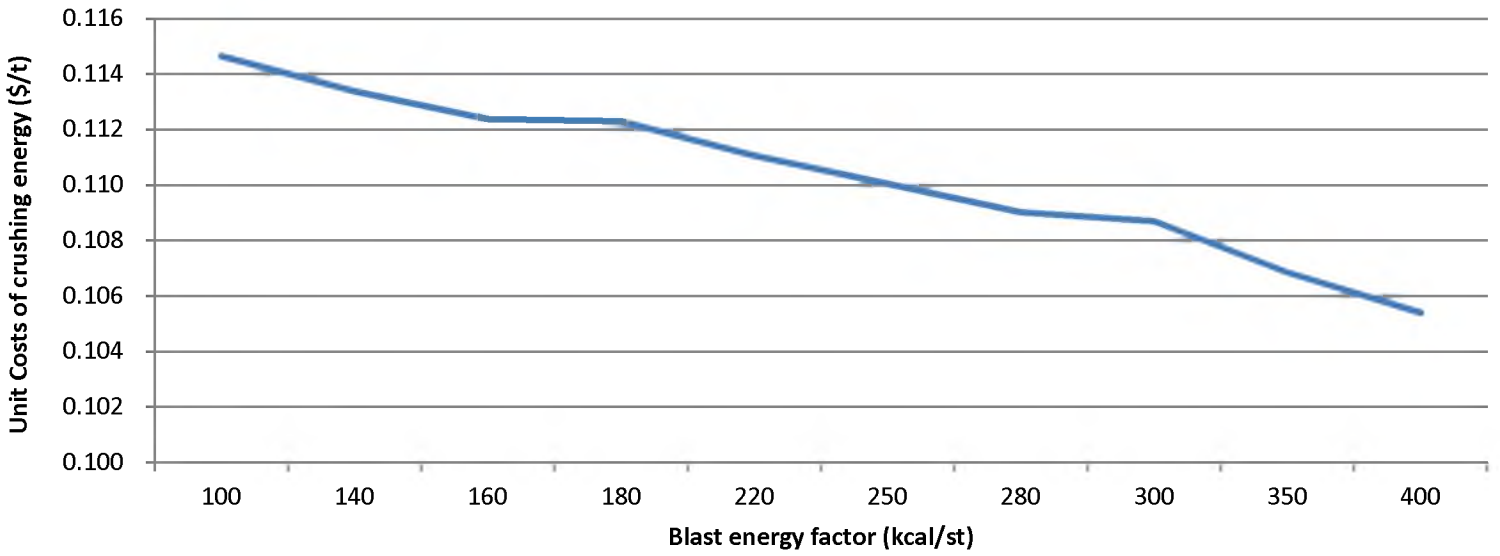

FIGURE 7.4 The variation of unit costs of crushing specific energy with blast energy factor

TABLES 7 (7.1a to 7.1h) Crushing rates, power draw, specific energy, and energy costs.

TABLE 7.1a: Feed rates through the crusher

Crusher throughput (t/h)

EF (kcal/st)	Avg: 142	100	140	160	180	220	250	280	300	350	400
Jaw	200.02	200.02	200.02	200.02	200.02	200.02	200.02	200.02	200.02	200.02	200.02
Cone 1	241.00	240.20	241.10	241.40	241.70	242.10	242.30	242.50	242.60	242.80	242.80
Cone 2	163.60	163.80	163.60	163.60	163.50	163.50	163.60	163.60	163.70	163.90	164.20

TABLE 7.1b: Percentage of fall-through material at the primary crusher

% Fall-through (bypass) Material

EF (kcal/st)	142	100	140	160	180	220	250	280	300	350	400
	34.16	32.62	34.13	35.33	36.71	39.81	42.3	44.87	46.59	50.88	55.04

TABLE 7.1c: Crusher power draw

Crusher Power Draw (kW)

EF (kcal/st)	Avg: 142	100	140	160	180	220	250	280	300	350	400
Jaw	81.0	83.7	81.2	79.7	78.1	74.6	71.9	69.1	67.1	62.0	56.9
Cone 1	101.0	101.0	101.0	101.0	101.0	101.0	101.0	101.0	101.0	101.0	101.0
Cone 2	131.0	132.0	131.0	130.0	131.0	131.0	131.0	131.0	132.0	132.0	133.0

TABLE 7.1d: Crushing specific energy

Specific Energy (kWh/t)

EF (kcal/st)	Avg:142	100	140	160	180	220	250	280	300	350	400
Jaw	0.40	0.42	0.41	0.40	0.39	0.37	0.36	0.35	0.34	0.31	0.28
Cone 1	0.42	0.42	0.42	0.42	0.42	0.42	0.42	0.42	0.42	0.42	0.42
Cone 2	0.80	0.81	0.80	0.79	0.80	0.80	0.80	0.80	0.81	0.81	0.81

TABLE 7.1e: Crushing energy unit costs

Unit Costs of Crushing Energy ($/t)

EF (kcal/st)	Avg: 142	100	140	160	180	220	250	280	300	350	400
Jaw	0.03	0.03	0.03	0.03	0.03	0.03	0.03	0.03	0.03	0.02	0.02
Cone 1	0.03	0.03	0.03	0.03	0.03	0.03	0.03	0.03	0.03	0.03	0.03
Cone 2	0.06	0.06	0.06	0.06	0.06	0.06	0.06	0.06	0.06	0.06	0.06

TABLE 7.1 (continued)

TABLE 7.1f: Crushing energy costs per hour

EF (kcal.st)	Avg: 142	100	140	160	180	220	250	280	300	350	400
Jaw	4.45	4.59	4.46	4.37	4.29	4.09	3.95	3.79	3.68	3.40	3.12
Cone 1	5.54	5.54	5.54	5.54	5.54	5.54	5.54	5.54	5.54	5.54	5.54
Cone 2	7.19	7.24	7.19	7.13	7.19	7.19	7.19	7.19	7.24	7.24	7.30
Total	17.18	17.38	17.19	17.05	17.02	16.83	16.68	16.53	16.47	16.19	15.97

TABLE 7.1g: Net crushing energy unit costs

EF (kcal.st)	142	100	140	160	180	220	250	280	300	350	400
Average $/st	0.078	0.079	0.078	0.077	0.077	0.076	0.076	0.075	0.075	0.073	0.072
Average $/t	0.086	0.087	0.086	0.085	0.085	0.084	0.083	0.083	0.082	0.081	0.080

TABLE 7.1h: Crushing monthly energy costs (12-hr day operation)

EF (kcal.st)	142	100	140	160	180	220	250	280	300	350	400
Costs ($)	6,183.71	6,256.81	6,187.66	6,132.75	6,126.42	6,057.27	6,003.93	5,948.61	5,928.85	5,828.10	5,747.10

CHAPTER 8

THE INFLUENCE OF FRAGMENTATION ON DRILLING AND BLASTING COSTS AND LOADING AND HAULING PRODUCTIVITY

8.1 Overview

In this chapter, an account is given of the investigations carried out to assess the effect of the degree of fragmentation on upstream stages of the mine-to-mill value chain. These stages are drilling, blasting, loading, and hauling. For the mining operation under review, it was found that fragmentation-induced variations in cost occur principally at the drilling and blasting end, with adverse influences reaching the crusher in the form of the oversize fragments. All costs arising from the various levels of oversize reaching the crusher are reckoned to be extra costs of blasting.

The average stripping ratio at the mine is 5:1. For this reason, it is crucial to evaluate the influences of blasting in waste as well as in ore. Blasting both materials could have a significant effect on the overall economics.

8.2 Oversize rock and its implications for secondary breakage and overall costs

Secondary breakage of both ore and waste are key considerations. Ore oversize diameter threshold is at 76.2 cm (30 inches). Above this, blockage of the crusher throat

could occur. Waste oversize threshold is at 213.36 cm (84 inches). The limit is imposed by the dimensions of the front end loader bucket.

From the Kuz-Ram predictions (see Section 5.4, and Table 5.9), there is a vast range of oversize ore quantities (of between 41.9% and 0.4%), corresponding to the full range of blast energy factors involved. Maximum waste oversize is at about 10% (Table 5.10).

All oversize must be reduced by secondary breakage methods, so that the downstream process can be carried out (crushing, in the case of ore, and dispatch to the waste dump, in the case of the waste). The cost of this secondary reduction is necessarily an extended blasting cost, and has been treated accordingly.

8.3 The effect of the degree of fragmentation on the costs of drilling and blasting

The degree of fragmentation is directly related to the amount of explosive energy infused into a unit mass or unit volume of rock. For a specified set of explosives, this energy is directly related to the amount of explosives in a hole as well as to the number of holes drilled and blasted per that unit volume or tonnage of ground. All conditions being equal, the energy infused has a direct relationship to the unit cost of fragmentation.

8.4 Estimation of the costs of drilling and blasting

As part of this evaluation, the costs of drilling and blasting were estimated. The basis of costing, as with the fragmentation prediction, was the use of ANFO as the main explosive, and optimal initiation. Specific additional details of the basis of the estimates are provided in the subsections on the costing of drilling (8.4.1) and blasting (8.4.2).

Estimates of the base case costs of drilling and blasting (which is the contract blast design) compared well with those currently borne by the mine, to within 10% for ore, and less than 15% for waste.

8.4.1 Drilling costs

The considerations made in drilling cost estimation are set out below.

i. Drill: The Atlas Copco model DM 45 drill, using a 17.145-cm (6.75-in) bit, is used as the basis for costing. This drill is operated by the mine in down-the-hole (DTH) mode.

ii. Hourly costs: Estimates of hourly operating costs for the DM 45 drill were developed from *Mine and Mill Equipment Costs – An Estimator's Guide* (2013). Costs of drill steel and bits were sourced from the *Guide for Estimating Drill Steel and Drill Bit Costs* from U.S. Army Corps of Engineers. Costs were adjusted for time, using cost indices from CostMine. Table 8.1 provides a summary of the components of that hourly cost. Table 8.2 shows an analysis of the bit and steel hourly costs.

iii. Bit performance and time analysis: The bits and rods for which costs were estimated were identical to those used at the mine. Penetration rates were estimated from the *Guide for Estimating Drill Steel and Drill Bit Costs* from U.S. Army Corps of Engineers. Table 8.3 outlines the bit performance in limestone, which compares well with observed performance on site. Time analysis (also shown in Table 8.3) was done to estimate the available operating time in a shift.

iv. Production analysis was done (Table 8.3), to determine the quantity of drilling possible within the shift.

v. Unit costs of drilling were then calculated from the hourly costs, the drill productivity, and the blast designs for each rock type. Tables 8.4 to 8.8 are summaries of the development of these unit costs of drilling for both the ore and waste rocks evaluated.

8.4.2 Blasting costs

The considerations made in blasting cost estimation were as follows:

i. Labor analysis, taking into consideration crew size and labor costs (Table 8.9).

ii. Time analysis, leading to a determination of available time for productive blasting activity in a shift. The number of holes that can be blasted in that time is also determined. Table 8.10 provides the analysis.

iii. Analysis of the production requirements. Annual production specified (ore and waste) was 114,683 m^3 (150,000 yd^3), at a stripping ratio of 5:1.

iv. The details and quantities of explosives and accessories per hole and per blast are specified. Unit costs for the explosives were obtained from Dyno Nobel. Details of this analysis are outlined in Tables 8.11 and 8.12.

The costs for drilling and blasting were combined and, for the ores of the three categories, namely Bom, Sembehun high-grade, and Sembehun low-grade, are summarized in Tables 8.13, 8.14 and 8.15, respectively. For each of these ores, the final drilling and blasting costs, at all blasting energy factors, take into account both the basic drill and blast costs and the extra costs of secondary breakage. The percentage of

oversize and undersize produced by the blast is presented. Table 8.16 outlines the mean fragmentation cost for the ores, based on a ratio of 1:1:1. From these analyses, ore oversize breakage potentially leads to increases over base case blasting costs of between 0.9% (Bom, at 400 kcal/st EF) and 355.7% (Sembehun low-grade, at 100 kcal/st EF). For the contract design specifications for ore blasting, a net increase in blasting costs (per ton) of up to 63% is expected.

Tables 8.17 and 8.18 provide summaries of drill, blast, and oversize reduction costs for the two types of waste rock considered in the study, namely, limestone and granodiorite, respectively. The size threshold for waste oversize characterization is 213.36 cm x 304.8 cm (84 inches x 120 inches), the limit being set by the capacity of the loader bucket. Reduction of waste oversize is by secondary blasting, although a mechanical breaker is also used. The unit cost of secondary reduction is $1.76/t ($1.60/st).

Secondary reduction is expected to be a major cost, for both ore and waste. To explore the impact of secondary reduction, Table 8.19 shows the costs of primary breakage, secondary breakage, and the overall cost of mining ore alone. Table 8.20 does the same for waste alone. To visualize the relative impacts on both types of rock, Figures 8.1 and 8.2 have been developed respectively from the two tables.

In the ore graph (Figure 8.1), a summation of the primary and secondary breakage costs produces a minimum in the region of 220 kcal/st. In the absence of waste, the 220 kcal/st design would produce the optimal blast, in terms of cost of ore fragmentation.

In the waste graph (Figure 8.2), the cost minimum is produced at 140 kcal/st. The relative magnitudes of the breakage curves in Figures 8.1 and 8.2 demonstrate that

secondary breakage is not as significant a cost issue for waste as it is for ore. This difference in importance of secondary breakage costs is understandable in the light of the different thresholds at which oversize is reckoned for ore and for waste. For ore, all sizes greater than 76.2 cm (30 inches) are considered oversize; for waste, the threshold is at 213.36 cm (84 inches).

A discussion of the overall impact of secondary breakage (and its implications for primary breakage requirement) is not complete with the figures mentioned above. This is because the average stripping ratio (5:1) has not been factored into the above scenarios. These ratios are discussed in Chapter 9.

8.5 The influence of fragment size distribution on loading productivity

In order to evaluate and quantify a possible cause-and-effect relationship between mining productivity and the particle size characteristics of the blasted material, photographic methods, as described in Section 3.4.1, were used to sample fragmentation at the mining face at W.U.S. Copper's Sembehun Pit. Corresponding time-and-motion data were collected specifically for the loading segment of the mining activity.

Fifteen sets of photos were shot across a blasted face of ore and waste (an average of four photos per set). Each set of photos was shot across about 20 m (66 ft) of the mining face. On the average, this width of face had enough rock for about five truckloads of a CAT 777 truck. The set of four photos was considered enough to assess the fragmentation across that face and to aid the evaluation of the impact of the particle size distribution on loading in that relatively small area.

To take a photo, two buckets were positioned for scale in the muck pile, about 4 m apart. One bucket was lined up behind the other to provide depth of view. After the image of a desired area had been captured in this manner, the buckets were relocated, and more photos taken.

Using a split-second stop watch, loading cycles from the photographed pile were timed. Each cycle started when the front end loader's bucket bit against the material in the stockpile, and ended when the material had been scooped, swung, and discharged into the truck, and the bucket teeth set against the face again to scoop the next load.

Each set of photos was processed in Split Desktop™ to estimate the particle size distribution. Figure 8.3 is a sequence of photos demonstrating various stages of image processing in Split Desktop™. Figures 8.4 and 8.5 are examples of the results obtained from the photo processing.

From the results of the analysis of each set of photos, the top size, 95%, 80%, 50%, and 30% passing sizes were extracted for all 15 sets of data. Table 8.21 is a summary of these data, including average size of load and single-pass load cycle of the CAT 992 loader.

8.6 Evaluation of loader cycle/productivity versus fragment size distributions

Using the data in Table 8.21, a statistical evaluation was carried out in Minitab™. Principally, linear regression relationships were explored between each of the size thresholds represented in the table (topsize, 95%, 80%, 50%, and 30% passing sizes) and,

separately, average cycle time for a single pass, and pass load (short tons). Simple linear regressions and multiple linear regressions were carried out.

In addition to the regular regressions that were run, a routine for stepwise regression in Minitab™ was used to rigorously assess the possibility that one or more of the available predictors might yield a significant regression.

Furthermore, a variety of different functional forms were explored, including exponential and logarithmic relationships, with subsequent linearization of the transformed values.

8.7 Results of statistical analysis

Figure 8.6 is a graph of cycle time vs. topsize, and Figure 8.7 is a graph of cycle time vs. mean size. The result (produced in Minitab™) of the regressions of cycle time on the entire set of predictors is presented in Figure 8.8. The criteria of interest in evaluating the regression equation are the F-statistic (f_0) and the coefficient of determination, R^2 (both shown within the ellipses in Figure 8.8). The hypothesis in the evaluation of the regression results is that the predictors (top size, F_{80}, F_{50}, etc.) have no significant impact on the loading cycle time. The alternative hypothesis is that the predictor(s) do(es) have an effect on the outcome. In the case of a simple linear regression, when $f_0 > f_{\alpha,1,n-2}$, the null hypothesis is rejected and the predictor does significantly affect the response variable. Hence, the model may be used to dependably predict the response. For multiple linear regression, the criterion for rejection is that: $f_0 > f_{\alpha,k,n-p}$ (Montgomery and Runger 2011).

However, in all cases considered, $f_{\alpha,1,n-2}$ and $f_{\alpha,k,n-p}$ obtained from the F distribution tables have been greater than 3, which is greater than all values of f_0 (shown only as F, in the Minitab™ results). These results lead to an acceptance of the null hypothesis, indicating that the various factors (top size, mean size, etc.) may not be used for the desired prediction purposes.

In all cases of the simple and multiple regressions, the value of R^2 shown in the results was low (most of them well below 50%), hence, indicating a poor fit of the model to the data.

The aim of the stepwise regression mentioned in Section 8.9 was to evaluate each of eleven possible predictors (including transforms and aggregates of some of the original variables) for their potential to validly predict either the cycle times or the size of the bucket load or to predict both. Figure 8.9 shows the result of the stepwise regression that was run between cycle time and 11 predictors. The result was that no variables passed the statistical criteria, and none of them could be "entered" into or used in the model to predict the cycle time. A similar result was obtained for the investigation of the prediction of mass in the bucket load.

Figure 8.10 is a plot of the residuals in the regression between cycle time and the various candidate regressors. The plot shows that the errors are normally and independently distributed with a mean of zero and a variance equal to the variance of the data. Normality and randomness are used as a test for the adequacy and validity of the regression. These residuals refer to the results in Figure 8.8.

In spite of the adequacy of the model (as demonstrated by the normality of the various plots), there was, however, no significant or meaningful relationship between the

particle size distribution of the blasted rock pile and either the loader cycle time (which impacts the loading speed) or the size (load) of the pass.

8.8 Implications

The conclusion is drawn that, if the fragment size distribution has no significant effect on the loader cycle time, then that fragment size distribution should not have any effect, either, on the haulage cycle times. No other data were collected to monitor such a relationship, nor could any other be conceived with reasonable chances to demonstrate impact better than the fragmentation data already evaluated.

Indeed, while this outcome does appear to challenge conventional wisdom, it may, however, actually bring sharply into focus an element that is generally disregarded when mine-to-mill issues are being discussed. This element is the human factor. It is conceivable that a loader operator's performance does rise and fall during an operating session, and that this performance may be susceptible to influence by extraneous factors, including operator competence and general circumstances. This explanation was not explicitly investigated. However, its validity is considered an important possibility.

In pursuing methods to evaluate the fragment size distribution and loading productivity relationship at an earlier stage of the research, discussions were held with John Floyd, of Blast Dynamics. Floyd had previously developed a system (ProDig) for characterizing this relationship, but appears to have abandoned the use of that system when his findings at several operations around the world demonstrated that "there is more deviation in cycle time due to operator experience than that related to fragmentation" (Floyd, 2014, pers. comm., August 4, 2014).

8.9 Estimation of wear and tear arising from degrees of rock fragmentation

Wear and tear is considered a major component of the effect of blasting on an operation's economic bottom line. However, it was not possible in this work to directly relate wear and tear effects to blasting energy or blast-generated particle size distribution. Certainly, such a relationship, if it exists, would be an important one to investigate.

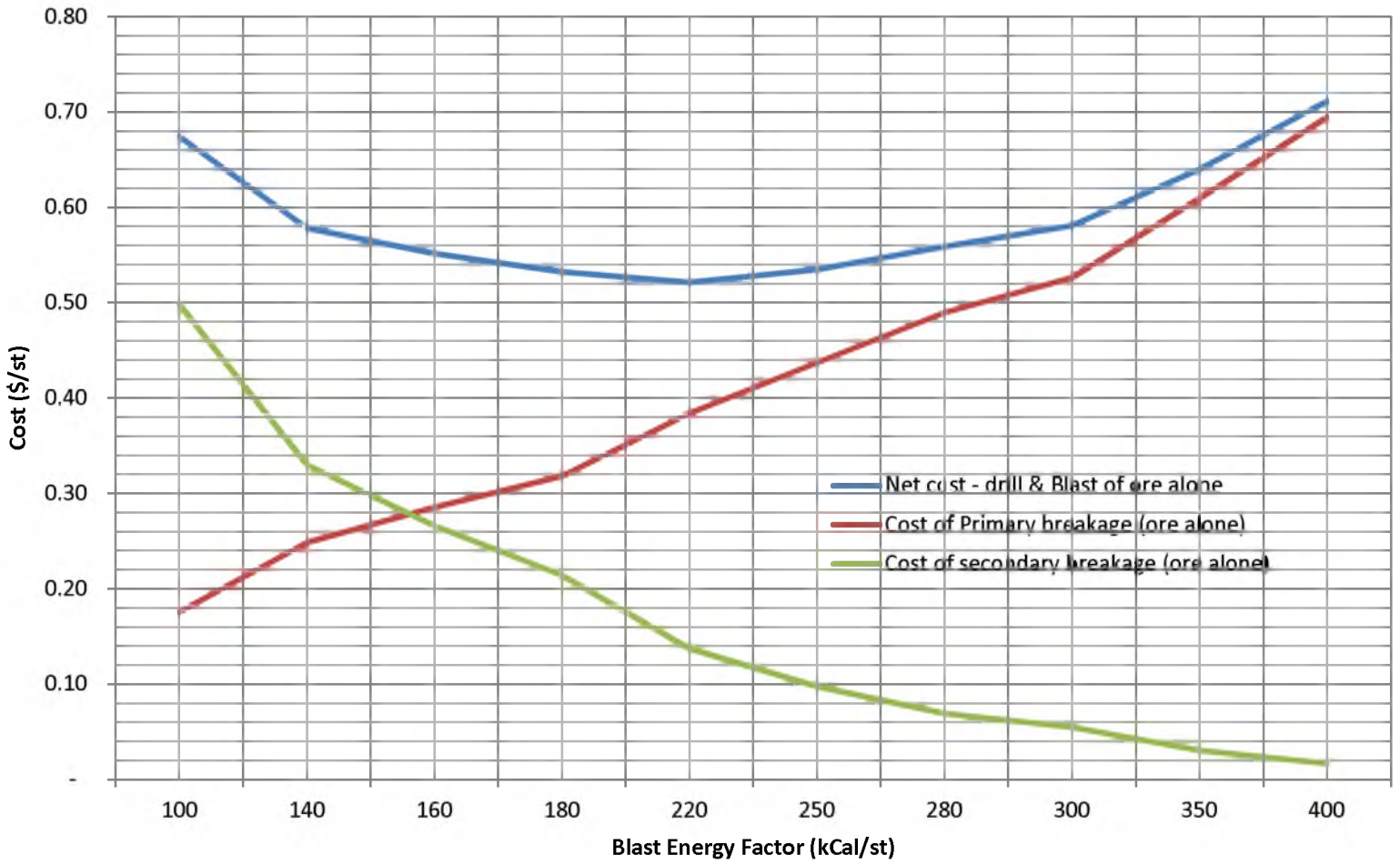

FIGURE 8.1 A plot of ore breakage costs versus energy factor

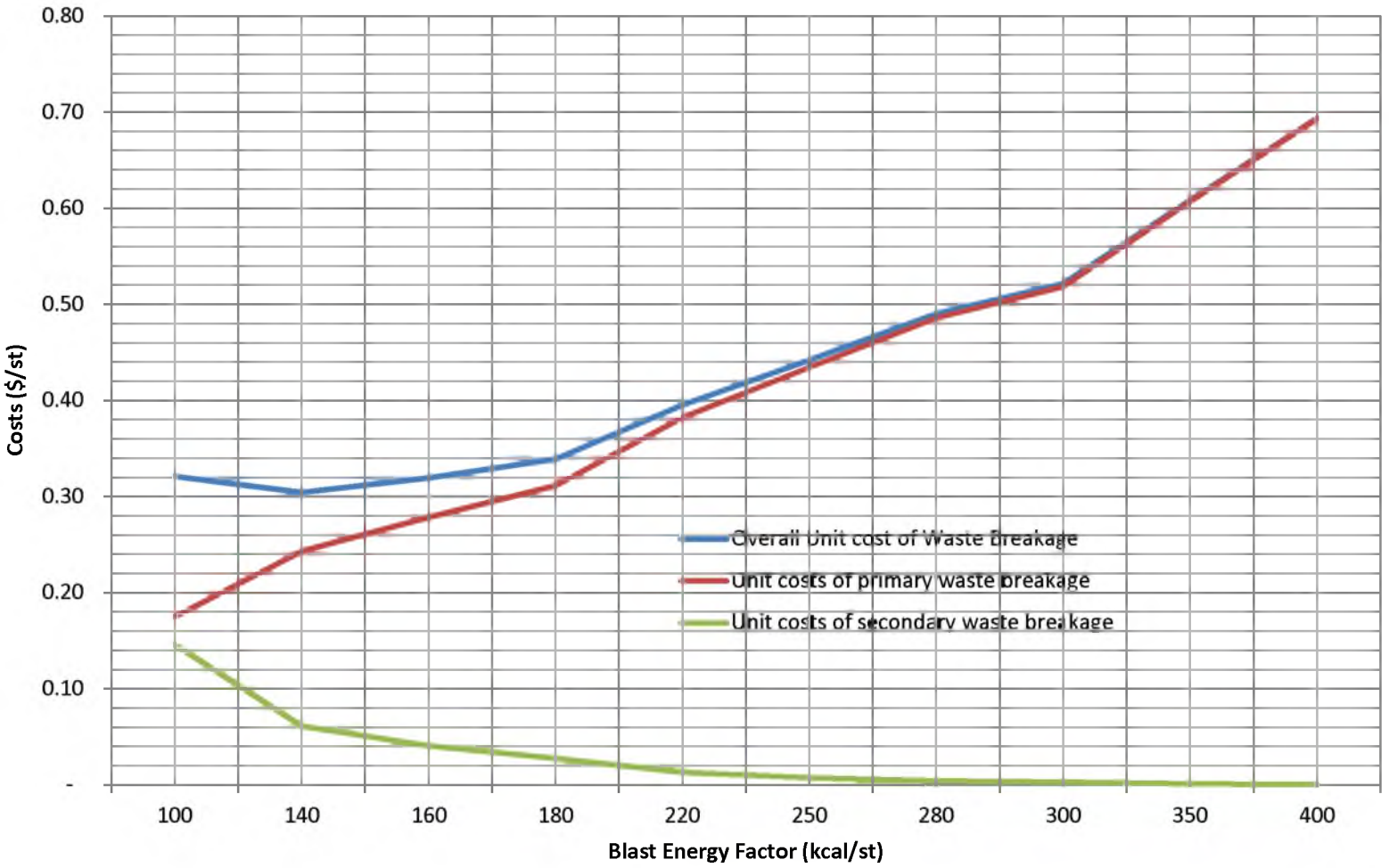

FIGURE 8.2 A plot of waste breakage costs against energy factor

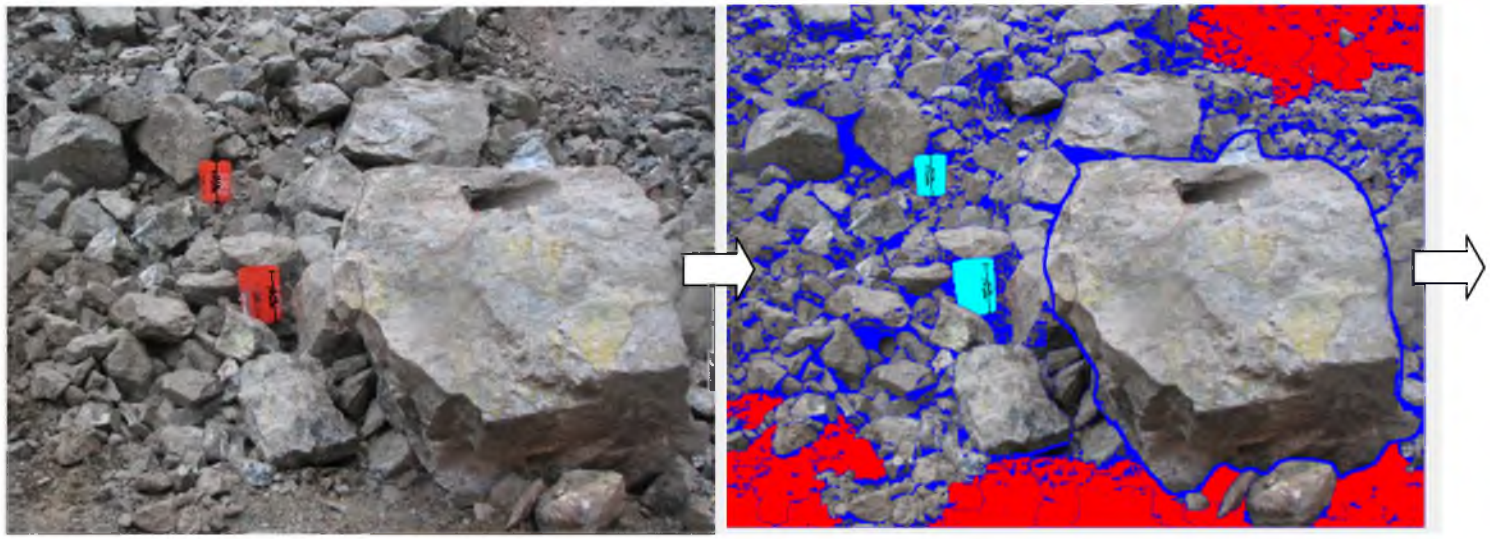

FIGURE 8.3 Images at various stages of processing for the estimation of fragmentation, using Split Desktop™

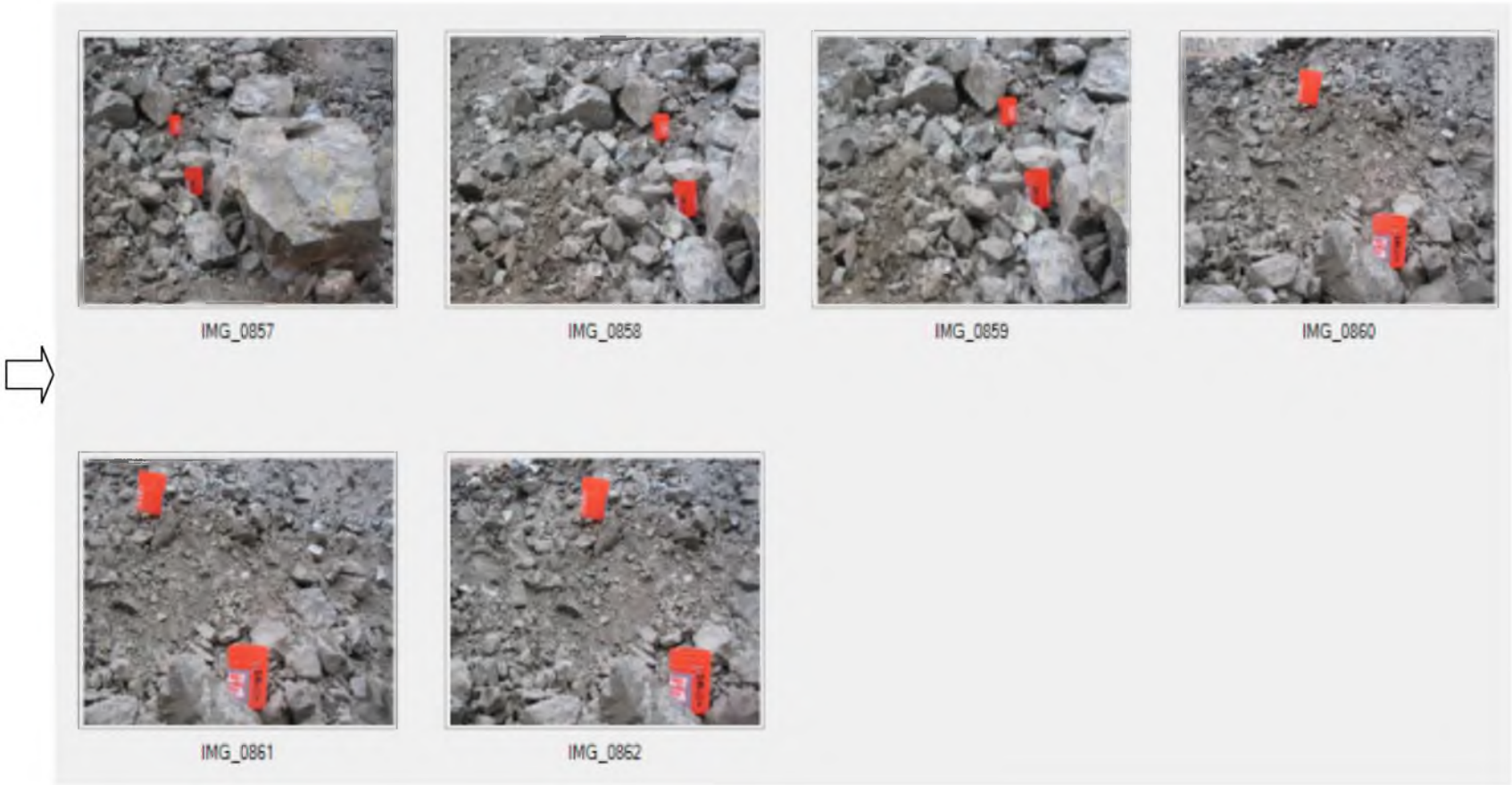

FIGURE 8.3 (CONTINUED)

Size[in]	Combined % Passing	IMG_0928 % Passing	IMG_0929 % Passing	IMG_0930 % Passing	IMG_0931 % Passing	IMG_0932 % Passing	IMG_0933 % Passing
75	100	100	100	100	100	100	100
50	99.88	100	100	99.49	100	100	100
30	79.47	75.12	71.27	83.88	81.63	74.68	84.31
25	70.51	64.52	61.44	77.85	73.76	63.38	75.14
15	48.71	44.51	40.62	60.01	57.38	40.95	50.87
10	37.73	34.51	27.75	50.78	49.85	31.39	36.81
8	33.75	29.5	22.74	47.57	46.86	28.34	32.77
6	30.13	24.82	18.57	43.41	44.41	25.85	30.01
4	25.05	19.18	13.79	37.03	39.75	19.95	26.93
2	17.78	12.34	7.93	28.18	31.92	12.8	19.79
1	12.8	7.93	4.56	21.42	25.61	8.2	14.52
0.75	11.21	6.59	3.62	19.11	23.36	6.82	12.77
0.5	9.32	5.08	2.62	16.26	20.52	5.25	10.64
0.38	8.2	4.22	2.08	14.49	18.71	4.36	9.35
0.25	6.86	3.25	1.5	12.32	16.43	3.35	7.78
0.19	6.05	2.7	1.19	10.97	14.97	2.77	6.83
0.08	4.21	1.54	0.59	7.77	11.36	1.58	4.62

% Passing	Combined Size[in]	IMG_0928 Size[in]	IMG_0929 Size[in]	IMG_0930 Size[in]	IMG_0931 Size[in]	IMG_0932 Size[in]	IMG_0933 Size[in]
F10	0.58	1.44	2.67	0.15	0.05	1.36	0.44
F20	2.54	4.27	6.72	0.84	0.46	4.02	2.05
F30	5.94	8.2	10.88	2.34	1.64	9.13	5.99
F40	11.08	12.52	14.74	4.87	4.08	14.53	11.28
F50	15.58	17.84	18.97	9.53	10.1	19.3	14.69
F60	19.93	22.81	24.16	14.99	16.69	23.58	18.36
F70	24.72	27.62	29.39	20.09	22.61	27.85	22.47
F80	30.31	32.29	34.19	26.72	28.99	32.5	27.63
F90	37.13	39.5	39.33	35.91	35.38	38.31	34.85
F95	42.06	43.99	43.34	42.22	39.47	41.74	40.62
Topsize (99.9	50.38	49.2	48.44	50.93	49.24	45.84	47.5

	Combined	IMG_0928	IMG_0929	IMG_0930	IMG_0931	IMG_0932	IMG_0933
Fines Cutoff[i	4.46	6.04	5.35	7.06	5.48	6.03	4.62
Fines Factor	50	50	50	50	50	50	50

FIGURE. 8.4 A screenshot example of the fragment size distribution results from blast image processing in Split Desktop ™

(1 inch = 2.54 cm)

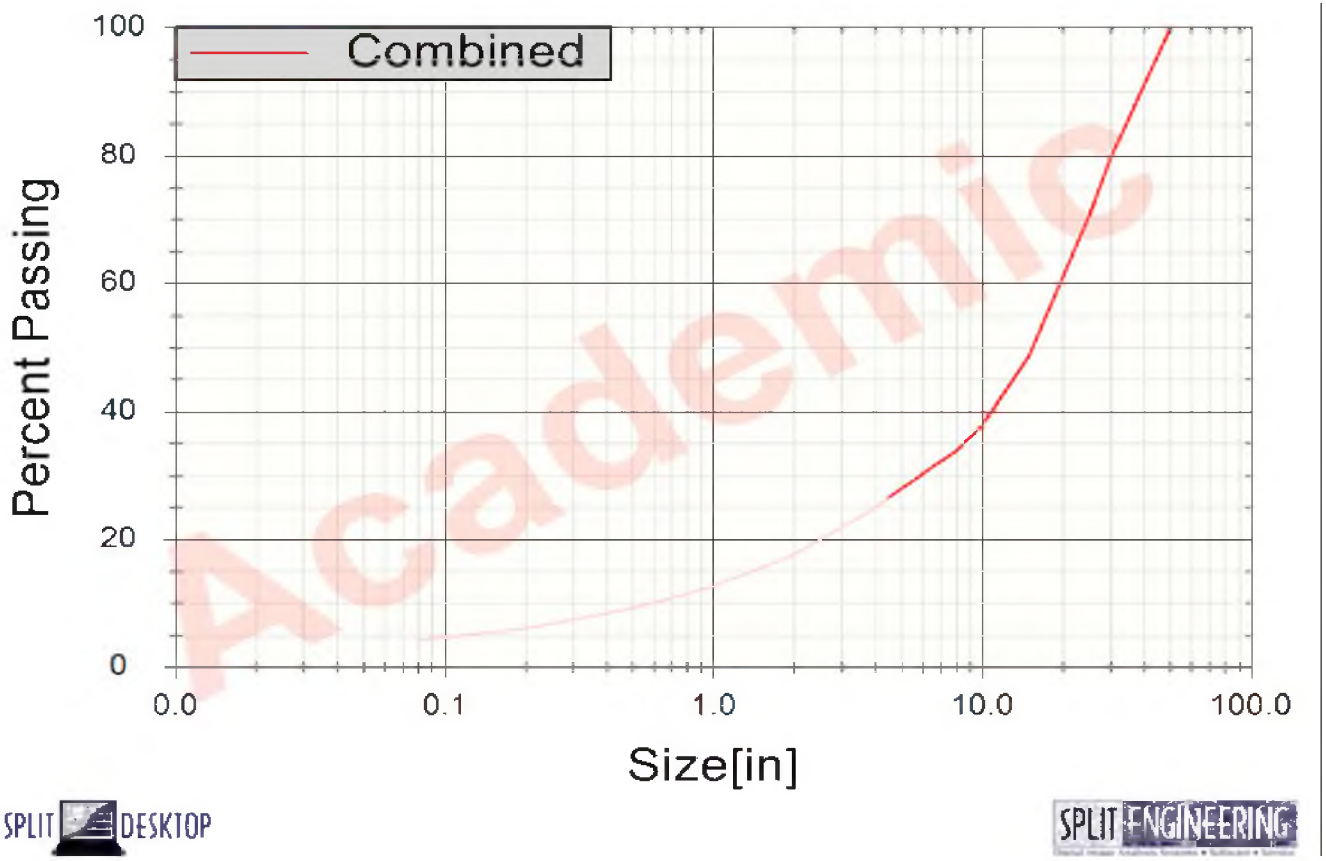

FIGURE. 8.5 A screenshot example of the fragment size distribution graph, obtained from blast image processing in Split Desktop™

(1 inch = 2.54 cm)

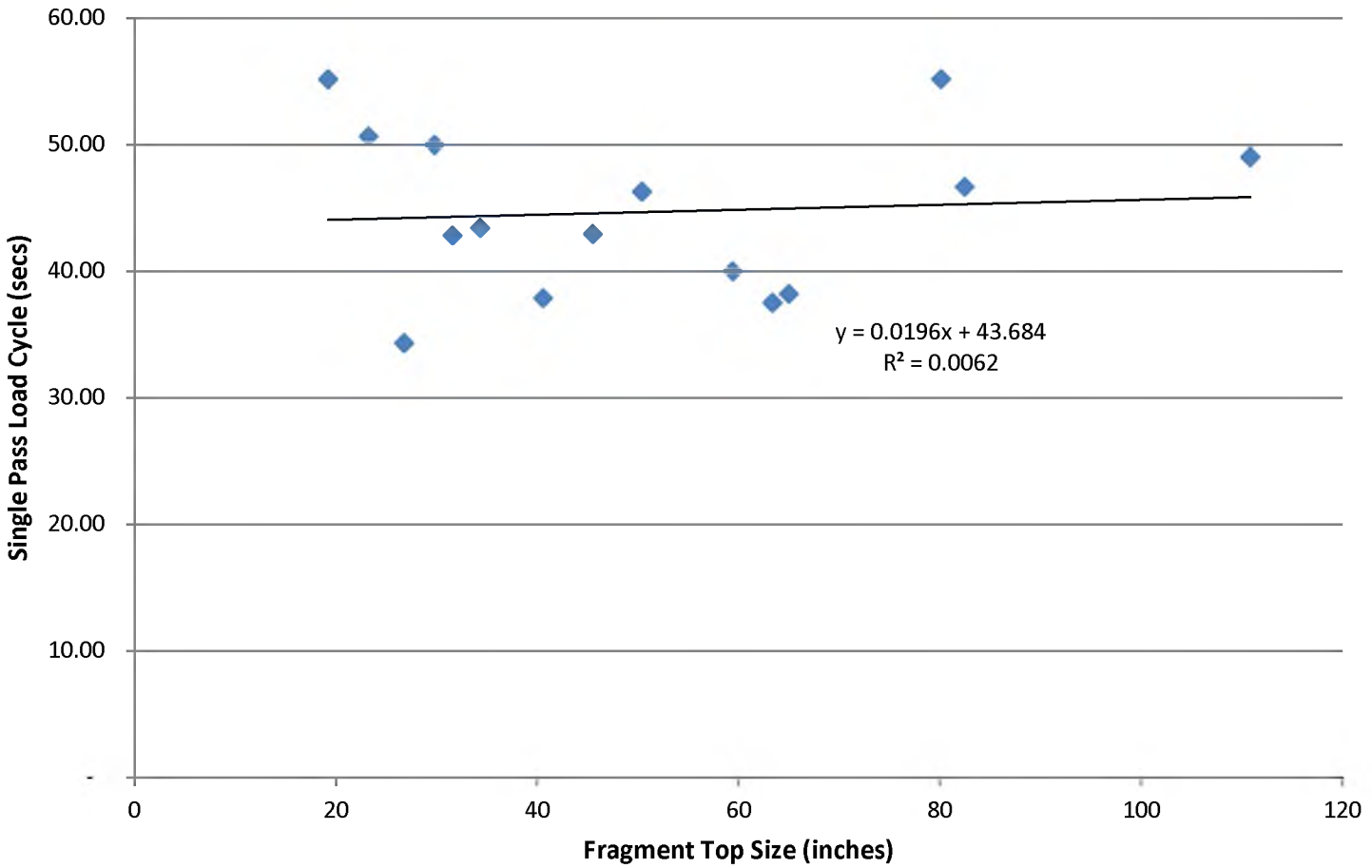

FIGURE 8.6 Regression plot of loading cycle time vs. top size.

1 inch = 2.54 cm

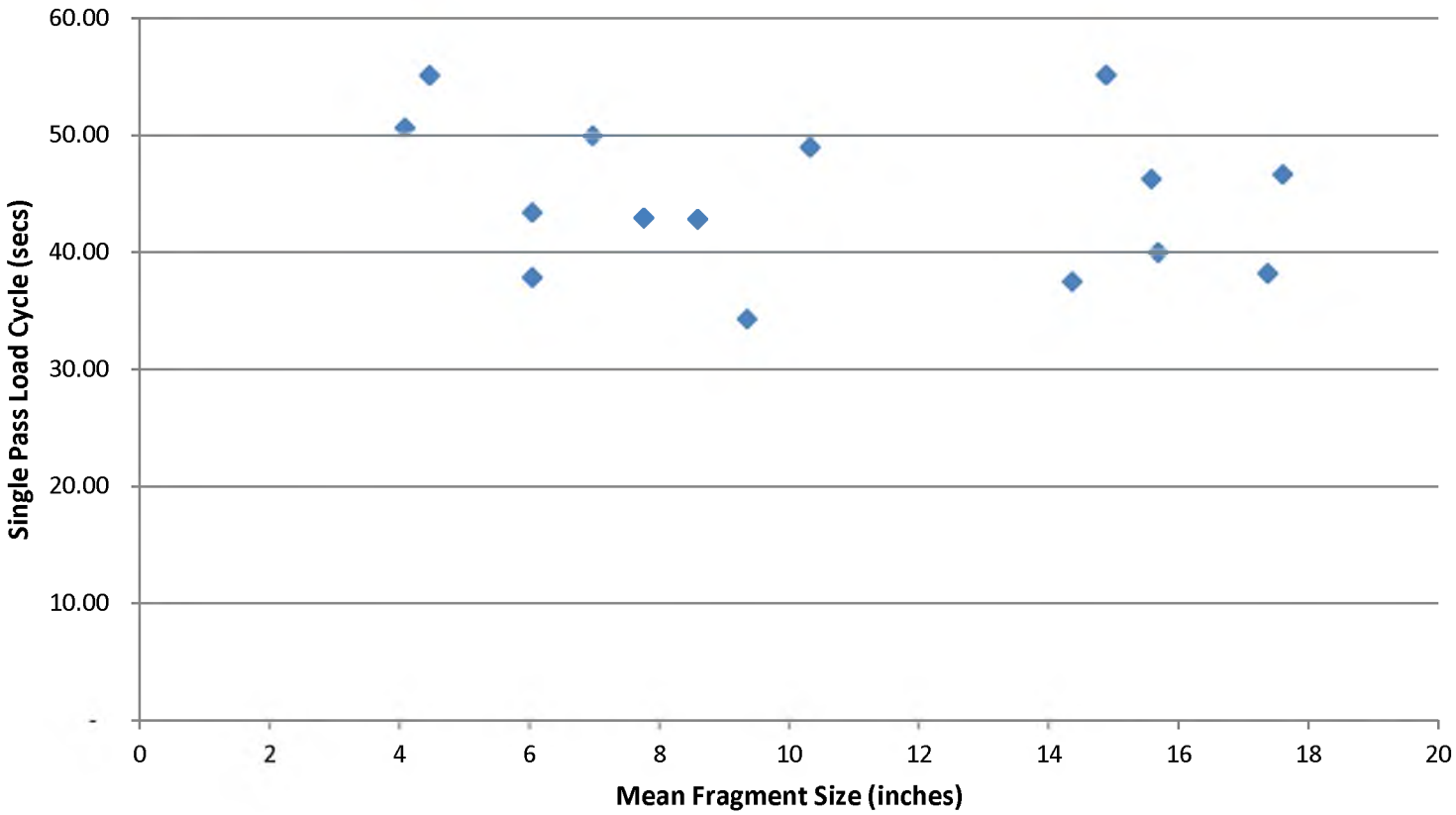

FIGURE 8.7 Regression plot of cycle time vs. mean size

1 inch = 2.54 cm

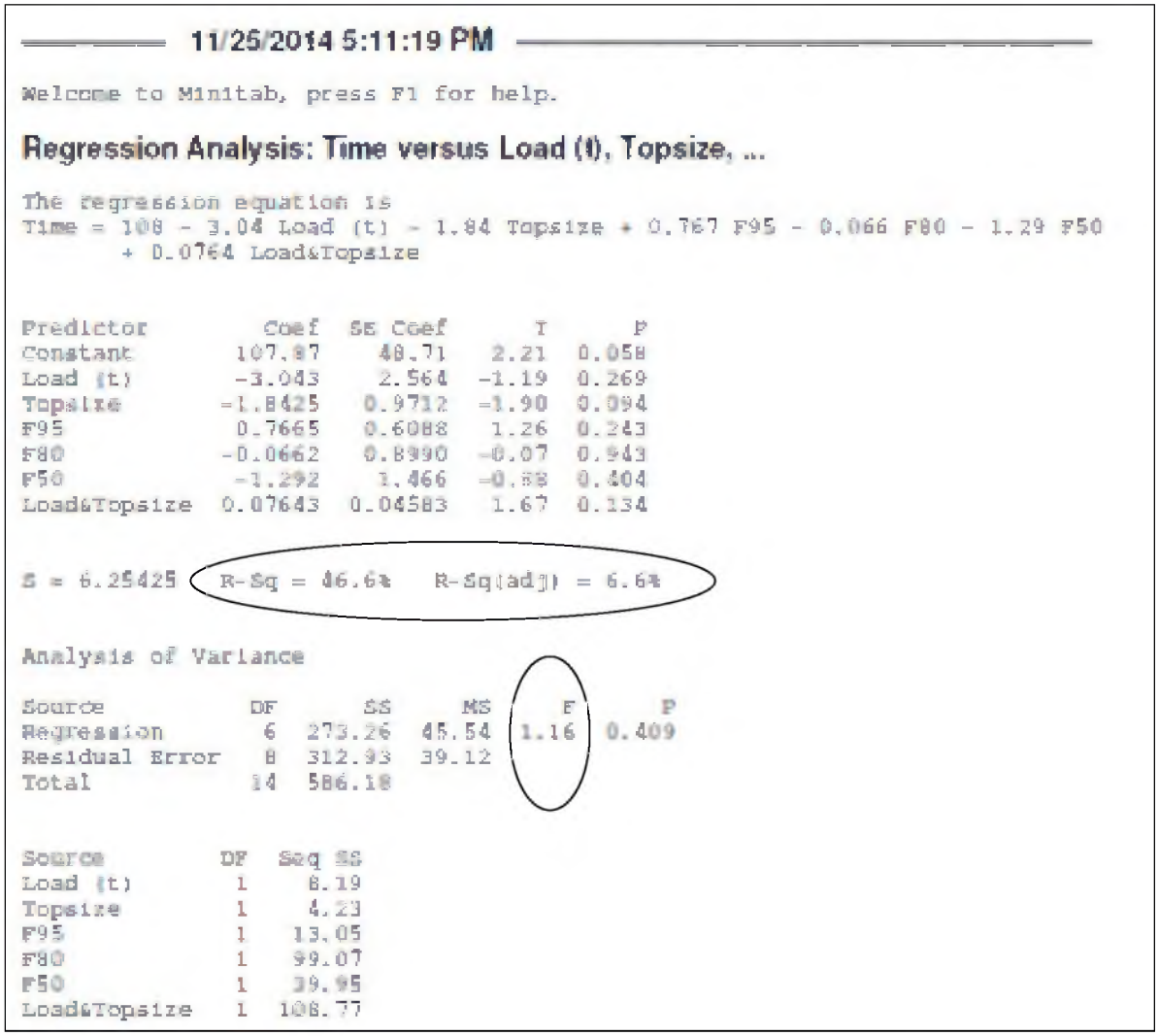

11/25/2014 5:11:19 PM

Welcome to Minitab, press F1 for help.

Regression Analysis: Time versus Load (t), Topsize, ...

The regression equation is
Time = 108 - 3.04 Load (t) - 1.84 Topsize + 0.767 F95 - 0.066 F80 - 1.29 F50
+ 0.0764 Load&Topsize

Predictor	Coef	SE Coef	T	P
Constant	107.87	48.71	2.21	0.058
Load (t)	-3.043	2.564	-1.19	0.269
Topsize	-1.8425	0.9712	-1.90	0.094
F95	0.7665	0.6088	1.26	0.243
F80	-0.0662	0.8990	-0.07	0.943
F50	-1.292	1.466	-0.88	0.404
Load&Topsize	0.07643	0.04583	1.67	0.134

S = 6.25425 R-Sq = 46.6% R-Sq(adj) = 6.6%

Analysis of Variance

Source	DF	SS	MS	F	P
Regression	6	273.26	45.54	1.16	0.409
Residual Error	8	312.93	39.12		
Total	14	586.18			

Source	DF	Seq SS
Load (t)	1	8.19
Topsize	1	4.23
F95	1	13.05
F80	1	99.07
F50	1	39.95
Load&Topsize	1	108.77

FIGURE 8.8 Results of regression of all cycle time on all factors shown in Table 8.21

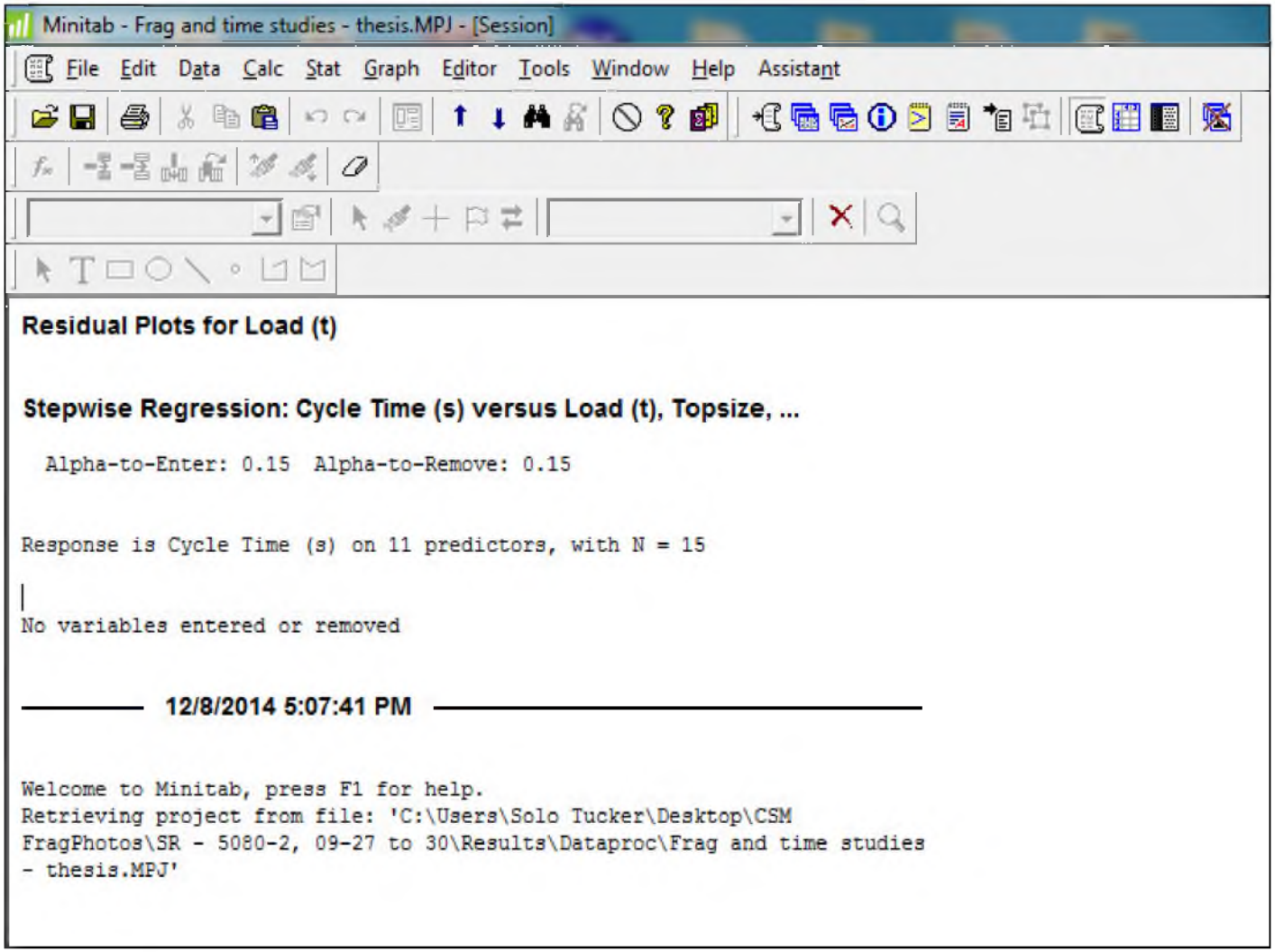

FIGURE 8.9 The results of stepwise regression on all factors shown in Table 8.21

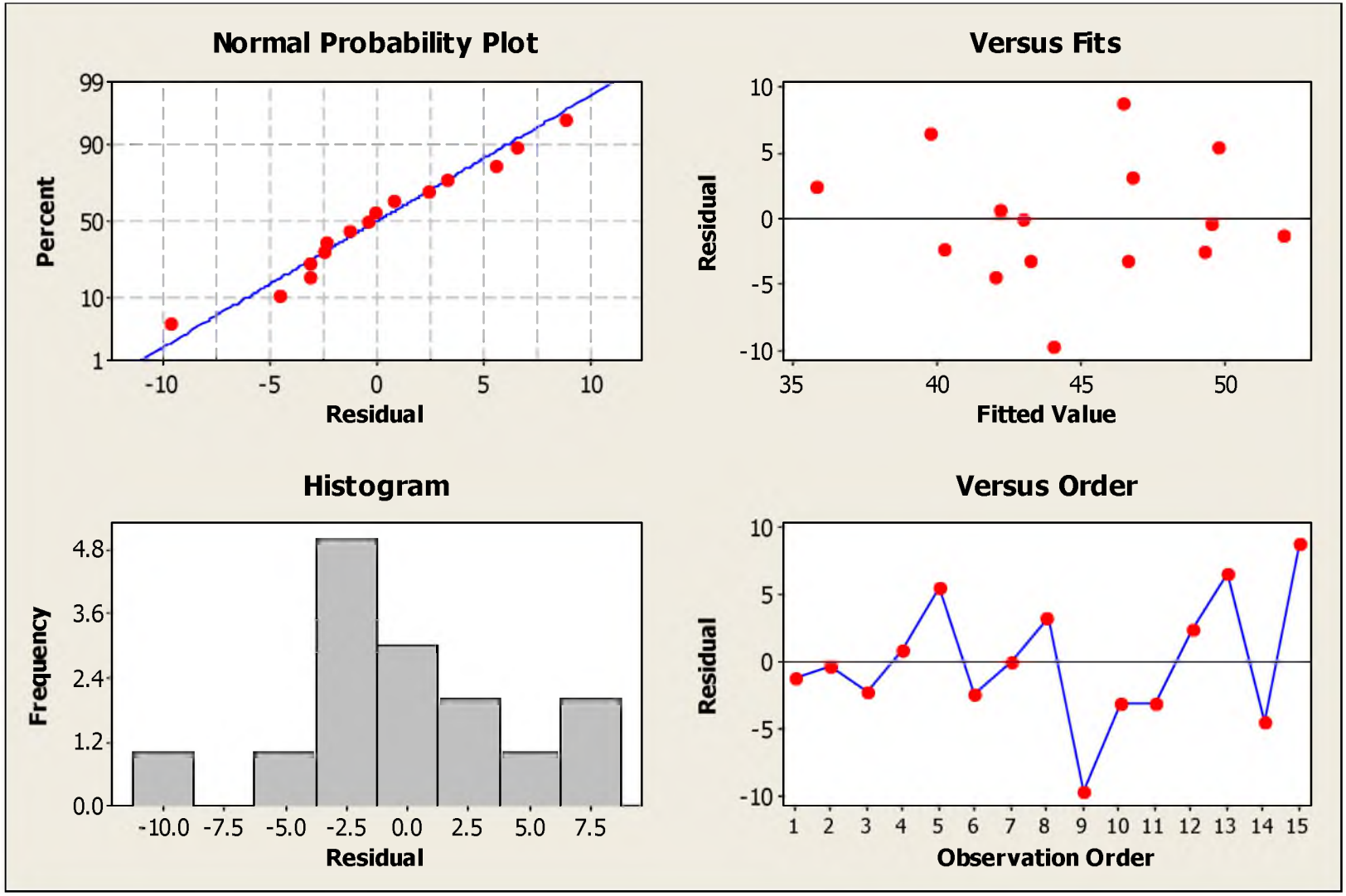

FIGURE 8.10 A plot of the residuals from the regression of cycle time on various factors

TABLE 8.1 Hourly operating costs for a DM 45 drill rig

Overhaul		Maintenance		Operating					Total
Parts ($/hr)	Labor ($/hr)	Parts ($/hr)	Labor ($/hr)	Diesel ($/hr)	Lube ($/hr)	Wear Parts ($/hr)	Total ($/hr)	Driller's net Wages+benefits ($/hr)	Grand Total (excl. ownership) ($/hr)
7.18	6.77	5.87	5.54	51.59	10.55	34.27	121.77	40.71	162.48

(Source: Infomine USA Inc. Costmine Division 2013; U.S. Army Corps of Engineers 2009)

TABLE 8.2 Development of costs for drill steel and bits

	Steel	Drill bit
Feet drilled/hole (approx)	24	
Rods	2	
$/ft/rod	0.0175	
Adj. Factor	1.5	
$/ft drilled	**0.02625**	**0.19**
Penetration rate (ft/hr)	127.5	127.5
$/hr = ft/hr * $/ft	3.346875	24.225
Total $/hr (2006 costs)	**27.571875**	
2006 Cost Index	186.5	
2014 Cost Index	231.8	
2014 Cost of wear items ($)	**34.27**	

Source: U.S. Army Corps of Engineers 2009

TABLE 8.3 Bit performance, time analysis and drill productivity in limestone

Time analysis		
Length of shift	10	hrs/shift
Less:		
Start up and Delays	0.25	hrs/shift
Lunch	0.50	hrs/shift
Major moves	–	hrs/shift
Misc Delays	0.25	hrs/shift
Total Delays	**1.00**	hrs/shift
Available Drilling time	9.00	hrs/shift

Penetration	2.125	feet/min
Hole length	23.9375	ft/hole
Drilling Rates:	11.3	mins/hole
Adding pipe	–	mins/hole
Pulling pipe	0.5	mins/hole
Maneuvering Time	3.0	mins/hole
Leveling Time	1.0	mins/hole
Total Drill Cycle	15.8	mins/hole
	0.26	hr/hole
Drill Productivity	3.81	holes/hour
	34.25	holes/shift

TABLE 8.4 A summary of the development of unit costs of drilling for Bom ore

EF (kwh/st)	100	129	140	160	180	220	250	280	300	350	400
Bench height (L) (ft)	20.00	20.00	20.00	20.00	20.00	20.00	20.00	20.00	20.00	20.00	20.00
Hole length (ft)	23.94	23.94	23.94	23.94	23.94	23.94	23.94	23.94	23.94	23.94	23.94
Burden, (B) (ft)	15.92	14.01	13.45	12.58	11.86	10.73	10.07	9.51	9.19	8.51	7.96
Spacing, (S) (ft)	18.30	16.12	15.47	14.47	13.64	12.34	11.58	10.94	10.57	9.78	9.15
yd^3/hole	215.79	167.28	154.14	134.87	119.89	98.09	86.32	77.07	71.93	61.66	53.95
yd^3/shift	7,391.75	5,730.04	5,279.82	4,619.84	4,106.53	3,359.89	2,956.70	2,639.91	2,463.92	2,111.93	1,847.94
yd^3/hr	821.31	636.67	586.65	513.32	456.28	373.32	328.52	293.32	273.77	234.66	205.33
st/hr	2,261.87	1,753.39	1,615.62	1,413.67	1,256.60	1,028.12	904.75	807.81	753.96	646.25	565.47
$/$yd^3$	0.20	0.26	0.28	0.32	0.36	0.44	0.49	0.55	0.59	0.69	0.79
$/st	0.07	0.09	0.10	0.11	0.13	0.16	0.18	0.20	0.22	0.25	0.29
$/t	0.08	0.10	0.11	0.13	0.14	0.17	0.20	0.22	0.24	0.28	0.32

TABLE 8.5 A summary of the development of unit costs of drilling for Sembehun high-grade ore

EF (kwh/st)	100	142	140	160	180	220	250	280	300	350	400
Bench height (L) (ft)	20.00	20.00	20.00	20.00	20.00	20.00	20.00	20.00	20.00	20.00	20.00
Hole length (ft)	23.94	23.94	23.94	23.94	23.94	23.94	23.94	23.94	23.94	23.94	23.94
Burden, (B) (ft)	16.71	14.02	14.12	13.21	12.45	11.26	10.57	9.98	9.65	8.93	8.35
Spacing, (S) (ft)	19.21	16.12	16.24	15.19	14.32	12.95	12.15	11.48	11.09	10.27	9.61
yd^3/hole	237.75	167.43	169.82	148.59	132.08	108.07	95.10	84.91	79.25	67.93	59.44
yd^3/shift	8,143.79	5,735.06	5,816.99	5,089.87	4,524.33	3,701.72	3,257.52	2,908.50	2,714.60	2,326.80	2,035.95
yd^3/hr	904.87	637.23	646.33	565.54	502.70	411.30	361.95	323.17	301.62	258.53	226.22
st/hr	2,261.87	1,592.87	1,615.62	1,413.67	1,256.60	1,028.12	904.75	807.81	753.96	646.25	565.47
$/$yd^3$	0.18	0.25	0.25	0.29	0.32	0.40	0.45	0.50	0.54	0.63	0.72
$/st	0.07	0.10	0.10	0.11	0.13	0.16	0.18	0.20	0.22	0.25	0.29
$/t	0.08	0.11	0.11	0.13	0.14	0.17	0.20	0.22	0.24	0.28	0.32

TABLE 8.6 A summary of the development of unit costs of drilling for Sembehun low-grade ore

EF (kwh/st)	100	155	140	160	180	220	250	280	300	350	400
Bench height (L) (ft)	20.00	20.00	20.00	20.00	20.00	20.00	20.00	20.00	20.00	20.00	20.00
Hole length (ft)	23.94	23.94	23.94	23.94	23.94	23.94	23.94	23.94	23.94	23.94	23.94
Burden, (B) (ft)	17.44	14.00	14.74	13.78	13.00	11.75	11.03	10.42	10.07	9.32	8.72
Spacing, (S) (ft)	20.05	16.10	16.95	15.85	14.94	13.52	12.68	11.98	11.58	10.72	10.03
yd^3/hole	258.95	167.07	184.97	161.85	143.86	117.71	103.58	92.48	86.32	73.99	64.74
yd^3/shift	8,870.10	5,722.65	6,335.79	5,543.81	4,927.83	4,031.86	3,548.04	3,167.89	2,956.70	2,534.31	2,217.53
yd^3/hr	985.57	635.85	703.98	615.98	547.54	447.98	394.23	351.99	328.52	281.59	246.39
st/hr	2,261.87	1,459.27	1,615.62	1,413.67	1,256.60	1,028.12	904.75	807.81	753.96	646.25	565.47
$/$yd^3$	0.16	0.26	0.23	0.26	0.30	0.36	0.41	0.46	0.49	0.58	0.66
$/st	0.07	0.11	0.10	0.11	0.13	0.16	0.18	0.20	0.22	0.25	0.29
$/t	0.08	0.12	0.11	0.13	0.14	0.17	0.20	0.22	0.24	0.28	0.32

TABLE 8.7 A summary of the development of unit costs of drilling for limestone

EF (kwh/st)	100	162.5	140	160	180	220	250	280	300	350	400
Bench height (L) (ft)	20.00	20.00	20.00	20.00	20.00	20.00	20.00	20.00	20.00	20.00	20.00
Hole length (ft)	23.94	23.94	23.94	23.94	23.94	23.94	23.94	23.94	23.94	23.94	23.94
Burden, (B) (ft)	17.86	14.01	15.09	14.12	13.31	12.04	11.30	10.67	10.31	9.55	8.93
Spacing, (S) (ft)	20.54	16.11	17.36	16.24	15.31	13.85	12.99	12.27	11.86	10.98	10.27
yd^3/hole	271.74	167.23	194.10	169.84	150.97	123.52	108.70	97.05	90.58	77.64	67.94
yd^3/shift	9,308.13	5,728.08	6,648.67	5,817.58	5,171.18	4,230.97	3,723.25	3,324.33	3,102.71	2,659.47	2,327.03
yd^3/hr	1,034.24	636.45	738.74	646.40	574.58	470.11	413.69	369.37	344.75	295.50	258.56
st/hr	2,261.87	1,391.92	1,615.62	1,413.67	1,256.60	1,028.12	904.75	807.81	753.96	646.25	565.47
$/$yd^3$	0.16	0.26	0.22	0.25	0.28	0.35	0.39	0.44	0.47	0.55	0.63
$/st	0.07	0.12	0.10	0.11	0.13	0.16	0.18	0.20	0.22	0.25	0.29
$/t	0.08	0.13	0.11	0.13	0.14	0.17	0.20	0.22	0.24	0.28	0.32

TABLE 8.8 A summary of the development of unit costs of drilling for granodiorite

EF (kwh/st)	**100**	**164.5**	**140**	**160**	**180**	**220**	**250**	**280**	**300**	**350**	**400**
Bench height (L) (ft)	20.00	20.00	20.00	20.00	20.00	20.00	20.00	20.00	20.00	20.00	20.00
Hole Length (ft)	23.94	23.94	23.94	23.94	23.94	23.94	23.94	23.94	23.94	23.94	23.94
Burden, (B) (ft)	17.97	14.01	15.19	14.21	13.40	12.12	11.37	10.74	10.38	9.61	8.99
Spacing, (S) (ft)	20.67	16.11	17.47	16.34	15.40	13.93	13.07	12.35	11.93	11.05	10.33
yd^3/hole	275.14	167.26	196.53	171.96	152.85	125.06	110.05	98.26	91.71	78.61	68.78
yd^3/shift	9,424.48	5,729.17	6,731.77	5,890.30	5,235.82	4,283.86	3,769.79	3,365.89	3,141.49	2,692.71	2,356.12
yd^3/hr	1,047.16	636.57	747.97	654.48	581.76	475.98	418.87	373.99	349.05	299.19	261.79
st/hr	2,261.87	1,375.00	1,615.62	1,413.67	1,256.60	1,028.12	904.75	807.81	753.96	646.25	565.47
$/$yd^3$	0.16	0.26	0.22	0.25	0.28	0.34	0.39	0.43	0.47	0.54	0.62
$/st	0.07	0.12	0.10	0.11	0.13	0.16	0.18	0.20	0.22	0.25	0.29
$/t	0.08	0.13	0.11	0.13	0.14	0.17	0.20	0.22	0.24	0.28	0.32

TABLE 8.9 Blasting labor analysis

Role	Qty	Wages &benefits ($/hr)	Hours	Cost ($/day)
Foreman	1	24	8	192
Powder Men	2	20	8	320
Drivers	1	20	8	160
Total				**672**

Note: No. of Teams = 1

TABLE 8.10 Time analysis for blasting

Available time Analysis		
Hours per shift	hours	8
Length of shift	mins	480
Startup	mins	45
Lunch	mins	20
Misc. delays	mins	15
Shutdown	mins	15
Available time	mins/shift	**385**
Time Utilization Analysis		
Connect time (@ 1min/hole)	mins	140
Load time (@ 1min/hole)	mins	140
Clear pit	mins	15
Shoot and clear shot	mins	30
R/T magazine	mins	45
Load time @ magazine	mins	15
Total time per shift	mins	**385**

TABLE 8.11 Unit costs of explosives products

Item	Unit	Value
Explosive		ANFO
Explosive Cost	$/lb	0.25
Booster Type	lb	1
Booster Cost	$ ea	6.00
Snap Line	$ ea	5.50
Nonel Detonators	$ ea	6.50

Source: DynoNobel

TABLE 8.12 Development of the cost of a single blast

Basis: NONEL Initiation				
Item	Unit	Qty	Unit cost ($/lb)	Cost ($)
Powder (Explosive)	lb	20,593	0.25	5,148.23
Boosters	ea	140	6	840.00
Nonel detonator	ea	140	6.5	910.00
Snap line	ea	119	5.07	603.33
Any other (det cord)	ea	2,000	0.124	248.00
Initiating cap (100 ft)	lot	1	12	12.00
Total: Explosives and accessories				**7,761.56**
Labor	Set	1	672	672.00
Total costs ($)				**8,433.56**

TABLE 8.13 A summary of the combined drilling, blasting, secondary breakage and mean blending fragmentation costs for Bom ore

Explosive energy (kcal/st)	100	129 Contract	140	160	180	220	250	280	300	350	400
Drill	0.07	0.09	0.10	0.11	0.13	0.16	0.18	0.20	0.22	0.25	0.29
Blast	0.10	0.14	0.15	0.17	0.19	0.22	0.26	0.29	0.31	0.36	0.41
Total	0.17	0.23	0.25	0.28	0.32	0.38	0.44	0.49	0.52	0.61	0.70
Secondary breakage ($/st)	1.50	1.50	1.50	1.50	1.50	1.50	1.50	1.50	1.50	1.50	1.50
% O/S	27.67%	18.34%	16.76%	12.92%	9.90%	5.74%	3.77%	2.46%	1.84%	0.88%	0.41%
% U/S	72.33%	81.66%	83.24%	87.08%	90.10%	94.26%	96.23%	97.54%	98.16%	99.12%	99.59%
Net blasting cost ($/st)	0.59	0.51	0.50	0.48	0.46	0.47	0.50	0.53	0.55	0.62	0.70
Net blasting cost ($/t)	0.65	0.56	0.55	0.53	0.51	0.52	0.55	0.58	0.61	0.68	0.78
% Increase in blasting cost	237.3%	118.3%	100.4%	68.4%	47.0%	22.5%	12.8%	7.5%	5.3%	2.2%	0.9%

TABLE 8.14 A summary of the combined drilling, blasting, secondary breakage and mean blending fragmentation costs for Sembehun high-grade ore

Explosive energy (kcal/st)	100	142 Contract	160	180	220	250	280	300	350	400	140
Drill	0.07	0.10	0.11	0.13	0.16	0.18	0.20	0.22	0.25	0.29	0.10
Blast	0.10	0.15	0.17	0.19	0.23	0.25	0.29	0.31	0.36	0.40	0.15
Total	0.18	0.26	0.29	0.32	0.38	0.43	0.49	0.53	0.61	0.69	0.25
Secondary breakage ($/st)	1.50	1.50	1.50	1.50	1.50	1.50	1.50	1.50	1.50	1.50	1.50
% O/S	30.08%	18.63%	15.05%	11.82%	7.20%	4.92%	3.34%	2.57%	1.32%	0.67%	19.07%
% U/S	69.92%	81.37%	84.95%	88.18%	92.80%	95.08%	96.66%	97.43%	98.68%	99.33%	80.93%
Net blasting cost ($/st)	0.63	0.54	0.51	0.50	0.49	0.51	0.54	0.56	0.63	0.70	0.54
Net blasting cost ($/t)	0.69	0.59	0.56	0.55	0.54	0.56	0.60	0.62	0.69	0.77	0.59
% Increase in blasting cost	256.6%	109.2%	79.1%	55.7%	28.1%	17.0%	10.1%	7.3%	3.2%	1.4%	113.3%

TABLE 8.15 A summary of the combined drilling, blasting, secondary breakage and mean blending fragmentation costs for Sembehun low-grade ore

Explosive energy (kcal/st)	100	155 Contract	140	160	180	220	250	280	300	350	400
Drill	0.07	0.11	0.10	0.11	0.13	0.16	0.18	0.20	0.22	0.25	0.29
Blast	0.10	0.17	0.14	0.17	0.19	0.23	0.26	0.28	0.31	0.36	0.41
Total	0.18	0.28	0.24	0.29	0.32	0.39	0.44	0.48	0.53	0.61	0.69
Ore secondary breakage ($/st)	1.50	1.50	1.50	1.50	1.50	1.50	1.50	1.50	1.50	1.50	1.50
% O/S	41.93%	26.41%	30.11%	25.27%	21.10%	14.51%	10.84%	8.03%	6.55%	3.88%	2.26%
% U/S	58.07%	73.59%	69.89%	74.73%	78.90%	85.49%	89.16%	91.97%	93.45%	96.12%	97.74%
Net blasting cost ($/st)	0.81	0.68	0.69	0.67	0.64	0.60	0.60	0.61	0.63	0.67	0.73
Net blasting cost ($/t)	0.89	0.74	0.77	0.73	0.70	0.67	0.66	0.67	0.69	0.74	0.80
% Increase in blasting cost	355.7%	141.9%	186.1%	131.9%	98.8%	56.4%	37.3%	24.8%	18.6%	9.5%	4.9%

TABLE 8.16 Mean blending fragmentation costs for ore

Explosive energy (kcal/st)	100	142	140	160	180	220	250	280	300	350	400
Mean blend blasting cost ($/st):	0.67	0.57	0.58	0.55	0.53	0.52	0.53	0.56	0.58	0.64	0.71
Mean blend blasting cost ($/t):	0.74	0.63	0.64	0.61	0.59	0.57	0.59	0.62	0.64	0.71	0.78

TABLE 8.17 A summary of the unit costs of drilling and blasting limestone

Explosive energy (kcal/st)	100	162.5 Contract	140	160	180	220	250	280	300	350	400
Drill	0.07	0.12	0.10	0.11	0.13	0.16	0.18	0.20	0.22	0.25	0.29
Blast	0.10	0.17	0.14	0.16	0.18	0.22	0.26	0.28	0.30	0.36	0.41
Total	**0.17**	**0.28**	**0.24**	**0.28**	**0.31**	**0.38**	**0.43**	**0.49**	**0.52**	**0.61**	**0.69**
Waste secondary brkage ($/st)	1.6	1.6	1.6	1.6	1.6	1.6	1.6	1.6	1.6	1.6	1.6
% O/S	10.31%	2.84%	4.42%	2.98%	2.03%	0.98%	0.57%	0.33%	0.23%	0.09%	0.03%
% U/S	89.69%	97.16%	95.58%	97.02%	97.97%	99.02%	99.43%	99.67%	99.77%	99.91%	99.97%
Added cost of blasting	0.16	0.05	0.07	0.05	0.03	0.02	0.01	0.01	0.00	0.00	0.00
Net blasting cost ($/st)	**0.34**	**0.33**	**0.31**	**0.33**	**0.34**	**0.40**	**0.44**	**0.49**	**0.52**	**0.61**	**0.69**
Net blasting cost ($/t)	0.37	0.36	0.35	0.36	0.38	0.44	0.49	0.54	0.58	0.67	0.77
% Increase in blasting cost	94.3%	16.0%	29.1%	17.1%	10.4%	4.1%	2.1%	1.1%	0.7%	0.2%	0.1%

TABLE 8.18 A summary of the unit costs of drilling and blasting granodiorite

Explosive energy (kcal/st)	100	164.7 Contract	140	160	180	220	250	280	300	350	400
Drill	0.07	0.12	0.10	0.11	0.13	0.16	0.18	0.20	0.22	0.25	0.29
Blast	0.10	0.17	0.14	0.16	0.18	0.22	0.26	0.29	0.30	0.36	0.40
Total	**0.18**	0.29	**0.24**	**0.28**	**0.31**	**0.38**	**0.43**	**0.49**	**0.52**	**0.61**	**0.69**
Waste secondary breakage ($/st)	1.6	1.6	1.6	1.6	1.6	1.6	1.6	1.6	1.6	1.6	1.6
% O/S	5.56%	1.15%	2.04%	1.28%	0.82%	0.34%	0.18%	0.10%	0.06%	0.02%	0.01%
% U/S	94.44%	98.85%	97.96%	98.72%	99.18%	99.66%	99.82%	99.90%	99.94%	99.98%	99.99%
Added cost of blasting	0.09	0.02	0.03	0.02	0.01	0.01	0.00	0.00	0.00	0.00	0.00
Net blasting cost ($/st)	**0.26**	**0.30**	**0.28**	**0.30**	**0.32**	**0.39**	**0.44**	**0.49**	**0.52**	**0.61**	**0.69**
Net blasting cost ($/t)	0.29	0.34	0.30	0.33	0.36	0.43	0.48	0.54	0.57	0.67	0.76
% Increase in blasting cost	50.8%	6.4%	13.4%	7.4%	4.2%	1.4%	0.7%	0.3%	0.2%	0.1%	0.0%

TABLE 8.19 Changes in primary and secondary mean breakage costs of ore, with energy factor

Explosive energy (kcal/st)	100	140	160	180	220	250	280	300	350	400
Primary breakage costs, ore alone ($/st)	0.18	0.25	0.29	0.32	0.38	0.44	0.49	0.53	0.61	0.69
Secondary breakage costs, ore alone ($/st)	0.50	0.33	0.27	0.21	0.14	0.10	0.07	0.05	0.03	0.02
Mean blend blasting cost ($/st):	0.67	0.58	0.55	0.53	0.52	0.53	0.56	0.58	0.64	0.71

TABLE 8.20 Changes in primary and secondary mean breakage costs of waste, with energy factor

Explosive Energy (kcal/st)	100	140	160	180	220	250	280	300	350	400
Primary breakage (waste alone) ($/st)	0.17	0.24	0.28	0.31	0.38	0.43	0.49	0.52	0.61	0.69
Secondary breakage (waste alone) ($/st)	0.15	0.06	0.04	0.03	0.01	0.01	0.00	0.00	0.00	0.00
Mean costs of waste breakage ($/st)	0.32	0.30	0.32	0.34	0.40	0.44	0.49	0.52	0.61	0.69

TABLE 8.21 A summary of the fragmentation description data, with timed motion study data for CAT 992 front end loader

Photo Set	Single pass Cycle Time (s)	Single pass load (short tons)	Top size (in.)	F95 size (in.)	F80 Size (in.)	F50 Size (in.)	F30 Size (in.)
1	50.67	16.00	23.23	17.15	10.79	4.08	1.33
2	49.02	17.5	110.85	86.15	28.29	10.32	4.32
3	37.88	20.71	40.56	18.85	11.06	6.04	3.37
4	42.95	21.00	45.51	26.22	15.8	7.76	4.26
5	55.19	20.67	80.11	61.81	36.01	14.88	7.24
6	46.68	21.27	82.47	64.07	37.2	17.6	7.93
7	42.83	20.46	31.57	23.94	16.94	8.59	4.63
8	49.99	18.69	29.77	23.72	16.39	6.97	2.42
9	34.33	18.75	26.75	22.57	16.4	9.35	5.09
10	40.01	20.33	59.41	48.23	36.33	15.68	3.47
11	43.43	20.50	34.31	25.23	15.31	6.04	2.64
12	38.22	18.88	64.98	47.03	33.57	17.37	4.69
13	46.30	18.11	50.38	42.06	30.31	15.58	5.94
14	37.52	18.00	63.35	51.38	35.43	14.36	4.88
15	55.17	19.43	19.19	14.3	9.94	4.46	1.82

CHAPTER 9

THE RELATIONSHIP OF BLAST-GENERATED FRAGMENT SIZE DISTRIBUTION AND UNIT MINING COSTS

9.1 Overview: The requirements and scope of evaluation

The overarching aim in conducting this research has been to assess and compare the impact of the degree of blast fragmentation on the economics of a hard-rock mining operation, and to determine in the process whether increasing the blast energy could lead to a cost minimization, or a net improvement in economics.

The minimum unit cost result would be a key indicator when only costs are being evaluated. The yardstick of net improvement in economics, that is, that the sum of revenues and costs is improved, is also a viable indicator, even when only costs are being impacted by the design action (namely the change in energy factors). In such an analysis, cost and revenue effects for all unit operations along the mine-to-mill pathway should be brought into consideration, including drill, blast, load, haul, crush, grind, and flotation to produce the valuable concentrate. For each investigated change in blast energy, the costs should be deducted from revenues for the chain, so that the economic outcome of each change can be compared to the others.

Investigating the net economic benefits (using revenues and costs) is definitely the appropriate approach if there is evidence that blast-induced fragment size reduction has a

direct revenue improvement effect (possibly, in addition to also decreasing costs). An example of such a situation is, if it is possible to show that liberation is improved when blasting energy is increased. Without such evidence, the better method is to evaluate only the impact on costs.

In this dissertation, only changes in unit costs arising from changes in blasting energy factor have been investigated. The following unit operations have been demonstrated to have variations in unit cost arising from changes in the degree of fragmentation. Those changing unit costs have been evaluated and presented in the sections indicated below:

i. Drilling (Section 8.3 to 8.4)

ii. Blasting (Section 8.3 to 8.4)

iii. Crushing (Section 7.2)

It has further been demonstrated that front end loader cycle time, and the mass of material in the bucket load are not significantly impacted by fragment size distribution (Section 8.5). As no other features of blast outcome (other than fragment size distribution) have been studied in this work, it is reasonable to conclude only that blast-generated fragment size distribution has been shown to have no impact on the loader's productivity.

Given the impact of loader productivity on haul truck productivity, and in the absence of any further evidence (conceptual or otherwise practical) of haulage productivity dependency on fragmentation sizes, the conclusion has been drawn that changes in blast-generated fragment size distribution do not significantly impact or influence haul truck productivity or its unit costs.

Grinding is the last of the unit operations considered in this study to investigate the economic impact of blast-generated fragment size distribution. The range of crusher product size distributions for each blast energy input was investigated in Sections 7.2.1 and 7.2.2. These particle size distributions are plotted in Figure 7.1.

Without exception, the plots of simulated crusher product show a uniform profile, coincident with the profile of the mill feed that was sampled as feed for the grinding tests (mentioned in Section 6.2.2 and shown in Figure 6.2; size analysis reported in Section 2.1.1.2 of Appendix A). The conclusion was therefore drawn that the mill feed size distribution is independent of the blast energy intensity. Instead, the crusher configuration and settings, especially the size of the screen perforations, were seen as the determiners of the mill feed product. In the absence of measurements or data for any other mill feed characteristics to be reliably related to mill performance outcomes, the conclusion was drawn that, as far as blast-generated particle size distributions are concerned, there is no significant or identifiable impact on the grinding mill performance.

The discussions above have compelled the conclusion that there is no merit in including the stages which are not impacted by blast fragmentation in an economic evaluation in this research. Those stages include loading, haulage, and grinding. Although cost impacts of blasting on the crushing costs are negligible, the differences in unit costs of crushing are real and, hence, justify the inclusion of crushing as an important unit operation in the current economic evaluation.

9.2 The method of economic evaluation

The choice has been made to evaluate the relative effect of blast energy intensity (including its impact through fragment size distribution) by summing and comparing the various unit costs of drilling, blasting, and crushing as presented by MacKenzie (1966, 1967).

For proper rationalization, these costs must all be expressed per short ton of ore produced. This step would recognize not only the unit costs of mining waste, but also recognize that, in order for a unit mass (example, short ton) of ore to be considered mined, a certain mass of waste must be stripped off. The ratio of the mass of waste mining required to allow one unit mass of ore to be mined is the stripping ratio.

The average stripping ratio at the mine is 5:1. The unit cost of breaking a short ton of ore by blasting and crushing (taking the stripping ratio into consideration) is systematically developed in Table 9.1 (with its inset Tables 9.1a to 9.1e).

Figure 9.1 depicts the overall influence of blast energy factor on breakage costs of ore (involving drilling and blasting of ore and waste, secondary reduction of ore and waste, and crushing of ore).

The following important outcomes are observed in Table 9.1 and Figure 9.1:

i. A cost minimum **is** achieved with increasing blast energy factor, which confirms the hypothesis laid out in Section 1. 2.

ii. This cost minimum occurs at 140 kcal/st, which is a fairly low energy level, compared to the rest of the energy levels considered in the research. Being the lowest-cost design energy factor, 140 kcal/st is to be considered the optimal blast energy design factor for both ore and waste. The average energy of the contract

blast design for ore at the mine (142 kcal/st) coincides with this optimal energy. However, the average contract design energy factor for waste (180 kcal/st) costs much more, and is clearly suboptimal.

iii. The cost summation curve starts just before the graph hits minimum. It seems to imply that the unit costs would indeed go higher at lower energy levels, hence supporting MacKenzie (1966, 1967). This cost increase with lowering energy levels is expected to arise more from the cost of secondary breakage than from primary breakage

9.3 Costs of wear and tear

The costs analyzed and presented above do not include the costs of wear and tear on the mining and processing equipment (bucket teeth, tires, truck beds, crusher linings). Short of preferentially and exclusively exposing the wear surfaces of these equipment to blast rock with size distribution characteristics corresponding to the predictions for the various energy factors considered here, then assessing resulting differences in wear rates, it is unclear how to relate wear and tear trends to specific blast energy inputs. Consequently, such an analysis has not been attempted in this dissertation.

9.4 The effects on slope stability costs

It has been outside the scope of this research to evaluate the effect of changes in blasting energy on the stability of the pit slopes. However, it is conceivable that increasing blasting energy will not only exacerbate large-scale pit slope failures but also lead to back break of individual benches. Back break is ubiquitous but large-scale failure

is site-specific and hard to put a cost on. The cleanup of catch benches, which may be required by MSHA, is a significant cost, in addition to being potentially dangerous.

While these potential effects may appear obvious, there would be considerable difficulty in establishing a dependable predictive relationship with blasting energy, without a detailed and time-consuming study. Such a study should take into account the myriad other influences on the slope stability, including natural inhomogeneities. The value of such an investigation would be enhanced if it is supplemented with detailed risk assessment.

9.5 Implications for grade control, ore loss, and dilution

Grade control is impacted significantly by blasting strategy and practice (Rogers et al. 2012a, 2012b; Thornton et al., 2005). Economic gains made in achieving optimal blast fragment size may be compromised through ore losses, dilution, and miscategorization of ore. However, this research has not considered these impacts. Methods to mitigate the possibility of economic losses from these means are being well developed in industry and are effective, but require a deliberate and often studied implementation to ensure the benefits of desired blasting strategy are maintained.

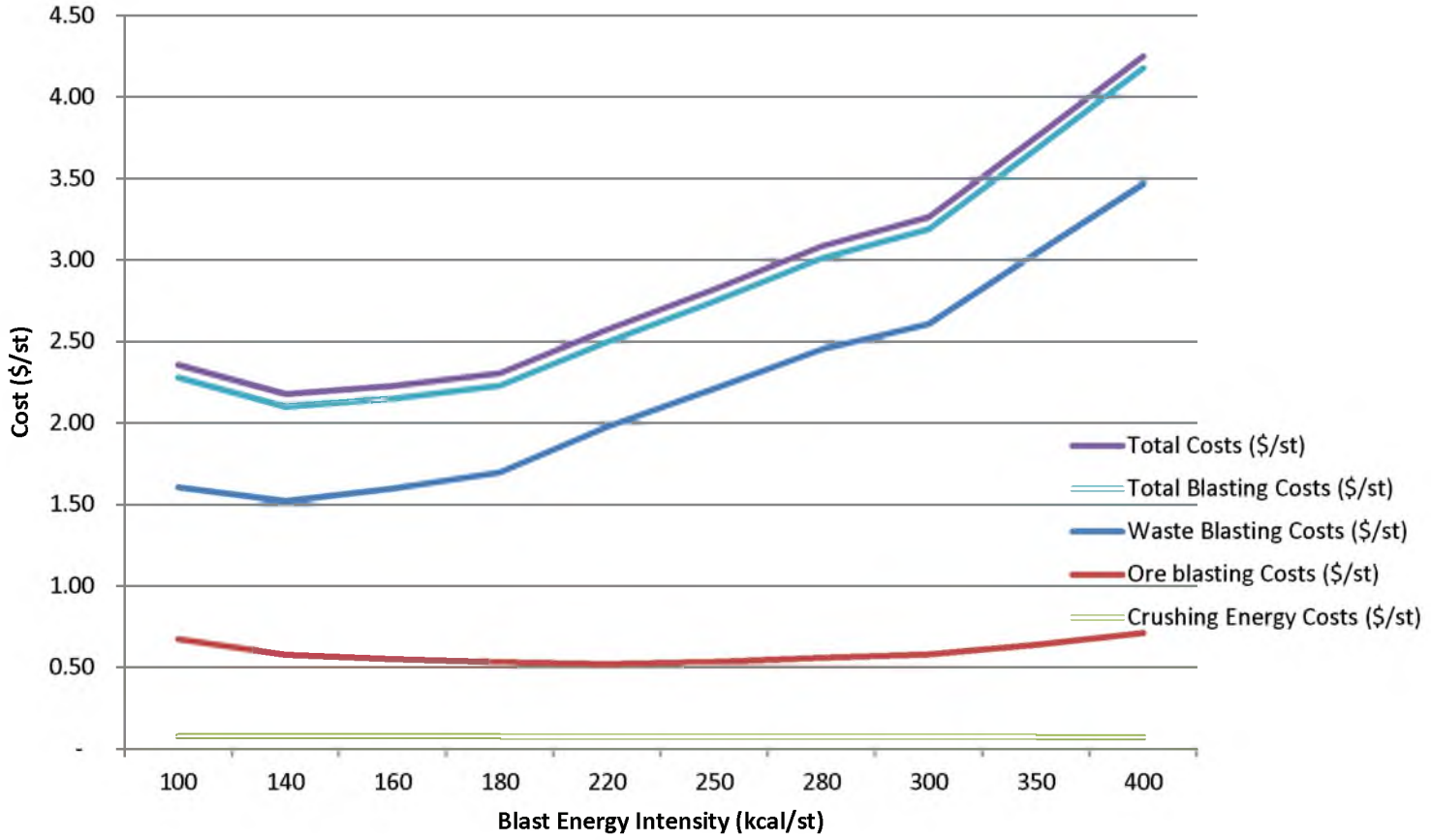

FIGURE 9.1 A plot of changes in unit cost of unit operations with blasting energy intensity

TABLE 9.1 A summary of unit costs of unit operations impacted by variations in blast-generated particle size distribution

Table 9.1a The mean cost of ore blasting

	Mean cost of ore blasting									
Explosive Energy (kcal/st)	100	140	160	180	220	250	280	300	350	400
Mean Blend blasting cost ($/st):	0.67	0.58	0.55	0.53	0.52	0.53	0.56	0.58	0.64	0.71

Table 9.1b The mean cost of waste blasting

	Mean Net Waste drilling & blasting cost ($/st) (Ratio = 0.75 Limestone : 0.25 Granodiorite)									
Explosive Energy (kcal/st)	100	140	160	180	220	250	280	300	350	400
$/st	0.32	0.30	0.32	0.34	0.40	0.44	0.49	0.52	0.61	0.69

Table 9.1c The combined cost of waste and ore blasting ($/st of ore mined)

	Combined cost of drilling and blasting ore and waste (Ratio: 5 Waste : 1 Ore) ($/st of ore)									
Explosive Energy (kcal/st)	100	140	160	180	220	250	280	300	350	400
Waste	1.60	1.52	1.60	1.70	1.98	2.21	2.45	2.61	3.04	3.47
Ore	0.67	0.58	0.55	0.53	0.52	0.53	0.56	0.58	0.64	0.71
Total	2.28	2.10	2.15	2.23	2.50	2.75	3.01	3.19	3.68	4.18

Table 9.1d Crushing energy costs

	Crushing Energy Costs									
Explosive Energy (kcal/st)	100	140	160	180	220	250	280	300	350	400
$/st	0.079	0.078	0.077	0.077	0.076	#####	0.075	0.075	0.073	#####

Table 9.1e The combined cost of breakage (per st of ore)

	Combined unit cost of breakage - mine and crusher									
Explosive Energy (kcal/st)	100	140	160	180	220	250	280	300	350	400
$/st	2.36	2.18	2.23	2.31	2.57	2.82	3.09	3.26	3.75	4.25

CHAPTER 10

SUMMARY, OBSERVATIONS, DISCUSSIONS, RECOMMENDATIONS, AND CONCLUSIONS

10.1 Summary of research process

The object of this dissertation was to provide an answer to questions about the validity of often-repeated claims in the mining industry that reduction of the size of fragmented rock through increasing blasting energy eventually leads to improved mine economics. The claim has been demonstrated as true for the operation in this research. However, the improved economics have been only in a cost minimization sense (rather than in an increased revenue sense), and apply principally to the costs of primary blasting and secondary reduction. The impact on crushing energy costs is negligible, and grinding costs do not appear to be affected by blasting energy.

This research was carried out at a copper mining operation in southern Utah, and involved the use of a range of modeling and simulation techniques. The procedure for the investigation involved initially carrying out rock characterization for ore and waste at the mine. This characterization involved recording various in situ rock mass characteristics, and then sampling and coring of materials for laboratory testing for geotechnical properties. Crusher products (grinding mill feeds) were also sampled and later processed in a laboratory, through a structured set of grinding tests.

Data obtained from the geotechnical tests were used to estimate the Kuz-Ram rock factor, A. Data from batch grinding tests were used to generate population balance modeling parameters for eventual use in milling simulation. However, it was later determined that the particle size distributions resulting from blasting may not bring any noticeable benefits into grinding mill performance. As a result, all grinding simulation-related work done for the purpose of this research was discontinued.

In addition to a base case set of blast designs that are in use by the host mine for this research, ten blast designs were developed and the fragmentation outcomes for each of them were simulated using the Kuz-Ram model. Oversize and undersize estimates were made.

Crushing simulation was done for a three-stage crushing plant, and the impact of various blast-generated feed size distributions on crushing energy and crushing product size distribution was investigated. Crushing simulation was done using MODSIM™.

Time and motion studies were conducted, and photogrammetric and statistical analyses were done to evaluate the effect of particle size distribution on load and haul productivity.

Costs were estimated for drilling, blasting, and crushing, which were the principal unit operations inferred to be affected in some meaningful way by the varying intensities of blast energy input.

Using costs alone, and no revenue streams, cost performances were investigated corresponding to the range of blast energy factors, and conclusions were drawn about the validity of the claim about the benefits of increasing blast energy intensity. Those conclusions are outlined along with the findings in the next section.

A schematic, summarizing the research process, is outlined in Figure 10.1.

10.2 Summary of findings

The following findings were made:

i. The blast-generated fragment size distribution does not significantly impact the loader and haul truck productivity.

ii. The impact of the crusher feed size distribution (blast-generated fragment distribution) on the crusher energy is limited to the primary crusher, where various fractions of feed may fall through, unmodified. However, the energy savings from increasing blasting intensity are negligible and do not justify the additional blasting energy costs.

iii. The restrictions imposed by the gape of the crusher are significant. These restrictions lead to substantial additional operational costs in secondary breakage. In general, jaw crushers are relatively inexpensive compared to gyratory crushers, and are often preferred at the start of projects because of minimizing start-up capital cost requirements. However, considering the significant increase in operating costs that may be imposed by the feed size restrictions, the economic merit in the long-term use of the jaw crusher is questionable.

iv. Beyond the primary crusher, the energy consumption and final product particle size distribution have no relationship to the size distribution characteristics of the crusher head feed (the blasting product).

v. In the crushing circuit, the finest screen openings impose an overwhelming influence on the size distribution of the final product, far more than any influence possibly contributed by the blast energy intensity.

vi. There has been no evidence from this work that any beneficial influences of blast-generated fragment size distribution reach the grinding mill.

10.3 Other observations

i. While there is fall-through material in the crusher feed at the prevailing fragment size distribution, the quantities thereof and the throughput advantage arising from installing a scalping apparatus does not suggest there will be a sufficiently large economic benefit to justify such an investment.

ii. Secondary size reduction is a significant cost that impacts both ore and waste rock handling. Due to contract obligations at the host mine, in which the costs of oversize are often shared, it is not often seen as a significant enough issue. However, if blasting was a fully in-house task, the full cost of inevitable secondary reduction would be carried by the mine owner. Hence, operating within the optimal blast range is desirable.

iii. The prediction of blast fragmentation outcomes is a highly imprecise engineering effort that is heavily subject to the technical judgment and perceptiveness of the evaluator. Much of the imprecision also arises from the inhomogeneities inherent in rock formations. As much as the prediction models are continuously refined, the vast array of factors that together have some impact on fragmentation outcomes will only continue to complicate prediction efforts in the future. More

comprehensive and efficient computing solutions are needed. Until these more efficient solutions are obtained, it is conceivable that the use of simpler prediction procedures like Kuz-Ram will continue to be the practical methods well into the future.

10.4 Discussions

i. The benefits of fragmentation-related mine-to-mill process optimization appear to be operation-specific. Benefits and solutions for one site may not apply at another.

ii. An operation that uses a crusher with a relatively low throat capacity is more likely to bear the costs of secondary breakage than another mine which, with otherwise the same circumstances of operation, uses a larger throat capacity, such as with a gyratory crusher. In the latter case, the optimal range of the cost curves would shift to the left, implying a lower unit cost of fragmentation.

iii. It is conceivable that blast-generated microfractures would be more beneficial to an operation using a SAG mill than one using exclusively equipment-induced breakage stresses, such as cone crushers or jaw crushers. Blast-generated micro-fractures may more gradually grow and yield their benefits within the context of a SAG mill.

iv. In an operating mine, the use of the energy factor strategy for mining cost optimization, as demonstrated in this research, must always consider the short-term stripping ratio, rather than the overall stripping ratio as done here. Optimal ranges of blast energy factor may shift through the months with the changes in

tonnages of ore and waste. Also, such a strategy would work best when blasting is carried out in-house, since blasting contracts would normally require a more fixed set of terms for blasting patterns.

v. Before implementing the energy factor strategy arising from this research, the operation will need to review the rocks that are being mined at some time in the future. This research has been mostly based on rocks that were in the path of mining between February and October 2014, and different rocks with other characteristics may impact the costs differently.

10.5 Future research

A major realization in this research is that fragment size distribution alone may not suffice in the study of the impact of blasting on the economics of the mine-to-mill pathway. A deeper understanding of the interaction of fragment size distribution and other muck pile characteristics as well as the size and method of a mining operation may bring further clarity to the question of the impact of blasting. In view of this realization, the following suggestions are made as useful directions for the advancement of knowledge in this field:

i. Investigate the impact of the degree of interlock of rock fragments on loading rates and mining productivity.

ii. Evaluate the impact of blast-generated microfractures on the crushing and grinding energy requirements of ore

iii. Explore the development of models for microfracture development in a given blast design.

iv. Investigate the changes, if any, in mineral liberation that may arise from blast-induced microfractures.

v. Evaluate the impact of the scale (size) of a mining operation on the benefits of a mining optimization strategy that is based on blasting energy factors.

vi. Assess the blasting energy factor strategy implications for operations using jaw crushers, gyratory crushers, or SAG mills.

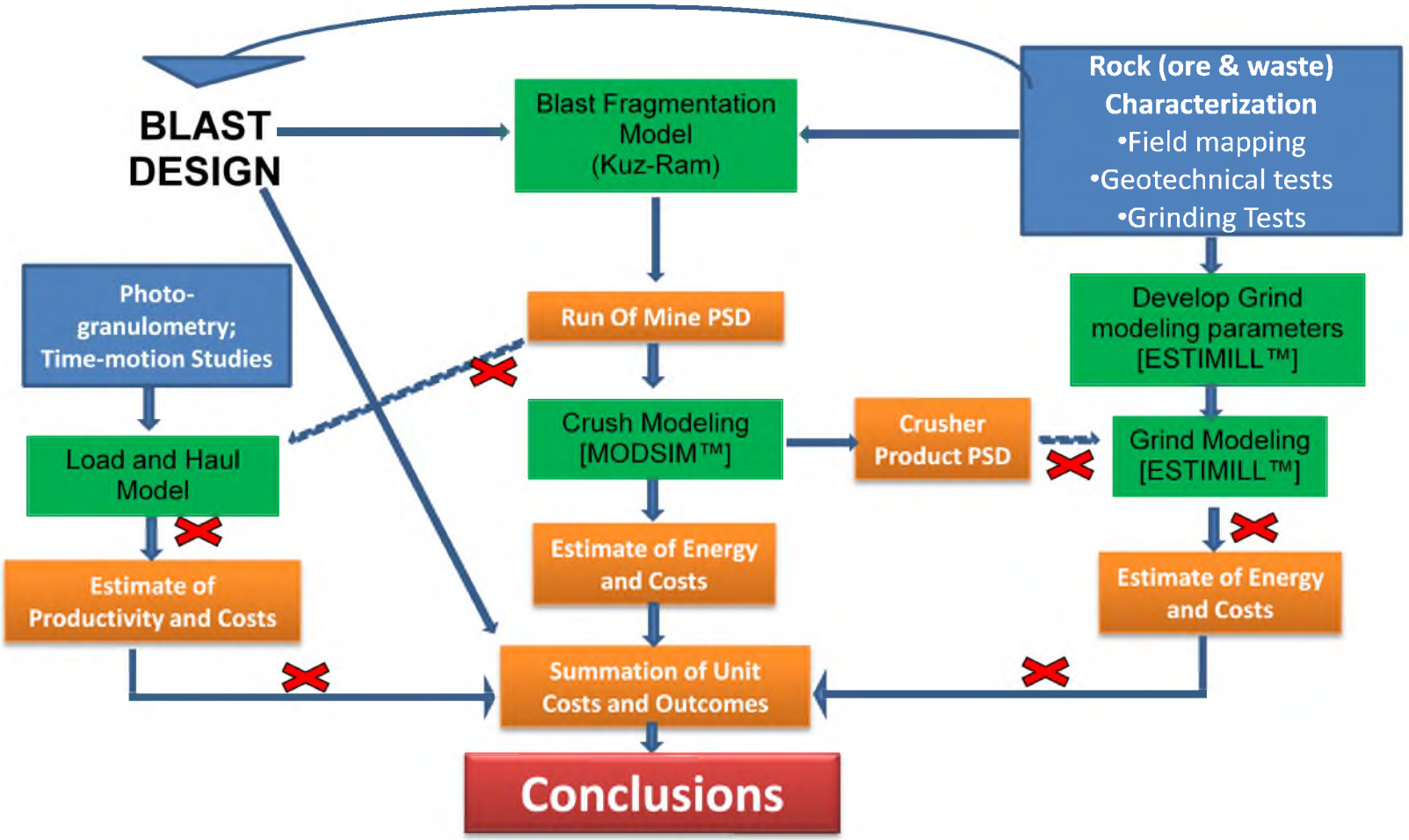

FIGURE 10.1 A schematic of the research process

Note: Framework of summary was adapted from JKMRC 2012

APPENDIX A

GRINDING REPORT

A REPORT ON THE MODELING AND SIMULATION OF GRINDING AT

THE W.U.S. COPPER PROCESSING PLANT

CONTENTS

A REPORT ON THE MODELING AND SIMULATION OF GRINDING AT THE W.U.S. COPPER PROCESSING PLANT

A.1 Background and overview

The development of this report in an appendix, rather than as part of the central dissertation report, became necessary after the observation had been made that the particle size distributions produced from crushing feeds from the range of blast designs are invariant (see Chapter 7). No matter what the blast design and the resulting blast product, the particle size distribution of the crusher product (mill feed) remained approximately the same. The conclusion was thus drawn that, if the crusher products for all streams of blasting product (low, medium, and high energy factor blasts) gave rise to essentially the same particle size distribution of grinding mill feed, then there was no justification in carrying out simulations for more than one grinding head feed. All head feed size distributions would be the same.

In other words, if the size distribution of the crushing product is influenced more by the crushing circuit than by the blast energy infusion, then a dedicated discussion of grinding theory and an account of the grinding tests within the main text of the dissertation is not justified. Such a discussion of the grinding exercise adds no significantly beneficial insight to the central question in the research.

The reader is urged to note that the conclusions above were made without an investigation into the issue of blast-generated micro-fractures. Indeed, it remains to be seen whether the influences of micro-fractures generated within the crushing circuit do or do not exceed those generated within a blast.

In spite of the recognition that this grinding report would not lend significantly to the discussion in the main part of the report, the author is of the view that an understanding of the grinding behavior of the ore may find use in other efforts.

This report is prefaced by the theory underlying the method of simulation, namely the population balance model. The development of the grinding equations and the phenomenological representation of the grinding sub-processes is outlined, followed by a detailed account of the procedures implemented in the grinding test.

A.2 Population balance models for grinding simulation: The linear breakage kinetics model and its batch solution

According to Herbst et al. (1968), perhaps the most practical form of the grinding models arising from the population balance approach is the linear lumped parameter models describe in this section. Expressed as linear, size-discretized kinetic mass balanced expressions, the models are obtained by dividing the particulate assembly being milled into n narrow size intervals, (x_i, x_{i+1}), where i = 1, 2,..,n.

The strength of these models lies in their ability to mathematically describe the key grinding sub-processes of breakage, classification and material transport.

The breakage component of the grinding process is characterized by two physically interpretable quantities, namely, the selection function and the breakage function. The

selection function gives the fractional rate of breakage of particles within each size interval. The breakage function gives the average size distribution of daughter fragments resulting from the primary breakage events. Together, these two quantities allow the mathematical representation and modeling of the behavior of each size fraction in the mill.

Consider a batch milling situation. For size interval i = 1, 2,…., n, the mass balance in the i^{th} size interval within this mill at time t is given by:

$$\frac{d[Hm_i(t)]}{dt} = -S_i Hm_i(t) + \sum_{j=1}^{i-1} b_{ij} S_j Hm_j(t) \qquad (A.1)$$

Where:

$m_i(t)$ is the mass fraction of material in the i-th size interval

H is the total mass of material being ground

S_i is the size-discretized selection function for the i-th size interval; it denotes the fractional rate at which material is broken out of the i-th size interval

b_{ij} is the size discretized breakage function; it represents the fraction of the primary breakage product of material in the j-th size interval that appears in the i-th size interval

When the selection and breakage function parameters are independent of both the size consist in the batch mill and time, this kinetic model is linear with constant coefficients (Herbst et al. 1977).

The set of n simultaneous differential equations in Equation 1 above may be conveniently represented by a single matrix equation,

$$\frac{d[\underline{H}\underline{m}(t)]}{dt} = -[\underline{I} - \underline{B}]\underline{S}\underline{H}\underline{m}(t) \qquad (A.2)$$

For a batch mill with feed size distribution $\underline{m}_{BATCH}(0)$, H is a constant. This equation allows an analytical solution to be readily obtained by standard matrix techniques:

$$\underline{m}_{BATCH}(t) = \exp(-[\underline{I} - \underline{B}]\underline{S}\,t)\underline{m}_{BATCH}(0) \qquad (A.3)$$

For the situation where no two selection functions are equal, the matrix exponential is then readily simplified by a similarity transformation to give:

$$\underline{m}_{BATCH}(t) = \underline{T}\,\underline{J}(t)\underline{T}^{-1}\underline{m}_{BATCH}(0) \qquad (A.4)$$

Where:

$$T_{ij} = \begin{cases} 0 & i < j \\ 1 & i = j \\ \sum_{k=j}^{i-1} \frac{b_{ik}S_k}{S_i - S_j} T_{kj} & i > j \end{cases}$$

$$J_{ij}(t) = \begin{cases} \exp(-S_i t) & i = j \\ 0 & i \neq j \end{cases}$$

This equation plays a central role in describing both batch mill and continuous grinding simulation situations.

A.2.1 Material transport and product size distributions

In the use of the population balance model, the continuous grinding environment must be represented not only by breakage kinetics, but also by a mathematical description of the material transport though the mill. Ideally, a distributed parameter model should be used to account for variations down the length of the mill providing the desired relationship between input and output mass flow rates and size distributions (Mika, 1970). However, a relative simplification is obtained on the basis that linear kinetics prevail and that all particle sizes are characterized by a single residence time distribution. Hence, a general relationship is obtained without requiring a detailed model for particle transport within the mill.

In the analysis to formulate the mill transport model, Herbst et al. (1977) recognized that linear systems have the properties of additivity and homogeneity (Himmelblau et al., 1968; Levenspiel and Bischoff 1963). The additive properties of the linear system mean that arbitrary inputs can be represented as the sum of responses of the system to a series of appropriately-weighted impulses. Thus, at steady state, the product size distribution from an open circuit mill, $\underline{m}_{MP}$, is determined by the sum of the responses of the mill to the feed size distribution $\underline{m}_{MF}$, introduced as a sequence of impulses. Hence the product size distribution is given by:

$$\underline{m}_{MP} = \int_0^{\infty} \underline{m}_{BATCH}(t)E(t)dt \qquad (A.5)$$

Where:

$\underline{m}_{BATCH}(t)$ is the response of the mill, operated in a batch fashion with an initial size distribution, $\underline{m}_{BATCH}(0)$. $\underline{m}_{BATCH}(0)$ is equivalent to the steady state size distribution of the mill feed, $\underline{m}_{MF}$.

E(t)dt is the exit age (residence time) distribution of the material. The residence time distribution is an experimentally-determinable function which denotes the mass fraction of material in the mill discharge which has resided in the mill for a time interval t to t+dt.

The residence time distribution function that is applicable in the above grinding solution depends on the kind of flow regime under consideration. Latchireddi (2013) observed that several transport models are candidates for the description of the resident time distribution, E(t), in mills, of which the mixers-in-series model appears to be the most suitable. Indeed, Herbst et al. (1977) found it appropriate and highly flexible to use the mixers-in-series model (in addition to the plugflow model for batch mill situations) in the program Estimill, for the simulation of grinding circuits.

According to the mixers-in-series model,

$$E(t_i) = \frac{j^j}{\tau^j} \frac{t_i^{j-1}}{\Gamma(N)} \exp\left(-\frac{j}{t} t_i\right) \tag{A.6}$$

Where:

N is the number of mixers in series

τ is the mean residence time

Γ is the gamma function

By substitution of this model into Equation A.5, an open-circuit solution is obtained, which is written compactly as:

$$\underline{m}_{MP} = \underline{T}\,\underline{J}_C(\tau)T^{-1}\underline{m}_{MF} \qquad (A.7)$$

Where:

$$J_{ij}(t) = \begin{cases} \int_0^{\infty} \exp(-[S_i\tau]\theta)E(\theta)d\theta & i = j \\ 0 & i \neq j \end{cases}$$

A closed circuit solution is obtained by applying Equation A.7 above, and applying a mass balance around the classifier, yielding:

$$\underline{m}_{MP} = \underline{L}(H/M_{MF})\underline{m}_{MF} \qquad (A.8)$$

Where:

$\underline{T}\,\underline{J}_C(\tau)T^{-1}\underline{m}MF$ has been replaced by $\underline{L}(H/M_{MF})\underline{m}_{MF}$. In addition to reducing the complexity of the subsequent equations, this replacement also emphasizes the dependence of the product size distribution on the mass flow rate, M_{MF}, which has significant implications for optimization of grinding mill performance.

A fuller treatment of the residence time distribution, its development and the considerations and analyses that yield its contribution to the solution of the mill product size distribution equation (Equation A.5) for all circuits (plugflow, open, closed and reverse-closed) is outlined in the Estimill manual (Herbst et al. 1977).

A.3 Grinding parameter estimation

To be able to meaningfully use the kinetic model in the population balance framework demonstrated above, various parameters must be estimated. According to Herbst et al. (1977), the parameter estimation problem can be treated as an objective-function minimization problem such that, given a set of experimental grinding data (whether batch, open or closed-circuit type), the solution algorithm must find the selection and/or breakage function values which minimize the deviations between model predictions and the experimental data. Mathematically, the expression is:

Find: $(S_i, b_{ij}) = \hat{S}_i, \hat{b}_{ij}$ such that $\hat{S}_i, \hat{b}_{ij}$ yields the smallest possible value of the objective function:

$$\Phi = \sum_{k=1}^{m} \sum_{i=1}^{n} W_i \left(m_{ik_{exp}} - m_{ik_{model}}(S_i, b_{ij}) \right)^2 \qquad (A.9)$$

This estimation is mathematically complicated for the following reasons:

i. $m_i^{model}(S_i, b_{ij})$ is non-linear in the unknown parameters. Thus, the parameter estimation is not amenable to traditional linear regression procedures.

ii. $\hat{S}_i, \hat{b}_{ij}$ must satisfy certain physical constraints

iii. The number of parameter values is very large, generally on the order of 100 for a product size distribution consisting of 10 size fractions

A.3.1 Solution to the parameter estimation problem

Herbst et al. (1977) successfully solved the first two of these difficulties, using the more efficient modified Gauss-Newton non-linear regression solution procedures. These

procedures are based on a linear Taylor series expansion of the model equations around a set of initial estimates of the parameters. The approximate model arising from each expansion is linear in a set of parameters that can be solved by conventional linear regression methods. The expansion is a stage-wise process, such that parameter estimates at each stage feed as a base point into the next stage. After numerous iterations, convergence is achieved that satisfies the optimization conditions set forth in Section A.3.

To be valid, non-negativity constraints are imposed on the solutions. A computational loop is created to produce ever declining values of the parameters, until convergence is achieved.

A.3.2 Reduction of the number of parameters

Herbst et al. (1977) overcame the third and final obstacle to effective parameter estimation, namely the large number of values of (S_i, b_{ij}), by adopting the use of two functional forms, one each for the selection and breakage functions.

The functional form chosen for the breakage function was a three-parameter formulation representing the cumulative function $\left(B_{ij} \equiv \sum_{k=1}^{n} b_{kj}\right)$, that is:

$$B_{ij} = \alpha_1 \left(\frac{X_i}{X_{j+1}}\right)^{\alpha_2} + (1 - \alpha_1)\left(\frac{X_i}{X_{j+1}}\right)^{\alpha_3} \qquad \text{(A.10)}$$

This equation is a weighted sum of two normalizable Gaudin-Schuhmann distributions. It yields a breakage function that is linear on log-log plot in the fines range

of particle sizes. At larger fragments, approaching the parent fragment size $\left(\frac{X_i}{X_{j+1}} \rightarrow 1\right)$, linearity is lost.

The functional form chosen to represent the selection function was a log-polynomial of adjustable order. The equation is:

$$S_i = S_1 \exp\left(-\sum_{j=1}^{J} \zeta_j \left[\ln\left[\sqrt{X_i X_{i+1}}/\sqrt{X_1 X_2}\right]\right]^j\right) \qquad \text{(A.11)}$$

This is a J-th order polynomial on log-log paper. Typically, J = 1, a straight-line dependence in log-log space (a power law), or J = 2, which is a quadratic dependence, is sufficient to describe experimental selection functions.

As a result of this simplification of the parameter representation, a several-fold decrease is achieved in the number of both the breakage and selection functions. The number of parameters required to describe the breakage function is three (α_1, α_2, α_3), and two or three for the selection function (S_1, ζ_1, and ζ_2).

A.3.3 Initial parameter estimates

The generation of final parameters in Estimill requires the use of initial estimates of [S1, ζ_1….] and/or [α_1, α_2, α_3]. There are two methods normally used for these initial estimates, namely, the Direct Measurement Method and the General Starting Point, called here, *the rough approximation*.

A.3.3.1 Direct Measurement Method *(Source: Estimill Manual, Page 13)*

This method involves performing a series of batch grinding experiments on a single monosize feed to determine the top size selection and breakage function values directly (Mika et al., 1967; Herbst and Fuerstenau 1968). The initial estimates of α_1, α_2, α_3 ($\alpha_3 > \alpha_2$) can be determined by plotting the experimentally measured breakage function on log-log space. Typically, for small fragment sizes, ($X_i/X_{j+1} \rightarrow 0$), since $\alpha_3 > \alpha_2$, Equation 10 reduces to:

$$B_{ij} = \alpha_1 \left(\frac{X_i}{X_{j+1}}\right)^{\alpha_2} \tag{A.12}$$

This equation of a straight line of slope α_2, and intercept (at $x_i/x_{j+1}=1$) of α_1. Thus, α_1 and α_2 are obtained by drawing a straight line through the fines range of the breakage function (see Figure A1). Knowing α_1 and α_2, α_3 is obtained as the gradient of a log-log plot of the following rearranged form of Equation 4.22:

$$\frac{B_{ij} - \alpha_1 (X_i/X_{j+1})^{\alpha_2}}{1-\alpha_1} = \left(\frac{X_i}{X_{j+1}}\right)^{a_3} \tag{A.13}$$

Herbst et al. (1977) note that S_1 should be taken as the experimentally measured value from the monosize grind results (also: Mika et al., 1967; Herbst and Fuerstenau 1968), and ζ_1 can be chosen as approximately equal to α_2 above.

A.3.3.2 General starting point estimates

An alternative approach to the above method for generating the range of parameters is to use a rough approximation (*general starting point* or *rough approximation*). Values recommended by Herbst et al. (1977) are:

$\alpha_1 = 0.8$; $\alpha_2 = 0.5$ $\alpha_3 = 2.5$

$\zeta_1 = 0.5$; $\zeta_2 = \zeta_2 = 0$

A.3.4 Refined estimates of breakage parameters

After the initial estimate of the breakage function parameters, a least squares adjustment may be done, to minimize the difference between model and experimental values for the parameters. Note that a similar least squares adjustment is done for S_1, as will be described in Section A.7.1. Beyond this point, a Gauss-Newtonian refinement of the range of parameters (selection, breakage, and adjustable parameters) is done in Estimill to facilitate grinding prediction. There is an option to either estimate selection functions only (given breakage functions), or to simultaneously estimate both selection functions and breakage functions. According to Rajamani (pers. comm. July 2014) experience has shown that the option of estimating selection functions only (given breakage functions), is sufficient for purposes of simulation. The estimation of both breakage and selection functions together does not meaningfully improve the preliminary estimates of breakage function. On the other hand, it could reduce the overall quality of the parameter estimates, yielding larger residuals of estimation.

A.4 Scale up and grinding simulation/prediction issues

It is known (Herbst 1971; Herbst et al 1973; Malghan and Fuerstenau 1976) that, for dry grinding situations, the size-discretized selection functions are proportional to the specific power draft input to the mill (P/H), so that:

$$S_i = S_i^E(P/H) \tag{A.14}$$

Where:

S_i^E is termed the "specific selection function", with units of t/kWh

P is the net power draft (in kilowatts) of the mill in which the data to be used for estimation is to be obtained

H is the mass holdup of material in the mill (in tons, t).

Unlike dry grinding, wet grinding is inherently non-linear. The spatial distribution and characteristics of material in the mill is believed to play an important role. According to Herbst (1971), Kim (1974), Siddique (1977), and Bhattacharyya (2014), apparently, the fine particles tend to suspend in the water, while the coarse particles are settled in the ball mass, resulting in an increased probability of breakage of the coarse particles. Thus, values of S_i and S_i^E are influenced by the mill consist, and therefore, may give inaccurate predictions in scale-up situations.

However, if estimates of specific selection function are obtained in the batch mill for "a similar fineness of grind" to that for which predictions are required in the larger mills, these values should allow predictions of large mill behavior in the "neighborhood" of the size distribution used for estimation. The procedure for similar-fineness-of-grind

estimates are well described by Siddique (1977). The procedure was implemented in this research, as reported in Section A.7.5.

A.5 Size classification: Screens and cyclones

One of the strengths of the population balance model is the ability to account for size classification, which is one of the key sub-processes in grinding. The tool that provides the means to track classification in the grinding system is the performance curve (also known as a partition curve or partition function). To estimate the parameters for a cyclone partition function, the following data are required:

i. The particle size distribution of the cyclone feed (which is also the particle size distribution of the mill product
ii. The particle size distribution of the cyclone overflow
iii. The particle size distribution of the cyclone underflow
iv. The percent solids of all three streams

The procedure to construct the partition curve is well documented in *Wills' Mineral Processing Technology* (Wills 2006).

A.6 Grinding test work

Grinding tests were carried out as part of this work to enable the estimation of the breakage parameters for simulation of grinding of the W.U.S. Copper ore. The key breakage parameters required in the use of the population balance model for the simulation of grinding are the selection function, the breakage function, and the set of associated adjustable parameters. In addition, the cyclone classification function is

required. The procedure used to develop these parameters in this work, from sampling to parameter estimation, is outlined in the following sub-sections.

A.6.1 Sample collection and preparation

Samples for the grinding test were obtained from the mill feed stockpile at the W.U.S. Copper ball mill plant. Feed on this stockpile was typically a crushed mix of ore from the Bom and Sembehun pits, blended in the ratio 1:2, with the Sembehun high and low grade ores being in the ratio 1:1. Ore blending at the site is primarily on the basis of grade, but also of hardness, and is carried out by front-end loader as the crusher is fed. The end product is a fully mixed feed, representing the intended blend. This ratio has been assumed in constituting the hypothetical feed of blast end products into the virtual crusher in the MODSIM simulation (see Section 6.2.1, iv of main report).

Two sets of sample were prepared, a monosize sample and a natural size distribution feed sample.

A.6.1.1 Preparation of monosize feed sample

A monosize 4 x 6 Tyler mesh (minus 4 mesh plus 6 mesh) sample was prepared, corresponding to -4760 microns (-4.760 mm) +3360 microns (+3.36 mm). This preparation was done in two stages. In the first stage, the air-dried crusher run (fresh mill feed) was randomly grab-sampled from various parts of the stockpile using a spade. The sample was rough-screened directly at the stockpile site. Two sizes of screens, the Tyler 4 mesh and the Tyler 6 mesh screens, were used for this purpose. The two-screen stack was agitated by hand until little or no more undersize discharge was observed. The plus-

4 mesh and minus-6 mesh materials were discarded. Batch after batch of material was grab-sampled and processed as above, until a total of about 15 kg of rough monosize material had been obtained.

The second stage of monosize sample preparation was at the grinding laboratory at the University of Utah. In a repeated process, until the entire set of roughly-screened sample described above had been processed, approximately 2 kg of rough-monosize material at a time was placed in a bank of three screens, of Tyler size sequence 4mesh, 6mesh, 8mesh and pan. This stack of screens, with their content of about 2 kg of material, was set up on a Retsch™ AS 200 vibratory sieve shaker and vibrated for 10 minutes, to obtain a "clean" monosize 4 x 6 mesh sample. A total of approximately 14 kg of "clean" monosize fraction was acquired through this process.

Calculations were performed to determine the amount of feed that would constitute the required slurry density and percent mill filling. This quantity was determined to be 2.0017 kg. From the clean set of monosize material, 5 lots of 2.0017 kg were weighed out for grinding. Details of the grinding conditions at the mine-site mills which the test grinding conditions would mimic, are specified in Table A1. Table A2 provides details of quantities used at all stages of the monosize grind.

A.6.1.2 Preparation of natural size distribution feed sample

As with the monosize material, the natural size distribution feed sample was grab-sampled from the crusher run pad. Careful steps were taken to ensure that none of the oversize or undersize rejects from the monosize sample rough preparation mentioned in

Section A.6.1.1 was used in this stage of sample collection. About 20 kg of un-screened sample, so obtained, was transferred to the grinding laboratory at the University of Utah.

The preparation of the sample for the natural size grind was more complicated and painstaking than that for the monosize grind sample. The objective was to obtain about 6 lots of 2.0017 kg, all identical in terms of content and particle size distribution. One of these identical samples would be used for size analysis. To achieve representative sampling, approximately 10 kg of the material was placed into a 12-cup spinning automatic sampler. Six fractions (each in a separate cup) were selected and weighed. The selected fractions were labeled A to F. In all cases, the weight was less than the desired 2.0017 kg. The remaining 6 cups were discharged again into the sampler's bin and split into another 12 fractions. From this, six fractions were selected and each selected fraction added to one of the first six samples A to F. The rest were returned to the sampler's hopper and split again. Thus, progressively, samples A to F were built up into approximately 2.0017 kg, each expected to be representative of the natural size feed.

One of the six sets of samples obtained by the procedure above was used to estimate the particle size distribution of the natural size feed. Using the automatic sampler, about 0.3313 kg of sample was obtained for the size distribution analysis (see mass of sample at zero minutes grind in Table A3).

A.6.1.3 Grinding test equipment

A 10-inch diameter stainless steel laboratory-scale batch ball mill, 11.5 inches long, was used in this work (see Figure A2). The mill is fitted with eight lifter bars of 19mm wide x 5mm high cross-section. It is opened (or shut) using a lid that fits firmly into a

rectangular opening on the side of the mill drum. This opening is used to load and/or discharge feed, balls, water and slurry into or out of the mill. The lid is locked into place with a set of bolts, driven by a powered hand-drill. The contact between the mill body and the lid is sealed with a polyurethane gasket, to ensure a firm fit while preventing leakages during milling.

The mill is equipped with a Graham variable speed transmission. The transmission shaft is fitted with a Futek model torque sensor that measures power draft (torque), and provides a serial interface for digital recording on a computer. Maximum capacity of the sensor is 100 Nm. Readouts of torque were obtained as voltage units, and converted to torque values in Nm by a multiplier of 2.0931. This conversion was obtained through a previous calibration process analogous to the use of a Prony brake absorption dynamometer.

Since the purpose of the grinding test was to generate parameters for simulation of an actual operating plant at the W.U.S. Copper mine, the decision was made to operate the test (batch) mill using grinding conditions identical to those in use at the full-scale mill. This similarity of operating conditions would minimize complications in scale up and simulation, and generally justify the application of prevailing scale up models. In line with this philosophy, the tests were designed based on details obtained about the standard operating conditions of the mill at mine site. These conditions included 35% ball filling, 70% solids, 100% slurry filling, 65-70% of critical speed (N_c*), and 100% slurry filling. Steel balls were used as grinding media, with the distribution of ball diameters approximating an equilibrium charge distribution. Ball top size used was 50.8mm (2 inches) and the scrap size 12.7mm (0.5 inches) (see Table A1). The equilibrium ball size

distribution was calculated based on linear wear theory (Vermeulen et al. 1983; Scaw Metals Group). A string of balls fitting this distribution, and weighing a total of 24.2 kg (see Table A1), was constituted in the grinding laboratory and used in the experimental runs.

A.6.2 Testing procedure

A.6.2.1 Monosize feed grind

Wet grinding of the monosize sample was carried out. The grinding procedure followed a basic set of steps conventionally used for batch grinding in comminution laboratories, and is well described in existing literature and publications (Siddique 1977; Herbst et al., 1983). The sequence was as follows:

i. The mill was charged with balls and feed material in a layer loading manner, with alternating layers of balls and feed. This layering was intended to improve the mixing process at the start of the test. Using a measuring cylinder, 858 cm^3 of water was added to the mill, which was the amount of water required to achieve the desired percent solids in the mill charge (see Table A1). The lid was screwed on and checked to ensure there was no leakage.

ii. A computer was connected to the torque sensor of the milling apparatus, via serial-USB and batch milling software interface, to record the milling torque. The speed of rotation had been pre-set at approximately 66 % of critical speed. This preset speed was not modified, but was verified in several preliminary runs, using a laser tachometer with a digital readout.

iii. The batch mill was run in the following five different successions of time: 1, 3, 5, 7 and 9 minutes. In each instance, a fresh lot of feed was used. This use of fresh feed at each run represented a major departure from traditional tests. In traditional procedures, the same material is used as feed in each grind and subsequently reconstituted for the next run after particle size analyses of the previous run's product had been measured (Siddique 1977).

iv. Ball wear was assumed to be sufficiently negligible to be invariant in the entire series of tests. This assumption was made in consideration of the relatively short durations of milling run, the small quantities of feed and balls used in this experiment, and the typical wear rates of steel media in mills.

v. After each of the five grinds, the mill was opened, emptied and washed thoroughly. The contents (ball and slurry) were carefully discharged into a receiving chamber located beneath the mill. The base of this chamber was equipped with gratings that retained the ball media while letting the grinding product through into a bucket located below. Care was taken to minimize or prevent loss of content.

vi. Due to the large amount of wash water used to clean out the mill, the milling product needed to be filtered. Pressure filtration was carried out using a filter press and the filter cake obtained was oven-dried, typically for about 8 hours. The dried product, which was moderately compacted and hardened by the accreted fines content and the drying process, was loosened by hand to facilitate accurate particle size analysis. Using the rotary sampler, two representative samples were obtained from the batch of grinding products, and dry-screened over a series of $\sqrt{2}$

screens on a Retsch vibratory shaker. Dry screening was perceived to be effective to about 60 mesh in the vast set of cases and to 100 mesh in a few. Material below this size was wet-screened on the Retsch shaker, down to 400 mesh (see Figure A3). The sub 400 mesh size slurry was collected in a bucket, pressure-filtered, dried, and weighed. Details of the grinding data for the monosize feed are shown in Table A4, and a plot of the products is shown in Figure A4a.

A.6.2.2 Natural size distribution feed grind

Grinding of the natural size distribution feed was carried out as per the procedure employed with the monosize grind (Section A.6.2.1). The difference was in the duration of the grinds, the natural size grind being done for 1, 2, 4, 5 and 6 minutes. Details of the resulting grinding data are shown in Table A5, and a plot of the products in Figure A5.

A.7 Parameter estimation and refinement

The preliminary estimation of breakage parameters was carried out in Microsoft Excel, using the monosize grinding data shown in Table A4. The theory for the procedure is as discussed in Section A.3.3.1.

A.7.1 Selection function

The objective was to obtain an estimate of S_1 and the adjustable parameter, ζ_1. The procedure used for the estimation of S_1 is as follows:

i. The mass fraction of feed size (m_1) remaining at each grind time was determined after each grind (see Table A4).

ii. $m_1(t)$ was plotted against grind time in semi-log space, such that the experimental slope, S_1, which is the selection function of the monosize feed, was obtained from the relation:

$$\frac{dm_1(t)}{dt} = -S_1(t)m_1(t) \tag{A.15}$$

so that

$$S_1(t) = -\frac{d[\ln m_1(t)]}{dt} \tag{A.16}$$

The result acquired from this experimental plot was 0.242. See Figure A6.

iii. A least-squares fit was done for the set of data of $m_1(t)$ vs. t, using the equation

$$m_1(t) = m_1(0)e^{-s_1 t}$$

The value of S_1 obtained was 0.3870 (see Table A6).

iv. An estimate of $\zeta_1$was done after obtaining B_{ij} as described in Section A.7.2.

v. These preliminary values of S_1 and ζ_1 obtained at this stage were subsequently refined in Estimill, by Newton-Gaussian non-linear regression procedures, as described in Section A.3.1.

The entire set of data from grinding the natural size distribution feed was used for the refinement in Estimill. The intermediate and refined sets of selection function and related

parameters are presented with the breakage function and its related parameters further on in this appendix.

As would also be noted, later, the scale-up procedure for industrial scale grinding simulation required a further refined estimation of the selection function, S_1, and the specific energy selection function, S_1^E.

A.7.2 Breakage function

i. The first step in this process was to generate F_i, which is the zero order rate constant inferred from the data in Table A4 (Herbst and Furstenau, 1968). To obtain this rate constant for all sizes, i, a plot was done of Y_i (the cumulative fraction finer than size i) vs. time, such that: $Y_i = f(t)$, (Figure A7). From this plot, a truncated range of the dataset was extracted and re-plotted. See Figure A8 for the results. Then,

$$\mathrm{Lim}_{t=0}\, F_i = \frac{d(Y_i)(t)}{dt} \tag{A.17}$$

The most suitable time range of the data was from zero to 1 minute.

ii. For all values of F_i, values of B_{i1}, the cumulative breakage function at size, i, was developed such that:

$$B_{i1} = \frac{F_i}{S_1} \tag{A.18}$$

The results of this step are presented in Table A7.

From principles, the breakage function and its related adjustable parameters (whose estimation is described below) are, for all intents and purposes, invariant, whether in dry or wet grinding (Siddique 1977). Once formulated as described in these sections, there was no longer any need to refine them in Estimill.

A.7.3 The adjustable parameters, ζ_1, α_1, α_2, and α_3

ζ_1, the distribution modulus, is obtained by plotting the feed size cumulative functions B_{ij} (Table A7) against the particle size on a log-log plot. ζ_1 is the slope of the plot in the fine particle size range. Figure A9 is the plot used to generate this value. The value obtained was 0.585. With S_1 and ζ_1 calculated, preliminary estimates of S_i were obtained for all other sizes other than i=1, using the relationship:

$$S_i = S_1 \left(\frac{\sqrt{x_i x_{i+1}}}{\sqrt{x_1 x_2}} \right)^{\zeta_1} \qquad \text{(A.19)}$$

where all terms are as defined in earlier sections.

Based on the procedures outlined in Section A.3.3.1 (and shown in Figure A1) first estimates were made for the normalizable breakage function parameters α_1, α_2, and α_3 ($\alpha_3 > \alpha_2$). As in those principles, this determination was made using the experimental values of B_{ij} outlined in Table A7. The procedure for generation of α_1 is the same as that for the generation of ζ_1. The respective plots in Figures A8 and A9 demonstrate that $\zeta_1 = \alpha_2 = 0.585$. $\alpha_1 = 0.375$.

A.7.4 Improvement of estimates

The above initial values above for the breakage function parameters α_1 and α_2 and α_3, were subsequently optimized using a least squares adjustment as described in Section A.3.4. These refined values have been called "Intermediate values" in Table A8. Because the normalizable breakage function parameters are adequate in this "intermediate" least-squares adjusted form, they have been retained as "refined" in that table, and no further refinement of them was done in Estimill. Only the selection function parameters were refined further.

A.7.5 The specific energy selection function and its refinement

As Siddique (1977) has outlined (see Section A.4), wet grinding is inherently non-linear, and the selection function parameters (as well as the energy selection function) are environment dependent. Consequently, these parameters estimated by the linear model are not strictly valid for extended grinding situations, especially for fine grinds. However, the model can be fitted to wet grinding data in the non-linear range, and kinetic parameters obtained can be used to predict the grinding behavior in the "neighborhood" of the data used for estimation. The grinding parameters that describe such an identical environment have been shown (Siddique, 1977) to lead to more effective predictive simulation for mills operating in that neighborhood of similar fineness of grind. By using this concept, narrow ranges of values of specific energy input into the batch mill were explored, and the range with product grind that is identical to the large-scale mill at W.U.S. Copper was chosen for estimation of selection function and specific selection function. The values inferred are presented in Table A9.

A.7.6 Estimation of cyclone partition curve

In this work, the cyclone performance data listed in Section A.5 were obtained from staff at the mill, and were used to estimate the partition curve for the cyclone. However, at a test simulation, inconsistencies were observed between the expected P_{80} of overflow, and that seen at the mill. Adjustments were therefore made, and Table 10 was inferred as the cyclone performance data.

A.8 Grinding simulation using Estimill

Only one grind was simulated, to explore the concept of closed-circuit grinding simulation in Estimill. This single simulation was carried out for the first stage of one of the two parallel two-stage grinding circuits shown in Figure A11 (Ball Mill 1). As at the operating plant, itself, the objective was to produce a P_{50} size of 150 mesh at the first stage grind.

The key inputs for grinding simulation in Estimill are the feed particle size distribution, the breakage parameters (selection function/specific energy selection function), and the classification function. The number of mixers in series was indicated as 2. Using the grinding parameters in Table A9, along with the natural feed particle size distribution in Table A5, and the cyclone performance curve in Table A10, the simulation was carried out.

Figure A12 is a screen dump of the data file prepared for use in Estimill for this exercise.

Figure A13 is the output file, demonstrating that the target 50% passing size of 150 mesh was achieved at the first stage of grinding. The power draw of the mill is 244 kW,

the fresh feed rate is 25 tons per hour, a previously determined circulating load of 550 %, thus yielding a total mill feed of 163.46 tons, and a mill specific energy 1.4927 kWh/ton.

A.9 Considerations for grinding optimization

The input parameters used in this simulation, along with knowledge of the potential feed rates for fresh feed to the various mills and the power at normal operating settings can be used to explore for possible energy savings in an optimization drive for this grinding circuit.

The initial objective of this work was not to do a grinding optimization, but to predict mill performance based on various head feed particle size distributions as part of the central research investigation. Even though no variety emerged in the crushing product size distribution to allow that initial scope of work to be completed, the performance of one of the mills has been validated.

The parameters used in the simulation remain valid for simulation-driven optimization efforts at this mill, until the ore characteristics themselves change. In that case, a fresh set of grinding tests must be carried out.

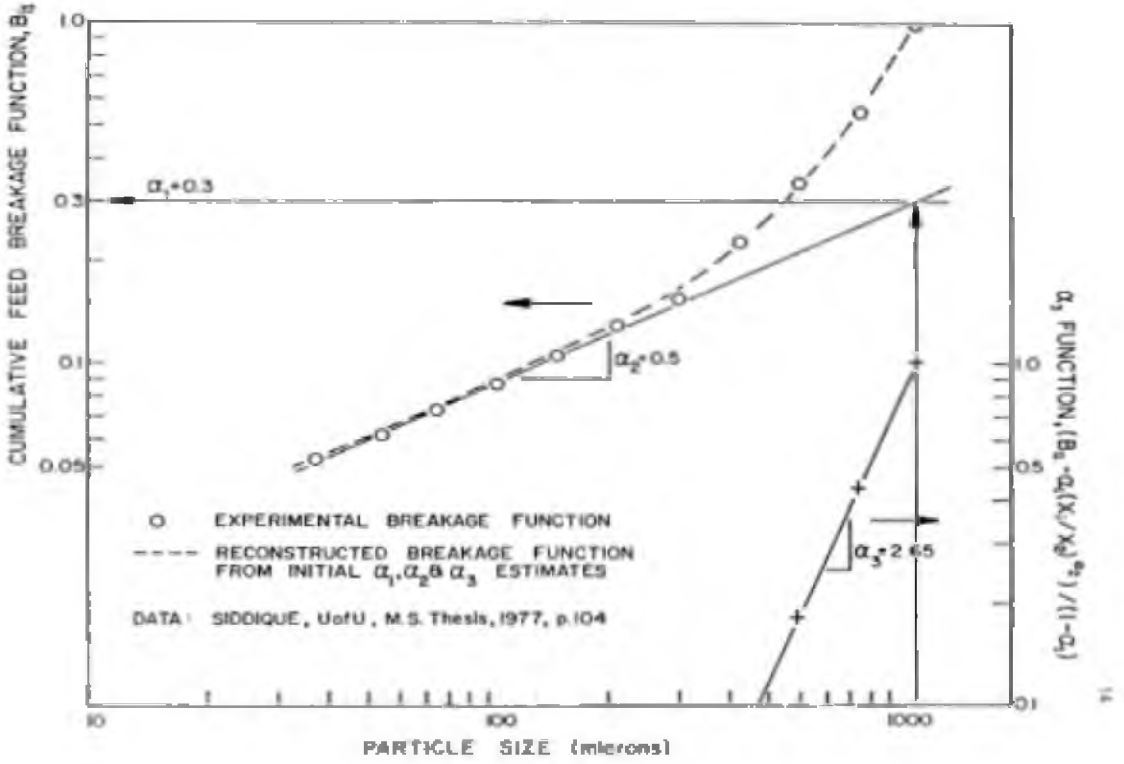

After Herbst et al. 1977

FIGURE A1 A schematic for estimating α_1, α_2, α_3

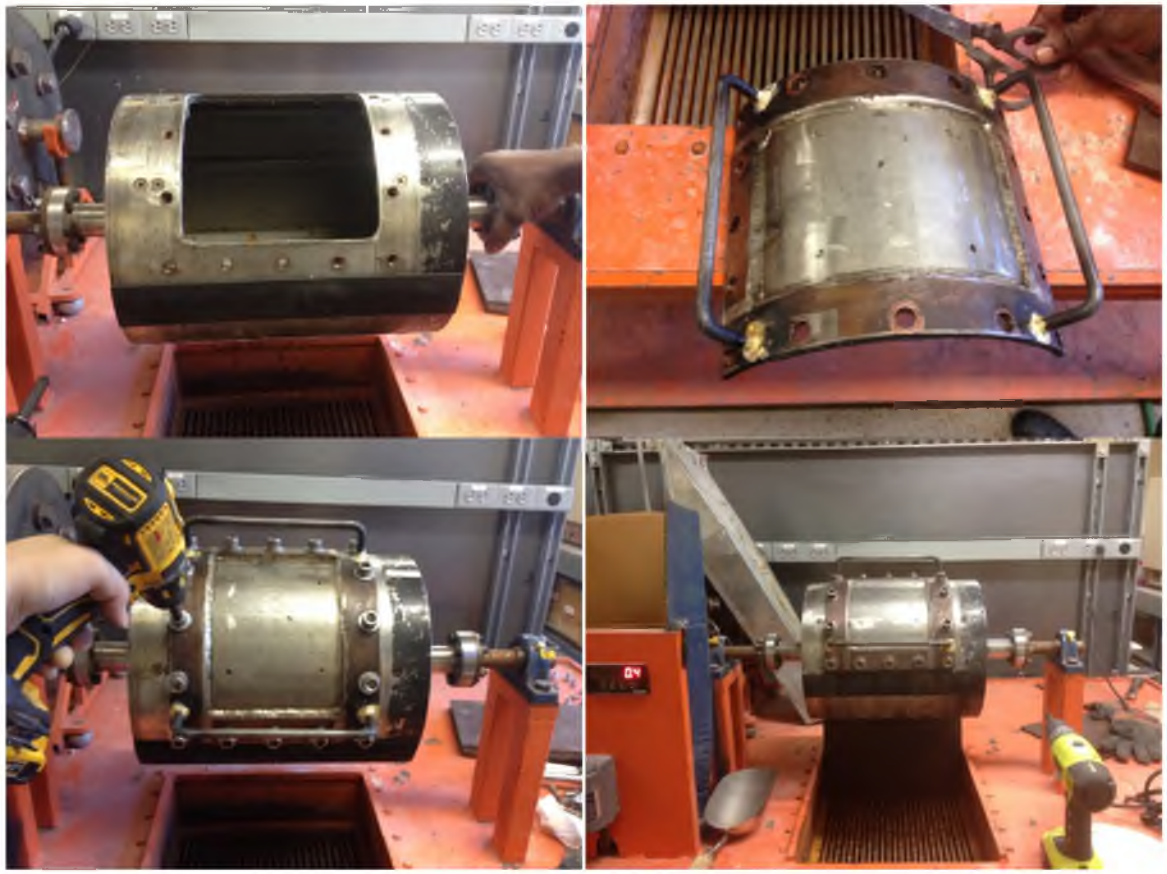

FIGURE A2 The 10-inch ball mill used in the grinding test *(courtesy: Anirban Bhattacharyya)*

FIGURE A3 Wet screening, using the Retsch 200 shaker (*courtesy: Anirban Bhattacharyya*)

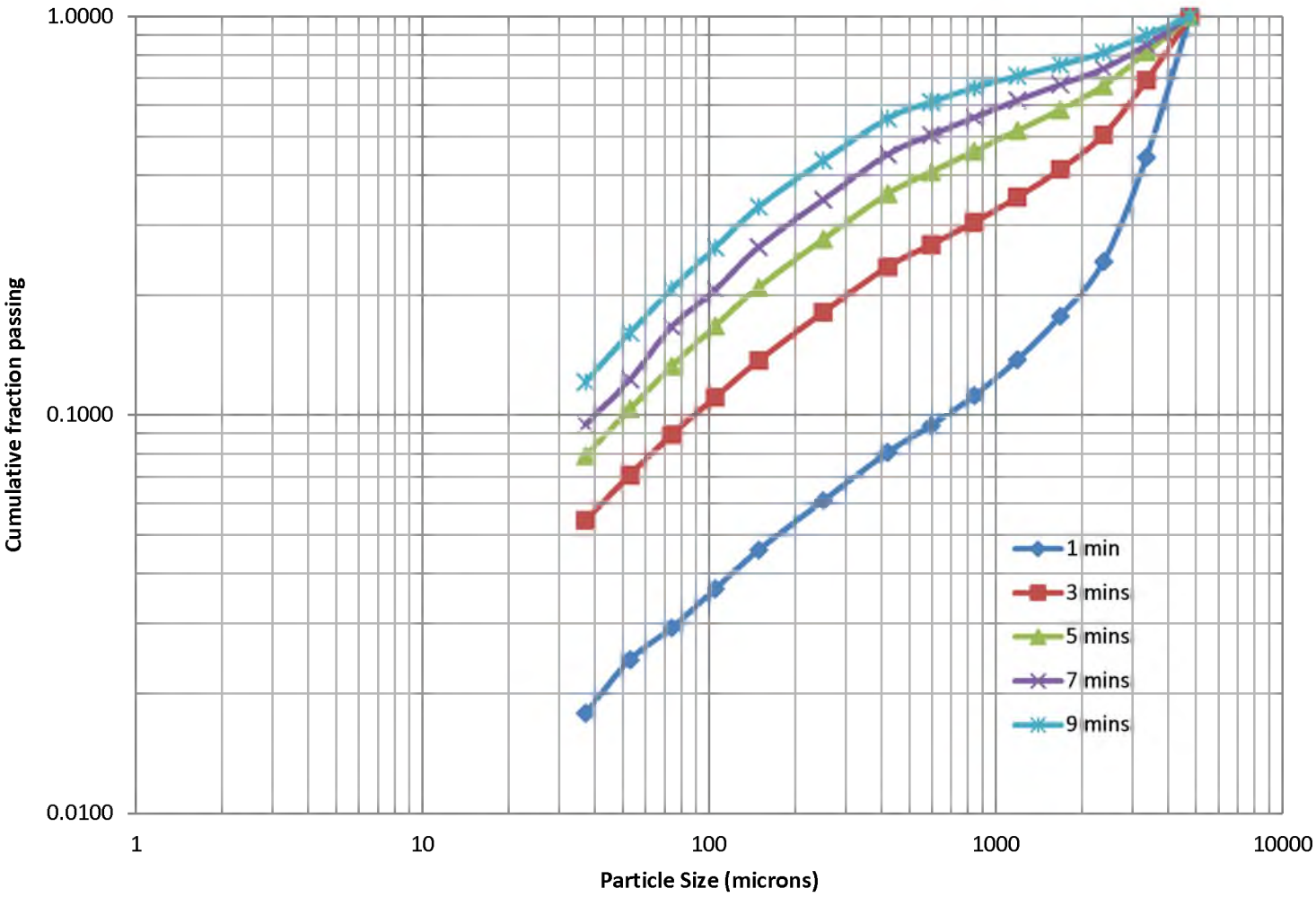

FIGURE A4 A plot of the particle size distributions of the various monosize grinds

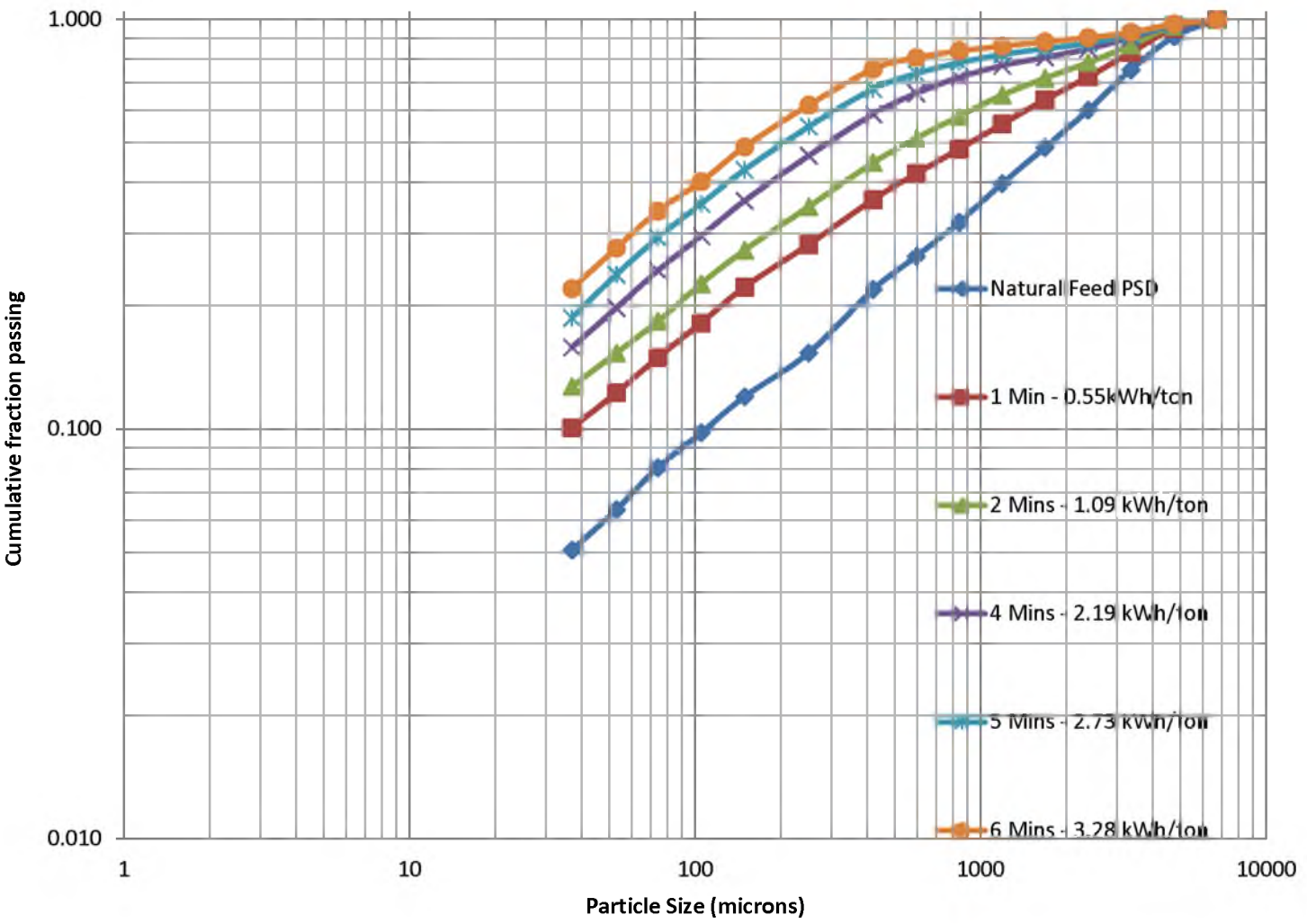

FIGURE A5 A plot of the particle size distributions of the various natural size feed grinds

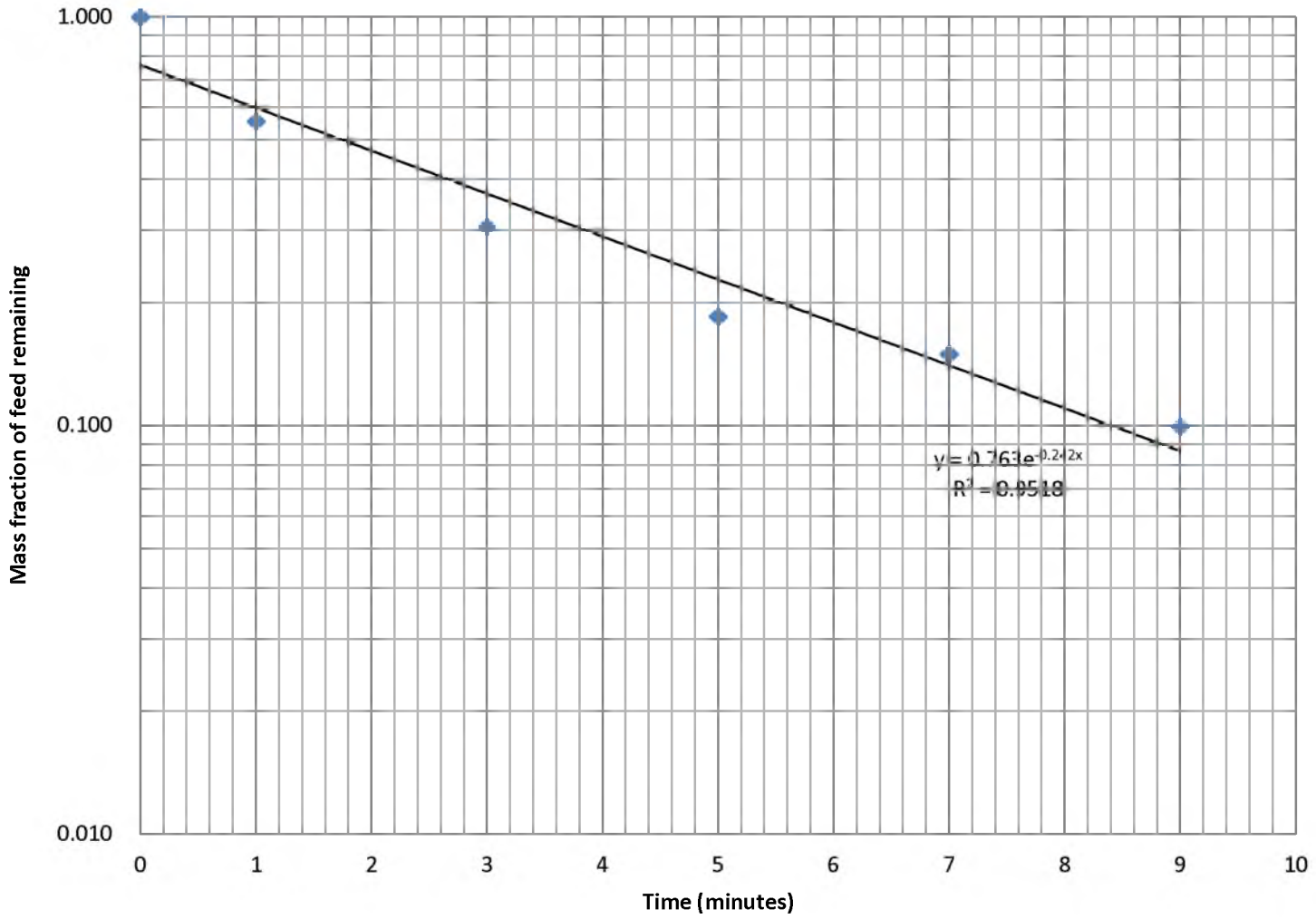

FIGURE A6 First stage of preliminary estimation of the monosize feed selection function, S_1

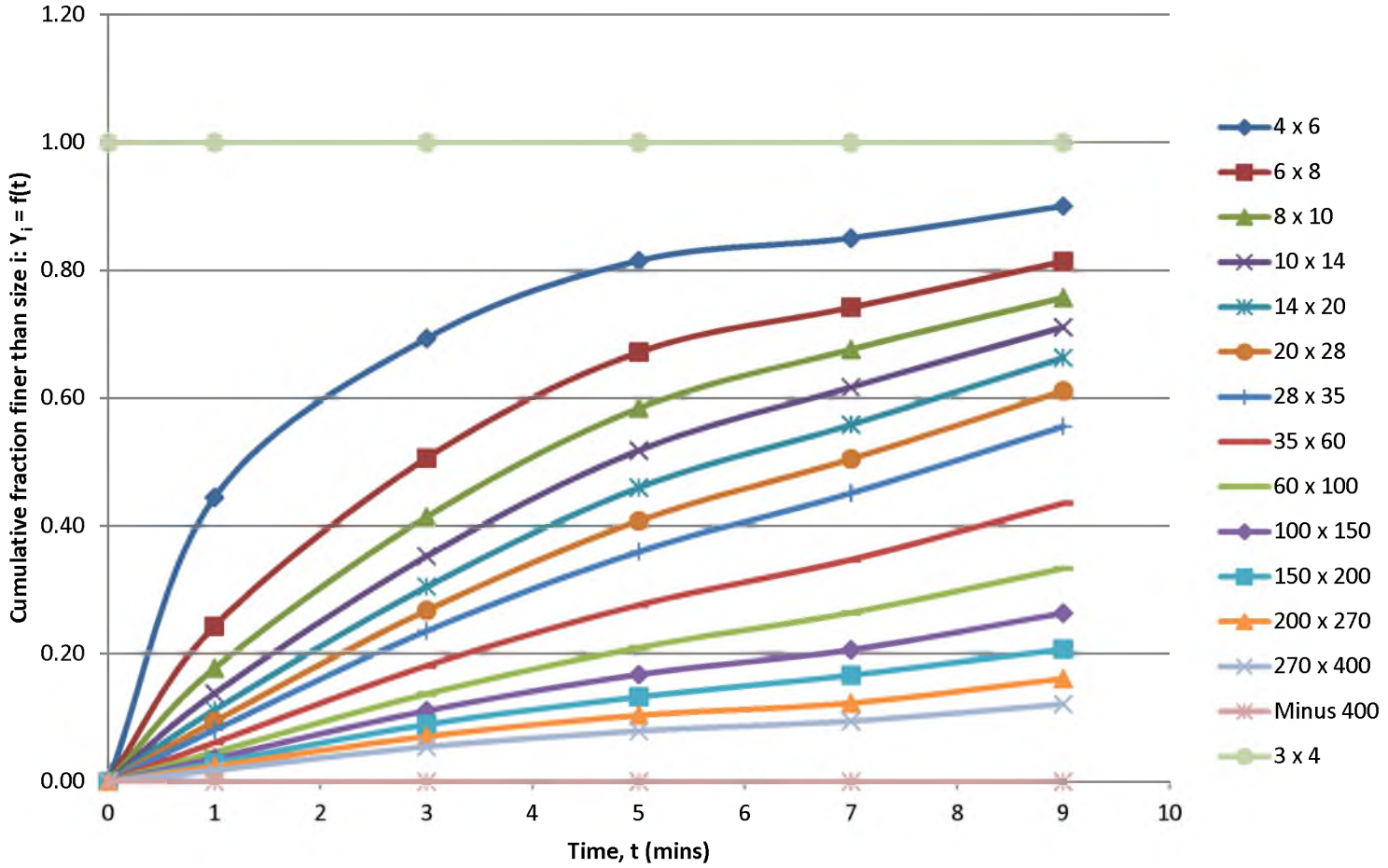

FIGURE A7 Stage 1 for the estimation of F_i: the derivation of b_{i1}

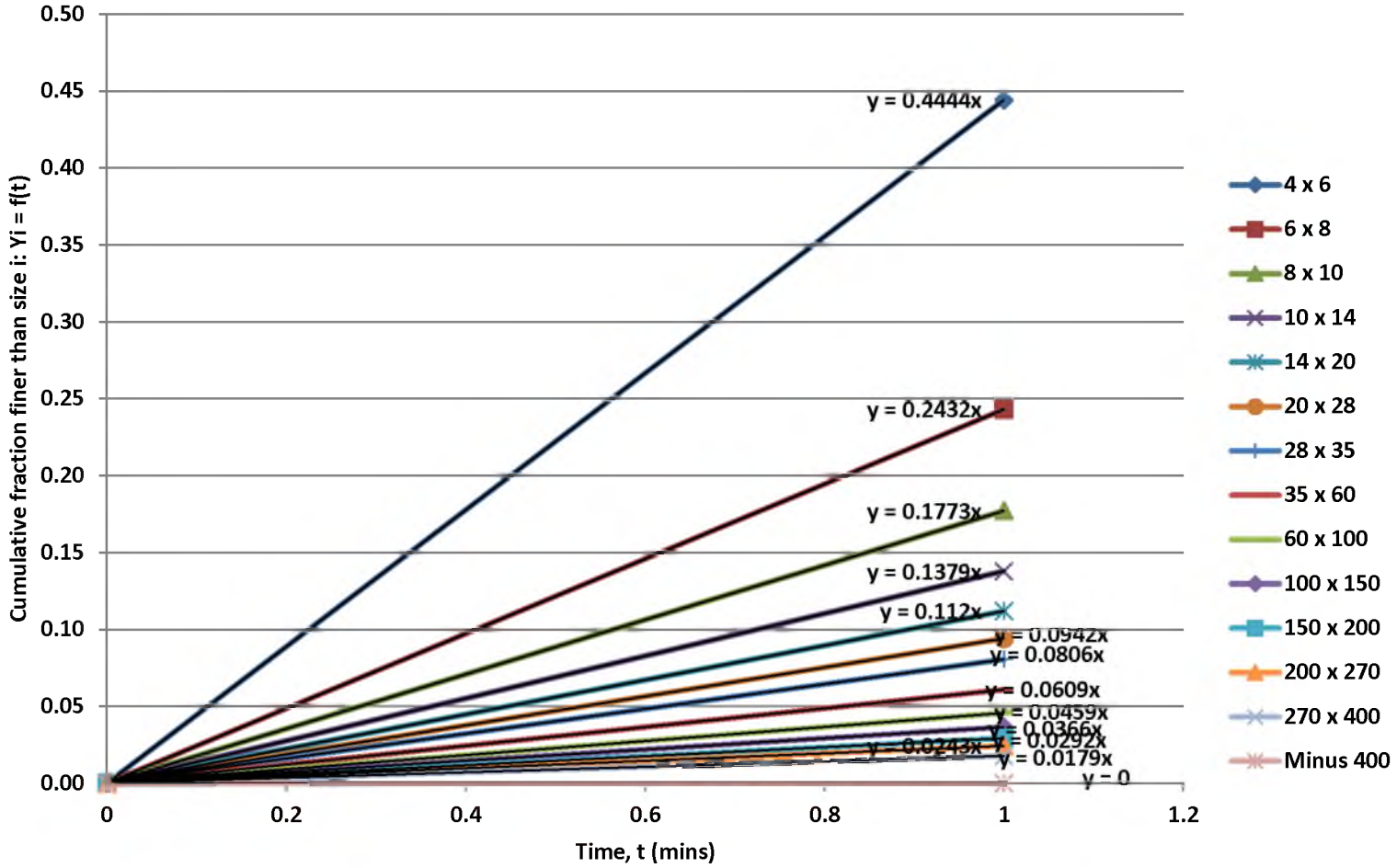

FIGURE A8 A plot of truncated Y_i vs t data, for the estimation of F_i.

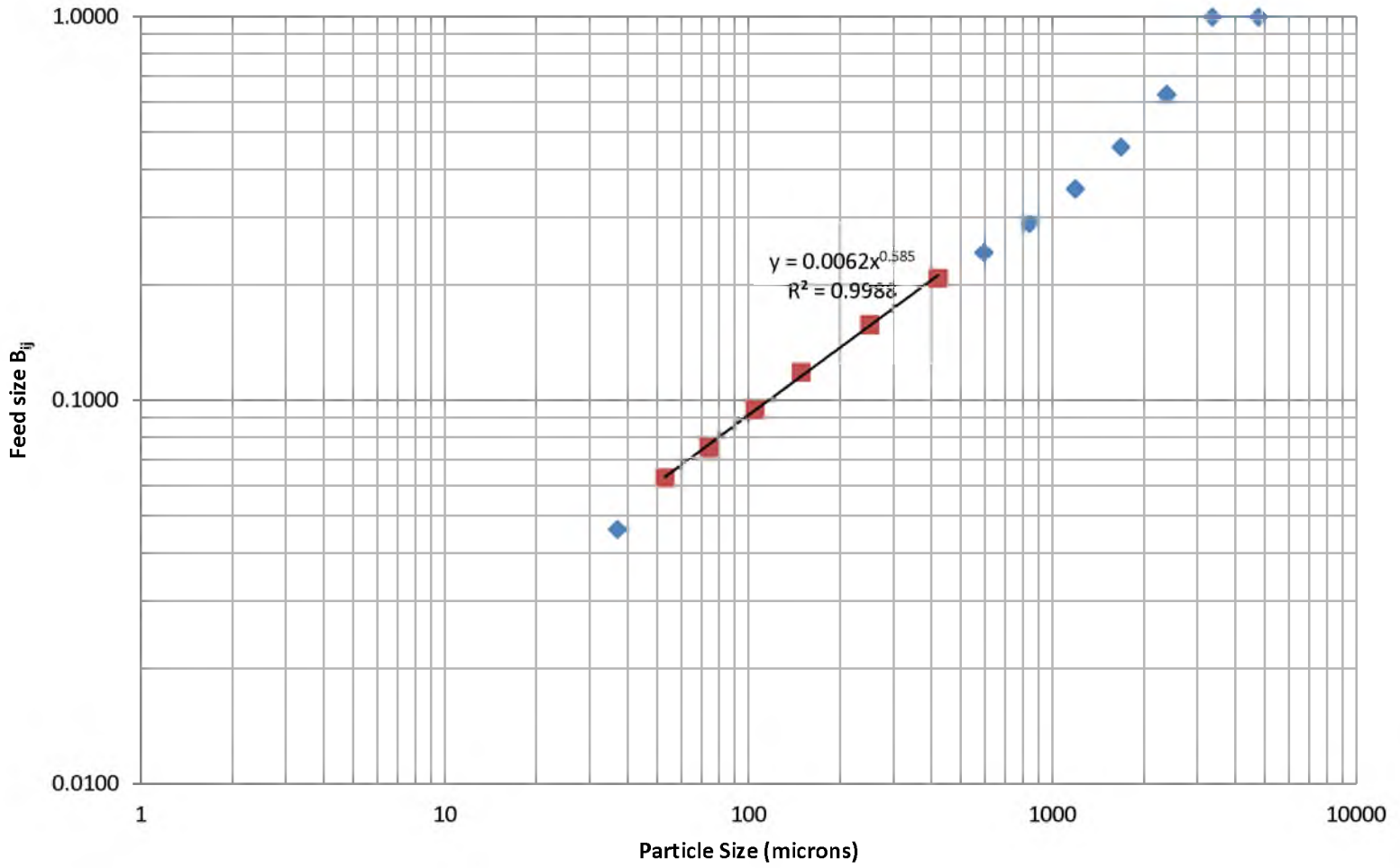

FIGURE A9 Estimation of ζ_1 (ref. Section A.3.1.3). Note that $\zeta_1 = 0.585$. ζ_1 is the distribution modulus of the breakage function

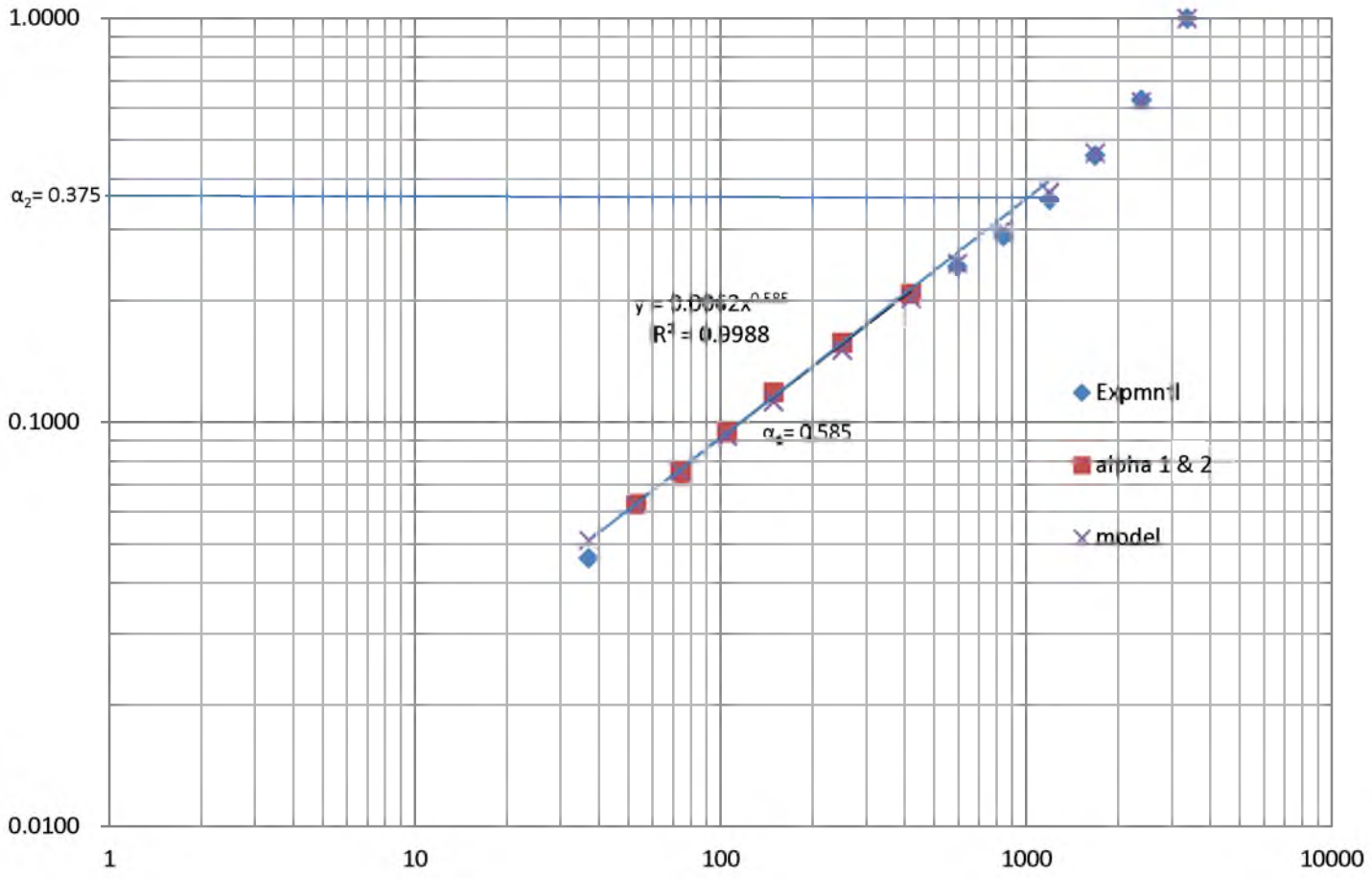

FIGURE A10 Procedure for the preliminary generation of adjustable breakage parameters

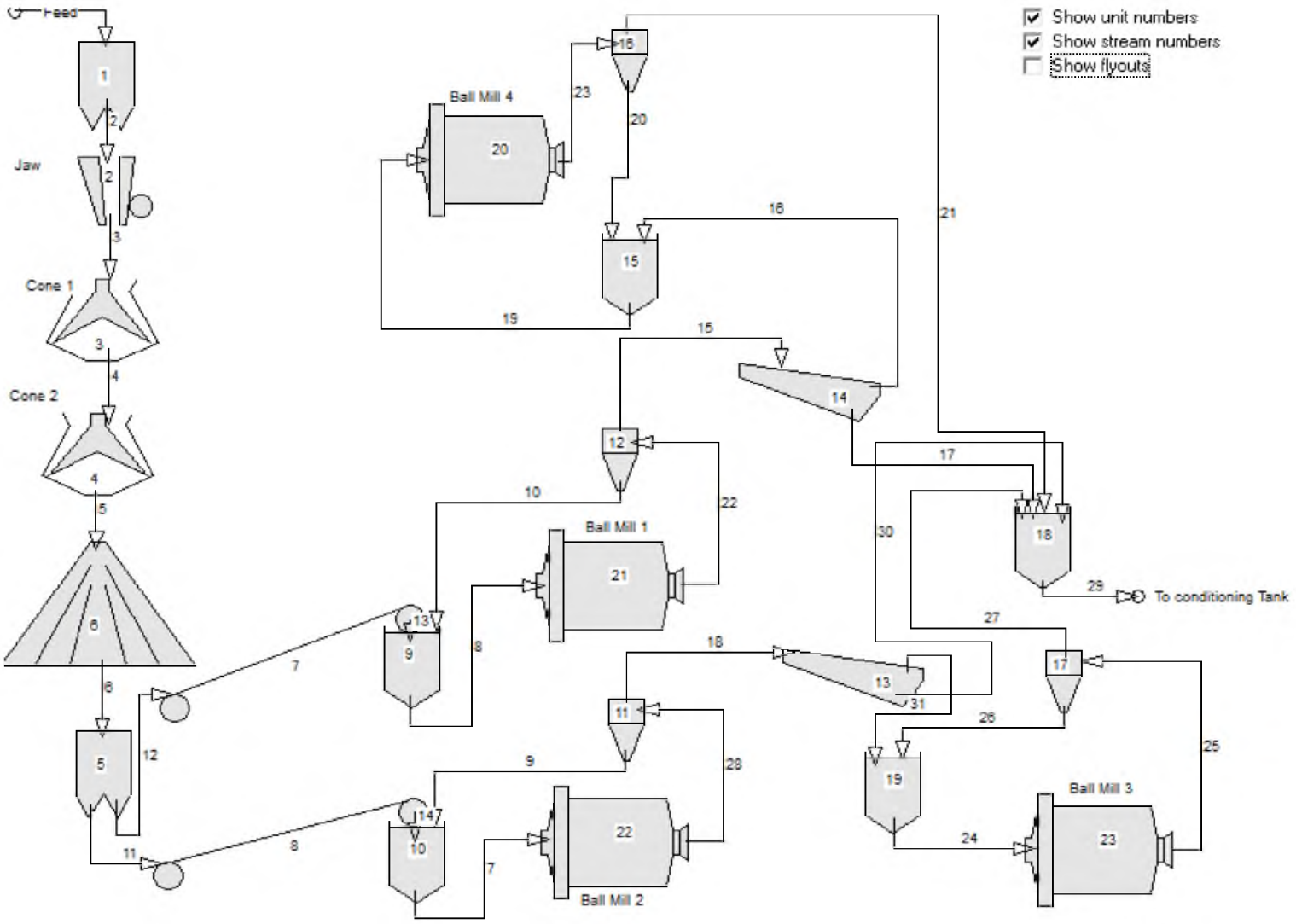

FIGURE A11 The configuration of the grinding circuit at W.U.S. Copper

```
WUSCopperSim1
0       0       1       1       15       1       1       2       1       1       2       2
3       4       6       8       10       14      20      28      35      60      100     150     200     270     400
1
2.0
1.0010 1 0.4722
0.6610  0.5681  4.2207
1.0000 1.0000 0.9999 0.9522 0.9213 0.8934 0.7654 0.6710 0.6387 0.5900 0.5043 0.4256 0.3565 0.2978 0.2100
1.4927
1.0000  0.9088  0.7543  0.6010  0.4878  0.3981  0.3206  0.2644  0.2194  0.1536  0.1201  0.0981  0.0806  0.0637  0.0507
6730    4760    3360    2380    1680    1190    841     595     420     250     149     105     74      53      37
0
```

FIGURE A12 A screen dump of the Estimill data file prepared for the first-stage grind.

File Edit Format View Help

```
          IDENT      CIRCUIT     IDEAL      RESIDENCE
          NUMBER      TYPE       MIXERS       TIME

            1          1         2.00         1.493
2


  STEADY-STATE CLOSED CIRCUIT SIMULATION:
  ---------------------------------------

    *** STANDARD CLOSED CIRCUIT: FRESH FEED TO MILL ***

          NUMBER OF IDEAL MIXERS =    2.00

          RESIDENCE TIME         =    1.493

          FEED RATIO             =    3.062 (MILL/FRESH)

          RELATIVE GRINDABILITY  =     .219 (WT/MIN)/(HOLD-UP)

          CIRCULATING LOAD       =  206.24  PERCENT

          CUMULATIVE DISTRIBUTION:

      SIZE     FRESH      ----- MILL ------    ------- CLASSIFIER --------
     (MESH)    FEED       FEED      PRODUCT    FEED    OVERSIZE  UNDERSIZE

      -   3    1.0000     1.0000    1.0000     1.0000    1.0000    1.0000

      -   4     .9088      .9557     .9855      .9855     .9785    1.0000

      -   6     .7543      .8667     .9470      .9470     .9212    1.0000

      -   8     .6010      .7552     .8854      .8854     .8299    1.0000

      -  10     .4878      .6474     .8111      .8111     .7248     .9891

      -  14     .3981      .5391     .7253      .7253     .6075     .9684

      -  20     .3206      .4269     .6281      .6281     .4784     .9367

      -  28     .2644      .3393     .5376      .5376     .3756     .8717

      -  35     .2194      .2700     .4563      .4563     .2946     .7898

      -  60     .1536      .1916     .3671      .3671     .2100     .6911

      - 100     .1201      .1360     .2914      .2914     .1437     .5961

      - 150     .0981      .0988     .2318      .2318     .0991     .5056

      - 200     .0806      .0733     .1854      .1854     .0697     .4239

      - 270     .0637      .0544     .1480      .1480     .0500     .3503

      - 400     .0507      .0415     .1189      .1189     .0371     .2875
Stop - Program terminated.
```

FIGURE A13 Part output from the grinding simulation done for Ball Mill 1 in Figure A11. The desired output is accentuated in the rectangular box

TABLE A1 A summary of support calculations for monosize grind sample preparation

Spreadsheet format courtesy of Anirban Bhattacharyya

W.U.S. Copper Grinding Research (Copper Skarn)

Batch tests conditions

data input					Mass Calculation for the batch test				
Ore =	Copper Skarn	wet	% solids (wgt) =	70	Mill Volume =	903.2	in^3	14800.9	cm^3
Feed Size =	6 x 8	esh	mono size		Media Volume =	316.1	in^3	5180.3	cm^3
Mill Size =	10.0	in	0.254	m	Void Volume =	126.4	in^3	2072.1	cm^3
Length Size =	11.5	in	0.292	m	Ore_{app} Volume =	126.4	in^3	2072.1	cm^3
M_B* =	0.35	ball charge, %			Ore mass =	2001.7	g	2.00	kg
M_p =	0.6	% filling of the interstices - dry ore			Hold-up (H) =	2001.7	g	0.0020017	ton
p_{bulk} =	1.65	g/cm^3							
p_{slurry} =	1.38	g/cm^3			Ideal Max Mass lost =	2.00	kg	Check % Solids =	70%

data input					Ball Mass Calculation for the batch test				
Ball Top Size (mm) =	50.8	mm	0.0508	m	Total Ball mass =	24.2	Kg	Ball volume (cm^3)	Number of Balls
Scrap Size (in) =	0.5	in	12.7	mm	2.00	10.61	Kg	68.64	20
		ρ_{ball} = 7.77	g/cm^3		1.50	10.23	Kg	28.96	45
Ball Size Distribution Calculation					1.00	2.73	Kg	8.58	41
Ball Diameter (inches)	Mid Point	String 1	Percent (by wgt)	MolyCop	0.67	0.51	Kg	2.58	25
2.00	2.000	100.00	44%	2.0	0.50	0.08	Kg	1.07	9
1.50	1.732	56.08	42%	1.5				Total of Balls	141
1.00	1.225	13.73	11%	1.0					
0.67	0.819	2.42	2%	0.5	check =	24.2	Kg		
0.50	0.579	0.31	0%	0.5					
			100%						

Critical Speed, N_c = 93.84

Water Calculation for the batch wet test		
Water Mass =	857.86	g
p_{water} =	1.00	$g/cm^3 = kg/l = t/m^3$
Water Mass =	0.86	Kg
Water Volume =	0.86	liters
Slurry Calculation		
slurry Mass =	2859.5	g
Slurry Volume =	2072.1	cm^3
Slurry % filling =	100.0	%

TABLE A2 Masses of sample used at various stages of the monosize grind

Mass of Material used in grinding test (g)					
0 mins	1 min	2 mins	3 mins	4 mins	5 mins
2001.7	2001.7	2001.7	2001.7	2001.7	2001.7
Weight after grinding (g)					
2001.7	1980.5	1992.6	1996.2	1996.1	1978.2
Losses (%)					
0.00%	1.06%	0.45%	0.27%	0.28%	1.17%
Mass of Sample used in post-grind size Analysis (g)					
0.0	324.9	326.7	328.9	331.9	331.1

TABLE A3 Masses of sample used at various stages of the natural size distribution grind

Mass of Material used in natural size feed grinding test (g)					
0 mins	1 min	2 mins	4 mins	5 mins	6 mins
2001.9	2001.9	2001.4	2001.7	2001.8	2002.1
Weight after grinding (g)					
2001.9	1980.4	1968.7	1975.8	1980.5	1982.8
Losses after grinding (%)					
0.00%	1.07%	1.63%	1.29%	1.06%	0.96%
Mass of Sample used in Size Analysis (g)					
331.3	335.5	334.3	342.1	330.1	329.7

TABLE A4 Monosize grinding data

				Grinding Product Sieved weights (g)						Mass fraction at stated size (sample only)						Cumulative Mass Fraction Passing					
			Time (mins)	0	1	3	5	7	9	0	1	3	5	7	9	0	1	3	5	7	9
i	Mesh	Size (mm)	Size (microns)	G1-0	G1-1	G1-2	G1-3	G1-4	G1-5	G1-0	G1-1	G1-2	G1-3	G1-4	G1-5	G1-0	G1-1	G1-2	G1-3	G1-4	G1-5
1	4	4.76	4760	0.0	0.0	0.0	0.0	0.0	0.0	0.000	0.000	0.000	0.000	0.000	0.000	1.000	1.000	1.000	1.000	1.000	1.000
2	6	3.36	3360	333.6	180.5	100.1	60.8	49.6	32.9	1.000	0.556	0.306	0.185	0.149	0.099	0.000	0.444	0.694	0.815	0.851	0.901
3	8	2.38	2380	0.0	65.4	61.2	47.1	36.0	28.7	0.000	0.201	0.187	0.143	0.108	0.087	0.000	0.243	0.506	0.672	0.742	0.814
4	10	1.68	1680	0.0	21.4	30.1	28.8	21.8	18.7	0.000	0.066	0.092	0.088	0.066	0.056	0.000	0.177	0.414	0.584	0.676	0.757
5	14	1.19	1190	0.0	12.8	20.1	21.8	19.7	15.4	0.000	0.039	0.062	0.066	0.059	0.047	0.000	0.138	0.353	0.518	0.617	0.711
6	20	0.841	841	0.0	8.4	15.6	19.1	19.4	15.8	0.000	0.026	0.048	0.058	0.058	0.048	0.000	0.112	0.305	0.460	0.559	0.663
7	28	0.595	595	0.0	5.8	12.1	17.1	17.8	17.2	0.000	0.018	0.037	0.052	0.054	0.052	0.000	0.094	0.268	0.408	0.505	0.611
8	35	0.42	420	0.0	4.4	10.5	15.9	17.8	18.4	0.000	0.014	0.032	0.048	0.054	0.056	0.000	0.081	0.236	0.360	0.451	0.556
9	60	0.25	250	0.0	6.4	17.8	27.4	34.5	39.8	0.000	0.020	0.054	0.083	0.104	0.120	0.000	0.061	0.181	0.276	0.347	0.436
10	100	0.149	149	0.0	4.9	14.4	22.0	27.6	33.8	0.000	0.015	0.044	0.067	0.083	0.102	0.000	0.046	0.137	0.209	0.264	0.333
11	150	0.105	105	0.0	3.0	8.6	13.8	19.2	23.1	0.000	0.009	0.026	0.042	0.058	0.070	0.000	0.037	0.111	0.168	0.206	0.264
12	200	0.074	74	0.0	2.4	7.0	11.5	13.2	18.7	0.000	0.007	0.021	0.035	0.040	0.056	0.000	0.029	0.089	0.133	0.167	0.207
13	270	0.053	53	0.0	1.6	6.1	9.5	14.5	15.3	0.000	0.005	0.019	0.029	0.044	0.046	0.000	0.024	0.071	0.104	0.123	0.161
14	400	0.037	37	0.0	2.1	5.3	8.1	9.4	13.2	0.000	0.006	0.016	0.025	0.028	0.040	0.000	0.018	0.054	0.079	0.095	0.121
15	Pan			0.0	5.8	17.8	26.0	31.4	40.1	0.000	0.018	0.054	0.079	0.095	0.121	0.000	0.000	0.000	0.000	0.000	0.000
			Measrd Pan	0.0	5.0	16.1	24.4	31.1	37.1	Mass fraction of feed remaining						1.000	0.556	0.306	0.185	0.149	0.099
			Adjstd totals	333.62	324.9	326.7	328.9	331.9	331.1												
			True totals	333.62	324.10	325.00	327.30	331.60	328.10												
			True losses	0.00	0.02	0.05	0.07	0.09	0.11												
			Adjstd Losses	0.00%	0.00%	0.00%	0.00%	0.00%	0.00%												

TABLE A5 Natural size distribution feed grind

			Grinding Product Sieved weights (g)						Mass fraction at stated size (sample only)						Cumulative Mass Fraction Passing					
		Time (mins)	0	1	2	4	5	6	0	1	2	4	5	6	0	1	2	4	5	6
i	Mesh	Size (microns)	G2-0	G2-1	G2-2	G2-3	G2-4	G2-5	G2-0	G2-1	G2-2	G2-3	G2-4	G2-5	G2-0	G2-1	G2-2	G2-3	G2-4	G2-5
1	3	6730	0.0	0.0	0.0	0.0	0.0	0.0	0.000	0.000	0.000	0.000	0.000	0.000	0.955	0.912	0.890	0.868	0.849	0.827
2	4	4760	30.2	15.6	11.3	10.4	9.2	7.4	0.087	0.042	0.030	0.026	0.024	0.019	0.868	0.870	0.860	0.841	0.825	0.809
3	6	3360	51.2	40.7	33.5	22.1	18.2	15.2	0.148	0.111	0.089	0.056	0.047	0.038	0.720	0.759	0.771	0.785	0.779	0.770
4	8	2380	50.8	36.1	26.8	19.3	13.4	8.8	0.146	0.098	0.071	0.049	0.034	0.022	0.574	0.661	0.700	0.736	0.744	0.748
5	10	1680	37.5	29.3	22.2	13.5	8.9	7.2	0.108	0.080	0.059	0.034	0.023	0.018	0.466	0.581	0.640	0.702	0.721	0.730
6	14	1190	29.7	27.3	21.8	12.6	8.9	7.1	0.086	0.074	0.058	0.032	0.023	0.018	0.380	0.507	0.582	0.670	0.698	0.712
7	20	841	25.7	24.4	24.4	16.8	12.3	7.4	0.074	0.066	0.065	0.043	0.032	0.019	0.306	0.441	0.517	0.627	0.667	0.694
8	28	595	18.6	20.9	22.7	21.3	15.4	10.3	0.054	0.057	0.060	0.054	0.040	0.026	0.252	0.384	0.457	0.573	0.627	0.668
9	35	420	14.9	19.2	22.0	25.0	20.3	16.6	0.043	0.052	0.059	0.063	0.052	0.042	0.210	0.332	0.398	0.510	0.575	0.626
10	60	250	21.8	27.2	32.8	41.9	42.6	45.8	0.063	0.074	0.087	0.106	0.110	0.115	0.147	0.258	0.311	0.404	0.465	0.512
11	100	149	11.1	20.2	25.4	35.7	39.0	42.6	0.032	0.055	0.068	0.091	0.100	0.107	0.115	0.203	0.243	0.313	0.365	0.405
12	150	105	7.3	13.6	15.7	22.1	24.7	28.7	0.021	0.037	0.042	0.056	0.064	0.072	0.094	0.166	0.202	0.257	0.301	0.333
13	200	74	5.8	10.8	14.4	18.0	20.3	20.2	0.017	0.029	0.038	0.046	0.052	0.051	0.077	0.136	0.163	0.212	0.249	0.282
14	270	53	5.6	9.0	10.0	15.8	18.2	21.1	0.016	0.024	0.027	0.040	0.047	0.053	0.061	0.112	0.137	0.171	0.202	0.229
15	400	37	4.3	7.4	8.8	13.4	17.0	18.6	0.012	0.020	0.023	0.034	0.044	0.047	0.048	0.092	0.113	0.137	0.159	0.182
	Pan (actual)		15.7	32.3	41.2	52.2	58.7	68.9	0.045	0.088	0.110	0.132	0.151	0.173	0.000	0.000	0.000	0.000	0.000	0.000
16	Pan (assigning losses to fines)		16.8	33.8	42.5	54.2	61.7	72.7	0.048	0.092	0.113	0.137	0.159	0.182	0.000	0.000	0.000	0.000	0.000	0.000
		Totals	347.00	367.8	375.5	394.3	388.8	398.6												
		Losses	0.33%	0.45%	0.39%	0.58%	0.91%	1.15%												

TABLE A6 Results from the least-squares adjustment of the preliminary S_1 estimate

Refinement of S1

Time	Mass fraction Remaining	Prediction (Theory)
0	1.000	1.000
1	0.556	0.679
3	0.306	0.313
5	0.185	0.144
7	0.149	0.067
9	0.099	0.031

: m1(t)=m1(0)*exp(-S1*t)

Initial S1	0.242
S1 Opt	**0.3870**
SSR =	0.0285

TABLE A7 Development of the cumulative breakage function

			Zero Order Formation of fines		s1 =	0.3870
i	Mesh	Size (microns)	$F_{i\ (calc)}$	$F_{i\ (Graph)}$		$B_{i1}=F_i/S_1$
1	4	4760	1.0000	1.0000	$B_{1\ 1}$	**1.0000**
2	6	3360	0.4444	0.4444	$B_{2\ 1}$	**1.0000**
3	8	2380	0.2432	0.2432	$B_{3\ 1}$	**0.6282**
4	10	1680	0.1773	0.1773	$B_{4\ 1}$	**0.4581**
5	14	1190	0.1379	0.1379	$B_{5\ 1}$	**0.3563**
6	20	841	0.1120	0.1120	$B_{6\ 1}$	**0.2895**
7	28	595	0.0942	0.0942	$B_{7\ 1}$	**0.2433**
8	35	420	0.0806	0.0806	$B_{8\ 1}$	**0.2084**
9	60	250	0.0609	0.0609	$B_{9\ 1}$	**0.1575**
10	100	149	0.0459	0.0459	$B_{10\ 1}$	**0.1185**
11	150	105	0.0366	0.0366	$B_{21\ 1}$	**0.0946**
12	200	74	0.0292	0.0292	$B_{12\ 1}$	**0.0755**
13	270	53	0.0243	0.0243	$B_{13\ 1}$	**0.0628**
14	400	37	0.0179	0.0179	$B_{14\ 1}$	**0.0461**
15	Pan		0.0000	-	$B_{15\ 1}$	**0.0000**

TABLE A8 Intermediate and refined values of the selection function, breakage function, and their related adjustable parameters

Parameter	Intermediate Value	Refined Value
S_1	0.387	0.6777
ζ_1	0.585	0.4680
α_1	0.6610	0.6610
α_2	0.5681	0.5681
α_3	4.2207	4.2207

TABLE A9 Values of selection function and energy specific selection function generated from the "neighborhood of similar fineness of grind" method.

Parameter	Value
$\mathbf{S_1}$	0.5474
ζ_1	0.4722
S_1^E	1.0010

TABLE A10: The classification function for Ball Mill 1 cyclone

Tyler Mesh	3	4	6	8	10	14	20	28	35	60	100	150	200	270	400
Size microns	6730	4760	3360	2380	1680	1190	841	595	420	250	149	105	74	53	37
Class Function	1	1	1	0.95	0.92	0.89	0.77	0.67	0.64	0.59	0.5	0.43	0.36	0.3	0.21

APPENDIX B

A SELECTION OF CONVERSIONS OF THE UNITS USED IN THIS RESEARCH

A SELECTION OF THE UNIT CONVERSIONS USED IN THE RESEARCH

Convert from		Physical Quantity	To		Multiply by
Unit	Symbol		Unit	Symbol	
Centimeter	cm	Length	Inch	in	0.3937008
Cubic foot	ft^3	Volume	Cubic yard	yd^3	0.03703704
Cubic yard	yd^3	Volume	Cubic meter	m^3	0.7645549
Foot	ft	Length	Meter	m	0.3048
Gram	g	Mass	Pound	lb	0.002204623
Gram	g	Mass	Kilogram	kg	0.001
Grams per cubic centimeter	g/cc	Density	Pounds per cubic foot	lb/ft^3	62.42796
Kilogram	kg	Mass	Pound	lb	2.204623
Kilogram	kg	Mass	Ton (metric ton)	t	0.001
Pound	lb	Mass	Short ton	st	0.0005
Pounds per cubic foot	lb/ft^3	Density	Short tons per cubic yard	st/yd^3	0.02309492
Pounds per square inch	psi	Pressure	Pascal	Pa	6894.757
Pounds per square inch	psi	Pressure	Megapascal	MPa	0.006894757
Short tons	st	Mass	Ton (metric ton)	t	0.9071847
Short tons per cubic yard	st/yd^3	Density	Tons per cubic meter	t/m^3	1.1865528

APPENDIX C

DEVELOPMENT OF THE KUZ-RAM ROCK FACTORS

EXHIBIT C1

DEVELOPMENT OF THE KUZ-RAM ROCK FACTOR FOR SEMBEHUN HIGH-GRADE ORE

Estimation of the Kuz-Ram Rock Factor, A

A = 0.06 * (RMD + RDI + HF) * C(A)

A = Kuz-Ram Factor RDI = Rock Density Influence Factor

RMD = Rock Mass Description HF = Hardness Factor C(A) = Correction Factor

Rock Type: Sembehun High Grade Ore (Soft)

Section 1: RMD

RMD = 10 for powdery/friable rock; RMD = 50 for massiver Rock; RMD = JF, for vertically jointed

Section 1a: Rock Mass Description (RMD)

Please choose **yes (Y)** *to* ***only one*** *of the following three questions:*

i. Is this rock friable n

ii. Is this rock massive, with no jointing, or with joint spacing > blast hole spacing ? (y/n) n

iii. Is the rock vertically jointed? y

Section 1b: Joint Factor, JF - ***(Only valid if you answered "Y" to Question iii in Section 1a, above)***

Note: **JF = (JCF * JPS) + JPA** JF = Joint Factor

JCF = Joint Condition Factor *JPA = Vertical Joint Plane Angle Factor*

JPS = Joint Plane Spacing Factor

JCF ***Range of values: 1 to 2***

Describe th joint condition in the box below. Please, choose only one of three options, namely:
"Tight", "Relaxed" or "Gouge-filled": if "Tight", input "1"; if "Relaxed", input "1.5";
If joint is "gouge-filled", input "2"

What is the condition of the joint? (1, 1.5 or 2)	1

JPS ***Range: 10 to 50***

Relevant factors: Reduced Pattern (P) and Joint Spacing (S)
P = Reduced Pattern = $(B*S)^{0.5}$

What is the average spacing of joints, in meters?	0.25	P =	4.29
What is the blast Burden (in meters)?	4	95% P =	4.08
What is the blast Spacing (in meters)?	4.6	JPS	20.00

JPA ***Note that only one answer can be "Yes", although all can be "No"***

Do the joints dip out of the face at >30°? (Y or N)	n		
Do the joints dip into the face at >30°? (Y or N)	y	JPA Value	30
Do the joints Strike out of the face? (Y or N)	n	**RMD**	**50**

Section 2: RDI (Rock Density Influence)

Rock Density (kg//m^3 2966

Rock Density Influence Factor (F **24.2**

Section 3: Hardness Factor

Young's Modulus, Y (Gpa)	48.98
UCS (MPa)	62.05

Hence, Hardness Factor, HF = **16.33**

Kuz-Ram Factor

Uncorrected Kuz-Ram Factor	5.43
Correction	1.2
Kuz-Ram Factor (Estimate)	**6.51**

EXHIBIT C2

DEVELOPMENT OF THE KUZ-RAM ROCK FACTOR FOR SEMBEHUN LOW-GRADE ORE

Estimation of the Kuz-Ram Rock Factor, A

A = 0.06 * (RMD + RDI + HF) * C(A)

A = Kuz-Ram Factor RDI = Rock Density Influence Factor

RMD = Rock Mass Description HF = Hardness Factor C(A) = Correction Factor

Rock Type: Sembehun Low Grade Ore (Hard)

Section 1: RMD

RMD = 10 for powdery/friable rock; RMD = 50 for massiver Rock; RMD = JF, for vertically jointed

Section 1a: Rock Mass Description (RMD)

Please choose **yes (Y)** *to* ***only one*** *of the following three questions:*

i. Is this rock friable n

ii. Is this rock massive, with no jointing, or with joint spacing > blast hole spacing ? (y/n) n

iii. Is the rock vertically jointed? y

Section 1b: Joint Factor, JF - ***(Only valid if you answered "Y" to Question iii in Section 1a, above)***

Note: **JF = (JCF * JPS) + JPA** JF = Joint Factor

JCF = Joint Condition Factor *JPA = Vertical Joint Plane Angle Factor*

JPS = Joint Plane Spacing Factor

JCF Range of values: 1 to 2

Describe th joint condition in the box below. Please, choose only one of three options, namely:
"Tight", "Relaxed" or "Gouge-filled": if "Tight", input "1"; if "Relaxed", input "1.5";
If joint is "gouge-filled", input "2"

What is the condition of the joint? (1, 1.5 or 2)	1

JPS Range: 10 to 50

Relevant factors: Reduced Pattern (P) and Joint Spacing (S)

P = Reduced Pattern = $(B*S)^{0.5}$

What is the average spacing of joints, in meters?	1.5	P =	4.29
What is the blast Burden (in meters)?	4	95% P =	4.08
What is the blast Spacing (in meters)?	4.6	JPS	20.00

JPA Note that only one answer can be "Yes", although all can be "No"

Do the joints dip out of the face at >30°? (Y or N)	y		
Do the joints dip into the face at >30°? (Y or N)	n	JPA Value	40
Do the joints Strike out of the face? (Y or N)	n	**RMD**	**60**

Section 2: RDI (Rock Density Influence)

Rock Density (kg//m^3) 2723

Rock Density Influence Factor (F **18.1**

Section 3: Hardness Factor

Young's Modulus, Y (Gpa) 80.87 Est. from SR Waste

UCS (MPa) 199.51 Point Load estimate

Hence, Hardness Factor, HF = **39.90**

Kuz-Ram Factor	
Uncorrected Kuz-Ram Factor	7.08
Correction	1.2
Kuz-Ram Factor (Estimate)	**8.49**

EXHIBIT C3

DEVELOPMENT OF THE KUZ-RAM ROCK FACTOR FOR LIMESTONE

(WASTE ROCK)

Estimation of the Kuz-Ram Rock Factor, A

A = 0.06 * (RMD + RDI + HF) * C(A)

A = Kuz-Ram Factor ***RDI = Rock Density Influence Factor***
RMD = Rock Mass Description ***HF = Hardness Factor*** ***C(A) = Correction Factor***

Rock Type: Limestone (Sembehun Pit Waste)

Section 1: RMD

RMD = 10 for powdery/friable rock; RMD = 50 for massiver Rock; RMD = JF, for vertically jointed rock

Section 1a: Rock Mass Description (RMD)

Please choose **yes (Y)** *to* ***only one*** *of the following three questions:*

i. Is this rock friable (powdery)?(y/n) n

ii. Is this rock massive, with no jointing, or with joint spacing > blast hole spacing ? (y/n) n

iii. Is the rock vertically jointed? (y/n) y

Section 1b: Joint Factor, JF - ***(Only valid if you answered "Y" to Question iii in Section 1a, above)***

Note: **JF = (JCF * JPS) + JPA** JF = Joint Factor
JCF = Joint Condition Factor *JPA = Vertical Joint Plane Angle Factor*
JPS = Joint Plane Spacing Factor

JCF ***Range of values: 1 to 2***

Describe th joint condition in the box below. Please, choose only one of three options, namely:
"Tight", "Relaxed" or "Gouge-filled": if "Tight", input "1"; if "Relaxed", input "1.5";
If joint is "gouge-filled", input "2"

What is the condition of the joint? (1, 1.5 or 2)	1

JPS ***Range: 10 to 50***

Relevant factors: Reduced Pattern (P) and Joint Spacing (S)
P = Reduced Pattern = $(B*S)^{0.5}$

What is the average spacing of joints, in meters?	1.5	P =	3.95
What is the blast Burden (in meters)?	3.6576	95% P =	3.75
What is the blast Spacing (in meters)?	4.2672	JPS	20.00

JPA ***Note that only one answer can be "Yes", although all can be "No"***

Do the joints dip out of the face at >30°? (Y or N)	y		
Do the joints dip into the face at >30°? (Y or N)	n	JPA Value	40
Do the joints Strike out of the face? (Y or N)	n	**RMD**	**60**

Section 2: RDI (Rock Density Influence)

Rock Density (kg//m^3) 2595

Rock Density Influence Factor (RDI) = **14.9**

Section 3: Hardness Factor (HF)

Young's Modulus, Y (Gpa)	66.85
UCS (MPa)	204.00
Hence, Hardness Factor, HF =	**40.80**

Kuz-Ram Factor

Uncorrected Kuz-Ram Factor	6.94
Correction	1.2
Kuz-Ram Factor (Estimate)	**8.33**

EXHIBIT C4

DEVELOPMENT OF THE KUZ-RAM ROCK FACTOR FOR GRANODIORITE

Estimation of the Kuz-Ram Rock Factor, A

A = 0.06 * (RMD + RDI + HF) * C(A)

A = Kuz-Ram Factor RDI = Rock Density Influence Factor
RMD = Rock Mass Description HF = Hardness Factor C(A) = Correction Factor

Rock Type: Granodiorite

Section 1: RMD
RMD = 10 for powdery/friable rock; RMD = 50 for massiver Rock; RMD = JF, for vertically jointed

Section 1a: Rock Mass Description (RMD)
Please choose **yes (Y)** *to* ***only one*** *of the following three questions:*

i. Is this rock friable n
ii. Is this rock massive, with no jointing, or with joint spacing > blast hole spacing ? (y/n) n
iii. Is the rock vertically jointed? y

Section 1b: Joint Factor, JF - ***(Only valid if you answered "Y" to Question iii in Section 1a, above)***
Note: **JF = (JCF * JPS) + JPA** JF = Joint Factor
JCF = Joint Condition Factor *JPA = Vertical Joint Plane Angle Factor*
JPS = Joint Plane Spacing Factor

JCF ***Range of values: 1 to 2***
Describe th joint condition in the box below. Please, choose only one of three options, namely:
"Tight", "Relaxed" or "Gouge-filled": if "Tight", input "1"; if "Relaxed", input "1.5";
If joint is "gouge-filled", input "2"

What is the condition of the joint? (1, 1.5 or 2)	1.5

JPS ***Range: 10 to 50***
Relevant factors: Reduced Pattern (P) and Joint Spacing (S)
P = Reduced Pattern = $(B*S)^{0.5}$

What is the average spacing of joints, in meters?	0.25	P =	3.95
What is the blast Burden (in meters)?	3.6576	95% P =	3.75
What is the blast Spacing (in meters)?	4.2672	JPS	20.00

JPA ***Note that only one answer can be "Yes", although all can be "No"***

Do the joints dip out of the face at >30°? (Y or N)	y		
Do the joints dip into the face at >30°? (Y or N)	n	JPA Value	40
Do the joints Strike out of the face? (Y or N)	n	**RMD**	**65**

Section 2: RDI (Rock Density Influence)
Rock Density (kg//m^3) 2563

Rock Density Influence Factor (F **14.1**

Section 3: Hardness Factor

Young's Modulus, Y (Gpa)	66.85
UCS (MPa)	225.00
Hence, Hardness Factor, HF =	**45.00**

Kuz-Ram Factor

Uncorrected Kuz-Ram Factor	7.44
Correction	0.7
Kuz-Ram Factor (Estimate)	**5.21**

APPENDIX D

CORE DIMENSIONS, SEISMIC VELOCITIES, AND DYNAMIC YOUNG'S MODULI

CORE DIMENSIONS, SEISMIC VELOCITIES, AND DYNAMIC YOUNG'S MODULI

						Uncorrected		Corrected				
						Arrival Times						
Sample ID	h (m)	D (m)	Vol (m3)	Mass (g)	ρ (kg/m3)	S-wave (μs)	P-wave (μs)	S-wave (μs)	P-wave (μs)	V_s (m/s)	V_p (m/s)	**E (Gpa)**
WUSCM-K1	0.0999	0.0537	0.0002264	665.5	2939.334141	29.51	17.73	29.3045	17.5309	3,410.40	5,700.79	83.51
WUSCM-K2	0.1087	0.0540	0.0002486	725.4	2,917.45	31.32	18.18	31.1145	17.9809	3,493.15	6,044.61	88.95
WUSCM-K3	0.1095	0.0539	0.0002496	734.1	2,941.03	30.5	17.86	30.2945	17.6609	3,615.67	6,202.12	95.55
WUSCM-K4	0.1132	0.0546	0.0002655	758.0	2,854.94	33.3	19.9	33.0945	19.7009	3,421.41	5,747.45	81.92
Avg	**0.1078**	**0.0540**	**0.0002475**	**720.8**	**2,913.2**					**3,485.16**	**5,923.74**	**87.48**
						Uncorrected		Corrected				
						Arrival Times						
Sample ID	h (m)	D (m)	Vol (m3)	Mass (g)	ρ (kg/m3)	S-wave (μs)	P-wave (μs)	S-wave (μs)	P-wave (μs)	**V_s (m/s)**	**V_p (m/s)**	**E (Gpa)**
WUSCM-L1	0.0588	0.0532	0.00013082	360.7	2,757.28	17.4	10.92	17.1945	10.7209	3,419.12	5,483.68	76.20
WUSCM-L2	0.0871	0.0536	0.00019635	546.0	2,780.78	24.6	15.9	24.3945	15.7009	3,568.43	5,544.27	81.19
WUSCM-L3	0.0875	0.0511	0.00017929	493.0	2,749.78	*33.8*	*19.9*	33.5945	19.7009	2,605.56	4,443.07	46.22
WUSCM-L4	0.0945	0.0537	0.00021404	594.9	2,779.45	26.6	16.42	26.3945	16.2209	3,580.42	5,826.02	85.27
WUSCM-L5	0.1052	0.0536	0.00023764	661.6	2,784.05	29.96	18.7	29.7545	18.5009	3,534.59	5,684.59	82.42
WUSCM-L6	0.1101	0.0520	0.00023363	645.0	2,760.75	-	-	-	-			
AVG					**2,768.68**					**3,341.62**	**5,396.33**	**74.26**
						Uncorrected		Corrected				
						Arrival Times						
Sample ID	h (m)	D (m)	Vol (m3)	Mass (g)	ρ (kg/m3)	S-wave (μs)	P-wave (μs)	S-wave (μs)	P-wave (μs)	**V_s (m/s)**	**V_p (m/s)**	**E (Gpa)**
WUSCM-M1	0.0323	0.0535	0.0000726	215.38	2,968.36	9.80	5.84	9.59	5.64	3,365.99	5,725.15	83.13
WUSCM-M2	0.0419	0.0534	0.0000937	266.74	2,845.63	13.48	8.28	13.27	8.08	3,154.73	5,182.28	68.29
WUSCM-M3	0.0652	0.0534	0.0001463	413.67	2,828.04	24.00	12.80	23.79	12.60	2,740.34	5,174.63	55.43
WUSCM-M4	0.1076	0.0534	0.0002412	702.90	2,914.70							
WUSCM-M5	0.1089	0.0536	0.0002459	742.00	3,017.32							
Avg					**2,914.81**					**3,087.02**	**5,360.69**	**68.95**
						Uncorrected		Corrected				
						Arrival Times						
Sample ID	h (m)	D (m)	Vol (m3)	Mass (g)	ρ (kg/m3)	S-wave (μs)	P-wave (μs)	S-wave (μs)	P-wave (μs)	**V_s (m/s)**	**V_p (m/s)**	**E (Gpa)**
WUSCM-N1	0.0211	0.0313	0.0000162	43.48	2,678.48	7.6	4.6	7.3945	4.4009	2,846.71	4,783.11	53.21
WUSCM-N2	0.0218	0.0314	0.0000169	46.31	2,745.30	7.4	3.6	7.1945	3.4009	3,025.92	6,401.25	68.18
WUSCM-N3-	0.0271	0.0314	0.0000211	55.24	2,624.15	12	6.2	11.7945	6.0009	2,298.95	4,518.49	36.76
WUSCM-N4	0.0344	0.0314	0.0000267	71.5	2,682.35	14	9	13.7945	8.8009	2,493.39	3,908.12	38.58
WUSCM-N5	0.0440	0.0314	0.0000341	93.11	2730.106825	20.4	11.2	20.1945	11.0009	2,178.81	3,999.67	33.41
WUSCM-N3	0.0237	0.0314	0.0000184	49.66	2,699.87	16.2	11.6	15.9945	11.4009	1,482.70	2,080.10	11.68
WUSCM-N7	0.0359	0.0538	0.0000816	216.18	2,648.54	10.9	6.9	10.6945	6.7009	3,353.59	5,352.27	70.11
WUSCM-N6	0.0313	0.0536	0.0000706			12.7	8.2	12.4945	8.0009			
Avg					**2,686.97**					**2,525.72**	**4,434.72**	**44.56**

APPENDIX E

PHOTO OF CORES USED IN ROCK CHARACTERIZATION

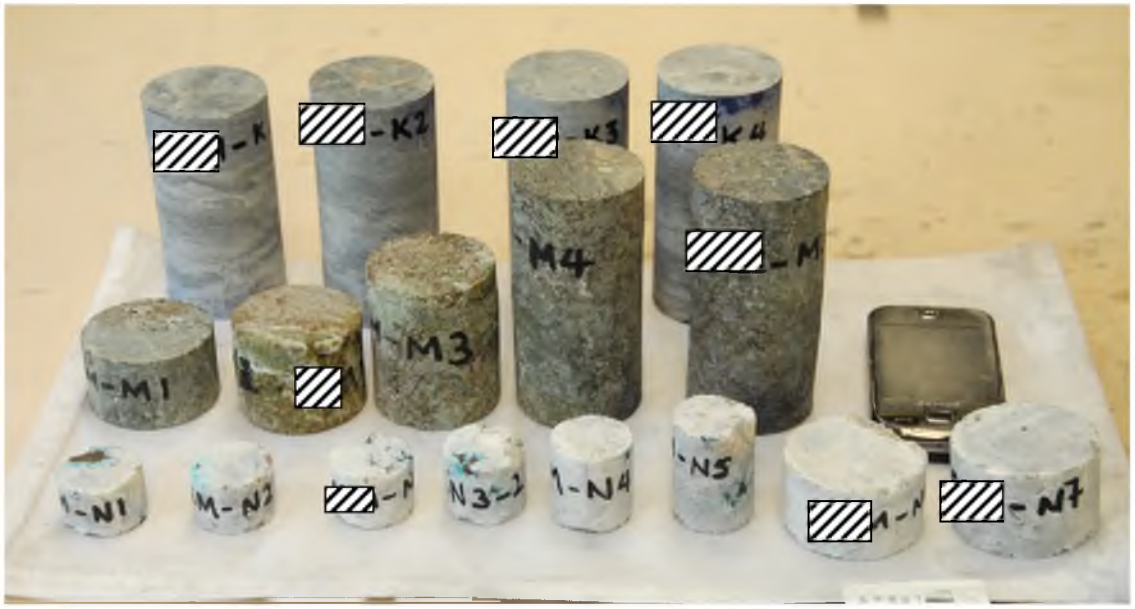

PHOTO OF CORES USED IN ROCK CHARACTERIZATION

Back row: Sembehun waste (limestone)

Middle row: Sembehun high-grade ore

Front row: Bom ore

Note: The initials of the host mine have been masked, in line with that host's request for anonymity

APPENDIX F

DENSITY DATA OBTAINED FROM W.U.S. COPPER'S GEOLOGY (ORE CONTROL) SECTION, WITH THOSE ESTIMATED IN THIS RESEARCH AT THE UNIVERSITY OF UTAH (U OF U)

DENSITY DATA OBTAINED FROM W.U.S. COPPER'S GEOLOGY (ORE CONTROL) SECTION, WITH THOSE ESTIMATED IN THIS RESEARCH AT THE UNIVERSITY OF UTAH (U OF U)

	W.U.S. Copper values				Estimated (U of U)
	s.t./ft^3	s.t./yd^3	t/yd^3	t/m^3	t/m^3
Bom ore	0.1020	2.75	2.50	3.268	2.687
Sembehun High Grade	0.0909	2.45	2.23	2.912	2.915
Sembehun Low Grade	0.0850	2.30	2.08	2.723	
limestone/dolomite	0.0810	2.19	1.98	2.595	2.769
monzonite	0.0830	2.24	2.03	2.659	
granodiorite	0.0800	2.16	1.96	2.563	

APPENDIX G

A SUMMARY OF DATA OBTAINED FROM UNIAXIAL COMPRESSIVE STRENGTH TESTING OF ROCKS FROM W.U.S. COPPER MINE

A SUMMARY OF DATA OBTAINED FROM UNIAXIAL COMPRESSIVE STRENGTH TESTING

OF ROCKS FROM W.U.S. COPPER MINE

Sample ID	Rock Description	D (m)	A (m^2)	mass (kg)	h (m)	Density (kg/m^3)	K_t (N/m)	K_{st} (N/m)	K_s (N/m)	E (GPa)	C_0 (MPa)
K1	East Side Sembehun Waste	0.053708	0.0022655	0.666	0.0999	2,939.3	1,108,429,643	3,654,842,846	1,590,918,609	70.18	178.6
K2		0.053970	0.0022877	0.725	0.1087	2,917.4	1,032,103,408	3,654,842,846	1,438,257,916	68.33	220.1
K3		0.053865	0.0022788	0.734	0.1095	2,941.0	993,353,415	3,654,842,846	1,364,104,843	65.57	196.2
K4		0.054640	0.0023448	0.758	0.1132	2,854.9	964,993,986	3,654,842,846	1,311,189,420	63.32	201.3
						2,913		Average	**1,426,117,697**	**66.85**	**199.1**
L2	West Side Sembehun Waste (5220 Bench)	0.05359	0.0022556	0.546	0.0871	2,780.8	1,107,952,985	3,654,842,846	1,589,936,849	61.36	191.1
L3		0.0510675	0.0020482	0.493	0.0875	2,749.8	830,036,163	3,654,842,846	1,073,932,510	45.90	165.7
L4		0.0537	0.0022648	0.595	0.0945	2,779.4	1,105,126,601	3,654,842,846	1,584,122,963	66.10	216.7
L5		0.0536375	0.0022596	0.662	0.1052	2,784.0	999,316,958	3,654,842,846	1,375,375,948	64.02	242.6
L6		0.051975	0.0021217	0.645	0.1101	2,760.8	878,611,362	3,654,842,846	1,156,671,001	60.03	70.3
										59.34	**204.04**
M4	Sembehun Ore (soft)	0.053425	0.0022417	0.703	0.1076	2,914.7	829,637,254	3,654,842,846	1,073,264,824	51.51	65.2
M5		0.0536275	0.0022587	0.742	0.1089	3,017.3	762,585,580	3,654,842,846	963,652,329	46.45	58.9
						2,966.0				48.98	62.05
N1	Bom Ore										
N2											
N3											27.15
N4											32.81
N5											26.31
						2686.97				**44.56**	**28.76**

APPENDIX H

POINT LOAD DATA USED TO ESTIMATE UNIAXIAL COMPRESSIVE STRENGTHS OF ROCKS

EXHIBIT H1

POINT LOAD DATA USED TO ESTIMATE UNIAXIAL COMPRESSIVE STRENGTH FOR BOM ORE

	Dimensions (cm)			Results				Dimensions (mm)									
Specimen	L (cm)	W (cm)	D (cm)	Ram PSI	Failure Load (lb)	Loading rate (lb/s)	Failure load, P (N)	L (mm)	W (mm)	D (mm)	Area, A (mm.sq.)	D_e^2	D_e	I_s (MPa)	F	$I_{s(50)}$	UCS (Mpa)
BLG-1	3.00	4.25	3.75	1,100	2,459.60	117.12	10,940.85	30.00	42.50	37.50	1,594	2,029	45.05	5.39	0.95	5.14	25.72
BLG-4	1.50	3.25	3.00	1,075	2,403.70	80.12	10,692.19	15.00	32.50	30.00	975	1,241	35.23	8.61	0.85	7.36	36.79
BLG-5	2.00	3.50	3.17	1,210	2,705.56	169.10	12,034.93	20.00	35.00	31.67	1,108	1,411	37.57	8.53	0.88	7.50	37.49
BLG-6	2.50	4.50	2.90	1,060	2,370.16	131.68	10,543.00	25.00	45.00	29.00	1,305	1,662	40.76	6.35	0.91	5.79	28.94
BLG-7-1	1.50	2.50	2.10	840	1,878.24	98.85	8,354.83	15.00	25.00	21.00	525	668	25.85	12.50	0.74	9.29	46.45
BLG-8	2.00	2.00	4.00	1,370	3,063.32	95.73	13,626.33	20.00	20.00	40.00	800	1,019	31.92	13.38	0.82	10.93	54.65
BLG-9	3.50	2.00	3.00	900	2,012.40	71.87	8,951.60	35.00	20.00	30.00	600	764	27.64	11.72	0.77	8.97	44.87
BLG-10-1	1.75	4.00	3.25	720	1,609.92	160.99	7,161.28	17.50	40.00	32.50	1,300	1,655	40.68	4.33	0.91	3.94	19.72
BLG-11	2.50	4.00	3.00	130	290.68	32.30	1,293.01	25.00	40.00	30.00	1,200	1,528	39.09	0.85	0.90	0.76	3.79
BLG-12	2.00	6.50	3.50	263	588.07	58.81	2,615.86	20.00	65.00	35.00	2,275	2,897	53.82	0.90	1.03	0.93	4.67
BLG-13	5.00	7.00	3.00	970	2,168.92	98.59	9,647.84	50.00	70.00	30.00	2,100	2,674	51.71	3.61	1.02	3.66	18.32
BLG-14	1.75	4.50	3.75	710	1,587.56	93.39	7,061.82	17.50	45.00	37.50	1,688	2,149	46.35	3.29	0.97	3.18	15.88
BLG-15	3.50	4.50	3.50	420	939.12	117.39	4,177.41	35.00	45.00	35.00	1,575	2,005	44.78	2.08	0.95	1.98	9.91
BLG-16	3.50	6.20	3.50	650	1,453.40	103.81	6,465.05	35.00	62.00	35.00	2,170	2,763	52.56	2.34	1.02	2.39	11.97
BLG-17	2.50	4.00	1.75	1,090	2,437.24	101.55	10,841.38	25.00	40.00	17.50	700	891	29.85	12.16	0.79	9.64	48.22
BLG-18	1.30	7.03	3.57	1,500	3,354.00	223.60	14,919.34	13.00	70.33	35.67	2,509	3,194	56.52	4.67	1.06	4.94	24.68
BLG-19	2.28	7.00	4.05	970	2,168.92	94.88	9,647.84	22.83	70.00	40.50	2,835	3,610	60.08	2.67	1.09	2.90	14.52
BLG-22-1	1.40	3.90	4.00	1,470	3,286.92	91.30	14,620.95	14.00	39.00	40.00	1,560	1,986	44.57	7.36	0.95	6.99	34.95
BLG-23	2.85	3.00	1.50	1,250	2,795.00	112.34	12,432.78	28.50	30.00	15.00	450	573	23.94	21.70	0.72	15.58	77.89
BLG-24-1	1.67	5.50	3.60	1,170	2,616.12	129.83	11,637.08	16.67	55.00	36.00	1,980	2,521	50.21	4.62	1.00	4.62	23.12
BLG-25-1	1.75	7.50	2.43	1,460	3,264.56	97.86	14,521.49	17.50	75.00	24.33	1,825	2,324	48.20	6.25	0.98	6.15	30.74
BLG-26	1.50	4.00	3.50	1,380	3,085.68	132.43	13,725.79	15.00	40.00	35.00	1,400	1,783	42.22	7.70	0.93	7.14	35.68
BLG-27-1	3.00	4.00	2.75	1,200	2,683.20	148.08	11,935.47	30.00	40.00	27.50	1,100	1,401	37.42	8.52	0.88	7.48	37.40
BLG-10-2	1.50	4.00	3.35	1,030	2,303.08	135.48	10,244.61	15.00	40.00	33.50	1,340	1,706	41.31	6.00	0.92	5.51	27.55
BLG-16-2	3.50	3.00	4.00	370	827.32	63.64	3,680.10	35.00	30.00	40.00	1,200	1,528	39.09	2.41	0.90	2.16	10.78
BLG-25-2	2.00	6.00	2.75	1,230	2,750.28	85.68	12,233.86	20.00	60.00	27.50	1,650	2,101	45.83	5.82	0.96	5.60	28.00
BLG-27-2	2.00	4.75	2.00	840	1,878.24		8,354.83	20.00	47.50	20.00	950	1,210	34.78	6.91	0.85	5.87	29.33
BLG-22-2	1.67	4.00	2.50	1,340	2,996.24		13,327.94	16.67	40.00	25.00	1,000	1,273	35.68	10.47	0.86	8.99	44.97
												Mean	41.53				29.54
																	28.76

Ram area (Sq. In.) : *2.236*

Site Constant, C = 5

EXHIBIT H2

POINT LOAD DATA USED TO ESTIMATE UNIAXIAL COMPRESSIVE STRENGTH

FOR SEMBEHUN HIGH-GRADE ORE

	Dimensions (cm)			Results			Dimensions (mm)									
Specimen	L (cm)	D (cm)	W (cm)	Ram PSI	Failure Load (lb)	Failure load, P (N)	L (mm)	W (mm)	D (mm)	Area, A (mm.sq.)	D_e^2	D_e	I_s (MPa)	F	$I_{s(50)}$	UCS (Mpa)
SRW-2	2.00	4.00	4.30	630	1,408.68	6,266.12	20.00	43.00	40.00	1,720	2,190	46.80	2.86	0.97	2.78	138.86
SRW-1	2.77	3.50	4.20	430	961.48	4,276.88	27.67	42.00	35.00	1,470	1,872	43.26	2.29	0.94	2.14	107.05
SRW-5	2.00	3.50	6.10	100	223.60	994.62	20.00	61.00	35.00	2,135	2,718	52.14	0.37	1.02	0.37	18.64
SRW-6	2.50	4.00	4.00	245	547.82	2,436.82	25.00	40.00	40.00	1,600	2,037	45.14	1.20	0.95	1.14	57.12
SRW-7	2.50	3.80	4.40	80	178.88	795.70	25.00	44.00	38.00	1,672	2,129	46.14	0.37	0.96	0.36	18.02
SRW-10	2.17	2.47	6.00	340	760.24	3,381.72	21.67	60.00	24.67	1,480	1,884	43.41	1.79	0.94	1.68	84.20
SRW-4	2.13	4.00	4.25	340	760.24	3,381.72	21.33	42.50	40.00	1,700	2,165	46.52	1.56	0.97	1.51	75.63
SRW-8	4.50	3.60	5.50	50	111.80	497.31	45.00	55.00	36.00	1,980	2,521	50.21	0.20	1.00	0.20	9.88
SRW-11	2.00	3.70	5.50	200	447.20	1,989.24	20.00	55.00	37.00	2,035	2,591	50.90	0.77	1.01	0.77	38.70
SRW-9	1.77	4.20	7.55	160	357.76	1,591.40	17.67	75.50	42.00	3,171	4,037	63.54	0.39	1.11	0.44	21.95
SRW-3	2.00	3.75	6.00	480	1,073.28	4,774.19	20.00	60.00	37.50	2,250	2,865	53.52	1.67	1.03	1.72	85.92
SRW-12	1.50	3.50	5.50	400	894.40	3,978.49	15.00	55.00	35.00	1,925	2,451	49.51	1.62	1.00	1.62	80.80
SRW-13	3.57	3.00	5.00	130	290.68	1,293.01	35.67	50.00	30.00	1,500	1,910	43.70	0.68	0.94	0.64	31.86
SRW-14	2.57	3.75	8.00	340	760.24	3,381.72	25.67	80.00	37.50	3,000	3,820	61.80	0.89	1.10	0.97	48.70
SRW-15	2.40	3.75	4.75	300	670.80	2,983.87	24.00	47.50	37.50	1,781	2,268	47.62	1.32	0.98	1.29	64.36
SRW-16	2.93	4.70	5.90	660	1,475.76	6,564.51	29.33	59.00	47.00	2,773	3,531	59.42	1.86	1.08	2.01	100.47
											Mean	50.23				61.38
																62.05

Ram area (Sq. In.) : *2.236*

Site Constant, C = 50

EXHIBIT H3

POINT LOAD DATA USED TO ESTIMATE UNIAXIAL COMPRESSIVE STRENGTH

FOR SEMBEHUN LOW-GRADE ORE

	Dimensions (cm)			Results			Dimensions (mm)									
Specimen	L (cm)	D (cm)	W (cm)	Ram PSI	Failure Load (lb)	Failure load, P (N)	L (mm)	W (mm)	D (mm)	Area, A (mm.sq.)	D_e^2	D_e	I_s (MPa)	F	$I_{s(50)}$	UCS (Mpa)
SRF-19	2.50	3.35	4.50	1,040	2,325.44	10,344.07	25.00	45.00	33.50	1,508	1,919	43.81	5.39	0.94	5.08	253.90
SRF-12	2.00	2.80	5.00	485	1,084.46	4,823.92	20.00	50.00	28.00	1,400	1,783	42.22	2.71	0.93	2.51	125.39
SRF-14	1.80	2.37	3.00	430	961.48	4,276.88	18.00	30.00	23.67	710	904	30.07	4.73	0.80	3.76	188.16
SRF-10	2.75	2.27	4.25	1,200	2,683.20	11,935.47	27.50	42.50	22.67	963	1,227	35.02	9.73	0.85	8.29	414.52
SRF-5	1.90	4.40	4.75	1,285	2,873.26	12,780.90	19.00	47.50	44.00	2,090	2,661	51.59	4.80	1.01	4.87	243.54
SRF-13	2.00	3.20	3.75	500	1,118.00	4,973.11	20.00	37.50	32.00	1,200	1,528	39.09	3.25	0.90	2.91	145.68
SRF-16	2.50	2.50	4.50	650	1,453.40	6,465.05	25.00	45.00	25.00	1,125	1,432	37.85	4.51	0.88	3.98	199.09
SRF-11	1.83	3.50	3.35	520	1,162.72	5,172.04	18.33	33.50	35.00	1,173	1,493	38.64	3.46	0.89	3.09	154.25
SRF-9	2.10	2.70	4.50	360	804.96	3,580.64	21.00	45.00	27.00	1,215	1,547	39.33	2.31	0.90	2.08	103.88
SRF-18	1.75	3.20	4.85	700	1,565.20	6,962.36	17.50	48.50	32.00	1,552	1,976	44.45	3.52	0.95	3.34	167.09
SRF-2	1.57	3.93	6.75	1,100	2,459.60	10,940.85	15.67	67.50	39.33	2,655	3,380	58.14	3.24	1.07	3.46	173.19
SRF-20	2.00	3.00	8.00	900	2,012.40	8,951.60	20.00	80.00	30.00	2,400	3,056	55.28	2.93	1.05	3.06	153.24
SRF-4	1.30	3.00	5.00	450	1,006.20	4,475.80	13.00	50.00	30.00	1,500	1,910	43.70	2.34	0.94	2.21	110.29
SRF-15	1.80	3.50	4.50	770	1,721.72	7,658.59	18.00	45.00	35.00	1,575	2,005	44.78	3.82	0.95	3.63	181.71
SRF-7	3.15	2.50	3.60	1,040	2,325.44	10,344.07	31.50	36.00	25.00	900	1,146	33.85	9.03	0.84	7.57	378.69
											Mean	**42.52**			**Mean**	**199.51**

Ram area (Sq. In.) : *2.236*

Site Constant, C = 50

APPENDIX I

CRUSHING CIRCUIT CHARACTERISTICS

CRUSHING CIRCUIT CHARACTERISTICS

Feature	Value
CRUSHERS	
Types	Jaw (x1) Cone (x2)
Feed rate through circuit	220(st/h) (200 t/h)
Hours of operation (per day)	12
Jaw Crusher Settings	
Gape	1117.6 mm x 787.4 mm (44 in. x 31 in.)
Open Side Setting (OSS)	177.8 mm (7 in.)
Closed Side Setting (CSS)	101.6 mm (4 in.)
Cone 1 Settings	
Gape	161.925 mm (6.375 in.)
Open Side Setting (OSS)	127 mm (5 in.)
Closed Side Setting (CSS)	12.7 mm (0.5 in.)
Cone 2 Settings	
Gape	73.025 mm (2.875 in.)
Open Side Setting (OSS)	44.45 mm (1.75 in.)
Closed Side Setting (CSS)	6.35 mm (0.25 in.)
SCREENS	
No. of Screens	2
Screen 1	
Dimensions of screen	6.096 m x 2.1336 m (20 ft x 7 ft)
No. of decks	3
No. of screen panels per deck	5
Dimensions of panel	1.2192 x 2.1336 m (4 ft x 7 ft)
Screen size on Deck 1	31.75 mm (1.25 inches)
Screen size on Deck 2	28.575 mm (1.125 inches) (x1); 9.525 mm (0.375 inches) (x4)
Screen size on Deck 3	6.35 mm (0.25 inches)
Inclination of screen	Horizontal
Screen 2	
Dimensions of screen	6.096 m x 2.1336 m (20 ft x 7 ft)
No. of decks	3
No. of screen panels per deck	5
Dimensions of panel	1.2192 x 2.1336 m (4 ft x 7 ft)
Screen size on Deck 1	15.875 mm (0.625 inches)
Screen size on Deck 2	12.7 mm (0.5 inches)
Screen size on Deck 3	6.35 mm (0.25 inches)
Inclination of screen	Horizontal

REFERENCES

Ash, R.L. 1963. The mechanics of rock blasting (Part 1). In *Pit and Quarry* 56(2): 98-100.

Bedair, A 1996. Digital Image Analysis of Rock Fragmentation from Blasting, Ph.D. thesis, Department of Mining and Metallurgical Engineering, McGill University, Montréal.

Bergmann, O.R., Riggle, J.W. and Wu, F.C. 1973. Model rock blasting – Effect of explosives properties and other variables on blasting results. In *Int. J. Rock Mechanics & Mining Sciences*, vol 10, pp 585-612.

Bergstrom, B.H. 1985. Crushability and grindability. In *SME Mineral Processing Handbook*, Ed: N.L. Weiss, New York, vol. 2, in Section 30 "Sampling and Testing", pp 65-68.

Bhattacharyya, A. 2014. Dependence of rates of breakage on fines content in wet ball mill grinding, M.S. thesis, Department of Metallurgical Engineering, University of Utah

BoBo, T. n.d. *What's new with the digital image analysis software Split-Desktop, Split Engineering*. Split Engineering, LLC, 110 S. Church St., Tucson, Arizona, USA

Bond, F.C. 1952. The Third Theory of Comminution. In *Trans. A.I.M.E.*, v. 193, pp. 484-494.

Brandt, D., Martinez, I., French, T., Slattery, L., Baker, G. 2011. *Better fragmentation through team work at Dos Pobres Mine, Safford, Arizona*. SME, November 2011

Csoke B, Petho S, Foldesi J and Meszaros, L. 1996. Optimization of stone-quarry technologies. In *Intl. Jnl. of Mineral Processing* 44-45. 447 - 459.

Chung, S.H. and Katsabanis, P.D. 2000. Fragmentation prediction using improved engineering formulas. In *Int J. Fragmentation by blasting*, vol 4, pp 198-207.

Cunningham, C.V.B. 1983. The Kuz—Ram model for prediction of fragmentation from blasting. In *Proceedings of the first international symposium on rock fragmentation by blasting*, Lulea, Sweden. p. 439–54.

Cunningham, C.V.B. 1987. Fragmentation estimations and the Kuz—Ram model - Four years on. In *Proceedings of the second international symposium on rock fragmentation by blasting*, Keystone, Colorado. p. 475–87.

Cunningham, C.V.B. 2005. The Kuz-Ram fragmentation model – 20 years on. In *Brighton Conference proceedings*. Ed. R. Holmberg et al.

Dance, A., Valery W., Jankovic, A., La Rosa, D., and Esen, S. 2007. *Maintaining the benefit – how to ensure Mine to Mill continues to work for you.* , Ninth Mill Operators Conference, Fremantle, WA, 19 to 21 March, 2007, pg. 1-8 (see pg 3)

Edgar, J and Pfleider, E.P. 1972. Mining and Milling, an Interrelated Fragmentation System. In *Society of Mining Engineers, AIME*, Transactions Vol 252, March 1972. Page 46 - 49

Eloranta, J. 2014. Non-ideal blasting for ideal grinding – Part Two. In The *Journal of Explosives Engineering*. Volume 31 Number 5, September/October 2014. Pg 26- 31.

Eloranta, J., Palangio, T., Palangio, T.C. and Workman L. 2007. Size matters on the Mesabi Range. In *International Society of Explosive Engineers*, 2007G Volume 1.

Floyd, J. n.d. *Efficient Blasting Techniques*

Hall, J. and Brunton, I. 2001. Critical Comparison of Julius Kruttschnitt Mineral Research Centre (JKMRC) Blast Fragmentation Models. In *EXPLO 2001*, Hunter Valley, NSW, 28 – 31 October 2001. Pages 207 – 212.

Herbst, J.A. 1971. *Batch Ball Mill Simulation: An Approach for Wet Systems.* D. Eng. Dissertation, University of California, Berkeley, California.

Herbst, J.A. and Fuerstenau, D.W. 1968. The zero order production of fine sizes in comminution and its implications in simulation. In *Transactions of SME, AIME, December 1968*, vol. 241. Pages 538 - 548

Herbst, J.A., Grandy, G.A., and Mika, T.S. 1968. *On the development and use of lumped parameter models for open- and closed-circuit grinding.* Trans. Inst. Min. Met. Section C, 77, pp. 193-198, (1968).

Herbst, J.A., Grandy, G.A. and Fuerstenau, D.W. 1973. *Population Balance Models for the Design o f Continuous Grinding Mills.* Paper 19 of International Mineral Processing Congress, London(1973).

Herbst, J.A., Rajamani, K. and Kinneberg, D.J. 1977. *ESTIMILL: A program for grinding simulation and parameter estimation with linear models.*

Herbst, J.A., Siddique, M., Rajamani, K. and Sanchez, E. 1983. Population Balance Approach to Ball Mill Scale-Up: Bench and Pilot Scale Investigations. In *SME of AIME Transactions Vol 272*. Pp 1945 – 1954.

Himmelblau, D.M., and Bischoff, K.B. 1968. *Process analysis and simulation: Deterministic systems*. J. Wiley, New York, 1968.

Hustrulid, W. 1999. *Blasting Principles for Open Pit Mining, Vol. 1: General Design Concepts*. CRC Press, Taylor & Francis Group, Boca Raton, London, New York

Infomine USA Inc. Costmine Division 2013. *Mine and Mill Equipment Costs – An Estimator's Guide*

Jankovic, A; Valery, W.; Davis, E., 2004. Cement Grinding Optimisation. In *Minerals Engineering*, vol 17 (2004), pp. 1075–1081.

Julius Kruttschnitt Mineral Research Center (JKMRC) 2012. *Mine to Mill Process Optimization* (Course notes for short course on Mine-to-mill process optimization at SME conference 2012). JK Tech SMI Technology Transfer

Kanchibotla, S.S., 2001. Optimum Blasting? Is it Minimum Cost Per Broken Rock or Maximum Value Per Broken Rock? In *EXPLO 2001* Hunter Valley, NSW, 28 - 31 October; pages 35 – 40.

Kanchibotla, S.S., Valery, W. and Morrell, S. 1999. Modelling Fines in Blast Fragmentation and its Impact on Crushing and Grinding. In *Explo '99*, Kalgoorlie, WA, November 7 – 11. pp 137 – 144.

Kemeny, J.M., Devgan A., Hagaman, R.M., Wu, X. 1993. *Analysis of rock fragmentation using digital image processing*

Kemeny, J.M., Mofya, E., Kaunda, R., and Lever, P. 2001. *Improvements in Blast Fragmentation Models Using Digital Image Processing.* EXPLO 2001, Hunter Valley, NSW, 28 - 31 October 2001

Kick, F. 1885. *Das Gesetz der proportionalen Widerstande und seine anwendung.(The law of proportional resistance and its application)* Leipzig, Germany.

Kim, J.H. 1974. *A Normalized Model for Wet Batch Ball Milling*. Ph.D. Dissertation, University of Utah, Salt Lake City, Utah.

King, R.P. 2012. *Modeling and simulation of mineral processing systems*. Second Edition. Ed. Schneider, CL and King, E.A. Society for Mining, Metallurgy and Exploration, Englewood, Colorado.

Konya, C. J. 1968. *Spacing of Explosive Charges.* MS Thesis, Department of Mining and Petroleum Engineering, University of Missouri at Rolla

Kou, S. and Rustan, A. 1993. Computerized design and result prediction of bench blasting. In *Proc 4th Int Symp on Rock Fragmentation by Blasting*, H-P Rossmanith ed, pp 263-271. Balkema, Rotterdam.

Kuznetsov, V.M. 1973. The mean diameter of fragments formed by blasting rock. In *Sov Min Sci*; 9:144–8.

Langefors, U., & Kihlstrom, B. 1963. *The modern technique of rock blasting*. Almqvist & Wicksell, Uppsala, Sweden

Larsson, B. 1974. Report on blasting of high and low benches – fragmentation from production blasts. In *Proc Discussion meeting* BK 74, pp 247 – 273. Swedish Rock Construction Committee, Stockholm

Latchireddi, S.R. 2013. Grate discharge vs overflow ball mills for fine grinding. M.S Thesis, University of Utah

Levenspiel, O., and Bischoff, K.B. 1963. Patterns of flow in chemical process vessels. In *Advances in Chemical Engineering,* edit. T.B. Drew, et. Al, Academic Press, New York, pp. 95-198, 1963.

Lilly, P.A. 1986. *An empirical method of assessing rock mass blastability*. The AusIMM/IE Aust Newman Combined Group, Large Open Pit Mining Conference October 1986. Pages 89 – 92.

Luz, J. A. M., Milhomem, F. O. 2013. *Scale-up of Crushing Tests*. Twenty-third International Mining Congress & Exhibition of Turkey, 16-19 April.

Lynch, A.J. and Morrison, R.D. 1999. Simulation in mineral processing history, present status and possibilities. In *The Journal of the South African Institutte of Mining and Metallurgy. October-December.* pp 283 - 288

Malghan, S.G., Fuerstenau, D.W, 1976. The Scale-up of Ball Mills Using Population Balance Models and Specific Power Input. In S*ymposium Zerkleinern, Dechma-Monographien*, Vol. 79, Part II No. 1586, p. 613.

McCarter, M.K. 2014. Unpublished, class notes on surface mining – University of Utah

MacKenzie, A.S. 1966. The Cost of Explosives, do you evaluate it properly? In *Mining Congress Journal*, Vol. 52 Issue 5. Pages 32 – 41.

MacKenzie, A.S. 1967. *Optimum Blasting;* 28th Annual Mining Symposium and the Fortieth Annual Meeting of the Minnesota Section, AIME.

Maerz, N. H., 1998. *Aggregate sizing and shape determination using digital image processing*. Center for Aggregates Research (ICAR) Sixth Annual Symposium Proceedings, St. Louis, Missouri, April 19-20, pp. 195-203.

Maerz, N.H., Palangio, T.C., Palangio, T.W., Elsey, K. 2007. Optical sizing analysis of blasted rock: lessons learned. In *European Federation of Explosives Engineers*

Maerz, N.H., Zhou, W. 1998. Optical digital fragmentation measuring systems – inherent sources of error. In *FRAGBLAST, the International Journal for Blasting and Fragmentation,* Vol. 2, No. 4, pp. 415 – 431.

Magdalinovic, N. 1989. A Procedure for Rapid Determination of the Bond Work Index. In *International Journal of Mineral Processing*, 25, 41-46.

Magdalinovic, N., 1990. Mathematical Model for Determination of an Optimal Crusher Product size. In *Aufbereitungs-Technik* 31, Nr 5

Magdalinovic, N., Magdalinovic, S., Jovanovic, R. and Stanujkic, D. 2011. Is there a material constant which characterises mineral resources grindability? In *Annual of the university of mining and geology "st. Ivan rilski"*, Vol. 54, Part II.

Mika, T.S. 1970. *Population balance models of a continuous grinding mill as a distributed process.* Doctor of Engineering dissertation, University of California, Berkeley, December 1970.

Mika, T.S., Berlioz, L.M. and Fuerstenau, D.W. 1967. An Approach to the Kinetics of Dry Batch Ball Milling". In *Zerkleinern, 2nd European Symposium on Comminution.* Edit. Rumpf, H. and Pietsch, W. Amsterdam Dechema-Monographien, 57, Part I, pp. 205 – 240.

Moser, P. 2003. Less fines production in aggregate and industrial minerals industry. In *Proc EFEE 2nd World Conf on Explo & Blasting.* R Holmberg ed, pp 335-343. Balkema, Rotterdam.

Montgomery, D.C. and Runger G.C. 2011. *Applied Statistics and Probability for Engineers.* Wiley & Sons, Inc.

Mular, A.L. 1989. Modelling, simulation and optimization of mineral processing circuits. In *Challenges in Mineral Processing*, ed. K.V.S Sastry and M.C. Fuerstenau, SME, Inc., Littleton, 323

Mwansa, S., Dance, A., Annandale, D., Kok, D., and Bisiaux B. 2010. *Integration and Optimisation of Blasting, Crushing and Grinding at the Newmont Ahafo Operation*

Nematollahi, H 1994. *New size laboratory ball mill for Bond Work Index determination.* SME non-meeting paper 93-315, 1993

Nielsen, K. and Kristiansen, J. 1996. Blasting-crushing-grinding: Optimization of an integrated comminution system. In *Proc 5th Int Symp on Rock Fragmentation by Blasting*, B Mohanty ed, pp 269-277. Balkema, Rotterdam.

Ouchterlony, F 2003. Influence of blasting on the size distribution and properties of muckpile fragments, a state-of-the-art review. In *MinFo project P2000-10: Energioptimering vid nedbrytning/Energy optimization in comminution.* Lulea University of Technology.

Ouchterlony, F. 2005. The Swebrec© function: linking fragmentation by blasting and crushing. In *Mining Technology* (Trans. Inst. Min. Metall. A) February 2005.

Palangio, T.W., Palangio T.C., Maerz, N 2005. Advanced automatic optical blast fragmentation sizing and tracking. In *Brighton Conference Proceedings*, R. Holmberg et al.

Preece, D.S., and Chung, S.H. 2003. *Blasting induced rock fragmentation prediction using the RHT constitutive model for brittle materials.*

Preece, D.S., Jensen R.P., and Chung S.H. 2001. *Development and Application of a 3-D Rock Blast Computer Modeling Capability Using Discrete Elements - DMCBLAST_3D**

Preece, D.S., and Lownds, C.M. 2008. *3D computer simulation of bench blasting with precise delay timing*

Rajamani, R.K. 2012. *Course notes* (unpublished), MetE 7910, Department of Metallurgical Engineering, University of Utah, Fall 2012.

Rittinger, R.P. 1867. *Lehrbuch der Aufbereitungskunde (Textbook of the Processing Art).* Ernst and Korn, Berlin, Germany.

Rogers, W., Kanchibotla, S.S., Tordoir, A., Ako, S., Engmann, E., and Bisiaux, B. 2012a. *Solutions To Reduce Blast-Induced Ore Loss & Dilution At Ahafo Gold Mine In Ghana.* SME Annual Meeting Feb. 19 - 22, 2012, Seattle, WA

Rogers, W., Kanchibotla, S.S., Tordoir, A., Ako, S., Engmann, E., and Bisiaux, B. 2012b. *Understanding blast movement and its impacts on grade control at Ahafo Gold Mine in Ghana*. International Society of Explosives Engineers. Nashville, Tennessee.

Rosin P, Rammler E. 1933. The laws governing the fineness of powdered coal. In *J. Inst Fuel* 1933;7:29– 36.

Rowland, C.A. Jr, and McIvor, R.E. 2009. The Bond Standard for Comminution Efficiency. In *Recent Advances in Mineral Processing Plant Design, SME*, 2009

Rustan, A. 1981. Fragmentation influencing factors in rock blasting. In *Teknisk rapport* 1981: 38T, Lulea University of Technology, Lulea, Sweden. In Swedish.

Sastry, K.V.S. and Lofftus, K.D. 1989. Challenges and opportunities in modeling and simulation of mineral processing systems. In *Challenges in Mineral Processing*, ed. K.V.S. Sastry and M.C. Fuerstenau, SME, Inc., Littleton, 369

Sastry, K.V.S. 1990. Principles and methodology of mineral processing modeling. In *Control '90 – Mineral and Metallurgical Processing*, ed. R.K. Rajamani and J.A. Herbst, SME Inc., Littleton, Colorado.

Scaw Metals Group n.d. Media Charge Strings Spreadsheet. In *Molycop Tools V.2.0*

Schuhmann R. 1940. *Technical publication 1189.* New York (NY). American Institute of Mining and Metallurgical Engineers; 1940.

Siddique, M. 1977. *A kinetic approach to ball mill scale-up for dry and wet systems.* MS thesis, Department of Mining, Metallurgical and Fuels Engineering, University of Utah

Singh, S.P. and Narendrula, R. 2005. Characteristics of the blasted muck and the loader's productivity. In *International Society of Explosives Engineers* 2005G Volume 2.

Tavares, L.M. and Carvalho, R.M. 2007. Impact work index prediction from continuum damage model of particle fracture. In *Minerals Engineering*, Elsevier. Vol. 20 pp1368–1375

Thomas, S., Rafiei, S., Maghsoodlou, S. and Afzali, A. 2014. *Foundations of Nanotechnology. Volume 2: Nanoelements Formation and interaction.* AAP Research notes on Nanoscience and Nanotechnology.

Thornton, D., Sprott, D., and Brunton, I. 2005. Measuring blast movement to reduce ore loss and dilution. In *International Society of Explosives Engineers*

Tucker, S.A. 2001. *Optimal open pit planning and design.* MSc thesis, Department of Mining Engineering, Kwame Nkrumah University of Science and Technology, School of Mines, Tarkwa, Ghana.

U.S. Army Corps of Engineers 2009. Appendix L - Guide for Estimating Drill Steel and Drill Bit Costs In *Construction Equipment Ownership and Operating Expense Schedule Region III.* EP 1110-1-8 Volume 3.

Utley, R. W. 2002. Selection and Sizing of Primary Crushers. In *Mineral Processing Plant Design, Practice, and Control: Proceedings - Volume 1.* Mular A. L.; Halbe, D. N.; Barratt D. J. (ed.), SME, Littleton, Colorado, pp. 584 - 605.

Valery, W and Jankovic, A 2002. *The future of comminution.* JKMRC, University of Queensland, Brisbane, Australia; 34th IOC on Mining and Metallurgy, 30 Sept.-3 Oct., Hotel Jezero, Bor Lake, Yugoslavia

Valery Jnr., W., La Rosa, D., Jankovic, A. 2004. *Mining and Milling Process Integration and Optimisation.* Presented at the SME 2004 Conference, Denver, CO. 23-25 February.

Vermeulen, L. A., Howat, D.D., and Gough, C. L.M., 1983. Theories of ball wear and the results of a marked-ball test in ball milling. In *Journal of Southern African Institute of Mining and Metallurgy.*

Whiten, W.J. 1973. The simulation of crushing plants with models developed using multiple spline regression. In *Application of computer methods in the Mineral industry* Eds MDG Salamon and Lancaster. S. Afr. Inst. Min. Metall. Johannesburg, 1973. P317-323

Whiten, W.J., Walter, G.W. and White, M.E. 1973. *A breakage function suitable for crusher models.* 4TH Tewksbury Symposium, Melbourne, Feb. P19.1-19.32

Widzyk-Capehart, E. and Lilly. P. 2001. A Review of General Considerations for Assessing Rock Mass Blastability and Fragmentation. In *Explo 2001*, Hunter Valley, NSW, October 28-31.

Wills, B. 2006. *Wills' Mineral Processing Technology;* Seventh Edition, Copyright 2006, ed. Napier-Munn

Workman, L. and Eloranta, J. 2003. The effects of Blasting on Crushing and Grinding Efficiency and Energy Consumption. In *Proceedings of 29th Conference on Explosives and Blasting Technique*, Nashville, TN, 2003